Routing and Protection in Flexible Optical Networks

Min Ju

▶ **To cite this version:**

Min Ju. Routing and Protection in Flexible Optical Networks. Hardware Architecture [cs.AR]. Université d'Avignon, 2018. English. NNT : 2018AVIG0226 . tel-01924170v1

HAL Id: tel-01924170

https://theses.hal.science/tel-01924170v1

Submitted on 15 Nov 2018 (v1), last revised 3 Dec 2018 (v2)

HAL is a multi-disciplinary open access archive for the deposit and dissemination of scientific research documents, whether they are published or not. The documents may come from teaching and research institutions in France or abroad, or from public or private research centers.

L'archive ouverte pluridisciplinaire **HAL**, est destinée au dépôt et à la diffusion de documents scientifiques de niveau recherche, publiés ou non, émanant des établissements d'enseignement et de recherche français ou étrangers, des laboratoires publics ou privés.

ACADÉMIE D'AIX-MARSEILLE
UNIVERSITÉ D'AVIGNON ET DES PAYS DE VAUCLUSE

THÈSE

présentée à l'Université d'Avignon et des Pays de Vaucluse
pour obtenir le diplôme de DOCTORAT

SPÉCIALITÉ : Informatique

École Doctorale 536 « Sciences et Agronomie »
Laboratoire d'Informatique (EA 4128)

Optimisation de la Protection des Réseaux Optiques de Nouvelle Génération

par
Min Ju

Soutenue publiquement Janvier 2018 devant un jury composé de :

M.	Bernard Cousin	Professeur, IRISA, Université de Rennes 1	Rapporteur
M.	Massimo Tornatore	Maître de Conférences, École polytechnique de Milan	Rapporteur
M.	Rami Langar	Professeur, LIGM, Université Paris-Est Marne-la-Vallée	Examinateur
M.	Bogdan Uscumlic	Ingénieur de Recherche, Nokia Bell Labs	Examinateur
M.	Juan-Manuel Torres	Maître de Conférences (HDR), LIA, Université d'Avignon	Directeur de thèse
M.	Shilin Xiao	Professeur, LOCT, Université de Shanghaï Jiao Tong	Co-directeur de thèse
M.	Fen Zhou	Maître de Conférences, LIA, Université d'Avignon	Co-directeur de thèse

Laboratoire d'Informatique d'Avignon

ACADÉMIE D'AIX-MARSEILLE
UNIVERSITÉ D'AVIGNON ET DES PAYS DE VAUCLUSE

THESIS

A thesis submitted at the University of Avignon
for the degree of Doctor of Philosophy

In : Computer Science

Doctoral School 536 «Sciences et Agroscience»
Laboratoire d'Informatique (EA 4128)

Optimization of Protection Schemes for Next Generation Optical Networks

by
Min Ju

Defended publicly January 2018 before the jury members:

M.	Bernard Cousin	Professor, IRISA, University of Rennes 1	Reviewer
M.	Massimo Tornatore	Associate Professor, Polytechnic University of Milan	Reviewer
M.	Rami Langar	Professor, LIGM, University Paris-Est Marne-la-Vallée	Examiner
M.	Bogdan Uscumlic	Research Engineer, Nokia Bell Labs	Examiner
M.	Juan-Manuel Torres	Associate Professor, LIA, University of Avignon	Supervisor
M.	Shilin Xiao	Professor, LOCT, Shanghai Jiao Tong University	Co-supervisor
M.	Fen Zhou	Associate Professor, LIA, University of Avignon	Co-supervisor

Laboratoire d'Informatique d'Avignon

Résumé

La tolérance aux pannes est une propriété très importante des réseaux optiques de nouvelle génération. Cette thèse aborde la conception des mécanismes de protection contre des pannes liées à la défaillance d'une fibre optique ou à une catastrophe naturelle. Deux systèmes de protection classiques, à savoir la protection par des cycles préconfigurés (p-cycles) et la protection du chemin de secours, sont étudiés pour atteindre une efficacité de protection élevée, tout en considérant le coût de l'équipement optique, la consommation d'énergie et l'utilisation de la ressource spectrale. Ces problèmes de survivabilité sont d'abord formulés en utilisant la programmation linéaire en nombres entiers (PLNE), et ensuite résolus soit par algorithmes heuristiques, soit par une approche de décomposition.

La panne d'une seule fibre optique est le scénario le plus courant. Nous allons donc considérer d'abord des pannes liées à la défaillance d'une fibre optique dans les réseaux optiques multi-débit. Pour réduire le coût des transpondeurs, un système de protection par p-cycles de longueur adaptable et peu coûteux est proposé. Spécifiquement, les p-cycles de longueur limitée sont conçus pour utiliser un débit approprié en fonction du coût du transpondeur et de la portée de transmission. Un modèle de programmation linéaire en nombres entiers (PLNE) sans énumération des cycles candidats est formulé pour générer directement les p-cycles de coût dépenses d'investissement minimum. De plus, un algorithme GPA (Graph Partitioning in Average) et un algorithme d'estimation des nombres de cycles (EI) sont développés pour rendre le modèle PLNE plus efficace au niveau du temps de calcul.

En ce qui concerne la consommation d'énergie des réseaux optiques élastiques résilients, nous proposons d'utiliser un schéma de p-cycles dirigés, efficaces en énergie, pour protéger le trafic asymétrique. En raison de l'avantage de distinguer du volume de trafic dans les deux directions, les p-cycles dirigés consomment peu d'énergie en attribuant de créneaux ou slots du spectre et des formats de modulation différents à chaque direction.

Un modèle PLNE est formulé pour minimiser la consommation d'énergie totale sous contraintes de génération du cycle dirigée, d'allocation de spectre, d'adaptation de modulation et de capacité de protection. Pour le passage à l'échelle, le modèle PLNE est décomposé en deux sous-problèmes: une méthode d'énumération de cycles améliorée et un modèle PLNE simplifié pour la sélection des cycles. Nous avons montré que les p-cycles dirigés obtiennent une meilleure performance comparant les p-cycles

non-dirigés pour le trafic asymétrique en termes de la consommation d'énergie et de l'utilisation du spectre.

Afin d'améliorer l'efficacité d'utilisation du spectre dans réseaux optiques élastiques, une protection par p-cycles (SS-p-cycle) à spectre partagé est proposée. Les SS-p-cycles permettent de réduire l'utilisation du spectre et le taux de fragmentation spectrale en exploitant un partage de spectre spécial entre plusieurs p-cycles ayant des liens communs. Les modèles PLNE est conçus dans les cas ≪sans≫ ou ≪avec≫ conversion spectrale afin de minimiser l'utilisation du spectre. Ces modèles peuvent obtenir la solution optimale pour un petit réseaux optiques élastiques, et une heuristique efficace est développée pour résoudre les instances à grande échelle. Les résultats de simulations montrent que les SS-p-cycles ont des avantages significatifs pour réduire l'utilisation de la ressource spectrale et la défragmentation des fréquence. De plus, la conversion du spectre aide les SS-p-cycles à acquérir une meilleure utilisation du spectre.

Finalement, bien que la panne de liaison unique est le scénario le plus courant, les défaillances à grande échelle dues aux catastrophes naturelles menacent la capacité de survie des réseaux de centres de données. Également, le problème d'approvisionnement de service de cloud après sinistre est étudié, en considérant la disposition du contenu, le routage, la protection du chemin et du contenu, et l'allocation du spectre. Les services cloud permettent d'utiliser un autre nœud centres de données avec du contenu répliqué pour garantir la survivabilité en cas de sinistre. Nous étudions deux modèles de protection contre les pannes liées aux catastrophes naturelles: la protection par chemin de secours de bout en bout dédiée et la protection par chemin de secours de bout en bout partagée, qui visent à minimiser l'utilisation du spectre. Un modèles PLNE est formulés pour chaque schéma de protection. Une approche de décomposition basée sur la génération de colonnes est proposée afin de trouver les solutions de chaque schéma de protection pour un réseaux optiques élastiques à l'échelle. Une évaluation approfondie a été réalisée pour étudier l'impact sur l'utilisation du spectre en termes de la quantité de trafic, du nombre de centre de données, du nombre de répliques et de topologies des réseaux.

Mots clés : Protection avec p-cycles, Routes de secours, Réseaux optiques multi-débit, Réseaux optiques élastiques, Génération de colonnes, Programmation linéaire en nombres entiers (PLNE), Algorithmes heuristiques.

Abstract

Network survivability is a critical issue for optical networks to maintain resilience against network failures. This dissertation addresses several survivability design issues against single link failure and large-scale disaster failure in optical networks. Two classic protection schemes, namely pre-configured Cycles (p-Cycle) protection and path protection, are studied to achieve high protection capacity efficiency while taking into account the equipment cost, power consumption and resource usage. These survivable network design problems are first formulated by mathematical models and then offered scalable solutions by heuristic algorithms or a decomposition approach.

We first consider single link failure scenario. To cut the multi-line rates transponders cost in survivable Mixed-Line-Rate (MLR) optical networks, a distance-adaptive and low Capital Expenditures (CAPEX) cost p-cycle protection scheme is proposed without candidate cycle enumeration. Specifically, path-length-limited p-cycles are designed to use appropriate line rate depending on the transponder cost and transmission reach. A Mixed Integer Linear Programming (MILP) model is formulated to directly generate the optimal p-cycles with the minimum CAPEX cost. Additionally, Graph Partitioning in Average (GPA) algorithm and Estimation of cycle numbers (EI) algorithm are developed to make the proposed MILP model scalable, which are shown to be efficient.

Regarding the power consumption in survivable Elastic Optical Networks (EONs), power-efficient directed p-cycle protection scheme for asymmetric traffic is proposed. Owing to the advantage of distinguishing traffic amount in two directions, directed p-cycles consume low power by allocating different Frequency Slots (FSs) and modulation formats for each direction. An MILP model is formulated to minimize total power consumption under constraints of directed cycle generation, spectrum assignment, modulation adaptation and protection capacity allocation. To increase the scalability, the MILP model is decomposed into an improved cycle enumeration and a simplified Integer Linear Programming (ILP) model. We have shown that the directed p-cycles outperform the undirected p-cycles in terms of power consumption and spectrum usage.

In order to improve the spectrum usage efficiency in p-cycle protection, a Spectrum Shared p-cycle (SS-p-cycle) protection is proposed for survivable EONs with and without spectrum conversion. SS-p-cycles permit to reduce spectrum usage and Spectrum Fragmentation Ratio (SFR) by leveraging potential spectrum sharing among multiple p-cycles that have common link(s). The ILP formulations are designed in both cases of

with and without spectrum conversion to minimize the spectrum usage of SS-p-cycles which can obtain the optimal solution in small instance, and a time-efficient heuristic algorithm is developed to solve large-scale instances. Simulation results show that SS-p-cycles have significant advantages on both spectrum allocation and defragmentation efficiency, and the spectrum conversion does help SS-p-cycle design to acquire better spectrum utilization.

Finally, large-scale disaster failures are being threatening the survivability of elastic optical Datacenter Networks (DCNs) although single link failure is the most common failure scenario. The disaster-survivable cloud service provisioning problem is investigated regarding the content placement, routing, protection of path and content, and spectrum allocation. Cloud services allow to use another DC node with replicated content to ensure disaster survivability. ILP models are formulated for Dedicated End-to-content Back-up Path Protection (DEBPP) and Shared End-to-content Back-up Path Protection (SEBPP), both of which aim at minimizing the spectrum usage. A decomposition approach based on Column Generation (CG) is proposed to increase the scalability of the ILP models of DEBPP and SEBPP. Extensive evaluation is performed to study the impact on the spectrum usage in terms of traffic amount, DCs, replicas, and network topologies.

Key-words: p-Cycle protection, Path protection, Mixed line rate networks, Elastic optical networks, Column generation, MILP, Heuristic algorithm.

Acknowledgements

This work is supported by China Scholarship Council and French Eiffel Scholarship.

First and foremost, I offer my gratitude to my supervisor, Dr. Fen Zhou, who supported me throughout my thesis with his guidance and encouragement. Without his effort, patience and availability during these three years, I would not have been able to complete this work.

I would like to thank my co-advisors, Prof. Shilin Xiao and Dr. Torres Juan-Manuel. They always give me very good advices and encourage me in my work. I am very grateful to them. I appreciate Prof. Shilin Xiao to encourage me to participate in the joint-supervision program.

I would like to thank Prof. Zuqing Zhu for his invaluable suggestions and kind encouragement. I appreciate the opportunity to work with him.

I also would like to thank my committee members for their prompt evaluation and comments to improve the quality of this dissertation.

I would like to thank my friends Minh Huong, Mohamed Amine Ait Ouahmed, Zakaria Ye, Haitao Wu, Jingyi Jiang, Weihua Wu and all the fellow graduate students in University of Avignon for their friendship during the three years of my stay in France. Special thanks to Haitao Wu and Weihua Wu for the opportunity of working together and valuable discussion.

I would like to thank fellow graduate students and friends Zhao Zhou, Meihua Bi, Tao Qi, Jia Peng in Shanghai Jiao Tong University for their friendship during my work. Special thanks to Zhao Zhou for the recommendation to work with Dr. Fen Zhou.

Last but not least, I would like to thank my family for their encouragement and support throughout my life.

Introduction

The past few decades have witnessed the evolution of optical networks from Single-Line-Rate (SLR) Wavelength-Division Multiplexing (WDM) towards Mixed-Line-Rate (MLR) WDM and Elastic optical networks (EONs) architectures [66, 94, 96, 122]. The network capacity and flexibility have been gradually improved in order to satisfy the requirements on high-bandwidth and on-demand applications [66, 107]. Also, network survivability is a key issue for optical networks to maintain operation against common network failures (*e.g.*, fiber cut), since a huge number of services are provisioned by the optical infrastructure [93]. In addition to the most common single link failure, the new failure scenario of large-scale disaster has threatened the optical Data Center Networks (DCNs), which can cause huge data loss and service disruptions [55].

There exist several protection schemes for survivable optical networks, such as link protection, path protection, ring protection and Pre-Configured-Cycle (p-Cycle) protection [33, 72, 116]. We first focus on the p-cycle protection scheme against single link failure owing to its distinct advantages that it has fast switching speed and provides protection capacity for both on-cycle links and straddling links [52]. Conventional p-cycle designs are required to enumerate candidate cycle set in advance, and to screen the most efficient p-cycles from the candidate cycle set. In contrast, we investigate p-cycle design principle without candidate cycle enumeration, which can overcome the drawback that it would be intractable to enumerate all the candidate cycles for large networks. In addition to p-cycle protection, path protection is also studied for disaster-survivable elastic optical DCNs. More specifically, Dedicated End-to-content Back-up Path Protection (DEBPP) and Shared End-to-content Back-up Path Protection (SEBPP) are explored for anycast traffic enabled by datacenter service.

Survivable optical networks encounter new challenges along with the evolution of optical network infrastructure with respect to equipment cost, power consumption and resource usage [107, 129]. However, this involves a very complex interdependencies optimization as the resource usage affects the protection capacity efficiency, equipment cost and power consumption. In MLR WDM optical networks, transponders operating at different line rates have different cost and transmission reach of the transmitted signal [18]. The situation becomes even more complex in EON because the Bandwidth-Variable Transponders (BVTs) work depending on not only the Frequency Slot (FS) usage but also the modulation format used, which will affect spectrum usage, cost, energy consumption and transmission reach together, and the use of Bandwidth-Variable Opti-

cal cross-Connects (BV-OXCs) in EONs also results in higher cost and energy consumption [129]. To deal with these challenges in next generation optical network protection, the objective of this thesis is to design efficient protection schemes in the consideration of spare capacity, network cost and network power consumption.

The rest of this chapter is organized follows:

- Motivation and Objectives
- Contributions of the Thesis
- Organization of the Thesis

Motivation and Objectives

Owing to the advanced technologies in optical networks, the transmission capacity has largely increased in which a single optical fiber can carry over 20 Tbps traffic transmission [10]. The network failures, such as fiber cut and large-area disaster, will cause huge loss for service providers and costumers. Thus, survivability of optical networks is of critical importance. This thesis concerns the design of efficient protection schemes using p-cycles and backup paths for next generation optical networks. Conventional protection schemes were mostly explored for minimizing protection capacity while our study focuses on joint optimization of both protection capacity and network performance metrics such as equipment cost, power consumption and spectrum usage. The main advantage of joint optimization is that it leads to more resource-efficient designs from the perspective of the network operator. However, it corresponds to a much more complex design problem thus efficient algorithms or decomposition approaches are needed against the scalability issue.

We first study p-cycle protection against single link failure. p-Cycle protection scheme has fast switching speed, and it provides protection capacity for both on-cycle links and straddling links [52]. Most of conventional p-cycle design schemes require to enumerate a candidate cycle set in advance and then optimize protection capacity to select p-cycles from the candidate set. However, optimal solution can not be reached with these methods as only partial cycles are formed in the candidate cycle set due to the scalability issue in large networks. We propose p-cycle design principle without cycle enumeration and integrate it with protection capacity constraint in mathematical formulation, which is guaranteed to obtain the optimal solution. Moreover, the advanced architecture of optical networks introduces additional network performance metrics for p-cycle protection. MLR optical networks add the line rate selection for p-cycle protection, which relates to not only wavelength usage but also transponder cost as well as transmission reach. EONs involve the spectrum allocation and modulation format selection as well power consumption, which further increases the complexity of the p-cycle protection problem. To achieve the high cost efficiency and power efficiency in survivable MLR and EONs, this thesis proposes joint optimization of p-cycle protection formulation and efficient algorithms.

To overcome the large area disaster threat on cloud service, path protection schemes are studied for survivable elastic DCNs, in which the service can be served by other Data Center (DC) replicas upon a disaster. In addition to spectrum allocation in survivable EONs, elastic optical DCNs are being faced with the problem of content placement, routing, protection of path and content. We first formulate the mathematical model for this problem and design DEBPP and SEBPP schemes. Then, to increase the scalability, DEBPP and SEBPP models are decomposed by Column Generation (CG) approach using a master problem and a pricing problem. This is solved iteratively, augmenting the number of columns until optimality of the original problem is proved with the available columns. To speed up the iteration, an algorithm is designed in the pricing problem to select the most promising columns rather than using all the columns. It has shown that CG is an intelligent way of generating promising working and backup lightpaths for survivable elastic optical data networks.

Contributions of the Thesis

This thesis investigates several protection schemes for next generation optical networks against single link failure and large area disaster failure. The contributions of these protection schemes in this thesis are listed and explained in detail below.

1. **Cost-effective p-cycle protection**: The unidirected p-cycle design model without candidate cycle enumeration is studied in MLR optical networks with respect to the transmission reach and transponder cost. Path-length-limited p-cycle is proposed to efficiently optimize the line rate selection, in which the transmission reach restricts the length of each protection path instead of the circumference of the cycle p-cycle. The Capital Expenditures (CAPEX) cost and the spare capacity are minimized by designing a Mixed Integer Linear Programming (MILP) model, which considers the cycle generation constraints, line rate assignment and protection capacity constraints together. In addition, Graph Partitioning in Average (GPA) heuristic algorithm is incorporated with the computation of number of required p-cycles approach to enable concurrent computation in sub-graphs with the proposed MILP model. Simulation results show that the proposed p-cycle protection scheme achieves significant CAPEX cost savings for MLR optical networks, especially the transponder cost savings, in comparison to conventional p-cycle protection with SLR and p-cycle protection with candidate cycle enumeration.

2. **Power efficient p-cycle protection**: A novel directed p-cycle protection scheme is proposed for asymmetric traffic in power-efficient EONs. Directed p-cycles benefit from distinguishing traffic amount in two directions and thus they are promising to consume low power by allocating different FSs and modulation formats for each direction. The directed p-cycle design, spectrum allocation, modulation adaptation and protection capacity are concerned by formulating an MILP model, which aims at minimizing the power consumption of optical equipments and the FS usage. The scalability issue of the MILP is solved by an improved cycle enumeration and a simplified Integer Linear Programming (ILP) model. The simulation results indicate the directed p-

cycles achieve power savings up to 47.9% in comparison with conventional undirected p-cycles. Moreover, it has been shown that the amount of power savings in directed p-cycles goes up when increasing the traffic asymmetry and anycast ratio of traffic patterns.

3. **Spectrum shared p-cycle protection**: A novel Spectrum Shared p-cycle (SS-p-cycle) protection scheme is proposed for survivable EONs with and without spectrum conversion. SS-p-cycles have the property that two p-cycles can share the same spectrum if and only if all of their protection paths do not have common links against any single link failure. SS-p-cycles permit to reduce spectrum usage and Spectrum Fragmentation Ratio (SFR) by leveraging potential spectrum sharing among multiple p-cycles. The design of SS-p-cycles is enabled by the ILP models, which check the promising spectrum sharing in terms of the protected link(s), and allocates the FSs for each SS-p-cycle. To overcome the lack of scalability in SS-p-cycle ILP, a fast and efficient SS-p-cycle Spectrum Allocation (SS-SA) algorithm is proposed to perform cycle selection and FSs allocation. The results indicate that SS-p-cycles significantly improve spectrum efficiency compared with conventional no-shared p-cycles in terms of maximum index of FSs and spectrum efficiency. The results also show that the spectrum conversion does help SS-p-cycle design to acquire better spectrum utilization, but it shows different impacts on maximum index of FSs and spectrum efficiency under different network nodal degree and network with/without spectrum conversion.

4. **Disaster-survivable path protection**: Disaster protection schemes, including DEBPP and SEBPP, are proposed for elastic optical DCNs. Mathematical models are formulated for DEBPP and SEBPP, respectively, taking into account content placement, routing, protection of path and content and spectrum allocation. The DEBPP and SEBPP models are further decomposed to increase the scalability, which is conducted by CG approach using a master problem and a pricing problem. The master problem optimizes the spectrum usage by selecting the working and backup paths from the paths set while pricing problem takes charge of generating new working and backup paths that may achieve a better solution. It has shown that CG achieves comparable results within an much shorter time than the joint ILP models. The spectrum usage of DEBPP and SEBPP is evaluated regarding the number of traffic amount, DCs, replicas, and different network topologies.

Organization of the Thesis

The thesis carried out studies on single link failure and large area disaster failure protection in next generation optical networks. Both p-cycle protection and path protection schemes are investigated. This thesis is organized according to the types of failure scenarios and protection schemes in terms of MLR optical networks, EONs and elastic DCNs.

The rest of the thesis is divided into four parts: Background and Technological Context (**Chapter**, 1), p-Cycle Protection Scheme for MLR WDM against Single Link Failure (**Chapter**, 2), p-Cycle Protection Schemes for EONs against Link Failure (**Chapters**, 3,

and 4) and Path Protection Schemes for Elastic DCNs against Disaster Failure (**Chapter**, 5).

The first part with **Chapter** 1 provides background information on optical networks, which covers the evolutions of optical backbone networks, key technologies of EONs, survivability in optical networks and literature review of classical protection schemes. The evolution of optical networks includes traffic-driven optical networks from SLR WDM to MLR WDM, and then EONs. Then, the property of flexible grid and bandwidth variable equipments in EONs are addressed. The survivability in optical networks is categorized into protection and restoration and involves the classic protection schemes and the challenges of survivable EONs. The literature review includes the existing p-cycle protection scheme and protection schemes that concern resource usage, cost, power consumption and cloud services issues.

The second part with **Chapter** 2 concerns the low-cost p-cycle protection for MLR optical network. It addresses the *voltage*-based undirected p-cycle design without candidate cycle enumeration in MLR optical networks, which concerns the line rate selection, transmission reach, transponder cost and wavelength assignment. The objective is to minimize the transponder cost and wavelength channel cost in p-cycle protection for MLR optical networks. Both ILP formulation and a network partition algorithm are developed to address this issue. The work of this chapter can be found in the publications **[J3]** and **[C5]**.

Concerning the network evolution from WDM optical networks to EONs, the third part comprising **Chapters** 3 and 4 address the p-cycle protection for EONs in terms of low power consumption and efficient spectrum usage. Specifically, **Chapter** 3 addresses the directed p-cycle design under asymmetric traffic scenario in EONs and concerns the power consumption and spectrum usage in survivable EONs. The objective is to minimize the spectrum usage and power consumption related to BVTs, BV-OXCs and Optical Amplifiers (OAs), which is accomplished by designing the MILP models and decomposition algorithms. The benefits of using directed p-cycle rather than unidrected p-cycle for asymmetric traffic protection is analyzed and evaluated. The work of this chapter can be found in the publications **[J2]** and **[C3]**. **Chapter** 4 concerns the efficient spectrum sharing among multiple p-cycles. The specific formulations for SS-p-cycles are developed in addition to the conventional spectrum allocation in survivable EONs with and without spectrum conversion. The performance of spectrum usage in SS-p-cycles is evaluated in comparison with conventional spectrum no-shared p-cycles. The work of this chapter can be found in the publications **[J1]** and **[C2]**.

Concerning the current large area disaster failure issue in DCNs, the fourth part with **Chapter** 5 further addresses the disaster-survivable DEBPP and SEBPP schemes in DCNs with EONs. The mathematical models of DEBPP and SEBPP schemes are first formulated. Then, the DEBPP and SEBPP formulations are further decomposed by CG approach to increase the scalability. A master problem, optimizing the spectrum usage of the selection of the working and backup lightpaths, and a pricing problem that generates the promising new working and backup lightpaths are addressed.

Finally, **Chapter** 6 concludes the thesis and envisages the future work.

Contents

Part I

Background and Technological Context

Chapter 1

Background and Technological Context

Contents

1.1 Evolution from fixed-grid to flexible-grid in optical networks

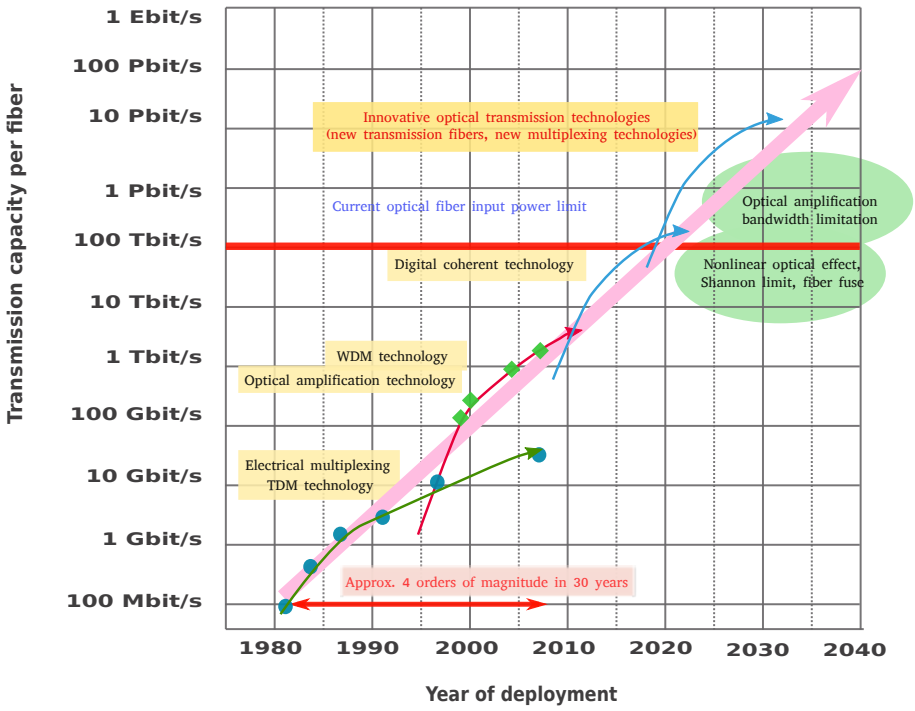

Figure 1.1: *Evolution in optical transmission technology [92].*

Several decades have witnessed the rapid development of optical networks towards high speed, high-capacity and long-distance since optical transmission was realized in 1970s [103]. As shown in Fig. 1.1, over the past several decades, the optical transmission technology has developed rapidly mainly through several technological innovations: Time Division Multiplexing (TDM) technology based on electrical multiplexing, optical amplification technology combined with WDM technology, and remarkably successful coherent technology with Digital Signal Processing (DSP) [64, 73, 92]. In the early 1990s, the transmission capacity of optical networks was dramatically increased in a cost-effective manner enabled by the development of WDM and Erbium-Doped Fiber Amplifier (EDFA) [9, 95]. WDM allows to concurrently multiplexe many optical wavelengths over a single optical fiber and each of the wavelengths is viewed as a separate channel for data transmission. In the early stage, WDM transmission systems operate in fixed grids with SLR transponders either 10Gb/s, 40Gb/s or 100Gb/s. It is broadly expected that with the advent of new networking capabilities and demanding cloud services, the evolution of optical networks will lead towards MLR WDM network and EON architectures [44, 107].

MLR WDM network is energy- and cost-effective by applying co-existing line rates (10/40/100 Gbps) transponders and multiple modulation formats [77, 96]. However, with high-bandwidth and on-demand applications continuing to emerge, WDM networks have limitations such as low spectrum utilization and rigidity in provisioning

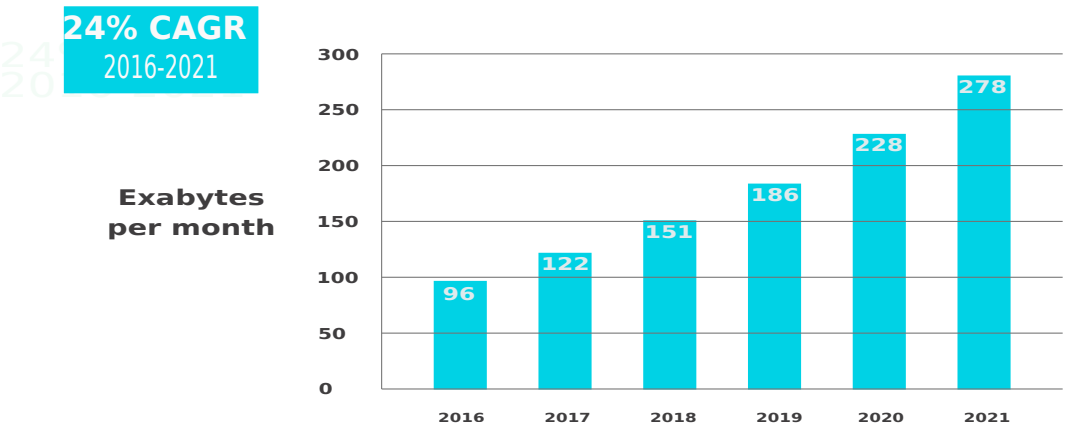

Figure 1.2: *Cisco global IP traffic forecast, 2016-2021 [22].*

for growing heterogeneous traffic demands. According to Cisco's report [22], the overall IP traffic is expected to grow to 278 Exabytes per month by 2021, up from 96 EB per month in 2016, a Compound Annual Growth Rate (CAGR) of 24 percent, as illustrated in Fig. 1.2. Representing the elastic allocation with sub-wavelength, super-wavelength, and multiple-rate data traffic accommodation, a more flexible optical network architecture was first named the spectrum sliced elastic optical path network architecture (SLICE) and is currently called the EON for simplicity [65, 66]. EONs enable flexible spectrum usage and adaptive modulation formats, which has been regarded as one of the most promising candidates for the next generation optical networks with respect to network spectrum cost, size, and power requirements [21, 127].

1.1.1 Fixed-grid WDM optical networks

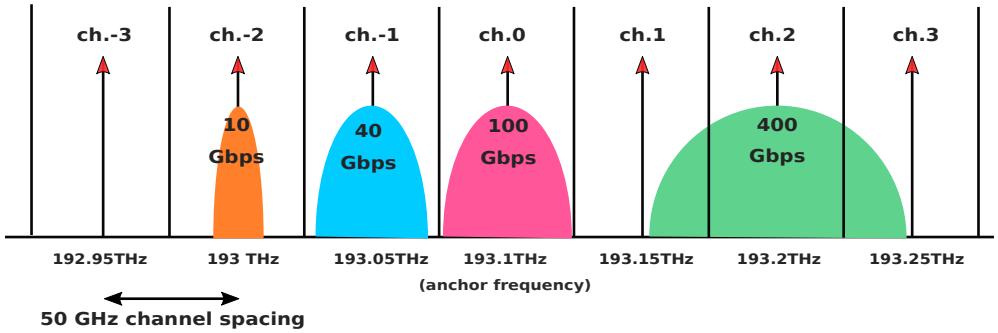

Figure 1.3: *ITU-T fixed-grid [117].*

In WDM optical networks, separate wavelengths or channels of optical signals are multiplexed and simultaneously transmitted in a single optical fiber. There is already commercial 100-Gb/s Dense Wavelength-Division Multiplexing (DWDM) transmission systems with a per fiber capacity of 10 Tb/s using the conventional 50 GHz frequency grid, as illustrated in Fig. 1.3 [1, 64]. DWDM technology is enabled by the advance of

optical components, such as Distributed Feedback (DFB) lasers, EDFAs, Wavelength-Selective Switches (WSS)-based Reconfigurable Optical Add/Drop Multiplexer (ROADM), and coherent techniques [120]. For each wavelength, the transmission line rate has been increased from 2.5 Gbps up to 100 Gbps with the improvements in transponder technology [58]. However, current DWDM systems with fixed grids are not able to accommodate heterogeneous traffic in an spectrum-efficient manner. Some traffic demands may occupy much less bandwidth than that provided by a full wavelength, which results in the bandwidth and spectrum waste while some may require multiple wavelengths. For example, one 50 GHz wavelength channel should be used for the 10 Gbps demand, while it can accommodate an 100 Gbps Dual-Polarization Quadrature Phase Shift Keying (DP-QPSK) signal, but it is not sufficient to transmit a 400 Gbps signal within the same spectral spacing.

1). SLR WDM

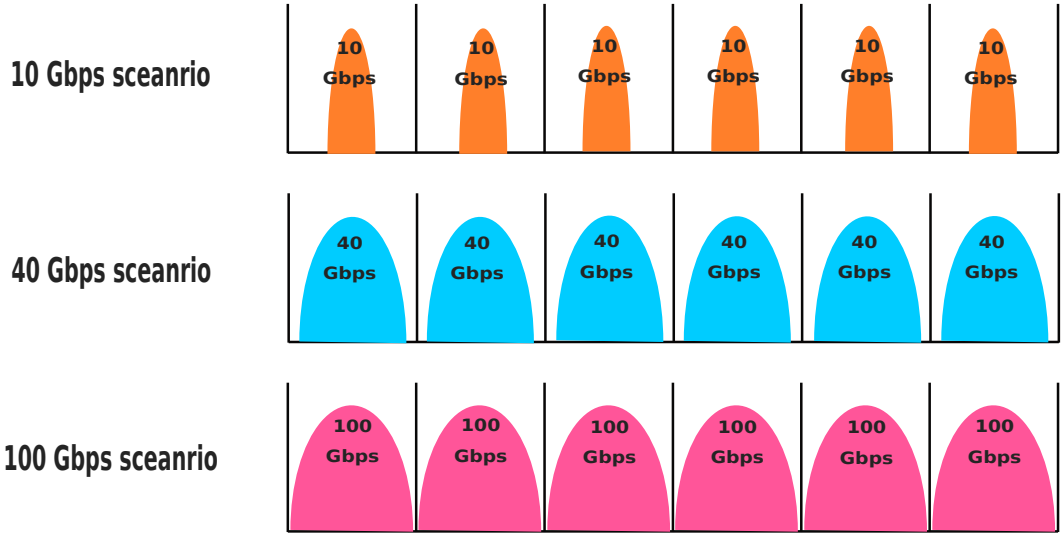

Figure 1.4: *SLR-WDM grid.*

SLR WDM offers only one line rate with specific transmission reach for all types of demands. The network can be configured with either 10 Gb/s, 40 Gb/s or 100 Gb/s line rate sceanrio, as shown in Fig. 1.4. SLR WDM needs to address the basic Routing and Wavelength Assignment (RWA) problem. The general definition of the RWA problem is as follows, given a set of communication requests, set up *lightpaths* by routing and assigning wavelengths to them, so as to minimize the network resources used or maximize the requests served. A *lightpath* is an optical communication path between two nodes without the Optical-Electrical-Optical (O/E/O) conversion, established by allocating the same wavelength throughout the route of the transmitted data. A *lightpath* is uniquely identified by a wavelength and a physical path. Two important issues should be addressed during the wavelength assignment process [20] :

- **Wavelength continuity constraint**: A *lightpath* must be assigned a common wavelength on each link it traverses except the utilization of wavelength converters

[101].

- **Distinct wavelength constraint**: Two *lightpaths* sharing a fiber link must occupy different wavelengths.

These two constraints of wavelength allocation are involved with the *lightpath* generation whose length should be less than the maximum transmission reach at a specific line rate. The RWA problem can be solved jointly or separately towards the routing problem and wavelength assignment problem. The objective of RWA problem can involve several issues, such as minimizing wavelength usage, minimizing network cost, minimizing energy, enabling survivability, *etc* [11, 24, 90].

2). MLR WDM

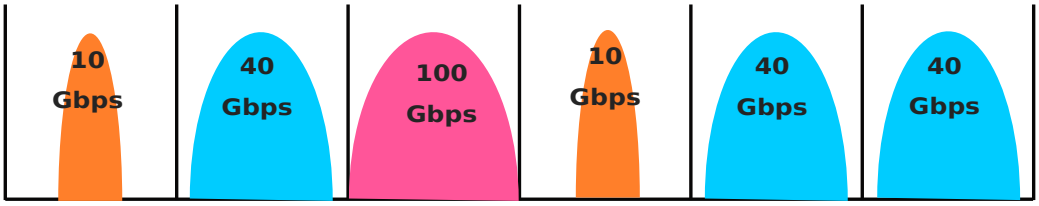

Figure 1.5: *MLR-WDM grid.*

Currently, WDM networks support mixed 10/40/100 Gbps per wavelength in the existing 50 GHz channels, as illustrated in Fig. 1.5. In MLR WDM, different types of transponders are configured to provision traffic at several line rates balancing the requirements on the capacity and transmission distance of the demand [18, 81, 151]. Thus, a single fiber link may carry various line-rate signals of 10/40/100 Gbps. MLR is leveraged to design a cost-effective network by exploiting the volume discount[1] of 40 and 100 Gbps transponders [81]. Then, the WDM network cost could be reduced because low-bitrate services will require less grooming (*i.e.*, less multiplexing with other low-bitrate services onto high-capacity wavelength), while high-bitrate services can be provisioned on an individual wavelength channel [96].

With the introduction of co-existing mixed line rates, the basic RWA problem in SLR WDM is enhanced to the Routing, Wavelength, and Rate Assignment (RWRA) problem [81]. However, due to the nonlinear effects induced by the co-propagating wavelengths with co-existing mixed line rates, the transmission reach and performance of 10/40/100 Gbps in MLR are further limited. According to the study in [18], the pure transmission reach of 10 Gbps with On/Off Key (OOK), 40 Gbps with Differential Phase Shift Keying (DPSK), and 100 Gbps with DP-QPSK are 1800 km, 2200 km, and 7000 km, respectively under a threshold Bit-Error Rate (BER) of 10^{-3}. Higher transmission reach of 100G is owing to the coherent reception technology which could be incorporated in commercially available 100 Gbps transponders. Nevertheless, in MLR WDM, the co-existing mixed line rates restricted the transmission reach of 10/40/100 Gbps to 1750/1800/900

[1]Volume discount means the cost of a resource increase at a line rate that is lower than the linear increase of the rate, *e.g.*, the cost of a 100 Gbps transponder can eventually be 4.5 times that of a 10 Gbps transponder under steady-state conditions, which is less than the line rate increase of ten times [81].

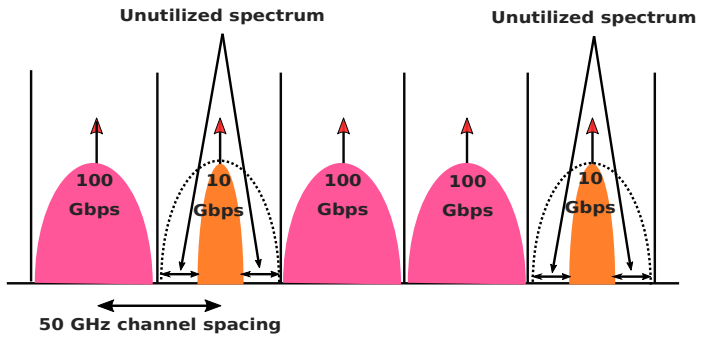

(a) Spectrum allocation in WDM fixed-grid optical networks

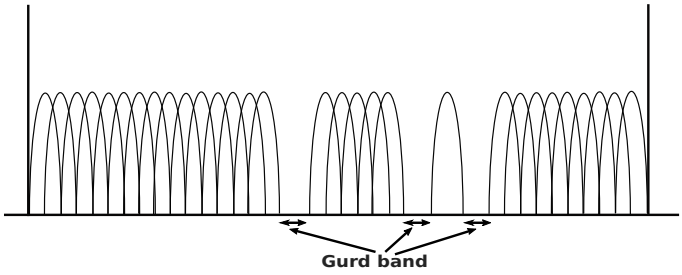

(b) Overlapping subcarriers caused by OFDM technology

Figure 1.6: *Flex-Grids in EONs [12].*

km, respectively [18].

In addition to **wavelength continuity constraint** and **distinct wavelength constraint** in SLR WDM optical networks, MLR WDM optical networks should consider the follow single line rate continuity issue:

- **Single line rate continuity constraint**: only single line rate can be used for a *lightpath* along all the traversing links even though multiple line rates are available.

The introduction of MLR offers an opportunity to design resource-efficient optical networks even though the involved RWRA problem increases the complexity of network design. The MLR network architecture has been shown to be energy- and cost-efficient in satisfying heterogeneous traffic demands than SLR network architecture [18, 87]. The joint optimization of line rate selection, *lightpath* generation and wavelength assignment contribute to the cost savings and energy savings in optical equipments.

1.1.2 Flexible-grid EONs

The burgeoning number of on-demand applications and instantaneously increasing cloud services require major evolution of the backbone network towards high bandwidth, high flexibility and high survivability [107, 127]. The conventional WDM optical

networks would waste a large portion of the spectrum if the channels carry only low bandwidth, and no traffic can be transmitted in the unused frequency gap between two adjacent channels, as reflected in Fig. 1.6. EONs can overcome the spectrum allocation limitations of the conventional WDM optical networks by utilizing the promising transmission techniques such as Nyquist Wavelength-Division Multiplexing (NWDM), Orthogonal Frequency-Division Multiplexing (OFDM), and Time Frequency Packing (TFP) [108]. EON architecture is one of the most promising candidates for optical networks to provision increasing traffic with fine-granularity flexible spectrum allocation and adaptive modulation formats. The term *elastic* refers to two key properties:

- **Elastic spectrum**: The optical spectrum can be divided into FS, having a spectral width of *e.g.* 12.5 GHz, 6.25 GHz or 5 GHz, and the channel can be a combination of a set of continuous FSs.
- **Elastic optical components**: The elastic optical paths can be accommodated with bitrate-variable equipments such as BVTs and BV-OXCs.

EONs alleviate the fixed-grid bandwidth issue of current WDM optical networks. Instead, EONs allow arbitrary contiguous concatenation of optical spectrum according to the traffic volume or user request in a highly spectrum-efficient and scalable manner [66]. The efficient spectrum usage in EONs comes from two factors. The first one is the Guard Bands (GB) are not "wasted" on two separate channels for the connection between two nodes. The second reason is that the spectrum assigned to each connection is "tailored" to their respective bandwidth, quality and reach requirements. The main characteristics of EONs are efficient accommodation of multiple data rates, elastic variation of allocated resources, reach-adaptable line rate, *etc*. Apart from the difference of allocating spectrum resources as the WDM optical networks, EONs employ adaptable transponders with different line rates and adaptive modulation formats. Thus, a number of transmission parameters, such as line rate, the FSs, the modulation format, will interact with each other, which directly or indirectly affects the resource allocation decision [125, 127].

EONs will bring lots of benefits for optical networks towards rate adaptive, distance adaptive, and availability adaptive service provision [65]. Nevertheless, EONs result in the increased complexity of network design and operation as the conventional RWA problem is modified to Routing and Spectrum Assignment (RSA) problem in EONs. Similar to the conventional *wavelength continuity constraint*, RSA needs to address the following spectrum allocation constraints [12]:

- **Spectrum continuity constraint**: All the links along a *lightpath* should use the same FSs.
- **Spectrum contiguity constraint**: The FSs allocated to a *lightpath* should be contiguous FSs.

As a result, the introduction of spectrum allocation dictates the enhancement of the network planning and optimization procedure to consider the resource-efficient network design. Cost- and energy-efficient EONs can be achieved by selecting the optimal combination of the parameters modulation level and the number of FSs. Recently,

several experimental demonstrations of EONs have been done to test the viability of the novel flexible optical networks with Software-Defined Network (SDN) technologies (*e.g.*, OpenFlow) [5]. However, there are still several challenges of EONs demonstration related to the routing, code and spectrum allocation, multi-domain and multi-technology orchestration, BVTs technology, monitoring aspects, *etc* [25].

To conclude, EONs are regarded as the promising solution to provision such traffic with flexible spectrum allocation. However, the requirements on BVTs and BV-OXCs are the main challenges of upgrading current WDM optical networks to EONs. Meanwhile, MLR optical networks with co-existing line rates (10/40/100 *Gbps*) can be the transitional solution, which has been proven to achieve the comparable performance as EONs [75].

1.2 Key technologies of EONs

The evolution towards EONs will bring several benefits for optical networks, such as the spectral savings, enhanced network availability, *etc*. These benefits require the key technologies existing in elastic optical provisioning, hardware equipment and network management and control, which are presented as follows.

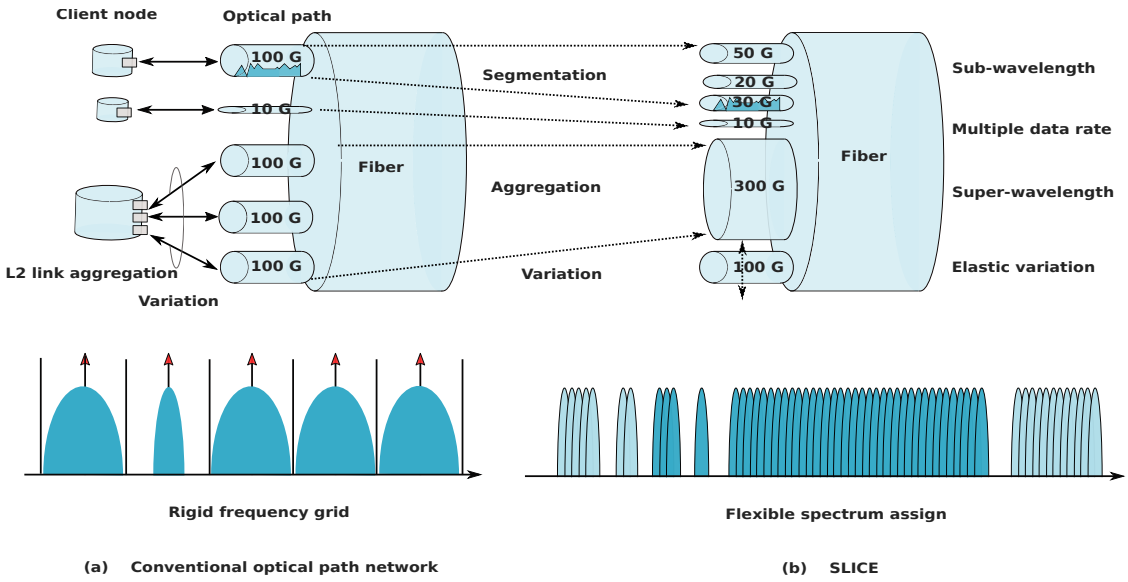

Figure 1.7: *Elastic optical path provisioning [66].*

1.2.1 Elastic optical path provisioning

EONs allow to accommodate each demand with a "proper size" of the spectrum based on its bitrate and the transmission distance. For a demand of more than 400 Gbps, WDM optical networks need to demultiplex it into small ones in order to fit the fixed

grid. In contrast, EONs support the high-capacity demands of 400 Gbps, 1 Tbps in a flexible optical grid, which eliminates most of the inefficient optical GBs and allows optical spectrum to be allocated to wavelengths as needed in FS increments [23] 2014. Thus, EONs allow to provision traffic demands with sub-wavelength, super-wavelength and multiple data rates, as illustrated in Fig. 1.7 [66].

- **Sub-wavelength provisioning**: For the traffic requiring only a fractional of bandwidth, EONs permit to accommodate it with just enough optical bandwidth. Every node on the *lightpath* allocates a cross-connection with an appropriate spectrum bandwidth to create an appropriate-sized end-to-end optical path. It allows to efficiently use the network resources by the cost-effective provisioning of fractional bandwidth service.
- **Super-wavelength provisioning**: EONs enable the super-wavelength provisioning by aggregating traffic from multiple physical ports/links in a switch/router into a single logical port/link. The super-wavelength provisioning can ensure high utilization of spectral resources. The aggregation technology can be realized by the OFDM SLICE transponders.
- **Multiple data rate provisioning**: EONs also allow to spectrally efficiently accommodate the mixed data bitrates owing to flexible spectrum allocation.

1.2.2 Enabling hardware technology

1). Bandwidth Variable Transponders

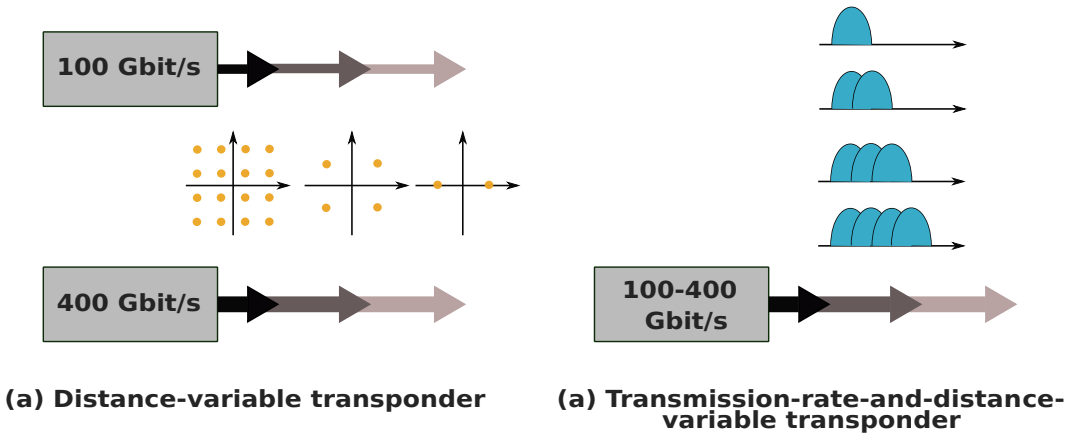

Figure 1.8: *BVT [92].*

BVTs, including flexible bandwidth transmitters and receivers, are used to tune the transmission bandwidth by adjusting several transmission parameters, such as the modulation format, number of bits per symbol, and spectrum used, as shown in Fig. 1.8. BVTs are able to trade spectral efficiency at different modulation formats against transmission reaches. For example, QPSK or Binary Phase-Shift Keying (BPSK) modu-

lation formats are more robust but less efficient, thus BPSK can support longer transmission distance, while 16-Quadrature Amplitude Modulation (16-QAM) modulation format is more efficient but with shorter transmission reaches [12].

Table 1.1: *Transmission rate, power consumption and transmission reach of a BVT with a single FS 12.5 GHz [129, 146]*

Modulation Formats	Transmission rate (Gbps)	Power Consumption (W)	Transmission Reach (km)
BPSK	12.5	112.374	9600
QPSK	25	133.416	4800
8QAM	37.5	154.457	2400
16QAM	50	175.498	1200

BVTs for EONs can be implemented with several multicarrier solutions, such as Coherent Wavelength-Division Multiplexing (CoWDM) [41], Coherent Optical Orthogonal Frequency-Division Multiplexing (CO-OFDM) [118] and dynamic Optical Arbitrary Waveform Generation (OAWG) [43]. Even though there is similarity among multicarrier signal generation between CO-OFDM, CoWDM, and OFDM transmitters, their operation principles and capabilities differ from each other [44].

Finally, the concept of Sliceable Bandwidth-Variable Transponder (S-BVT) has emerged in order to enable higher utilization of flexible transceivers [108]. The major property of S-BVT is the ability to allocate the capacity into one or several independent optical flows that are transmitted towards one or multiple destinations. An S-BVT can generate multiple optical flows that can be routed into different *lightpaths* flexibly towards different destinations. S-BVT is represented by a class of transponders able to dynamically tune the required optical bandwidth and transmission reach by adjusting parameters of bitrate, modulation format, Forward Error Correction (FEC) coding, and shaping of optical spectrum [108].

The deployment of BVTs introduces a trade-off between spectral efficient modulation format and transmission reach as well as network cost and power consumption related to optical module of ADC, DAC, I/Q modulators and the electronic processing [108]. The higher level modulation formats lead to increased effective capacity and spectral efficiency, however, they result in reduced transparent transmission reach, increased equipment cost and power consumption. Table 1.1 presents the transmission rate, power consumption and transmission reach of a BVT with a single FS (bandwidth 12.5 GHz) at different modulation formats [129, 146].

2). Bandwidth Variable Optical Cross-Connects

BV-OXCs allow to switch transmitted signals within their frequency bandwidth to appropriate switch output ports. They can allocate an appropriate-sized cross-connection with the corresponding spectrum bandwidth to support an elastic optical lightpath provisioning. The switching window of BV-OXCs needs to be configured according to the spectral width of the incoming optical signal in a flexible manner [12]. As shown in

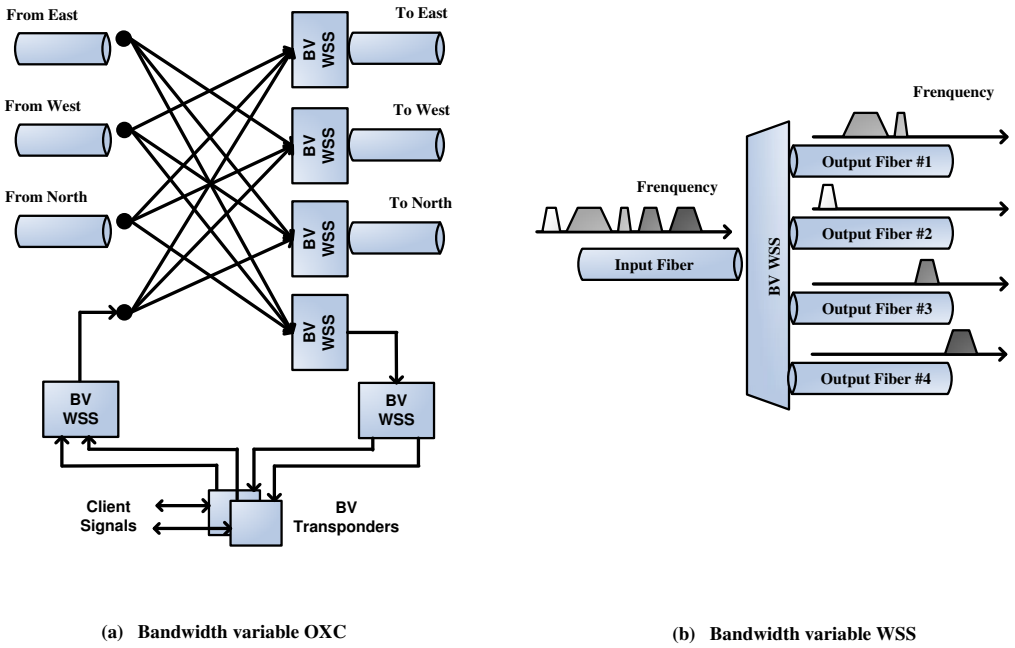

(a) Bandwidth variable OXC **(b) Bandwidth variable WSS**

Figure 1.9: *BV-OXC and BV-WSS. [66].*

Fig. 1.9, an BV-OXC is typically constructed out of several interconnected Bandwidth-Variable Wavelength Selective Switches (BV-WSS) and amplifiers. The BV-WSS is an 1 × N switch or filter providing a continuously tunable and variable seamless transmission spectrum. BV-WSSs can be implemented by one of the several technologies: optical Micro Electro Mechanical Systems (MEMS), Liquid Crystals On Silicon (LICOS), or silica Planar Lightwave Circuits (PLCs) [120]. BV-OXC design needs to consider the penalties introduced by the filtering characteristics and crosstalk between different channels, which can be alleviated by increasing the bandwidth of the optical filter and introducing higher GBs between super channels [122].

1.3 Survivability in optical networks

Survivability has critical importance for high-bandwidth optical backbone networks to provide resilience against network failures. The failures in fiber-optic networks occur often due to the cable-based technology and co-located infrastructure with other network utilities [35]. Furthermore, the transmission capacity in today's networks has largely increased in which a single optical fiber can carry over 20 Tbps traffic transmission, thus, the failures will cause huge loss for service providers and costumers [10]. The following text is organized as the concept of protection and restoration, classic protection schemes and challenges of next generation optical network protection.

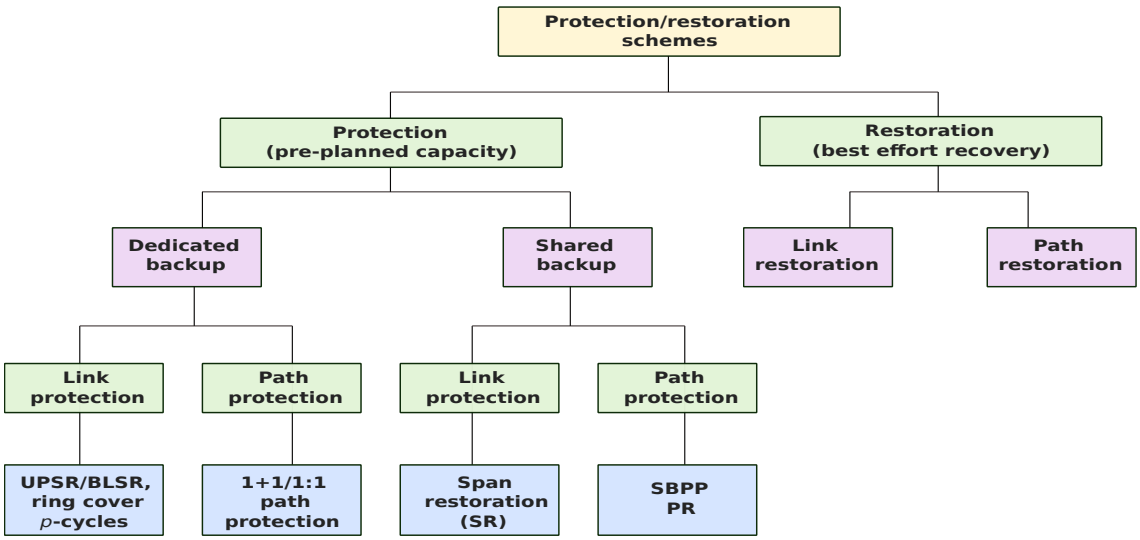

Figure 1.10: *Network protection/restoration schemes [116].*

1.3.1 Protection and restoration

Over the last few decades, several protection techniques have been investigated for optical networks. They can be classified under two general categories: *protection* strategy and *restoration* strategy depending on the establishment operation before or after the occurrence of a failure [150]. Figure 1.10 shows a classification of survivable techniques in terms of *protection* strategy and *restoration* strategy [102, 116]. Both *protection* strategy and *restoration* strategy offer the survivable technique on link level and path level. In link survivable scheme, the source and destination nodes of the connection are oblivious to the link failure, and only the two ending nodes of the failed link do the recovery operation. In path survivable scheme, the source node and the destination node of each connection are informed about the failure via messages from the nodes adjacent to the failed link [102].

1). Protection

Protection is used to configure pre-assigned capacity to ensure survivability by reserving the spare capacity dedicated to cover a specific set of failure scenarios. Protection strategy reserves resources for recovery from failures at either connection setup or network design time, and keeps idle when there is no failure. It results in short recovery time [2] but relatively non-efficient spare capacity [3]. The network resources used in protection strategy may be dedicated for each failure scenario, named *dedicated protection*; alternatively, the network resources can be *shared* against failures among different failure scenarios, named *shared protection*. For instance, under assumption of single span failure, Shared Backup Path Protection (SBPP) allows protection paths to share the pro-

[2]Recovery time is referred to as the time elapsed from when a failure occurs to the recovery of the failure.

[3]Spare capacity is referred to the total reserved protection capacity in the whole network.

tection capacity on their common spans as long as their corresponding working paths do not traverse any common span [115]. Shared protection schemes are generally more capacity-efficient than the dedicated protection schemes owing to the capacity sharing.

2). Restoration

Restoration is used to reroute the affected traffic after failure occurrence by using available capacity which is not dedicated to any specific failure but can be configured as needed [102]. The spare capacity available within the network is utilized for restoring services once a failure occurs. Generally, restoration strategy is more efficient in utilizing spare capacity due to the multiplexing of the spare-capacity requirements and provide resilience against different kinds of failures, but it requires more recovery time as the spare capacity has to be determined dynamically according to the available spare capacity. Moreover, the dynamic restoration algorithms are usually complicated.

Table 1.2: *Performance comparison among different protection schemes*

Protection schemes / Metrics	Dedicated protection	Shared protection	Path protection	Link protection
Spare capacity efficiency	Low	High	High	Low
Recovery time	Short	Long	Long	Short
Protection stability	Low	High	High	Low

We focus on protection schemes in this dissertation. Different protection schemes have their own properties and benefits, as shown in Tab.1.2. From the perceptive of spare capacity usage, path protection provides significant capacity savings over link protection, and shared protection provides significant savings over dedicated protection. From the perceptive of recovery time, dedicated protection requires less recovery time than shared protection, and link protection requires less recovery time than path protection. From the perceptive of protection stability, path protection is more susceptible to multiple link failures than link protection, and shared protection is more susceptible to multiple link failures than dedicated protection.

In our work, we only focus on single link failure and single disaster zone failure. Node failure and multiple failure are not considerded since the single failure happens the most.

1.3.2 Classic protection schemes

Protection schemes are by far the most studied for optical networks as dynamic algorithms for restoration are usually complicated. We focus on the protection schemes for next generation optical networks in this dissertation. Lots of protection schemes have been proposed for optical networks against different types of failures. Among

these protection schemes, single link failure protection schemes have drawn more attention as it is a common failure of fiber cuts during the operation of optical networks. Furthermore, network-area disaster failures, such as earthquake, hurricane, tsunami or human-made disasters, have started to attract more attention in today's DCNs due to the increasing traffic in cloud services [55].

We summarize the classical protection schemes in terms of failure type:

1). Link failure protection

In an optical network, each link carries many lightpaths, and the failure of a single link causes the failure of all the lightpaths traversing the link. Both link protection and path protection can be used to protect link failure.

- **Link protection**

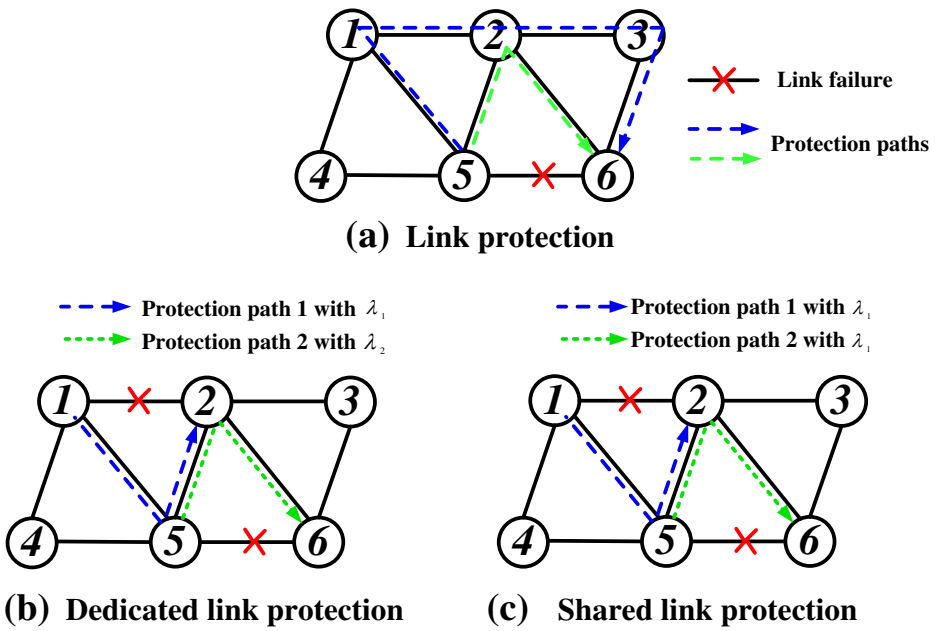

Figure 1.11: *Link protection against single link failure.*

The basic idea of link protection is that a protection path is reserved for each link, and when the link fails, traffic is rerouted around the failed link via the protection path. Link protection involves only the nodes adjacent to the failed link and switches the failed connections to the backup path around the link failure. Figure 1.11 shows an example of link protection against a link failure. In Fig. 1.11 (a), once the link failure occurs between nodes 5 and 6, the affected traffic is rerouted through the backup path 5-2-6 or the alternative one 5-1-2-3-6. The ending nodes 5 and 6 take charge of the recovery of the the failed link.

The link protection schemes can be further classified as dedicated or shared link protection depending on if the spare capacity is shared or not. Dedicated link protection

means that the spare capacity, *i.e.*, a wavelength is dedicated to a protection path on a particular link. Thus, different wavelengths must be assigned to the protection paths if they have common link(s). As shown in Fig. 1.11 (b), protection path 1 is assigned with λ_1 for a working channel traversing link 5-6 while protection path 2 is assigned with λ_2 for a working channel traversing link 1-2. The benefit of dedicated link protection is that it may offer protection against the failure of multiple links. Both protection path 1 and protection path 2 can be used if the links 5-6 and 1-2 fail simultaneously. Shared link protection allows different protection paths to share the wavelength on the common link(s). As shown in Fig. 1.11 (c), the protection path 1 and protection path 2 can share wavelength λ_1 on link 5–2. Shared link protection can utilize the spare capacity more efficiently than dedicated link protection [150].

- **Path protection**

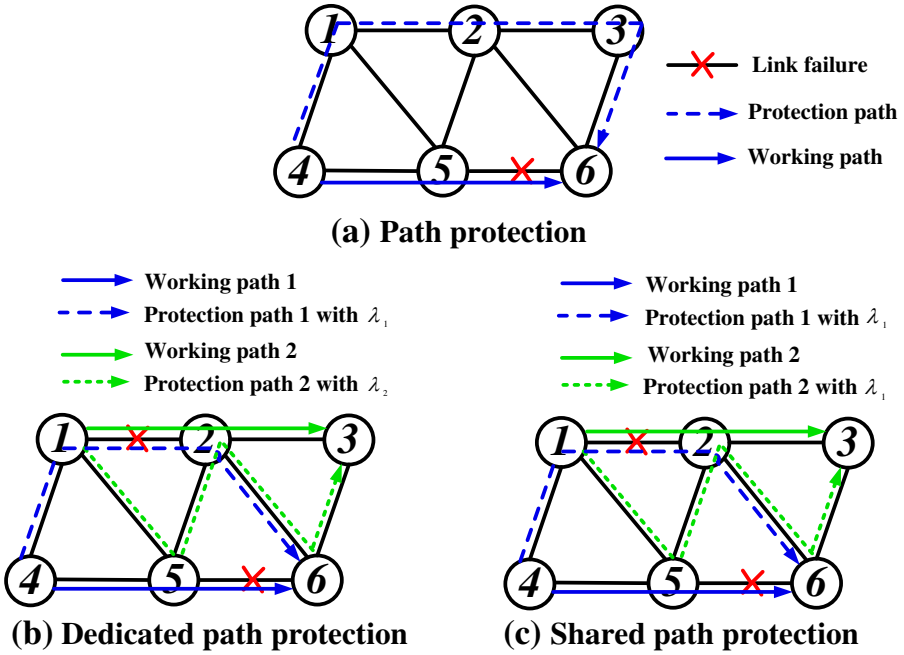

Figure 1.12: *Path protection against single link failure.*

In contrast to link protection, the source and destination nodes of the failed connection in path protection are conscious of the failure occurrence. They switch the traffic to the protection path and active the spare capacity reserved upon a link failure. Figure 1.12 shows an example of path protection against link failure. In Fig. 1.12 (a), once the link failure occurs between nodes 5 and 6 on the working path 4-5-6, the affected traffic is rerouted through the protection path 4-1-2-3-6. As a special case, the protection path 4-1-2-3-6 has no common link with the working path 4-5-6, then it can use the same or different wavelength resource for protection.

Path protection also has the dedicated scenario and the shared scenario. In dedicated path protection shown in Fig. 1.12 (b), for each working path, the spare wave-

length is reserved on the links of the protection path. Different wavelengths should be assigned for the protection paths if they have common link(s). The protection path 4-1-2-6 is provided for working path 4-5-6 while the the protection path 1-5-2-6-3 is provided for working path 1–2–3. As the two protection paths have the common link 2-6, they must use different wavelengths $\lambda 1$ and $\lambda 2$, respectively. Dedicated path protection requires a large amount of extra capacity for protection purposes and the reserved spare capacity is kept idle. However, the dedicated path protection has more protection stability as it is able to provide recovery from not only single-link failures, but also some multi-link failures. The shared path protection, known as the SBPP, allows to share the spare capacity on the common links of protection paths as long as the corresponding working paths are link-disjoint. Because in this case, the two working paths can not fail at the same time then the survivability can be ensured. As an example in Fig . 1.12 (c), the two protection paths can now share $\lambda 1$ on link 2–6. Therefore, they can just use the $\lambda 1$ for the protection of both working paths, as opposed to the dedicated path protection. The SBPP is able to utilize the capacity more efficiently, while still achieving 100% survivability from single-link failure [150].

- ***p*-Cycle protection**

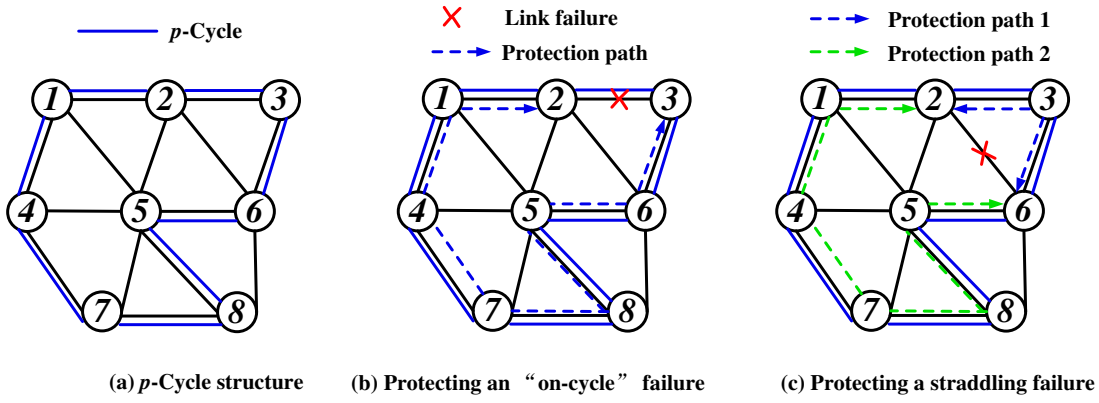

Figure 1.13: *p-Cycle protection against single link failure.*

The method of *p*-cycle protection has emerged as a topic of great importance over the past few years due to its ring-like short recovery time and mesh-like high efficiency in the use of spare capacity [52, 72]. There exist different types of *p*-cycle protection schemes, such as link-protecting *p*-cycle, path-protecting *p*-cycle and node encirling *p*-cycle [72]. It is assumed that the optical nodes are relatively reliable so that most of the studies in the literature focus on link- and path-protecting *p*-cycles. We focus on link-protecting *p*-cycle protection in this dissertation.

Figure 1.13 (a) illustrates the basic operation of a link-protecting *p*-cycle 1-2-3-6-5-8-7-4-1. All the links in this small network can be protected by the *p*-cycle as either "on-cycle" link [4] or "straddling" link [5]. The protection for "on-cycle" link case is illustrated

[4] An on-cycle link is a link of *p*-cycle, such as 1-2 and 2-3.

[5] A straddle link is a link which is connected between two nodes of *p*-cycle but does not belong to the

in Fig .1.13 (b), in which the end nodes of the failed link 2-3 loop back the traffic to the protection path 2-1-4-7-8-5-6-3 on the p-cycle. Figure 1.13 (c) shows the case of "straddling" link protection, in which the end nodes of failed link 2-6 can loop back the traffic to two alternative protection paths 2-3-6 and 2-1-4-7-8-5-6 on the p-cycle. The protection capacity of p-cycle is configured in advance, and only the two end nodes of the failed link switch the working traffic to pre-configured protection path. Specifically, one unit of protection capacity is provided for each on-cycle link in one p-cycle, while two units of protection capacity are provided for each straddling link.

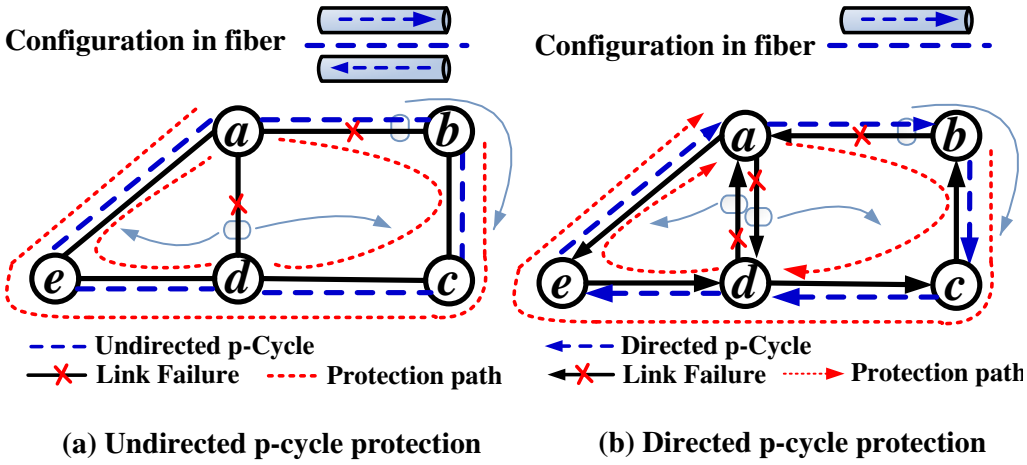

Figure 1.14: *Undirected and directed p-cycles.*

The previous concept of p-cycle in Fig. 1.13 refers to the undirected p-cycle strategy, and there exists another directed p-cycle strategy, as shown in Fig. 1.14. Undirected p-cycle is the common protection strategy, in which the same protection capacity is configured in the two directions according to the maximum traffic amount of the two directional links. It means that once the undirected p-cycle is determined, the same spare capacity are configured in the two parallel fiber links for opposite directions. Then, it enables to provide two units of protection capacity for each straddling link, like $a - d$ in Fig. 1.14 (a). However, directed p-cycle only configures protection capacity in one direction in the directed on-cycle links. Although a directed p-cycle provides one unit of protection capacity for each directed straddling link, *e.g.*, $a \rightarrow d$ and $d \rightarrow a$ in Fig. 1.14 (b), it can distinguish directional links and provide different protection capacity, which is beneficial for asymmetric traffic provisioning in two directions. Thus, the total protection capacity can be saved in directed p-cycles by efficiently allocating protection capacity for unidirectional links. Hence, directed p-cycles have the potential to protect the asymmetric traffic in a resource-efficient way.

2). Node failure protection

In optical networks, nodes failure occurs because of the equipments failure at optical cross-connect nodes. For instance, the malfunction of a transmitting or receiving line card. The resilience for this failure case can be provided by a redundant number of line

p-cycle, such as 1-5 and 2-6.

cards. Alternatively, a node is protected if the network is able to switch the lightpahts crossing this node to protection paths with spare resources. Generally, node failures in a service layer such as the failure of a network interface card on a router can only be recovered by node elements in peer-level not by other layers such as WDM physical layer [72].

- **Node-encircling *p*-Cycle**

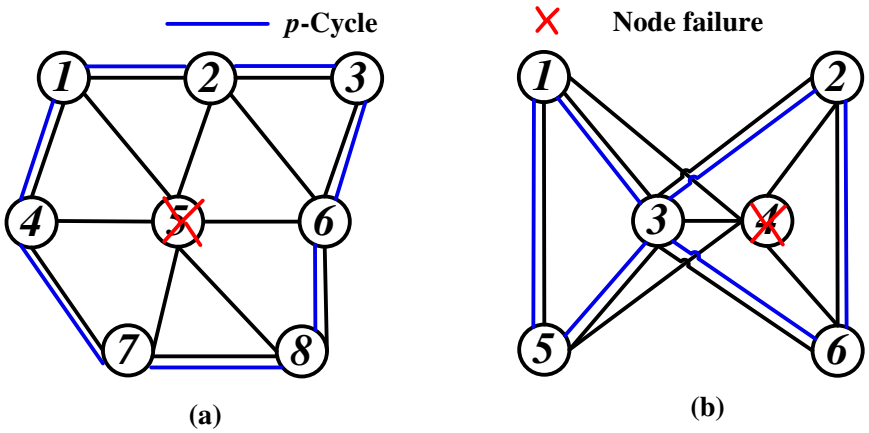

Figure 1.15: *Node-encircling p-cycles.*

The conventional link-protecting *p*-cycle protection has been extended to provide protection against node failure, called "Node-encircling *p*-cycle" [70]. Node-encircling *p*-cycle maintain the resilience followed by the two properties: First, it must not include the failed node that is protected by the node-encircling *p*-cycle, and second, it must contain all of the node that were adjacent to the failed node. Therefore, it is able to substitute failed routes for all of the possible flows that traversed them before node failure.

As illustrated in Fig. 1.15, the node-encircling *p*-cycle must cross all nodes immediately adjacent to the failed node but not the node itself. In Fig. 1.15 (a), the seven-node *p*-cycle 1-2-3-6-8-7-4-1 in blue crosses all six nodes adjacent to the failed node 5. Thus, upon failure of the encircled node, any lightpath transiting the failed node can be rerouted in either direction around the *p*-cycle. In addition to the simple *p*-cycle Fig. 1.15 (a) (*i.e.*, it does not cross the same node and/or span more than once), non-simple *p*-cycle also logically encircles the failed node, as illustrated in Fig. 1.15 (b).

3). Network-area disaster failure protection

In addition to the common single link failure and node failure, the network-area disaster failure is becoming a critical issue in communication networks. For instance, the earthquate and tsunami of 2011 in Japan and Sichuan earthquake of 2008 in China caused massive damage to telecom networks in large geographic areas. With the benefits from DCNs and the anycasting services, connection protection can be enhenced by serving from different DCs. Instead of providing a backup path from the source to the original DC node, using another DC node with replicated content is allowed to ensure

disaster survivability. Since the first study about disaster-resilient network design was conducted in 2011 [54], different approaches have been proposed for disaster protection in the consideration of disaster-disjoint path generation and content placement in DCNs. Most of the disaster protection schemes are path protection by assigning the alternative backup path from the backup DC upon a large-area disaster. Note that there exist lots of anycasting protection approaches against single link failure or DC node failure that also offer a backup path from another DC. These approaches can be applied into disaster protection involved with disaster area.

We classify the related path protection for disaster or anycasting below:

- **Dedicated/Shared End-to-content Backup Path Protection (DEBPP/SEBPP) [80]**

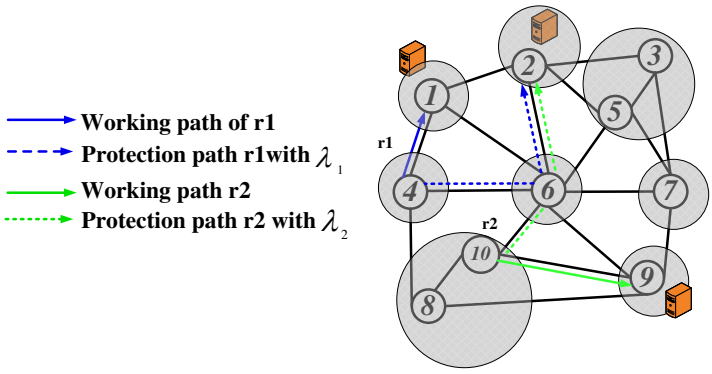

(a) DEBPP

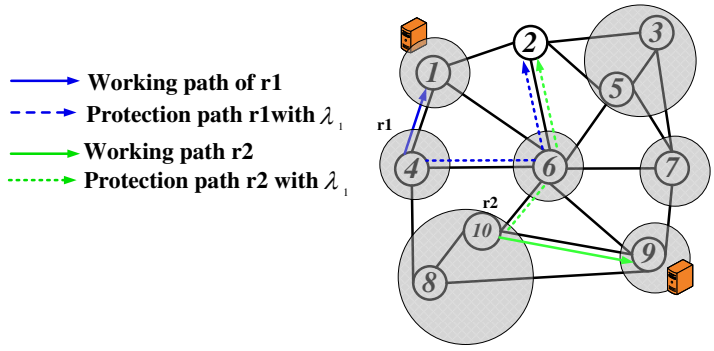

(b) SEBPP

Figure 1.16: *DEBPP and SEBPP in disaster protection.*

The path protection schemes against disaster failures concern the path protection and content protection simultaneously. A Disaster Zone (DZ) is defined as a set of nodes and links which might be affected simultaneously by a single disaster event. Thus, the primary and backup paths should be DZ-disjoint. Moreover, the specific content should be satisfied as the backup path uses a different DC node rather than the primary DC node. The end-to-content backup path protection can be divided into Dedicated End-to-content Backup Path Protection (DEBPP) and Shared End-to-content

Backup Path Protection (SEBPP) according to the spare capacity allocation mechanism.

As shown in Fig. 1.16, two requests originate from node 4 and node 10 respectively in the network with 3 available DCs and 8 DZs. The request r_1 is provisioned through 4-1 to DC 1, while it is protected through 4-6-2 to DC 2. The request r_2 is provisioned through 10-9 to DC 9, while it is protected through 10-6-2 to DC 2. Because the two protection paths have common link 6-2, the DEBPP scheme in Fig. 1.16 (a) uses different spectrum resources on them, while the SEBPP scheme in Fig. 1.16 (b) allows them to share the spectrum resource as their working paths do not fall into the same DZ. Thus, the DEBPP scheme reserves specific spare capacity for each backup path while the SEBPP scheme allows spare capacity sharing on common links among different backup paths as long as their primary paths do not fail simultaneously due to a single disaster.

- **Multiple-path protection [109]**

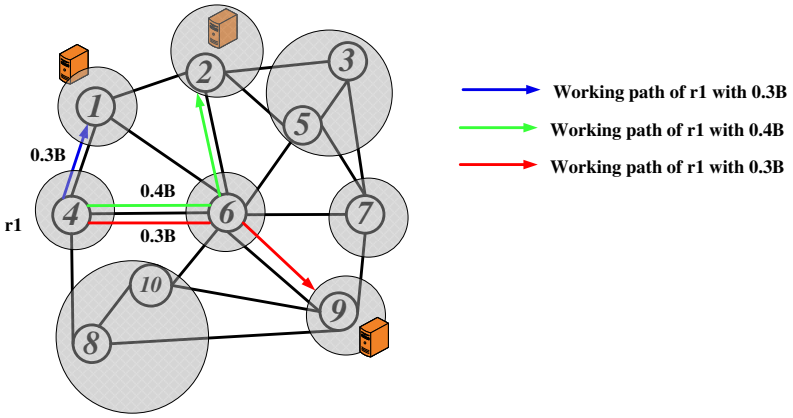

Figure 1.17: *Disaster-aware multipath provisioning scheme. (B is the bandwidth required by r_1.)*

Multipath protection scheme for disaster-aware service provisioning is conducted by multiplexing service over multiple paths destined to multiple DCs with manycasting [109]. Manycasting is referred to providing service from a subset of the DCs. Thus, the manycasting owns the advantage of resilience by allowing serving a cloud user from an intelligently selected subset of DCs having the requested service. Some services may accept a reduced level of bandwidth during failures, depending on their characteristics.

As shown in Fig. 1.17, the multipath provisioning scheme is enabled by the cloud services over DCNs so that the request can be provisioned from several different DC nodes. The request r_1 at node 4 can be provisioned by multipath routing through 4-1,4-6-2, and 4-6-9. Each of the multiple paths only provides partial bandwidth 0.3B, 0.4B and 0.3B respectively to maintain the survivability. As a result, for a multipath service provisioning, even if some paths are down due to a disaster failure, the other paths can maintain some bandwidth for degraded-service level.

- **Anycast-protecting p-cycle protection [119]**

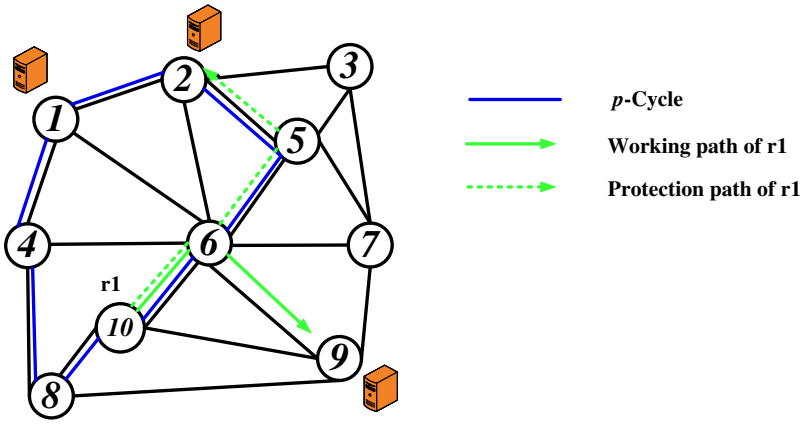

Figure 1.18: *Anycast-protecting p-cycle protection scheme.*

A p-cycle path protection for anycast traffic provisioning, named anycast-protecting p-cycles, was proposed in [119] even though there is no work about the p-cycle protection against disaster failure. It combines protection of physical links with protection of flow paths. The key idea of the anycast-protecting p-cycle is that it provided the backup path as long as the both the requesting node and the backup replica DC node are on a p-cycle. Thus, the protection can be provided on the flow level by the backup path as a straddling path or as an on-cycle path. In case of any link failure, the request can be provisioned from the replica DC instead of restoring the original working path.

An example is shown in Fig. 1.18, where request r_1 is provisioned though the DC 9 via 10-6-9. In order to provide the anycasting protection, the p-cycle 1-2-5-6-10-8-4-1 is designed to provide the protection path 10-6-5-2 for request r_1. The protection is enabled by the DC node 2 that is involved by the p-cycle. Note that the p-cycle can provide multiple protection for different requests as long as the request node and the backup DC are involved in the p-cycle. The advantage of the anycast-protecting p-cycle is that it can provide restoration of the entire working path using even one p-cycle for each request. Moreover, the backup DC can be available in any p-cycle protecting links of the entire working path [119].

1.3.3 Challenges of next generation optical network protection

In this dissertation, we focus on p-cycle protection for MLR optical networks and EONs, and path protection for disaster-survivable DCNs. Generally, both p-cycle protection and path protection provide efficient protection capacity with wavelength/spectrum to recover from the network failures. To concern the next generation optical network protection, we address several potential research challenge respect to network cost and energy issues, specific protection scheme for optical DCNs as well as the complexity of

protection design methodology, as shown in Fig. 1.19. The first challenge is to address the cost and energy performance of networking design for protection schemes as the continually increasing traffic and the advanced technologies in optical networks are requiring more network cost and power consumption [116, 122, 129, 144]. Secondly, for the optical DCNs, specific protection schemes need to study for efficiently protecting the new traffic scenarios with the introduction of today's new service, such as anycast service [131, 138]. To solve these survivability issues related to network performance metrics and new traffic scenarios, protection schemes can be explored with network design methodology either by mathematical formulation or heuristic algorithms. This addresses the third challenge of network protection design methodology as the multiple degrees of freedom and their interdependencies make the protection scheme designing more complicated. In the following text, we will address these three challenges and discuss about their impacts on next generation optical network protection.

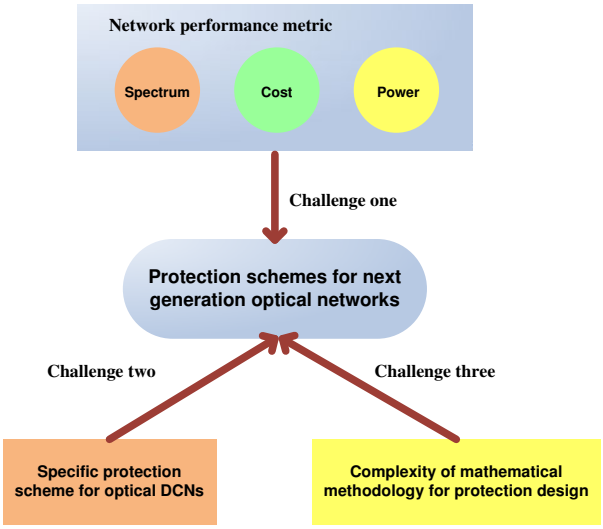

Figure 1.19: *Main considerations of next generation optical network protection.*

1). Spectrum-efficient, cost-efficient and energy-efficient network protection

The ever-increasing traffic demands supported by optical networks dramatically introduce new challenges of capital investment and energy consumption in addition to deploying enough capacity [129]. These growing traffic demands also consume increasing energy, which keeps an average annual growth rate of 10% in today's telecommunication networks since 2007 [144]. It becomes a key issue to investigate new protection mechanisms to improve the cost and energy efficiency for the next generation optical networks. The development of MLR optical networks and EONs permits to achieve potential cost and energy savings by more flexible network protection technology [27]. The network cost and power lie in optical equipments such as optical transponders, inline amplifiers and the nodal pre- and post-amplifiers, regenerator and the core switching elements. The network cost and power consumption mainly depend on the transmission line rate, which also restricts the transparent transmission reach [107]. It has been shown that EONs can achieve potential advantages with respect to energy and

spectral efficiency as well significant cost savings for the operators. However, the cost efficiency of EONs strongly depends on the main cost contributor BVT, and it differs in traffic conditions and network topologies [129]. Thus, it is of great importance to design cost- and energy-efficient protection schemes for next generation optical networks.

In both fixed-grid MLR WDM and EONs, network protection involves the solution of some sort of resource allocation problem, which lies in the transponders, the regenerators, and the spectrum units (wavelengths or FSs) on the links and the cross-connects [125]. Adaptable transponders can be used in MLR WDM and EONs so that the resource allocation decision can be affected by a number of transmission parameters directly or indirectly, such as the request capacity, transmission reach, modulation format, *etc*. Moreover, efficient resource allocation of wavelengths or FSs can achieve the savings of network protection cost and power [129]. This is because the resource usage, cost and energy interrelate the transmission reach, the transmission rate, and other parameters. Thus, the multiple degrees of freedom and their interdependencies make traffic protection establishment in new generation optical networks like MLR WDM and EONs more complicated than in conventional WDM networks.

2). Specific protection scheme for optical DCNs

DCNs interconnects all of the DC resources (computational, storage, network) together to handle the growing demands of cloud computing for end users [79]. DCNs accommodate multiple DC tenants with a variety of workloads, in which DCs are the components that provide users with requested services/contents. The studies on DCNs in the literature have generated solutions for many use cases such as cloud computing, Content Delivery Networks (CDNs), distributed storage, *etc* [131]. DCNs offer many features to help to organize the new applications with the following benefits [133]: (i) DCNs permit to expand the traffic provisioning in an efficient way by the connection of thousands of DC servers, (ii) DCNs allows traffic reliability and efficiency to massive machine-to-machine communications with the distributed workloads on DC servers, (iii) DCNs support various virtualization techniques related to Virtual Machine (VM), virtual network, and virtual function.

As an efficient traffic provisioning technique in DCNs, anycasting has been used to serve the customer with one-of-many destination DC as long as the service-level agreements (*e.g.*, bandwidth and computing requirements) are satisfied [147]. Anycasting communication scheme permits to utilize the optical spectrum more wisely owing to that the destination DC of a request is implicit. However, these new anycasting-enabled network services involve asymmetric traffic provisioning in addition to the conventional symmetric traffic provisioning [131]. Conventional symmetric traffic protection schemes assign the same amount of protection capacity in two directions between the same pair of nodes [130]. However, compared with the symmetric approach, it has been proven that asymmetric traffic provisioning can bring resource savings (up to 50% of spectrum usage and up to 30% of CAPEX cost) in EONs [131], thus protection schemes that focus on asymmetric traffic have big potential to achieve power savings.

3). Complexity of the protection design methodology

The protection scheme design concerns the different requirements on traffic characteristics and network property. The spare capacity allocation is involved in the optimization of resource usage related to the network cost, energy, *etc*. However, these areas are clearly interrelated and pose many trade-offs, such as the transmission reach with the spectral efficiency trade-off [125]. The spare capacity problem for the protection schemes is referred to the survivable RSA problem, which finds an appropriate working route and backup route for a source and destination pair and to allocate suitable FSs to the requested lightpaths. The RSA problem in EONs is quite similar to the RWA problem in WDM optical networks. The difference between RSA and RWA is due to the capability of the EON architecture to offer flexible spectrum allocation. In RSA, a set of contiguous FSs is allocated to a lightpath instead of the single wavelength by RWA in fixed-grid WDM networks [12]. The allocated FSs must be placed in an appropriate way to satisfy the spectrum contiguity constraint and spectrum continuity constraint. It has been stated that RSA is an $\mathcal{NP}$-hard problem in [12].

One methodology used to solve this complicated protection design problem is efficient MILP/ILP formulation, and alternative approach is designing algorithms. However, the optimal solution is not always guaranteed as the classical p-cycle generation, RWA and RSA problems are $\mathcal{NP}$-hard [12, 21, 51]. Heuristic algorithms have much lower computation complexity but it can not guarantee the optimal solution. Another alternative method for achieving the overall optimal design is the decompose technique, such as CG approach, which permits to get the optimal solution by generating promising columns iteratively [113].

1.4 Literature review

Survivability is always a key concern for optical network design to maintain the availability against network failures. A lot of protection schemes have been studied for MLR WDM optical networks and EONs due to the more resource allocation flexibility. Considering the advanced equipment requirements on the optical layer in MLR optical networks and EONs, most of these protection schemes shift the focus to the cost-effective and energy-efficient network protection rather than only the conventional wavelength/spectrum-efficient network protection [7, 13, 18, 32, 75, 81, 82, 84, 99, 123, 124, 128, 129]. Recently, disaster-survivable cloud service provisioning has been regarded as a crucial issue as more and more cloud traffic is delivered by DCNs. Some protection schemes have already been proposed to provide survivability against disaster failures [39, 45, 55, 109, 110, 142]. The approaches to solve these protection design problems were conducted by either ILP formulation or heuristic algorithms.

Below, we summarize different protection schemes for MLR WDM optical networks, EONs and optical DCNs with respect to different protection issues.

1.4.1 Cost-effective protection and power-efficient schemes for MLR WDM networks

In [81], cost-effective protection for transparent MLR WDM optical networks was studied with three dedicated-path protection mechanisms: MLR-at-*p*-lightpath protection (MLR-*p*), MLR-at-lightpath protection (MLR-*l*), and MLR-with-backup-flow-grooming protection (MLR-*g*). The goal is to minimize the network cost in terms of transponders at various bitrates. They first proposed an ILP-based two-step approach by relaxing the wavelength-clash constraint and solving the routing/rate assignment and first-fit wavelength assignment. It has been observed that MLR-*l* addressed a good trade-off between performance and complexity, achieving a significant cost reduction and being solved in a reasonable time. Thereafter, they proposed a heuristic approach for MLR-*l* and the simulation results showed that cost-effective MLR survivable networks can be designed by intelligent assignment of bitrates to the lightpaths while satisfying all the traffic demands.

The authors in [81] further proposed a Shared Subconnection Protection (SSP) scheme for MLR optical networks [82]. The SSP scheme addressed the cost-versus-capacity trade-off in providing shared protection for a transparent MLR network. They stated that SSP was an excellent candidate for protection in MLR networks for the following reasons: (i) Both working lightpaths and backup subconnections can take advantage of rate heterogeneity in MLR networks; (ii) SSP enabled low restoration time, which was crucial when transporting very high bitrates; (iii) SSP can avoid power transients that arose when the power level on a link was suddenly changed. A two-step approach was developed to formulate part of the problem as an ILP. The simulation results showed that SSP enabled higher sharing of backup capacity in an MLR network, in which the design cost was up to 37% less than an SLR network with SSP and around 40% less than MLR with dedicated protection.

In [124], a computation-efficient multipath routing scheme was proposed for survivable provisioning in MLR networks. They studied the degraded service in which certain services can accept a fraction of the requested bandwidth in the event of a failure in exchange of paying a lower cost. They concerned minimum-cost MLR network design by choosing which transponder rates to use at each node while considering the opportunity to exploit multipath routes to support degraded services. Both MILP solution and a heuristic were proposed for the partial-protection. The MILP formulation was proposed to minimize the total transponder cost while exploring various rate-assignment choices with respect to all possible grooming options. The proposed heuristic algorithm comprised of two major steps, *i.e.*, route assignment and rate assignment in computing a multipath routing solution. The results have shown that significant cost savings can be achieved with the help of partial protection versus full protection, which was highly beneficial for network operators. They also noted that multipath routing in MLR networks exploited volume discount of higher-line-rate transponders by cost-effectively grooming requests over appropriate line rates versus SLR.

In [32], a new solution for *p*-cycle design in MLR optical networks was developed and evaluated, which was the first *p*-cycle protection scheme for MLR networks to the

best of our knowledge. Considering the impact of multiple heterogeneous rates in MLR networks, a *p*-cycle protection scheme was proposed to exploit the under-utilization of *p*-cycles and protect additional demands. Both exact optimization formulation and a heuristic solution for this critical problem were proposed. Simulation results showed that *p*-cycle for MLR had increased protection efficiency over SLR networks.

[18], the authors first formulated mathematical models for designing energy- and cost-efficient MLR optical networks in transparent, translucent, and opaque IPoWDM networks. To evaluate these models, they further determined the maximum transmission reach of different line rates when they are mixed with other line-rate channels in the fiber transmission. They conducted several numerical simulations to study the energy consumption of MLR compared with the conventional SLR network, and investigated the relationship between energy-minimized and cost-minimized MLR network design. They found that energy-minimized design may not be the CapEx-minimized design depending on the relative values of transponders and amplifiers.

1.4.2 Cost-effective and power-efficient protection schemes for EONs

In [128, 129], the authors evaluated the energy- and cost-efficiency of different protection schemes in EONs and compared them with the protection schemes for conventional WDM networks. The energy efficiency and cost efficiency evaluation were conducted with three common path protection schemes: 1+1 Dedicated Protection (1+1 DP), 1:1 DP, and Shared Protection (SP). Transponders, OXC and OAs were considered as the dominant optical equipments of energy and cost issues. In order to address the spectral efficiency in addition to energy efficiency, the Energy efficiency per GHz (bits/Joule/GHz) was adopted from wireless networks to evaluate the protection performance. *BandwidthCBand* is the available ITU-T C-band spectrum, *i.e.* around 4 THz.

$$\frac{EnergyEfficiency(bits/Joule)}{AvgSpectrumOccupancy * BandwidthCBand(GHz)} \tag{1.1}$$

Considering the DP and SP protection schemes, they stated the differences in the constraints between the routing and resource allocation in SLR WDM networks, MLR WDM networks and EON, and provided a broad vision of the situations where a particular protection scheme or transmission technology was more beneficial in terms of energy and cost-efficiency. The results showed that the flexible resource allocation of the EONs can be beneficial in energy efficiency for a realistic survivable network, and the SP protection scheme offered the best energy efficiency at any traffic load value in their simulations.

In [99], the power consumption wastage for survivability in IP/Multi-Protocol Label Switching (MPLS) over DWDM multi-layer optical networks was studied. The authors focused on the design of survivable multi-layer optical networks over an SLR, MLR or an Elastic DWDM optical layer minimizing the total network CAPEX. Comparing with the existing works on optical layer energy-efficient design, multi-layer IP/MPLS over elastic DWDM optical networks was concerned with CAPEX and energy issues.

A two-step network design approach was proposed based on ILP. The first step was to determine the unprotected capacity with minimum total network CAPEX, and the second step conducted a joint optimization of the extra capacity to make the network survivable to all link failure scenarios with minimum CAPEX. From their results, EONs can yield up to 36% optical layer power consumption reduction when compared to SLR while this remarkable power consumption reduction was also translated into a significant 9.3% overall network power consumption reduction when considering IP and optical layers together.

In [84], a Differentiated Quality of Protection (Diff QoP) scheme was proposed to maintain high service availability with improved energy- and spectral-efficiency. The proposed Diff QoP schemes were able to match the actual client/service requirements for network protection in both static (offline) and dynamic (online) scenarios. A framework for implementation of Diff QoP was proposed in an optical transport network as well as a thorough explanation of the heuristic to improve both the energy- and spectral-efficiency of the networks. The performance of Diff QoP in terms of energy- and spectral-efficiency were comprehensively evaluated in both WDM (SLR and MLR) and EON network architectures with both static and dynamic traffic operation. They concluded that Diff QoP can be considered as a promising protection scheme for enhancing both the energy- and spectral-efficiency of optical transport networks while maintaining the heterogeneous reliability requirements of different services/users.

In [13], the authors addressed the minimum network cost problem for survivable virtual optical network mapping in flexible bandwidth optical networks. Dedicated-path protection was explored with an ILP model, the LBSD (the largest bandwidth requirement (LB) of virtual links versus the shortest distance (SD)) mapping approach and the LCSD (the largest computing (LC) resources requirement versus the shortest distance) mapping approach. The simulation results showed that the proposed approaches not only achieved the minimum total network cost but also minimum spectrum usage and minimum number of regenerators. In [123], an optimal cost-effective network dimensioning was studied for different configurations of optical slot switching metropolitan rings with elastic-rate transponders. MILP-based model was formulated to study the network cost depending on the protection type and the elasticity.

In [75], a real network with 1113 physical nodes and 1+1 protection was evaluated by varying the ratio of core/metro nodes to find the optimum network performance regarding cost and power efficiency of EONs. The protection scheme was designed to simultaneously minimize CAPEX and power consumption allowing for a mostly transparent (translucent) network. Their results confirmed that the use of the flex grid is beneficial for the EON scenario.

In [7], a hybrid protection approach based adaptive routing introducing the regenerator activation was proposed in the consideration of energy consumption. Both DP and SP protection schemes were designed by ILP formulation and greedy or heuristic algorithms. In their study, the first algorithm identified the primary path of each connection request and the second algorithm selected the path with minimal power consumption with their appropriate modulation formats. When a connection request

had no appropriate modulation format, the regenerator was placed to permit connection establishment with a good quality of signal. The simulation results showed that activation of the regenerators had a significant impact on energy consumption and network blocking probability.

1.4.3 Disaster-survivable cloud provisioning for optical DCNs

To the best of our knowledge, the study in [55] was the first work to address the content placement, routing, and protection of paths and contents subproblems together in disaster-survivable WDM optical DCNs. They first proposed an integrated ILP model to solve the subproblems simultaneously. In order to solve the problem for large networks, relaxations of the integrated ILP were proposed, including a two-step ILP and the LP relaxations. Since the LP-relaxed solution may not be a feasible one, they proposed heuristics to find a feasible solution from the LP-relaxed solution. In addition, they also explored a non analytical approach to solve the problem for large instances. They have shown that the proposed disaster protection scheme exploiting anycasting provided more protection, but used less capacity than dedicated single-link failure protection. They found that a reasonable number of DCs and selective content replicas with intelligent network design can provide survivability to disasters while supporting user demands. Their simulation results have indicated that the performances of the proposed relaxation scheme and the heuristics were quite close to the integrated ILP that gave the best-case scenario.

In [45], a survey of strategies for communication networks to protect against large-scale natural disasters was given. An overview of the vulnerability of communication networks to disaster-based disruptions was first presented, including the measures of network vulnerability, identification of vulnerable regions and vulnerability of physical infrastructures. Then, rules and techniques for making network architectures less vulnerable to disaster-based failures were analyzed. There were two complementary ways to proceed: Pre-disaster network robustness improvements such as in-network solutions and out-network solutions, and post-disaster network/service recovery methods such as rapid emergency communication network deployment and effective network maintenance. Finally, the disaster-resilient routing algorithms were discussed including tunable survivability against single link failure, resilience against multiple failures, spatio-temporal disaster-aware routing and post-disaster routing.

In [110], a Backup Reprovisioning with Partial Protection (BRPP) scheme was proposed to remedying the large-scale disaster failure problem as the providing 100% protection against disasters would require massive and economically unsustainable bandwidth overprovisioning. The BRPP scheme supported dedicated-path protection, where backup resources were reserved but not provisioned, such that the amount of bandwidth reserved for backups as well as their routings were subject to dynamic network state. The proposed BRPP framework consisted of various modules in the control layer of SDN, while implementing the algorithmic solutions for realizing BRPP in a network of OpenFlow-enabled switches and servers. The results have shown that,

with the added flexibility coming from incorporating degraded service in backup re-provisioning, it was able to utilize network resources better when network resources were scarce so that more connections can be provisioned with the extra capacity by degrading backup paths.

In [109], a novel disaster-aware service-provisioning scheme was proposed by multiplexing service over multiple paths destined to multiple servers/datacenters with manycasting. These applications can exploit multipath provisioning, which offered degraded service with degraded-service level in case of a failure. An ILP formulation was proposed based on the k-shortest paths from each node to each datacenter as an input. The objective was to minimize the expected bandwidth loss in the event of disasters and the network resource usage. To increase the scalability, heuristic optimization approaches were provided for disaster-aware service provisioning with manycasting in cloud networks. The numerical examples have shown that exploiting manycasting by intelligently selecting destinations in a risk-aware manner offered high level of survivability against disaster failures at no extra cost compared to the other survivable schemes.

In [39], a joint progressive recovery strategy of post-disaster cloud-network recovery was proposed for optical DCNs to maximize content reachability to users at each repair stage. Content connectivity was employed to ensure delivery of cloud services. A Joint Progressive Net-DC Recovery (JR) algorithm was designed to schedule repair of optical network nodes/links and DCs. The objective is to attain maximum possible cumulative weighted content reachability to users at each stage, including network node repair phase, network link repair phase and DC repair phase. The simulation results have shown that the proposed approach provided an efficient recovery strategy for post-disaster cloud networks. With joint progressive recovery of optical network and DCs, higher content reachability can be provided to users at each repair stage.

In [142], a shared protection scheme was proposed to maintain disaster survivability under both anycast method and unicast method in elastic optical DCNs. The anycast method had specific source node, the content, and the bandwidth of the content while its destination node can be one of potential DCs as every datacenter has same contents. The unicast method had specific source node, destination node, and the bandwidth requirement of the content. ILP formulations were developed to solve the problem of providing disaster survivability for RSA under the anycast method. It utilized the priori method to maximize the network throughput first, and then to minimize used spectrum resources. Simulations were conducted in a small 6-node network to investigate the throughput and spectrum usage as the number of requests increased. The results have shown that the network under anycast method provided the same throughput as that of unicast, but used much less spectrum resources.

Part II

p-Cycle Protection Scheme for MLR WDM against Single Link Failure

Chapter 2

Low-Cost p-Cycle Design Without Candidate Cycle Enumeration in MLR Optical Networks

Contents

2.1 Introduction

Previously, survivable WDM optical networks have been investigated intensively with several protection schemes [2, 33, 111, 139, 145]. However, these protection schemes only focus on network resources allocation under SLR. Survivability in MLR optical networks need to deal with line rate assignment related to protection cost and transmission reach. Thus, cost-effective protection approaches for MLR optical networks are increasingly important. Conventional p-cycle design schemes are required to enumerate candidate cycle set in advance, and to screen p-cycles from the candidate cycle set. Since the number of candidate cycles increases exponentially with the number of nodes and links in the network, it would be intractable to enumerate all the candidate cycles. Thus, some work on finding partial candidate cycles with high metric have been tried to form effective candidate cycle sets, nevertheless, optimal solution can not be obtained with them. In addition, p-cycles without candidate cycle enumeration are explored in [111, 139], but these methods are not valid in MLR optical networks due to the lack of line rate optimization. Moreover, p-cycles are rarely designed considering transmission reach, which is not realistic.

In this chapter, p-cycle protection scheme is studied against single link failure, which is regarded as the most common failure in optical networks. Specifically, a distance-adaptive p-cycle protection scheme without candidate cycle enumeration is studied in MLR optical networks. Path-length-limited p-cycles are designed to assign line rates depending on the length of each protection path. An MILP model is formulated to minimize CAPEX cost. Then, Graph Partitioning in Average (GPA) algorithm and Estimation of cycle numbers $|I|$ (EI) algorithm are designed to enable concurrent computation of MILP model in sub-graphs.

The significant aspects of this proposition are:

- Distance-adaptive p-cycle scheme is designed in the consideration of transmission reach at various line rates, thus the transmission quality of optical signal along protection path can be guaranteed.
- An MILP model without candidate cycle enumeration is formulated to directly generate p-cycles, thus it is guaranteed to obtain the optimal solution if possible.
- p-Cycles are generated with the path-length-limited constraint, which restricts p-cycles according to the length of each protection path instead of the length of cycle circumference. It is more accurate and cost-effective.
- A graph partitioning algorithm is developed to enable concurrent computations in sub-graphs in the proposed MILP model, which largely cuts computational time.

2.2 Related work

Even though survivable MLR optical networks are critical, very few related work has been done in this field [32, 81, 82, 124]. In [81], three dedicated protection approaches

at the lightpath level were studied in MLR networks. The authors further explored SSP in transparent MLR networks in [82], where they designed a two-step approach to solving the Routing/Rate Assignment (RRA) and Wavelength Assignment (WA). The authors in [124] investigated survivable provisioning with multipath routing to minimize overall transponder cost, in which partial requested bandwidth was provisioned on link-disjoint path. However, these protection schemes mainly focused on end-to-end path protection, thus they may suffer from relatively long restoration time since the working and protection paths had to be set up and turned down frequently.

p-Cycle protection scheme with fast switching time was introduced in 1998 [52]. In [112], link-based *p*-cycles were explored to protect individual links with and without wavelength conversion. *p*-Cycle was also developed to protect SRLG failure in [105], and to provide protection for link and node failures simultaneously [30]. In addition, the authors in [4] developed a new ILP model for enhanced failure-specific *p*-cycles with a specified minimum dual-failure restorability level. They showed that this new model provided significant capacity cost reductions compared with the original design model, which did not consider this enhanced dual-failure restorability. Moreover, the authors in [17] addressed the impact on reliability performance of *p*-cycles due to capacity sharing, and they concluded that there was a tradeoff between capacity sharing and reliability. For the reliability concern, they obtained that it is more reasonable to use *p*-cycles in smaller networks than in long haul networks.

All the *p*-cycle protection schemes above with SLR used a two-step approach to enumerating candidate cycles first, and then to screen *p*-cycles from the candidate cycles. However, enumerating all the candidate cycles would increase the computational complexity since the number of candidate cycles increases exponentially with the number of network links and nodes. The authors in [3] comprehensively analyzed the tradeoff among the size of eligible *p*-cycles, the optimality gap and computational time. To ensure a small enough optimality gap, a bigger eligible set of *p*-cycles needed to be selected, thus long computational time was also required. To address this issue, some heuristic algorithms for enumerating partial candidate cycles with high metric were proposed [31, 51]. Even though these partial candidate cycles were individually efficient, they generally provided only sub-optimal solutions when combined together. A single-step method using CG technique was proposed to reach optimal solution and own scalability in [113], but it relied on a decomposition of the initial problem into a master problem and a pricing problem.

p-Cycle design without candidate cycle enumeration was studied by ILP formulations in [111], however, the ILP was too complex so that a four-step heuristic was proposed to solve it. The authors further designed three efficient *p*-cycle design without candidate cycle enumeration for SLR optical networks in [139], which were based on recursion, flow conservation, and cycle exclusion, respectively. However, these optimal *p*-cycle design approaches without candidate cycle enumeration were only valid in SLR optical networks, and they can not be applied into MLR optical networks due to the lack of line rate optimization. More importantly, the transmission reach was ignored in their models, thus it can not guarantee the transmission quality along the protection path.

Even though a p-cycle design was investigated for MLR optical networks in [32], it still required candidate cycle enumeration in advance and screened p-cycles from candidate cycle set. More importantly, the authors in [32] did not consider various transparent transmission reach at different line rates, thus the quality of the optical signal on the protection path can not be guaranteed.

Hence, it is of great value to investigate distance-adaptive p-cycle design scheme without candidate cycle numeration in MLR optical networks.

2.3 Problem statement

The MLR optical network topology is modeled as $G(V, E)$, where V and E represent the sets of nodes and directed fiber links in G, respectively. A set of line rates, denoted by $R = 10/40/100\ Gbps$, is assumed to provision the traffic loads. p-Cycles are built to provide protection for single link failure under the transmission reach. We assume that the protection paths are provisioned in transparent optical networks without any O/E/O conversion in intermediate node(s), then only two transponders at the ending nodes are laid for each protection path. Thus, contiguous line rate should be guaranteed along the protection paths. The distance-adaptive p-cycles for MLR optical networks in this study are designed under the following considerations:

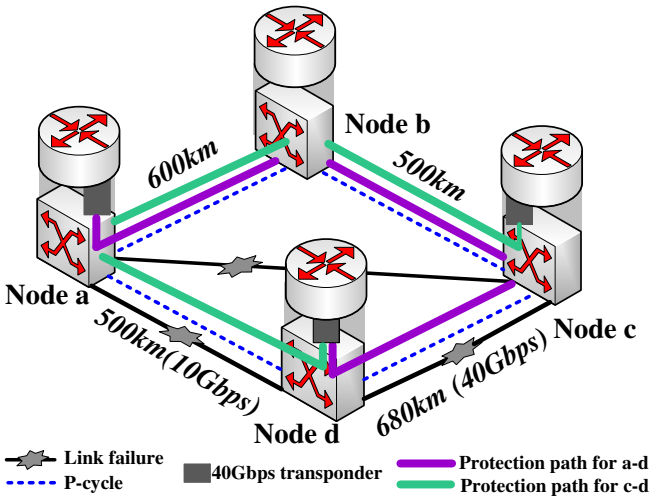

Figure 2.1: *p-Cycle protection in MLR optical networks.*

- *Transmission reach* [1]: The quality of an optical signal is degraded along a path due to Physical-Layer Impairments (PLIs) [98], and it becomes even worse in MLR optical networks with various co-existing line rates. The transmission reach of line rates at 10 $Gbps$, 40 $Gbps$, and 100 $Gbps$ are 1750 km, 1800 km, and 900 km at

[1] It is defined as the distance an optical signal can travel before the signal quality and the bit-error-ratio (BER) degrade to an unacceptable level and the communication is considered infeasible [19]

a threshold BER 10^{-3}, respectively [18]. The transmission reach in [18] was estimated with modulation formats of 10 *Gbps* OOK, 40 *Gbps* DPSK and 100 *Gbps* DP-QPSK. Moreover, the MLR optical networks was considered dispersion minimized for 10 *Gbps* (as in legacy systems). Transmission reach is a main consideration to determine the proper line rate for each *p*-cycle. As shown in Fig. 2.1, the protection path $a-b-c-d$ for failed link $a-d$ has a length of 1780 *km*, then only 40 *Gbps* can be assigned.

- *Transponders Cost*: The relative transponder cost is treated as 1 *unit*, 2.5 *units* and 3.75 *units* for 10 *Gbps*, 40 *Gbps* and 100 *Gbps*, respectively [18].
- *Spare Capacity Cost*: Spare capacity is required for each link on the *p*-cycles. We treat spare capacity cost as 1 for each link of the *p*-cycle.
- *Single Line Rate for One p-Cycle* : Only one single line rate can be selected for one *p*-cycle, even though several line rates are potential for individual protection path in the *p*-cycle. Again in Fig. 2.1, protection path $d-a-b-c$ with 1600 *km* length for failed link $d-c$ can be assigned 10 *Gbps* or 40 *Gbps*, but only 40 *Gbps* is allowable because another protection path $a-b-c-d$ with 1780 *km* length only can be assigned 40 *Gbps*.
- *p-Cycle Protection Capacity*: One unit of protection capacity is provided for each on-cycle link, while for each straddling link, two units of protection capacity are provided. For the on-cycle link $a-d$ in Fig. 2.1, the *p*-cycle provides 40 *Gbps* protection capacity via a-b-c-d, while it provides $2\times 40\ Gbps = 80\ Gbps$ protection capacity for straddling link $a-c$ via a-b-c and a-d-c. The protection capacity provided by all *p*-cycles should be sufficient to ensure 100% single link failure protection.

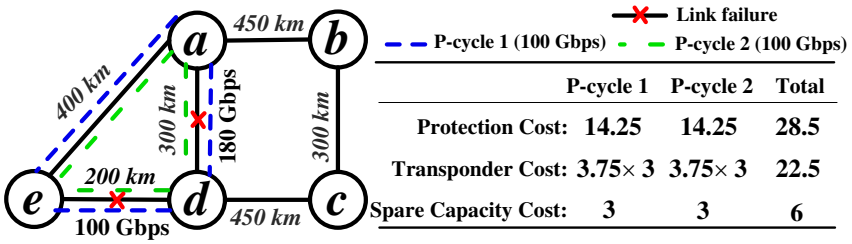

(a) Feasible solution of p-cycles

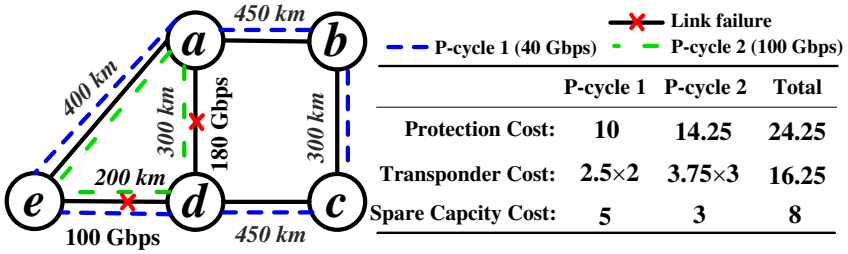

(b) Optimal solution of p-cycles

Figure 2.2: *Optimal p-cycle design with the minimum CAPEX cost.*

Table 2.1: *Parameters and variables in MILP model in* ***Chapter*** *2.*

Network Sets and Parameters	
$G(V, E)$	Network topology with node set V and link set E.
I	The set with the maximum number of p-cycles allowed in the MILP model. The size of I is estimated by (2.33) in Subsec. 2.5.2.
i	Cycle index where $i \in \{1, 2, \cdots, \|I\|\}$. I_i indicates the i-th p-cycle.
N_v	The neighborhood of a node v.
d_{vu}	The length between node v and node u, d_{max} indicates the biggest length in network $G(V, E)$.
R	The set of line rates, *e.g.*, $\{10, 40, 100\ Gbps\}$.
h_r	Transmission reach at line rate r, which is 1750, 1800 and 900 km at 10, 40 and 100 $Gbps$.
h_{max}	Maximum transmission reach among R, h_{max}=1800 km.
h_{min}	Minimum transmission reach among R, h_{min}=900 km.
t_r	Transponder cost at line rate r, which is 1, 2.5, and 3.75 at 10, 40 and 100 $Gbps$, respectively.
c_{vu}	The cost of adding one unit of spare capacity (*i.e.*, one wavelength) to link (v, u), which is treated as 1 for each link.
l_{vu}	Traffic load on undirected link (v, u). As we protect undirected links, only upper triangular matrix in the traffic matrix is valid.
α	A pre-defined fractional constant, $\frac{1}{\|V\|} \geq \alpha > 0$.
Variables	
$x^i_{vu} \in \{0, 1\}$	Equals 1 if link (v, u) is used by I_i, and 0 otherwise.
$y^i_v \in \{0, 1\}$	Equals 1 if node v is crossed by I_i, and 0 otherwise.
$f^i_v \in (0, 1)$	Virtual *voltage* value of node v in I_i.
$o^i_v \in \{0, 1\}$	Equals 1 if node v is root node in I_i, and 0 otherwise.
$b^i_r \in \{0, 1\}$	Equals 1 if I_i operates at line rate r, and 0 otherwise.
$z^i_{vu} \in \{0, 1\}$	Equals 1 if link (v, u) is potential to be protected by I_i, and 0 otherwise.
$q^i_{vu} \in \{0, 1\}$	Equals 1 if link (v, u) desires to be protected by I_i, and 0 otherwise.
$q^{ir}_{vu} \in \{0, 1\}$	Equals 1 if link (v, u) desires to be protected by I_i at line rate r, and 0 otherwise.
$y^{ir}_v \in \{0, 1\}$	Equals 1 if node v is crossed by I_i at line rate r, and 0 otherwise.
$p^{ir}_{vu} \in \{0, 1\}$	Protection capacity for link (v, u) if it desires to be protected by I_i at line rate r. It equals 1 if link (v, u) is an on-cycle link, and it equals 2 if link (v, u) is straddling link, and 0 otherwise.

In this study, the CAPEX cost is considered as the sum of transponder cost and spare capacity cost. Hence, MLR optical networks offer the potential to optimize line rates of p-cycles with respect to traffic amount, transmission reach, protection capacity and CAPEX cost. However, conventional p-cycle design with MLR only consider transponder cost, spare capacity cost and protection capacity. In our work, we further take into account the transmission reach and explore accurate line rate assignment for distance-adaptive p-cycle design for MLR optical networks.

Here, a simple example in Fig. 2.2 shows how we design distance-adaptive p-cycle with minimum CAPEX cost. The value next to each link indicates the physical length and the other value on links $a-d$, $e-d$ show the working traffic amount. To protect these two working links, several solutions can be performed under the previous considerations. One feasible solution is shown in Fig. 2.2(a) with two p-cycles operating at 100 $Gbps$ line rate. The feasible solution requires CAPEX cost 28.5, which is the sum of transponder cost 22.25 (p-cycle 1: $3.75(t_{100}) \times 3(nodes)$, p-cycle 2: $3.75(t_{100}) \times 3(nodes)$) and spare capacity cost 6 (p-cycle 1: $3(links)$, p-cycle 2: $3(links)$). However, CAPEX cost can be further minimized with optimal line rate assignment. Figure 2.2(b) shows the optimal p-cycle design, in which p-cycle 1 and p-cycle 2 are assigned with 40 $Gbps$ and 100 $Gbps$ line rates, respectively. The CAPEX cost 24.25, in which transponder cost is 16.25 (p-cycle 1: $2.5(t_{40}) \times 2(nodes)$, p-cycle 2: $3.75(t_{100}) \times 3(nodes)$) and spare capacity cost 8 (p-cycle 1: $3(links)$, p-cycle 2: $3(links)$). Thus, the optimal p-cycle solution saves 15% CAPEX cost than the feasible one in Fig. 2.2(b).

2.4 MILP formulation

In this section, we introduce the distance-adaptive p-cycle design for MLR optical networks. Specifically, instead of candidate cycle enumeration, we formulate an MILP model to generate optimal p-cycles with respect to line rate assignment, transmission reach, transponder cost and spare capacity cost. We further explore path-length-limited p-cycles to assign line rates depending on the length of each protection path. The notations and variables in the MILP model are given as in Tab. 2.1.

2.4.1 MILP model

For the sake of readability, we use $\forall i$, $\forall v$, $\forall u$, $\forall r$, and $\forall e$ to denote $\forall i \in \{1, 2, \cdots, |I|\}$, $\forall v \in V$, $\forall u \in N_v$, $\forall r \in R$, and $\forall e \in E$, respectively.

Objective:

The objective of our p-cycle design is to minimize the total CAPEX cost consisting of transponder cost and spare capacity cost in MLR optical networks protection. It should be noted in our p-cycle design, only one transponder is laid in one node if there exists at least a protection path incident to this node. It is more cost-effective compared with the conventional p-cycle design in which two transponders are laid at two ending nodes of each protection path, respectively.

$$\begin{aligned} \min \quad & \theta_1 \cdot C_T + \theta_2 \cdot C_L \\ C_T &= \sum_{i \in I} \sum_{r \in R} \sum_{v \in V} t_r \cdot y_v^{ir} \\ C_L &= \sum_{i \in I} \sum_{e \in E} c_e \cdot x_e^i \end{aligned} \tag{2.1}$$

where C_T and C_L are total transponder cost and total spare capacity, respectively.

Constraints:

The constraints in MILP model can be classifies into cycle generation constraints (2.2)-(2.6), line rate assignment constraints (2.9)-(2.10) and protection capacity constraints (2.11)-(2.17).

1). Cycle generation constraints:

$$x_{vu}^i + x_{uv}^i \leq 1, \qquad \forall i, \forall v, \forall u \tag{2.2}$$

$$\sum_{u \in N_v} (x_{vu}^i + x_{uv}^i) = 2y_v^i, \qquad \forall i, \forall v \tag{2.3}$$

$$f_u^i - f_v^i \geq (1+\alpha) \cdot x_{vu}^i - 1, \qquad \forall i, \forall v, \forall u \tag{2.4}$$

$$\sum_{v \in V} o_v^i \leq 1, \qquad \forall i \tag{2.5}$$

$$\sum_{u \in N_v} x_{vu}^i \leq 1 + o_v^i, \qquad \forall i, \forall v \tag{2.6}$$

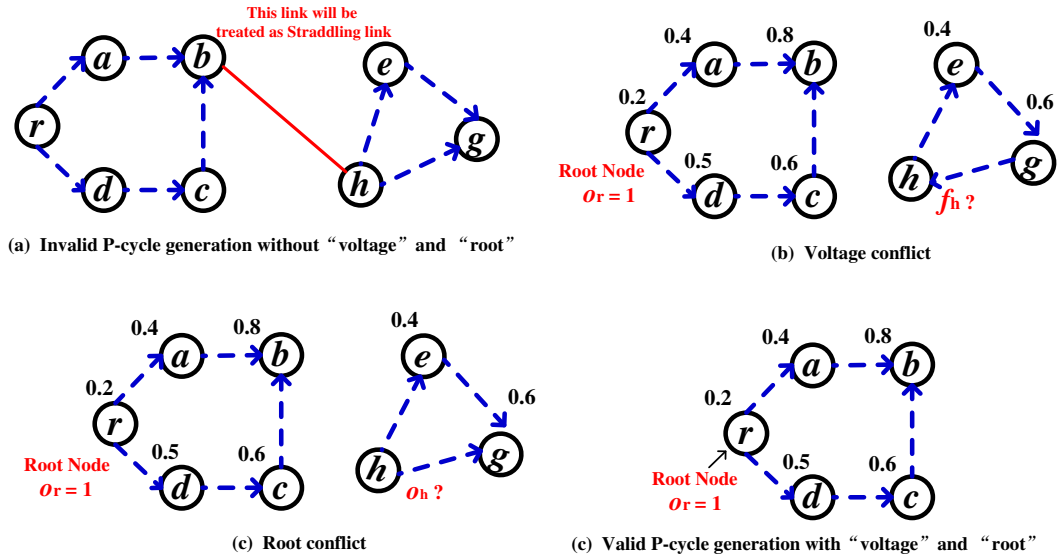

(a) Invalid P-cycle generation without "voltage" and "root"

(b) Voltage conflict

(c) Root conflict

(c) Valid P-cycle generation with "voltage" and "root"

Figure 2.3: *Cycle generation with and without "voltage".*

It should be noted that we design undirected p-cycles that protect undirected traffic, but directed links are used in the constraints (2.2)-(2.6) in order to generate cycles easily

from the formulation. Constraint (2.2) ensures that at most one link between two nodes can be used in a p-cycle. Constraint (2.3) implies that if node v is crossed by a p-cycle, then it should have two adjacent links. However, only these two constraints are not enough to guarantee the connectivity of the p-cycle (*i.e.*, there is always a path between every pair of nodes on the p-cycle). This results in the incorrect p-cycle that link (b,h) has the potential to be protected in Fig. 2.3(a). To eliminate this situation, $voltage$-based constraints (2.4)-(2.6) in [139] are used. Here, $voltage$ f_v^i a virtual variable assigned to node $v \in V$ as a way of expressing and verifying the connectivity of p-cycle. Constraint (2.4) ensures that the $voltage$ of node v should be bigger than that of node u if link (u,v) is used in a p-cycle. A single *root* node is defined with the minimum $voltage$ value, and it permits to have two outgoing links, which are ensured by constraints (2.5) and (2.6). An example is shown in Fig. 2.3, node r is assumed to be the *root* node, and the potential value $voltage$ is assigned next to each node except the node d. Once the connectivity of p-cycle is not guaranteed, either $voltage$ conflict or *root* conflict will happen.

- $voltage$ conflict:
  This conflict happens due to that constraint (2.4) is not satisfied. As we can see from Fig. 2.3(b), the links (h,e) and (g,h) are used on the p-cycle, then the $voltage$ conflict happens for f_h.

$$\begin{cases} x_{he} = 1, \quad x_{gh} = 1, \\ f_e = 0.4, \quad f_g = 0.6, \\ f_e - f_h \geq (1+\alpha) \cdot x_{he} - 1, \\ f_h - f_g \geq (1+\alpha) \cdot x_{gh} - 1, \end{cases} \Longrightarrow 0.6 \leq f_h \leq 0.4 \tag{2.7}$$

- *root* conflict:
  This conflict happens due to that constraint (2.6) is not satisfied. As we can see from Fig. 2.3(c), the outgoing links (h,e) and (h,g) of node h are used on the p-cycle while node h is not the *root* node, then the *root* conflict happens for o_h.

$$\begin{cases} x_{he} = 1, \quad x_{hg} = 1, \quad o_d = 0 \\ x_{he} + x_{hg} \leq 1 + o_h \end{cases} \Longrightarrow 1 \leq o_h = 0 \tag{2.8}$$

2). Line rate assignment constraints:

$$\frac{\sum_{e \in E} d_e \cdot x_e^i}{h_r} \leq \frac{h_{max}}{h_{min}} \cdot (1 - b_r^i) + b_r^i, \qquad \forall i, \forall r, \forall e \tag{2.9}$$

$$\sum_{r \in R} b_r^i \leq 1, \qquad \forall i \tag{2.10}$$

Constraint (2.9) permits to assign line rate for distance-adaptive p-cycles. Specifically, the p-cycle circumference should be less than the transmission reach h_r of the assigned line rate r. We call constraint (2.9) the cycle-circumference-limited constraint. Note that we assume that the impairments along the protection path are mainly due to long-distance transmission, and the impairments introduced by the intermediate nodes

are relatively small so that they can be compensated with a performance margin preset [46]. Constraint (2.10) ensures that only one line rate can be assigned for each p-cycle.

3). Protection capacity constraints:

$$z_{vu}^{i} \leq \frac{1}{2} \cdot (y_{v}^{i} + y_{u}^{i}), \qquad \forall i, \forall v, \forall u \tag{2.11}$$

$$q_{vu}^{i} \leq z_{vu}^{i}, \qquad \forall i, \forall v, \forall u, u > v \tag{2.12}$$

$$q_{vu}^{ir} = q_{vu}^{i} \cdot b_{r}^{i}, \qquad \forall i, \forall r, \forall v, \forall u, u > v \tag{2.13}$$

$$p_{vu}^{ir} = (2 \cdot z_{vu}^{i} - x_{vu}^{i} - x_{uv}^{i}) \cdot q_{vu}^{i} \cdot b_{r}^{i}, \qquad \forall i, \forall r, \forall v, \forall u, u > v \tag{2.14}$$

$$\sum_{i \in I} \sum_{r \in R} p_{vu}^{ir} \cdot r \geq l_{vu}, \qquad \forall v, \forall u, u > v \tag{2.15}$$

$$y_{v}^{ir} \geq q_{vu}^{ir}, \qquad \forall i, \forall r, \forall v, \forall u, u > v \tag{2.16}$$

$$y_{u}^{ir} \geq q_{vu}^{ir}, \qquad \forall i, \forall r, \forall v, \forall u, u > v \tag{2.17}$$

We give a limitation of the directed links used in the protection capacity constraints to guarantee the protection capacity for undirected traffic. Specifically, only the link (v, u) with u bigger than v is considered to be provided protection. Constraint (2.11) makes sure that only if both starting and ending nodes of a link (v, u) are crossed by I_i, then link (v, u) is potential to be protected by I_i. Constraint (2.12) implies the desire of link (v, u) to be protected by one p-cycle. Constraint (2.13) determines that if link (v, u) desires to be protected by I_i at line rate r. Constraint (2.14) determines the protection capacity for link (v, u) if it desires to be protected by I_i. Specifically, if link (v, u) is an on-cycle link, one protection capacity is provided, else if it is a straddling link, two protection capacity units are provided, otherwise, no protection capacity is provided. Constraint (2.15) ensures 100% single link failure protection. Constraints (2.16) and (2.17) ensure that one transponder at line rate r should be laid on node v in I_i if at least one link incident to v desires to be protected by this I_i at line rate r.

In order to ensure linearity in the MILP model, constraints (2.13) and (2.14) are rewritten as constraints (2.18) and (2.19) respectively.

$$\Longrightarrow \begin{cases} q_{vu}^{ir} \leq \frac{1}{2} \cdot (q_{vu}^{i} + b_{r}^{i}), & \forall i, \forall r, \forall v, \forall u, u > v \\ q_{vu}^{ir} \geq q_{vu}^{i} + b_{r}^{i} - 1, & \forall i, \forall r, \forall v, \forall u, u > v \end{cases} \tag{2.18}$$

$$\Longrightarrow \begin{cases} p_{vu}^{ir} \leq 2 \cdot q_{vu}^{i}, & \forall i, \forall r, \forall v, \forall u, u > v \\ p_{vu}^{ir} \leq 2 \cdot b_{r}^{i}, & \forall i, \forall r, \forall v, \forall u, u > v \\ p_{vu}^{ir} \leq 2 \cdot z_{vu}^{i} - x_{vu}^{i} - x_{uv}^{i}, & \forall i, \forall r, \forall v, \forall u, u > v \end{cases} \tag{2.19}$$

2.4.2 Computational complexity

The number of dominant variables and constraints of the MILP model are summarized in Tab. 2.2. Both of variables and constraints only increase linearly with the network size if $|I|$ is given.

Table 2.2: *Computational complexity of the MILP model.*

Computational complexities	
No. of dominant variables	No. of dominant constraints
$O(\|I\|\|E\|\|R\|)$	$O(\|I\|\|E\|\|R\|)$

2.4.3 Path-length-limited p-cycle

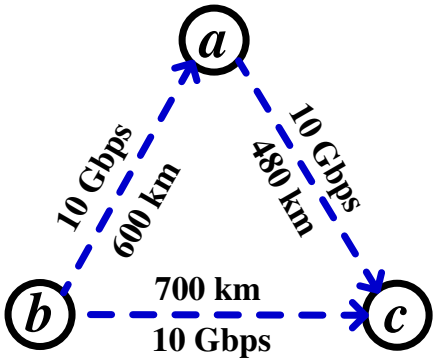

P-cycle generation with constraint (2.7)	
Line Rate:	40 Gbps
Protection Cost:	10.5
Transponder Cost:	2.5×3 nodes
Spare Capacity Cost:	3
P-cycle generation with constraint (2.20)	
Line Rate:	10 Gbps
Protection Cost:	6
Transponder Cost:	1×3 nodes
Spare Capacity Cost:	3

Figure 2.4: *Extra CAPEX cost in p-cycle using constraint (2.9).*

In Subsec. 2.4.1, we use simple and faster cycle-circumference-limited constraint (2.9) to assign line rate with transmission reach. In fact, both hop-limited and cycle-circumferences-limited constraints have been tried in [8, 78, 143]. In these studies, hop-limited p-cycle design excluded p-cycle directly with maximum H hops of any protection path, while cycle-circumferences-limited design restricted p-cycle with the maximum $H+1$ hops of the cycle circumference. They obtained the conclusion that simple and faster cycle circumference limited model provided an excellent approximation of the strictly hop-limited model. However, considering the transmission reach in MLR optical networks, cycle-circumference-limited constraint in p-cycle design will result in extra CAPEX cost and even infeasible solution as follows.

- **Extra CAPEX cost**. For instance in Fig. 2.4, all the links with traffic 10 $Gbps$ need to be protected. The p-cycle is assigned 40 $Gbps$ line rate by using constraint (2.9) as the length of the p-cycle circumference is 1780 km. Thus, the CAPEX cost is 10.5. However, if the line rate assignment depends on the length of each protection path, which are a-b-c (1300 km), a-c-b (1180 km) and b-a-c (1080 km), thus 10 $Gbps$ line rate can be assigned with a lower CAPEX cost of 6. We call p-cycle with such line rate constraint **path-length-limited p-cycle**.
- **Infeasible solution**. More importantly, in some cases, the cycle-circumference-limited constraint (2.9) results in infeasible solution even though there exists a feasible solution. For instance, constraint (2.9) will eliminate the p-cycle in Fig. 2.5 as its cycle circumference length 2620 km is bigger than the transmission reach (1800 km at 40 $Gbps$). Note that such p-cycle design with cycle-circumference-

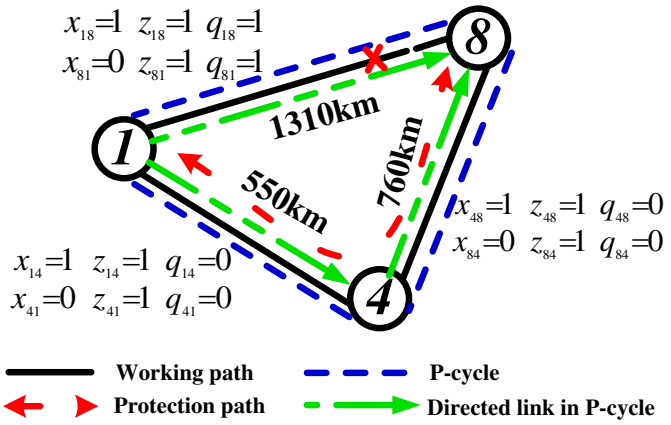

Figure 2.5: *The feasible solution acquired path-length-limited p-cycle with the value of variables x^i_{vu}, z^i_{vu} and q^i_{vu}.*

limited constraint also exists in [97, 139], in which the length of p-cycle circumference is used as transmission reach to determine line rate or modulation format. In fact, the p-cycle in Fig. 2.5 still enables the protection for link $1-8$ using protection path $1-4-8$, as the protection path length is only 1310 km, which is able to be assigned 10 or 40 $Gbps$ line rate.

We propose the following theorems to address path-length-limited p-cycle with transmission reach on each protection path.

Theorem 2.4.1. *A cycle (say I_i) is a path-length-limited p-cycle if the following two conditions are held:*

$$z^i_b = q^i_b = 1, \qquad \exists \quad b \in E \tag{2.20}$$

$$\sum_{e \in E} d_e \cdot x^i_e - d_b \cdot z^i_b \leq h_r, \qquad \exists \quad r \in R, \exists \quad b \in E \tag{2.21}$$

Proof. Equation (2.20) indicates that at least one link b can be protected by I_i and it also desires to be protected by I_i. In inequality (2.21), $\sum_{e \in E} d_e \cdot x^i_e$ calculates the length of cycle circumference of I_i, which consists of all the on-cycle links. Then, the length of protection path for link b in I_i depends on the nature of link b:

- **On-cycle link**. $\sum_{e \in E} d_e \cdot x^i_e - d_b$ represents the protection path length for link b. Obviously, if it is less than h_r, then at least one line rate r can be assigned for I_i.
- **Straddling link**. There are two protection paths for link b: $v - u_1 - \ldots - u_n - u$ and $v - v_1 - \ldots - v_n - u$ (here, u_i and v_i indicate the intermediate nodes along the protection path). Thus the corresponding lengths of these two protection paths are $D^1_{vu} = d_{vu_1} + d_{u_1u_2} + \ldots + d_{u_nu}$ and $D^2_{vu} = d_{vv_1} + d_{v_1v_2} + \ldots + d_{v_nu}$, respectively, and they should satisfy $D^1_{vu} + D^2_{vu} = \sum_{(v,u) \in E} d_{vu} \cdot x^i_{vu}$. It should be noted that for each link $v - u$ in almost all the backbone topologies, the inequality principle is

satisfied that $d_{vu} \leq D^1_{vu}, D^2_{vu}$ [2]. Then, $\sum_{(v,u)\in E} d_{vu} \cdot x^i_{vu} - d_{vu} \geq \sum_{(v,u)\in E} d_{vu} \cdot x^i_{vu} - D^1_{vu}$, $\sum_{(v,u)\in E} d_{vu} \cdot x^i_{vu} - d_{vu} \geq \sum_{(v,u)\in E} d_{vu} \cdot x^i_{vu} - D^2_{vu}$. Thus, if inequality (2.21) is held, then the two protection paths of b in I_i can at least operate at line rate r.

Hence, I_i is a path-length-limited p-cycle if conditions (2.20) and (2.21) are held. □

Theorem 2.4.2. *A path-length-limited p-cycle can be found by constraint (2.22) if it exists, and its appropriate line rate can also be determined by constraint (2.22).*

$$\frac{\sum_{e\in E} d_e \cdot x^i_e - q^i_{vu} \cdot d_{vu}}{h_r} \leq \frac{h_{max}}{h_{min}} \cdot (1 - b^i_r) + b^i_r + \frac{d_{max}}{h_r} \cdot (1 - q^i_{vu}) \quad \forall i, \forall r, \forall v, \forall u, u > v \tag{2.22}$$

Proof. In constraint (2.22), x^i_{vu} represents whether link (v,u) is used as on-cycle link in I_i, and q^i_{vu} indicates whether link (v,u) desires to be protected by I_i. For an on-cycle link (v,u), the length of the corresponding protection path is $D_{vu} = \sum_{(v,u)\in E} d_{vu} \cdot x^i_{vu} - d_{vu}$, while for a straddling link (v,u), the lengths of the two protection paths are $D^1_{vu} = d_{vu_1} + d_{u_1u_2} + \ldots + d_{u_nu}$ and $D^2_{vu} = d_{vv_1} + d_{v_1v_2} + \ldots + d_{v_nu}$, respectively. The line rate assignment constraint depends on the lengths of protection paths for different types of links.

- **Link (v,u) with q^i_{vu} = 1.**
  1. **On-cycle link (v,u) with q^i_{vu} = 1.** Then length of protection path for link (v,u) should be shorter than h_{max}, *i.e.*, $D_{vu} = \sum_{(v,u)\in E} d_{vu} \cdot x^i_{vu} - d_{vu} \leq h_{max}$.

     The line rate b^i_r for D_{vu} is restricted by the following constraint:

     $$\frac{\sum_{e\in E} d_e \cdot x^i_e - d_{vu}}{h_r} \leq \frac{h_{max}}{h_{min}} \cdot (1 - b^i_r) + b^i_r \tag{2.23}$$

  2. **Straddling link (v,u) with q^i_{vu} = 1.** Based on the inequality principle, it is obvious that $d_{vu} \leq D^1_{vu}$, $d_{vu} \leq D^2_{vu}$. Thus, the line rate r for D^1_{vu} and D^2_{vu} also can be restricted by constraint (2.23).
- **Link (v,u) with q^i_{vu} = 0.** In this case, we need to guarantee that the line rate previously assigned still works. In other words, whatever the value of b^i_r, the

[2] For instance in German, European and NSFNET networks [91]. Note that only one link $8-10$ in COST239 network is 1.4% longer than $D^1_{(8)(10)} = d_{(8)(9)} + d_{(9)(10)}$ and only one link $24-27$ in US Backbone network is 1.0% longer than $D^1_{(24)(27)} = d_{(24)(28)} + d_{(28)(27)}$ [68, 69]. To simplify, we assume that all the links in COST239 and US Backbone networks studied in this work satisfy the inequality principle. However, future work should be done to deal with this situation, especially for the networks, where more links do not satisfy the inequality principle.

following constraint (2.24) is always held, which is derived from constraint (2.22) by restituting $q_{vu}^i = 0$.

$$\frac{\sum_{e\in E} d_e \cdot x_e^i}{h_r} \leq \frac{h_{max}}{h_{min}} \cdot (1 - b_r^i) + b_r^i + \frac{d_{max}}{h_r} \tag{2.24}$$

Let d_{max} indicate the longest links in a network topology, then the longest p-cycle circumference will be $(h_{max} + d_{max})$, thus for any p-cycle, $\sum_{e\in E} d_e \cdot x_e^i \leq h_{max} + d_{max}$. When $b_r^i = 0$, constraint (2.24) is held. When $b_r^i = 1$, it means that there exits a least a link b desiring to be protected by I_i, no matter it is on-cycle link or straddling link, we can get from Theorem 1 that $\sum_{e\in E} d_e \cdot x_e^i - d_b \leq h_r$. Since $d_b \leq d_{max}$, we have $\sum_{e\in E} d_e \cdot x_e^i \leq h_r + d_{max}$. As a result, we can see that constraint (2.24) is always satisfied for the case $q_{vu}^i = 0$ whatever the value of b_r^i, and the line rate previously assigned (restricted by the links with $q_{vu}^i = 1$) still works.

Thus, the path-length-limited p-cycle can be found with constraint (2.22) as well as its proper line rate. □

Considering all the situations that whether the link (v, u) has the desire q_{vu}^i to be protected by I_i, appropriate line rate is assigned for I_i with the constraint (2.22). This constraint will overcomes the shortcomings of extra CAPEX cost and infeasible solution in constraint (2.9). We use the novel constraint (2.22) to replace constraint (2.9) in the p-cycle design MILP model.

2.4.4 Discussion

The proposed MILP model enables to guarantee the optimal p-cycle design in transparent optical networks. Meanwhile, our MILP model can be easily extended to translucent or opaque optical networks with O/E/O regenerators [152]. In these optical networks, the introduction of O/E/O regenerators extends transmission reach and enables more flexible line rate assignments. However, the regenerators also add CAPEX cost. Thus, both extended transmission reach and added CAPEX cost need to be taken into account. These considerations can be formulated by adding two variables g_v and g_v^i, where g_v indicates whether a regenerator needs to be placed in node v and g_v^i indicates whether p-cycle I_i uses the regenerator in node v, respectively. Only objective function in equation (2.1) and line rate assignment constraint (2.22) need to be modified as follows:

$$\min \quad \theta_1 \cdot C_T + \theta_2 \cdot C_L + \theta_3 \cdot C_R \tag{2.25}$$

$$C_R = \sum_{v\in V} e_{O/E/O} \cdot g_v \tag{2.26}$$

Where $e_{O/E/O}$ is the cost of one O/E/O regenerator, and θ_3 is an adjustable parameters for weighting of C_R.

$$\frac{\sum_{e\in E} d_e \cdot x_e^i - q_{vu}^i \cdot d_{vu} - \sum_{v\in V} g_v^i \cdot D_R}{h_r} \leq \frac{h_{max}}{h_{min}} \cdot (1 - b_r^i) + b_r^i + \frac{d_{max}}{h_r} \cdot (1 - q_{vu}^i) \quad \forall i, \forall r, \forall v, \forall u, u > v \tag{2.27}$$

$$g_v^i \leq y_v^i, \qquad \forall i, \forall v \tag{2.28}$$

$$g_v \geq g_v^i, \qquad \forall i, \forall v \tag{2.29}$$

Here, we consider the impact of regenerators by introducing a constant extended distance D_R, then line rate assignment can be achieved by constraints (2.27)-(2.29). Moreover, these constraints involve Regenerator Placement Problem (RPP), which has been considered as a high complexity problem [40].

2.5 Algorithms for time-efficient MILP model

In this section, we develop two algorithms to solve the MILP model time-efficiently. Even though the proposed model manages to obtain the optimal solution in small network topologies, as the network size increases, it takes a long time to get the optimal solution. To increase the scalability, *Algorithm* 1 Graph Partitioning in Average (GPA) is designed to partition the network topology into small sub-graphs in average, then the optimal p-cycles can be obtained in different sub-graphs in parallel. We further observe that the number of required p-cycles (*i.e.*, $|I|$) in the MILP model largely affects computational time, and design *Algorithm* 2 Estimation of $|I|$ (EI) to estimate the enough number of required p-cycles. Then, the p-cycle results can be obtained by the proposed MILP model with the help of GPA and EI algorithms.

Algorithm 1: Graph Partitioning in Average (GPA) Algorithm

Input: Network topology $G(V, E)$ and traffic matrix, number of sub-graphs k
Output: The optimal p-cycles

1 calculate matrix W and D in $G(V, E)$, where W is the adjacency matrix of G and D is an $n \times n$ diagonal matrix composed of the degree of each node in G ;
2 compute the Laplacian matrix $L = D - W$;
3 compute the eigenvalues and eigenvectors of L;
4 choose k eigenvectors of L corresponding to the smallest k eigenvalues ;
5 partition $G(V, E)$ into sub-graphs in average using k-means algorithm [88] ;
6 distribute inter-links to be protected among these sub-graphs in average ;
7 solve the MILP model in Subsec. 2.4.1 for sub-graphs in parallel ;
8 obtain the optimal p-cycles.

2.5.1 GPA algorithm

Inspired by the graph partitioning method for multi-domain optical networks in [33], we propose a Graph Partitioning in Average algorithm based on spectral clustering [88] to perform concurrent computation in p-cycle design for MLR optical networks.

In GPA algorithm, we first compute the Laplacian matrix $L = D - W$ where D is the degree matrix and W is the adjacency matrix of graph $G(V, E)$, and obtain its eigenvalues and eigenvectors. Then, according to the number of sub-graphs (say k), we choose k eigenvectors corresponding to the k smallest eigenvalues, and apply k-means algorithm [88] to minimize the number of inter-links connecting different sub-graphs. We also use k-means algorithm to guarantee that the sub-graphs have as equal number of intra-links as possible, which is efficient for concurrent computation. Regarding the inter-links, we distribute them averagely to be protected by different sub-graphs so as to let the working links in each sub-graph as equal as possible. In each sub-graph, p-cycles are generated using MILP model in Subsec. 2.4 based on intra-links, inter-links to other sub-graphs, and the links connecting the nodes of inter-links in other sub-graphs. However, for a specific sub-graph, not all the links need to be protected, only intra-links in the p-cycle and partial inter-links are required to be protected.

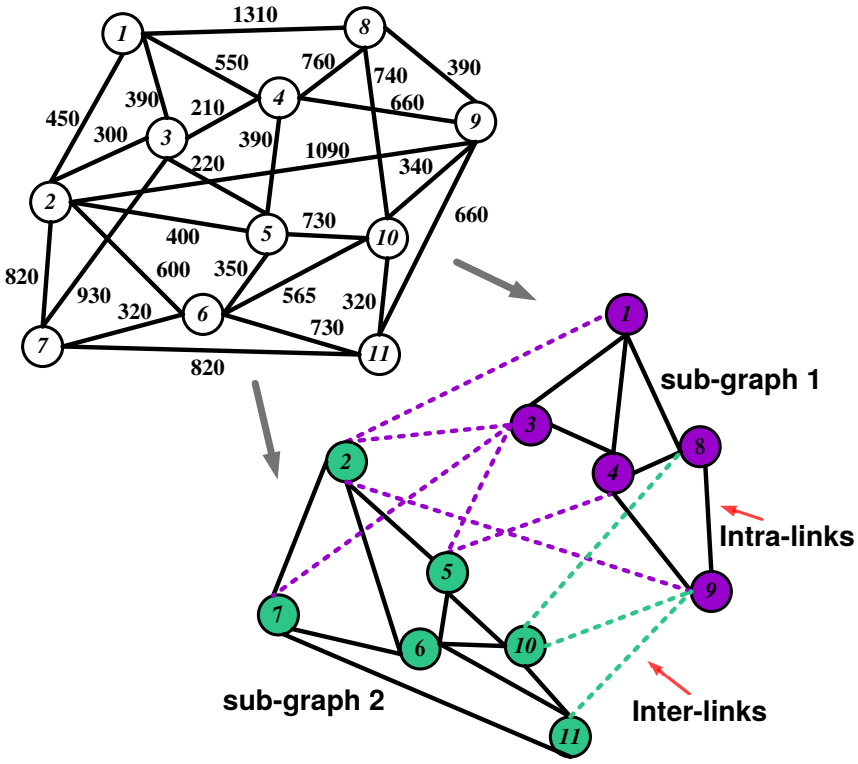

Figure 2.6: *2 sub-graphs partitioning of European COST239 Network.*

We give an example to illustrate the GPA algorithm with 2 sub-graphs partitioning in European COST239 network [151] in Fig. 2.6. In sub-graph-1, p-cycles are generated based on intra-links in sub-graph-1, inter-links (*i.e.*, (1,2), (3,2), (3,5), (3,7), (4,5), (8,10),

(9,10), (9,2) and (9,11)), and links connecting the nodes of inter-links in sub-graph-2 (*i.e.*, links (2,5), (2,7), (5,10), (7,11) and (10,11)). However, only a sub-set of inter-links (1,2), (3,2), (3,5), (3,7), (4,5) and (9,2) are chosen to be protected in sub-graph-1 so that sub-graph-1 and sub-graph-2 have the same number of working links (13 links). The p-cycles in sub-graph-2 can be obtained using the same method.

2.5.2 EI algorithm

Algorithm 2: Estimation of $|I|$ (EI) Algorithm

Input: Traffic matrix, transponder cost t_r at line rate $r \in R$
Output: The number $|I|$ of p-cycles required in MILP model

for *each link* $(v,u) \in E$ *with traffic load* l_{vu} **do**
  choose the p-cycles with cost-effective transponders to protect the traffic load l_{vu} ;
  calculate the total number of required p-cycles at 100 $Gbps$ with equation (2.30);
  calculate the total number of required p-cycles at 40 $Gbps$ with equation (2.31);
  calculate the total number of required p-cycles at 10 $Gbps$ with equation (2.32);
  sum the total number of p-cycles for protecting traffic loads l_{vu};
end
obtain the total number of required p-cycles for protecting all the traffic load with (2.33).

The value of $|I|$ should be sufficiently large to ensure that the proposed MILP model manages to obtain optimal solution. However, a larger $|I|$ will slow down the computational time. In [139], $|I|$ is estimated by tending to straddle the heaviest load links whose incident nodes have degrees larger than 2. But this method is not valid in our model, since they do not consider different protection capacity provided by different line rates in the p-cycles.

Table 2.3: *The method for choosing the number of cost-effective p-cycles.*

Traffic $l_{vu}(Gbps)$	$[1,10]$	$[11,20]$	$[21,40]$	$[41,50]$	$[51,100]$
Required p-cycle	⊕	⊕⊕	⊙	⊕⊙	⊗
Optimal cost t_r	1	2	2.5	3.5	3.75

⊕ 10 $Gbps$ p-cycle ⊙ 40 $Gbps$ p-cycle ⊗ 100 $Gbps$ p-cycle

In EI algorithm, we estimate the number of p-cycles $|I|$ required in MILP model according to traffic loads and transponder cost. For each link in $G(V,E)$, we choose the p-cycles with minimum transponder cost to protect the traffic load. Table 2.3 explains how to choose such p-cycles for protecting traffic load below 100 $Gbps$. Note that the

method can be simply applied for larger traffic load. We summarize the following Equations (2.30)-(2.32) to calculate the total number of required p-cycles to protect traffic load l_{vu} on link (v,u) at 10, 40 and 100 $Gbps$ line rates, respectively.

$$C_{100} = \lfloor \frac{l_{vu} + 49}{100} \rfloor \tag{2.30}$$

$$C_{40} = \lfloor \frac{max\{19 + l_{vu} - C_{100} \cdot 100, 0\}}{40} \rfloor \tag{2.31}$$

$$C_{10} = \lceil \frac{max\{9 + l_{vu} - C_{100} \cdot 100 - C_{40} \cdot 40, 0\}}{10} \rceil \tag{2.32}$$

If we assume that each link $(v,u) \in E$ is protected by one or multiple p-cycles, then the number of total required p-cycles for protecting all the links in $G(V,E)$ can be estimated as $\sum_{(v,u)\in E} C_{100} + C_{40} + C_{10}$ using (2.30), (2.31) and (2.32). However, each p-cycle has the ability to protect at least 3 links because there exists at least 3 links consisting the p-cycle. Thus, the total number of estimated p-cycles $|I|$ is obtained by equation (2.33). δ is added as a small positive integer in case that $|I|$ is not large enough because the 100 $Gbps$ line rate p-cycle does not always exists for protecting each link regarding to the transmission reach.

$$|I| = \delta + \frac{1}{3} \sum_{(v,u)\in E} (C_{100} + C_{40} + C_{10}) \tag{2.33}$$

2.6 Simulation and performance evaluation

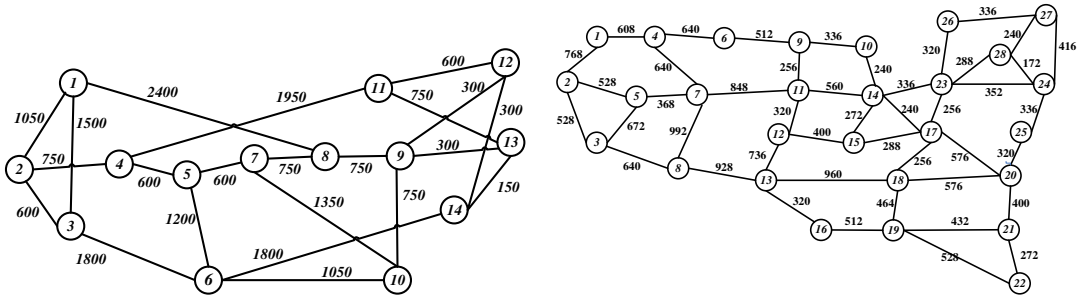

(a) The NSF network [46] (b) The US Backbone network [46]

Figure 2.7: *The network typologies used in the simulations.*

We use CPLEX 12.06 to solve the proposed MILP model on an Intel Core PC equipped with a 3.5 GHz CPU and 8 GBytes RAM. Three networks are used as test beds: European COST239 (11 nodes, 52 directed links, and average nodal degree 4.7 in Fig. 2.6 [18], NSFNET (14 nodes, 44 directed links and average nodal degree 3.1) [46] and US Backbone networks (28 nodes, 90 directed links and average nodal degree 3.2) [46]. In order to guarantee there always exists at least one protection path ($\leq$ 1800 km) for each

working link, the link length in real optical networks NSFNET and US Backbone is divided by 3 and 2, respectively. Note that the divisor can be modified according to the real network. In this study, we regard both of parameters θ_1 and θ_2 as 1.

We first evaluate the proposed algorithms for our p-cycle design MILP model in COST239, NSFNET and US Backbone networks. GPA algorithm partitions COST239, NSFNET and US Backbone networks into 2 sub-graphs, 3 sub-graphs and 4 sub-graphs scenarios, respectively. EI algorithm estimates enough number of required p-cycles in each sub-graph. Thereafter, we compare our method with p-cycle design without cycle enumeration in SLR optical networks [139] and p-cycle design with cycle enumeration in MLR optical networks [32].

2.6.1 The efficiency of GPA and EI

We first verify the efficiency of GPA and EI algorithms in COST239 network by solving the MILP model in four cases, *i.e.*, No GPA or EI, EI, GPA and EI+GPA. Due to the computational complexity, we use a server with 500 GBytes RAM for the cases of No GPA or EI, and EI. For the other cases, only the PC with 8 GBytes RAM is used. The traffic is generated between each two nodes in the network and the traffic amount is generated randomly. Note that the maximum amount of traffic load on each link is about 10, 30, 50 and 100 *Gbps* after Dijkstra's shortest-path routing, respectively.

The results are shown in Tab. 2.4. We observe that when neither GPA nor EI is used, the computation time increases dramatically as the amount of traffic increases. For the traffic large than 30 *Gbps*, even feasible solution can not be achieved after it exceeds the memory with computation time more than 70000 *s*. However, EI algorithm largely reduces computation time and achieves comparable solution compared with the optimal solution in case of No GPA or EI, but it still requires a long computation time for large traffic. Note that the solution 62 for the case of No GPA or EI is even worse because it is obtained with a relative gap 33.11% to the lower bound in CPLEX, and this value does not decrease from computation time 709.42 *s* to 71809.43 *s*. GPA algorithm can achieve sub-optimal solution and reduce computation time for larger traffic. Moreover, in more sub-graphs scenario, larger computation time reduction and bigger optimality gap are observed. Finally, we see that using both GPA and EI algorithm further reduces computation time and does not affect the quality of solution.

We can conclude that it is the GPA algorithm that mainly reduces computation time at the expense of introduced optimality gap, however, with both EI and GPA, more computation time reduction can be achieved.

2.6.2 p-Cycle design with GPA and EI

Then, we perform simulations with both GPA and EI algorithms in COST239, NSFNET, US Backbone networks, respectively. Maximum link traffic loads are about 50, 100, 150 and 200 *Gbps*, respectively. The results are shown in Fig. 2.8 and Tab. 2.5. The following

Table 2.4: *Computation time and optimality gap with different approaches (No EI or GPA, EI, GPA and GPA+EI) in COST239 network.*

Maximum link traffic		No EI or GPA	EI		GPA			GPA+EI		
		1 graph	1 graph	2 sub-graphs	3 sub-graphs	4 sub-graphs	2 sub-graphs	3 sub-graphs	4 sub-graphs
10 *Gbps*	Objective	38.5	38.5	49	63	75	49	63	75
	Time	421.38 *s*	169.43 *s*	24.43 *s*	6.24 *s*	2.12 *s*	1.34 *s*	1.35 *s*	0.33 *s*
	Gap *	–	0%	21.4%	38.8%	48.6%	21.4%	38.8%	48.6%
30 *Gbps*	Objective	62	58	63	67	80.5	63	67	80.5
	Time	71809.43 *s*	26124.48 *s*	54.14 *s*	10.78 *s*	23.75 *s*	2.62 *s*	2.13 *s*	0.63 *s*
	Gap *	–	0%	7.9%	13.4%	27.9%	7.9%	13.4%	27.9%
50 *Gbps*	Objective	–	76.5	80	80	94	80	80	94
	Time	79045.77 *s*	39468.50 *s*	6325.95 *s*	38.94 *s*	7.92 *s*	4.12 *s*	3 *s*	0.12 *s*
	Gap *	–	0%	4.4%	4.4%	18.6%	4.4%	4.4%	18.6%
100 *Gbps*	Objective	–	108	115.5	114	128.75	115.5	114	128.75
	Time	76213.17 *s*	46343.75 *s*	27135.7 *s*	7143.32 *s*	409.56 *s*	633.01 *s*	11.42 *s*	0.69 *s*
	Gap *	-	0%	6.5%	5.3%	16.2%	6.5%	5.3%	16.2%

- Feasible solution can not be obtained after exhausting all the memory. * Gap means the optimality gap to the solution with only EI algorithm.

two metrics are used to evaluate the performance of p-cycles in different sub-graphs scenarios:

- ***CAPEX Cost***: CAPEX cost is evaluated as total protection cost of p-cycles generated by the MILP model.
- ***Computation Time***: Computation time is used to evaluate the GPA and EI algorithms.

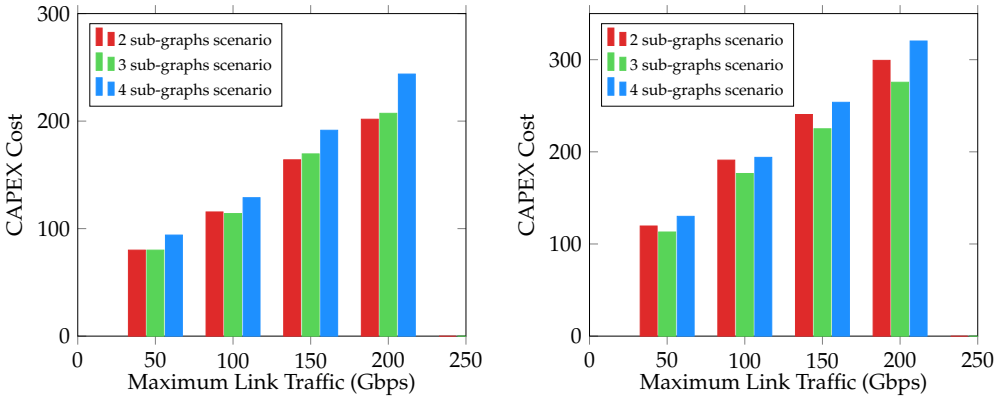

(a) p-Cycle Results in COST239 network

(b) p-Cycle Results in NSFNET network

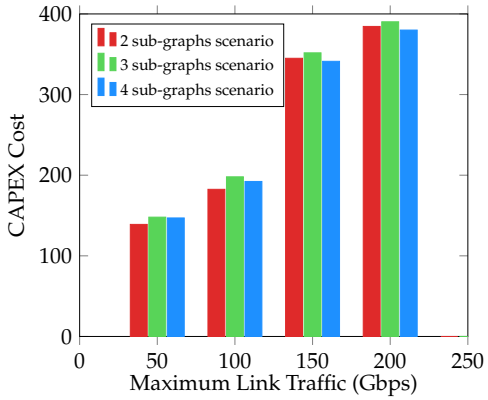

(c) p-Cycle Results in US Backbone network

Figure 2.8: *CAPEX cost of p-cycles in different sub-graphs scenarios in COST239, NSFNET and US Backbone networks.*

In COST239 network, we can see that the CAPEX cost in Fig. 2.8(a) increases with the number of sub-graphs, while the computation time in Tab. 2.5 is greatly reduced. Specifically, at low traffic, the CAPEX cost in 4 sub-graphs scenario is approximately 17% and 17% bigger at 50 *Gbps* traffic and 11% and 12% bigger at 100 *Gbps* traffic in comparison to 2 sub-graphs scenario and 3 sub-graphs scenario, respectively. Whereas, the computation time in these sub-graphs scenarios does not differ too much. As the traffic increases, the computation time in 2 sub-graphs scenario is 10446.41 s (nearly 3 h) at 150 *Gbps* traffic, and 53961.45 s (nearly 15 h) at 200 *Gbps* traffic, however, 4 sub-

Table 2.5: *Computation time in different sub-graphs scenarios in COST239, NSFNET and US Backbone networks.*

Traffic	2 sub-graphs	3 sub-graphs	4 sub-graphs
COST239			
50 *Gbps*	4.12 *s*	3 *s*	0.12 *s*
100 *Gbps*	633.01 *s*	11.42 *s*	0.69 *s*
150 *Gbps*	10446.41 *s*	507.12 *s*	109.13 *s*
200 *Gbps*	53961.45 *s*	5218.17 *s*	29.16 *s*
NSFNET			
50 *Gbps*	4.52 *s*	3.02 *s*	0.56 *s*
100 *Gbps*	463.17 *s*	8.85 *s*	2.03 *s*
150 *Gbps*	7426.19 *s*	59.78 *s*	4.42 *s*
200 *Gbps*	31676.07 *s*	100.78 *s*	253.34 *s*
US Backbone			
50 *Gbps*	9523.91 *s*	20.14 *s*	0.56 *s*
100 *Gbps*	12635.45 *s*	5681.74 *s*	3.64 *s*
150 *Gbps*	34786.53 *s*	13785.17 *s*	75.36 *s*
200 *Gbps*	57841.06 *s*	34561.04 *s*	1252.27 *s*

graphs scenario largely decreases the the computation time to only 109.13 *s* at 150 *Gbps* traffic and 29.16 *s* at 200 *Gbps* traffic with the low CAPEX cost expense, which are 16% and 28% bigger than that in 2 sub-graphs scenario, respectively.

In NSFNET network, it shows some differences from COST239 network. As we can see from Fig. 2.8(b) and Tab. 2.5, 3 sub-graphs scenario achieves the lowest CAPEX cost and also the shortest computation time. Specifically, at the traffic 50 *Gbps*, 100 *Gbps*, 150 *Gbps* and 200 *Gbps*, the CAPEX cost in 3 sub-graphs scenario is 5% and 2%, 8% and 9%, 6% and 11%, 5% and 2% lower than that in 2 sub-graphs scenario and 4 sub-graphs scenario, respectively. Compared with the computation time about 31676.07 *s*(nearly 8 *h*) at traffic 200 *Gbps* in 2 sub-graphs scenario, it is only 100.78 *s* in 3 sub-graphs scenario.

To show the scalability of our method, we also show the p-cycle results in US Backbone network in Fig. 2.8(c) and Tab. 2.5. It is worth noting that differences of CAPEX cost in various sub-graphs are quite small (less than 8%). The 4 sub-graphs scenario even spends lower CAPEX cost than 2 sub-graphs scenario and 3 sub-graphs scenario as we set a gap at high traffic (10% for 2 sub-graphs scenario and 5% for 3 sub-graphs scenario) in CPLEX to ensure the feasible solution with limited memory. Meanwhile, since the US Backbone network has big node set and link set, it takes a long time to generate p-cycles in 2 sub-graphs scenario, whereas the computation time in 4 sub-graphs scenario is largely reduced.

The p-cycle results on these three networks indicate that the proposed MILP model is efficiently solved with the help of GPA and EI algorithms, which permit to largely reduce computation time. p-Cycles are generated in the balance between CAPEX cost and

computation time in 4 sub-graphs scenario in COST239 and US Backbone networks, 3 sub-graphs scenario in NSFNET network.

2.6.3 Comparison to SLR-NCE-40 and MLR-CE

The *p*-cycle results in Subsec. 2.6.2 show that our *p*-cycle design MILP model is efficient to achieve relatively low cost and low computation time with GPA and EI algorithms. In this Subsection, we further compare our *p*-cycle results with *p*-cycle design without cycle enumeration in SLR optical networks in [139], and *p*-cycle design with cycle enumeration in MLR optical networks in [32]. For the sake of readability, we call the *p*-cycle design in [139] as SLR-NCE-40, the *p*-cycle design in [32] as MLR-CE and our *p*-cycle design as MLR-NCE.

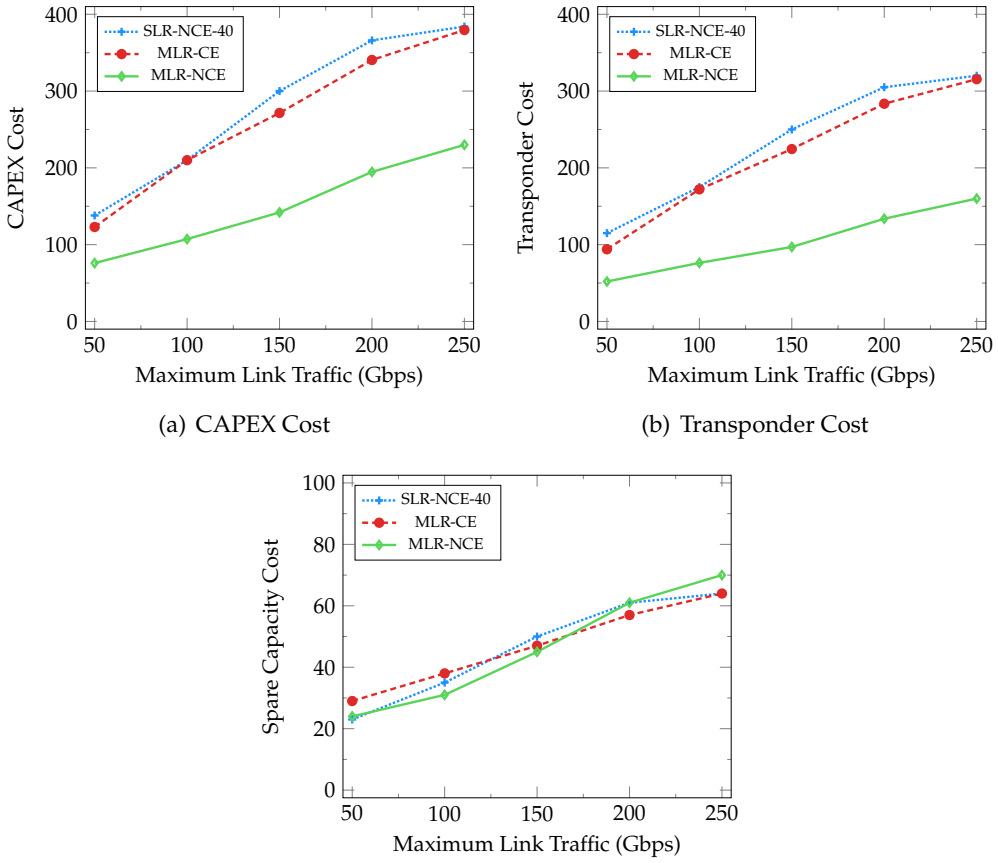

(a) CAPEX Cost

(b) Transponder Cost

(c) Spare Capacity Cost

Figure 2.9: *Protection cost comparison among SLR-NCE-40, MLR-CE and MLR-NCE in COST239 Network.*

To conduct the comparison, we use the results of MLR-NCE in 4 sub-graphs scenario in COST239 and US Backbone networks, and 3 sub-graphs scenario in NSFNET network. In SLR-NCE-40, only 40 *Gbps* line rate is assigned as either 10 *Gbps* or 100 *Gbps*

line rate for p-cycles will increase CAPEX cost. In order to make a fair comparison, we add the transmission reach on p-cycles with cycle-circumference-limited constraints in SLR-NCE-40 and MLR-CE. Thus, we have to remove the traffic in some links in the networks as SLR-NCE-40 and MLR-CE are not able to protect all the traffic with such transmission reach, which we discuss in Subsec. 2.4.3. It should be noted that our path-length-limited p-cycles in MLR-NCE enables to protect all the traffic in these networks. The traffic in the following links are removed: $1-8$, $2-9$, $4-8$, $4-9$ and $7-11$ in COST239 network, $1-8$, $4-11$ and $6-14$ in NSFNET network, $8-13$ in US Backbone network. The performance of SLR-NCE-40, MLR-CE and MLR-NCE are evaluated with the following metrics:

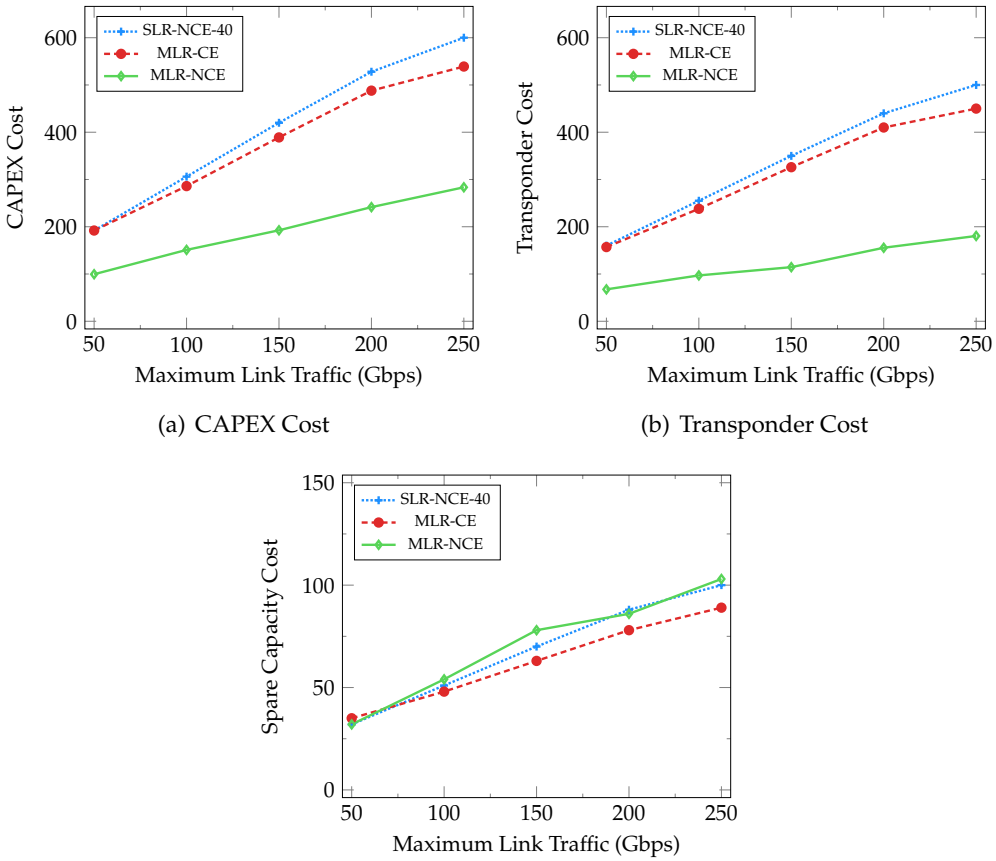

(a) CAPEX Cost

(b) Transponder Cost

(c) Spare Capacity Cost

Figure 2.10: *Protection cost comparison among SLR-NCE-40, MLR-CE and MLR-NCE in NSF Network.*

- ***CAPEX Cost***: CAPEX cost is the total protection cost for p-cycle design. It consists of transponder cost and spare capacity cost, both of which are weighted 1 in this study.
- ***Transponder Cost***: Transponder cost is the main protection cost in CAPEX cost.

- ***Number of Transponders***: In MLR-CE and MLR-NCE, transponders are set at 10/40/100 Gbps line rates, while in SLR-NCE-40, only 40 *Gbps* line rate is assigned. It is valuable to investigate the number of transponders used at each line rate.
- ***Spare Capacity Cost***: Spare capacity is pre-configured on each link in *p*-cycles for potential failures. It is also a significant metric for CAPEX cost.

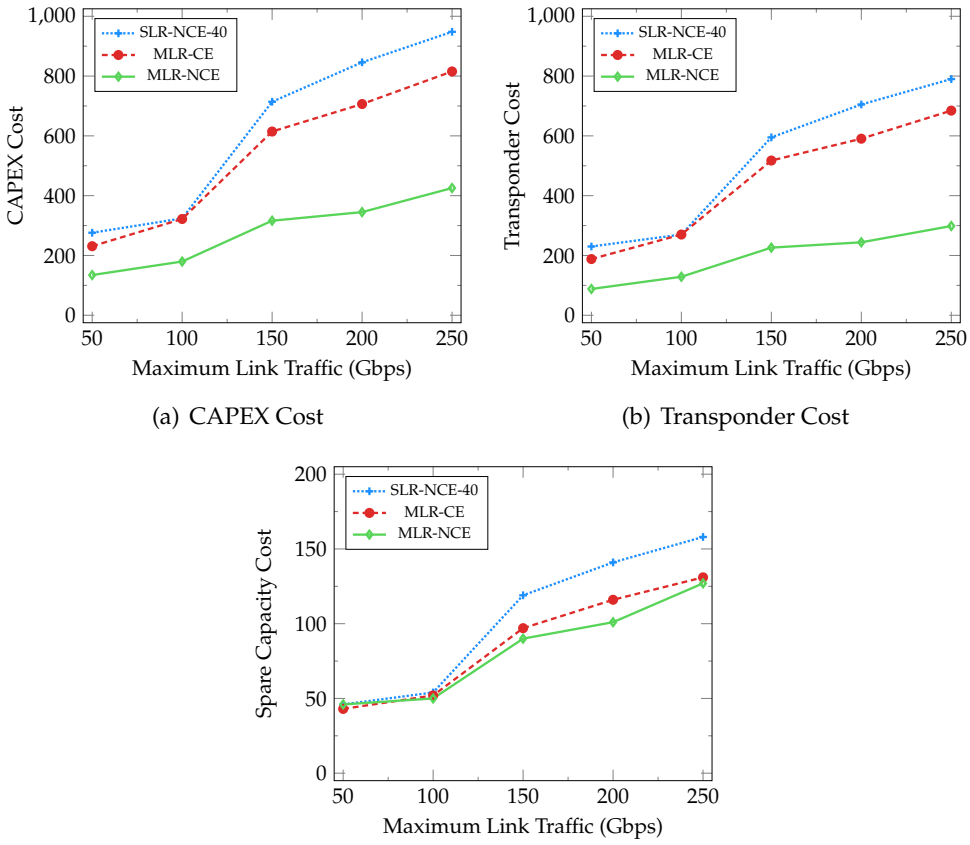

(a) CAPEX Cost

(b) Transponder Cost

(c) Spare Capacity Cost

Figure 2.11: *Protection cost comparison among SLR-NCE-40, MLR-CE and MLR-NCE in US Backbone Network.*

We observe that MLR-NCE achieves significantly lower CAPEX cost in comparison to SLR-NCE-40 and MLR-CE in all the network instances in Fig. 2.9(a), 2.10(a), 2.11(a). Specifically, compared with SLR-NCE-40 that generates *p*-cycles at 40 *Gbps* without cycle enumeration, MLR-NCE achieves CAPEX cost savings about 46.68% in average in COST239 network, 52.00% in average in NSFNET network and 53.18% in average in US Backbone network. The valuable CAPEX cost reduction comes from the optimal line rate assignment in MLR-NCE for MLR optical networks. Meanwhile, compared with MLR-CE that generates *p*-cycles at 10/40/100 *Gbps* with cycle enumeration, the average CAPEX cost savings in MLR-NCE are 43.40% in COST239 network, 48.76% in NSFNET network and 46.70% in US Backbone network. It indicates that more CAPEX

Table 2.6: *Number of transponders used at each line rate in SLR-NCE-40, MLR-CE and MLR-NCE.*

Traffic		COST239			NSFNET			US Backbone		
		SLR-NCE-40	MLR-CE	MLR-NCE	SLR-NCE-40	MLR-CE	MLR-NCE	SLR-NCE-40	MLR-CE	MLR-NCE
50 *Gbps*	⊕	—	34	2	—	12	0	—	18	16
	⊙	46	24	20	64	58	27	92	68	29
	⊗	—	0	0	—	0	0	—	0	0
	Total	46	58	22	64	70	27	92	86	45
100 *Gbps*	⊕	—	12	0	—	8	2	—	0	0
	⊙	70	64	26	102	80	38	108	96	47
	⊗	—	0	3	—	8	0	—	8	3
	Total	70	76	29	102	96	40	108	104	50
150 *Gbps*	⊕	—	12	2	—	6	12	—	10	0
	⊙	100	76	35	140	104	35	238	146	71
	⊗	—	6	2	—	16	4	—	38	25
	Total	100	94	39	140	126	51	238	194	96
200 *Gbps*	⊕	—	6	10	—	0	3	—	38	4
	⊙	121	102	42	176	140	55	282	140	54
	⊗	—	6	5	—	16	4	—	54	28
	Total	121	114	57	176	156	62	282	232	86
250 *Gbps*	⊕	—	8	11	—	10	8	—	32	11
	⊙	128	114	44	200	152	63	316	168	67
	⊗	—	6	6	—	16	4	—	62	32
	Total	128	128	61	200	178	75	316	262	110

⊕ 10 *Gbps* p-cycle ⊙ 40 *Gbps* p-cycle ⊗ 100 *Gbps* p-cycle

cost in MLR-NCE is reduced compared with SLR-NCE-40, this is because that SLR-NCE-40 uses only 40 *Gbps* line rate for all the *p*-cycles.

Next, we conduct clear presentation of transponder cost and spare capacity cost of the CAPEX cost in these three network instances. From Fig. 2.9(b)(c), 2.10(b)(c) and 2.11(b)(c), we can see that the transponder cost in MLR-NCE is much lower than in SLR-NCE-40 and MLR-CE, while the spare capacity cost does not show many differences. Specifically, comparing with SLR-NCE-40, MLR-NCE achieves average transponder cost savings about 55.71% in COST239 network, 63.12% in NSFNET network and 60.73% in US Backbone network, while, in comparison to MLR-CE, the average transponder cost savings in MLR-NCE is 51.85% in COST239 network, 60.62% in NSFNET network and 55.37% in US Backbone network. The spare capacity cost in MLR-NCE is reduced less than transponder cost. In comparison to SLR-NCE-40, the spare capacity cost savings are 1.54% and 15.95% in average in COST239 network and in US Backbone network, respectively. While compared with MLR-CE, the spare capacity cost savings are 4.71% and 4.01% in average in COST239 network and in US Backbone network, respectively. However, in NSFNET network, the spare capacity cost in MLR-NCE is even 3.61% and 10.74% bigger than in SLR-NCE-40 and MLR-CE, respectively. This is because that the inter-links among sub-graphs in MLR-NCE may be used several times, thus it requires more spare capacity.

It can be concluded that transponder cost savings mainly contributes to the reduction of CAPEX cost in MLR-NCE. As the transponders used in MLR-CE and MLR-NCE distribute in various line rates, then we make a deeper insight into the number of transponders used at various line rates in Tab. 2.6. We observe that SLR-NCE-40 uses the biggest number of transponders for *p*-cycle protection as only 40 *Gbps* line rate is assigned. Even though the *p*-cycles in MLR-CE and MLR-NCE are able to be assigned 10/40/100 *Gbps*, most of the transponders are set at 40 *Gbps* line rate, this is because 40 *Gbps* line rate for *p*-cycle reaches a compromise between the transmission reach and transponder cost. However, in MLR-NCE, fewer than half of the transponders in SLR-NCE-40 and MLR-CE are used. There are several reasons for the reduction. First of all, just enough transponders are laid for each *p*-cycle in MLR-NCE. Specifically, unlike the layout of transponders in SLR-NCE-40 or MLR-CE, in which one pair of transponders are laid on each protection path, only one transponder is laid on the node that incident to the protection path in MLR-NCE. Thus, it will reduce the number of transponders. Moreover, path-length-limited *p*-cycles are generated in MLR-NCE, while SLR-NCE-40 and MLR-CE generate the cycle-circumference-limited *p*-cycles, which bring extra protection cost, as discussed in Subsec. 2.4.3. In addition, MLR-NCE offers a way to directly generate the optimal *p*-cycles in MILP model without candidate cycle enumeration.

The comparison results demonstrate that our *p*-cycle design MLR-NCE achieves significant CAPEX cost savings (more than 40%) in comparison to SLR-NCE-40 and MLR-CE. The main cost savings comes from the transponder cost, which is further optimized in our path-length-limited *p*-cycles. Moreover, the *p*-cycle design MILP model manages to obtain the optimal solution which uses exactly the minimum CAPEX cost in *p*-cycle protection for MLR optical networks.

2.7 Conclusion

In this chapter, we investigate distance-adaptive p-cycle design for MLR optical networks. Based on path-length-limited p-cycles with transmission reach consideration on each protection path, we propose an MILP model to directly generate optimal p-cycles with the minimum CAPEX cost instead of candidate cycle enumeration. We also develop GPA algorithm and EI algorithm to make the proposed MILP model scalable, which are proved to largely reduce computation time. Extensive simulations demonstrate that our proposed p-cycle design achieves significant CAPEX cost savings for MLR optical networks, especially the transponder cost savings, in comparison to p-cycle design with SLR and p-cycle design with candidate cycle enumeration.

p-Cycle protection for MLR optical networks enables to offer a cost-effective protection scheme against single link failure. However, the proposed p-cycle protection with MLR no long works for the next generation EONs, which has more flexible spectrum allocation and new network services. In addition to the cost-effective network protection, reducing power consumption in EONs protection is of great importance as due to the introduction of advanced optical equipments BVTs and BV-OXCs [7, 84, 85, 129, 144]. We further address these issues in the next chapter.

Part III

p-Cycle Protection Schemes for EONs against Single Link Failure

Chapter 3

Power-Efficient Protection With Directed p-Cycles for Asymmetric Traffic in EONs

Contents

3.1 Introduction

Survivable green EONs need to address both survivability and energy consumption mainly comes from BVTs, BV-OXCs and OAs [129, 144]. Moreover, EONs begin to support new networking capabilities and demanding network services, such as anycast service, which brings *asymmetric traffic* supported by DCs, *e.g.*, CDNs, distributed storage and Virtual Private Networks (VPN) in addition to the conventional *symmetric traffic* [131]. It has been shown that compared with the symmetric approach,asymmetric traffic provisioning can bring resource savings (up to 50% of spectrum usage and up to 30% of CAPEX cost) in EONs [131], thus protection schemes that focus on asymmetric traffic have big potential to achieve power savings. However, most protection schemes for EONs only aimed at improving spectrum efficiency by solving the RSA problem [15, 16, 63, 116, 137, 141]. Even though these protection schemes benefit from efficient spectrum allocation, they may consume more power due to the absence of power-aware optimization. In EONs, the power consumption of optical devices . To meet the requirements on low power consumption, protection schemes for EONs need to take into account both power efficiency and spectrum efficiency.

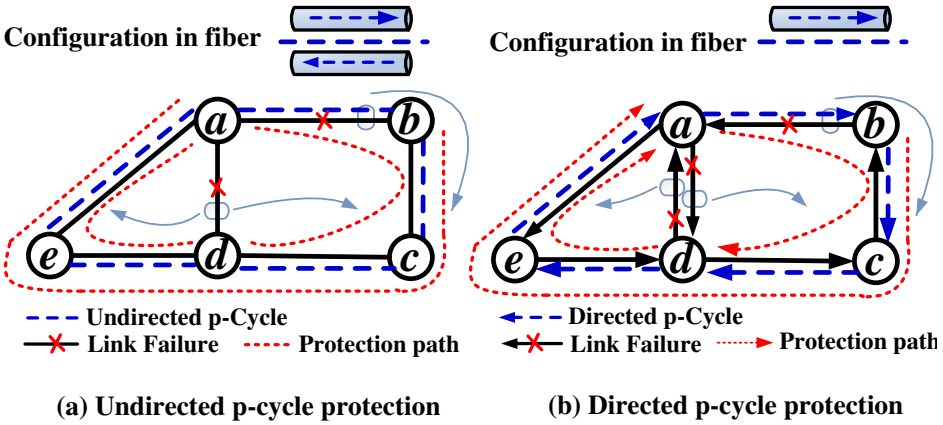

Figure 3.1: *Undirected and directed p-cycles.*

We study the directed p-cycle protection for EONs with asymmetric traffic services from a perspective of reducing power consumption. Figure 3.1 shows the directed p-cycle compared with the common undirected p-cycle. In undirected p-cycle, the same protection capacity is configured in the two directions according to the maximum traffic amount of the two directional links. It means that once the undirected p-cycle is determined, the same FSs and modulation format are configured in the two unidirectional fibers. Then, it enables to provide two units of protection capacity for each straddling link, as shown in Fig. 3.1(a) for $a - d$. However, directed p-cycle only configures protection capacity in one direction in the directed on-cycle links. Although a directed p-cycle provides one unit of protection capacity for each directed straddling link, *i.e.*, $a \rightarrow d$ and $d \rightarrow a$ in Fig. 3.1(b), it can distinguish directional links and provide different protection capacity for asymmetric traffic in two directions. Thus, the total protection capacity can be saved in directed p-cycles by efficiently allocating protection capacity for unidirec-

tional link. Hence, directed p-cycles have the potential to protect the asymmetric traffic in a power-efficient way.

In this chapter, we explore directed p-cycle design for EONs and investigate the power savings of directed p-cycles for protecting asymmetric traffic. Specifically, an MILP model called EDPC is formulated to minimize total power consumption in the considerations of directed cycle generation, spectrum allocation, modulation adaptation and protection capacity. Thereafter, to increase the scalability, EDPC is decomposed, and a two-step approach is proposed: an improved cycle enumeration and a simplified ILP model called De-EDPC. We conduct extensive simulations to evaluate the power savings of proposed directed p-cycles compared with undirected p-cycle in terms of diverse Traffic Asymmetry ($TASY$), Anycast Ratio (AR) and the number of DCs.

The key contributions of this proposition are summarized as follows:

- To the best of our knowledge, this is the first work on power-efficient protection for asymmetric traffic in EONs. Specifically, directed p-cycles are studied to earn power savings compared with traditional undirected p-cycles which are designed for symmetric traffic protection.
- Directed p-cycles are explored in the considerations of cycle generation, spectrum allocation and adaptive modulation formats under transmission reach limits.
- An MILP model is formulated to integrally generate directed p-cycles without candidate cycle enumeration so that it is guaranteed to reach the optimal solution. To enable the scalability, a two-step approach is developed to solve the MILP model.
- Extensive simulations are carried out to explore the power savings of directed p-cycles in terms of TASY, AR and the number of DCs in EONs. It is observed that directed p-cycles achieve power savings up to 47.9% compared with undirected p-cycles.

3.2 Related work

Table 3.1: *Protection schemes in EONs.*

Objective	Symmetric traffic	Asymmetric traffic (including anycasting)
Spectrum-efficient	[5-9]	[18], [20]
Energy-efficient	[10], [15-17]	—-

We summarize the existing protection schemes in EONs in terms of objective and traffic patterns in Tab. 3.1. Most of these schemes focus on improving spectrum efficiency for either symmetric or asymmetric traffic protection, and energy-efficient pro-

tection schemes have been aroused to be investigated for symmetric traffic recently. However, there is no work on the energy-efficient protection scheme for asymmetric traffic in the consideration of new asymmetric services in EONs.

For the energy-efficient protection schemes, the authors in [144] addressed that energy efficiency and resilience needed to be combined in network design, and they also identified several challenges for energy-efficient survivable optical network design. In [85], the protection scheme under hourly traffic bandwidth requirement was studied in an energy-efficient way in SLR, MLR and EON scenarios. In [84], the energy efficiency was evaluated in a Diff QoP scheme by providing different protection levels for each connection, according to the client protection requirements. An energy-efficient hybrid path protection approach based on adaptive routing was studied with the introduction of regenerator activation in [7]. The authors in [129] discussed three power-aware protection schemes, referred to 1+1 DP, 1:1 DP and SP, and evaluated the cost efficiency and energy efficiency improvement in EONs in comparison with WDM networks.

For the asymmetric traffic provisioning in EONs, the authors in [132] investigated both symmetric and asymmetric models for lightpath provisioning with Dedicated Path Protection (DPP), and they concluded that asymmetric traffic protection acquired significant savings of BVT up to 25%. The similar conclusion was obtained in [131], in which the authors concluded that asymmetric traffic provisioning can bring significant resource savings compared with the symmetric approach (up to 50% spectrum usage savings and 30% CAPEX cost savings). Moreover, for the new anycast service, the authors in [50] proposed a novel Tabu Search (TS) approach to simultaneously covering unicast and anycast traffic routing in EONs. In [49], the joint optimization of anycast and unicast traffic with survivability consideration in EONs was studied with the DPP scheme.

These path protection schemes may suffer from long restoration time when a failure happens, as a cooperation among several nodes is required to notify the affected connections, please refer to [57, 102, 150] for an extensive review of restoration time. As opposed to path protection, p-cycle protection schemes benefit from ring-like recovery speed, in which only the ending nodes of the failed link do the switching operation [52, 57]. Moreover, it earns mesh-like capacity efficiency, as both on-cycle links and straddling links can be protected [52]. These benefits of p-cycle protection have driven several related investigations in WDM optical networks even though it has not been implemented in current optical networks. Recently, p-cycle protection scheme has been studied for EONs [16, 63, 137, 141]. The authors in [63] investigated dynamic p-cycle protection in EONs with spectrum planning related to Protected Working Capacity Envelope (PWCE) p-cycle design and Hamiltonian cycle. They further studied Failure-Independent Path protection (FIPP) p-cycles taking into account routing, modulation formats and spectrum allocation in [16]. In [141], an ILP model for p-cycle design in EONs was developed to minimize total spectrum usage with load balancing in the working paths. An optimal design for p-cycle in EONs was studied with and without spectrum conversion in [137].

However, these p-cycle protection schemes only focused on minimizing spectrum

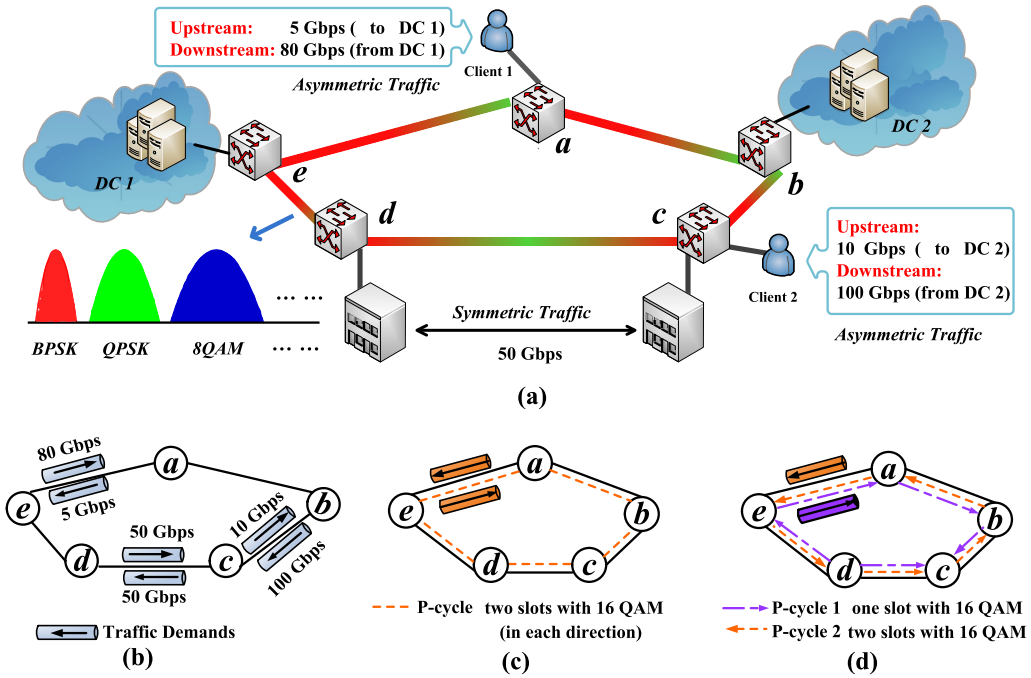

Figure 3.2: *(a) Symmetric and asymmetric services in EONs. (b) The traffic demands. (c) Undirected p-cycle protection. (d) Directed p-cycle protection.*

usage without the consideration of power consumption. Meanwhile, most of the studied p-cycle designs were undirected p-cycles, which were not efficient for asymmetric traffic protection in EONs with new services. Directed p-cycle design has been carried out by Jaumard et al. in WDM networks [62], in which they concluded that using undirected p-cycles for asymmetric traffic protection required more resources than directed p-cycles (45% higher for pure asymmetric traffic). Nevertheless, their directed p-cycle scheme is no longer valid for EONs due to the absence of spectrum allocation and modulation format adaptation. Hence, power-efficient directed p-cycle design is urgent to be investigated for protecting asymmetric traffic in EONs.

3.3 Problem statement

In EONs, asymmetric traffic between the clients and DCs become critical in addition to conventional symmetric traffic due to the new services such as anycast supported by DCs. Anycast service is defined as one to one-of-many transmission, in which client node v is fixed while the server node can be chosen among the set of admissible replica DCs [50]. Different from the conventional *symmetric traffic* which has the same traffic amount ($l^{Up} = l^{Down}$) in the upstream and downstream direction, *asymmetric traffic* differs in the two directions. More specifically, the upstream traffic l^{Up} is much smaller

than the downstream traffic l^{Down}. We introduce a parameter called $TASY$ to describe the average traffic asymmetry in the network by Eq. (3.1). Specifically, for each pair of source node s and destination node d, l_{sd} and l_{ds} indicate the traffic demand in each direction, then the traffic asymmetry $TASYsd$ between s and d is calculated by Eq. (3.1) [62]. $TASY = 0\%$ represents symmetric traffic while $TASY = 100\%$ indicates pure asymmetric traffic.

$$\begin{aligned} TASYsd &= \frac{max\{l_{sd}, l_{ds}\} - min\{l_{sd}, l_{ds}\}}{max\{l_{sd}, l_{ds}\} + min\{l_{sd}, l_{ds}\}} \times 100\% \\ TASY &= \overline{TASYsd} \end{aligned} \tag{3.1}$$

For instance, Fig. 3.2(a) illustrates the symmetric and asymmetric services in EONs. The symmetric service consists of associated bidirectional symmetric traffic with the same volume in each direction, and asymmetric service with asymmetric traffic has different volumes in the upstream and downstream directions. Figure 3.2(b) clearly illustrates the symmetric and asymmetric traffic. We assume EONs support contiguous FSs with spectral width 12.5 GHz. To protect the traffic with p-cycles, EONs support flexible FSs allocation and adaptive modulation formats (*i.e.*, BPSK, QPSK, 8-QAM and 16-QAM), which will be presented in the following part of power consumption. For simplicity, we assume that only 16-QAM with 50 $Gbps$ protection capacity per slot is used in this example. Figure 3.2(c) shows the conventional undirected p-cycle protection without consciousness of different traffic volumes in two directions, thus it assigns the same protection capacity (two FSs) in each direction to guarantee the protection. However, by distinguishing the different volume in each direction, directed p-cycle protection assigns one FS for clockwise p-cycle 1 and two FSs for counterclockwise p-cycle 2, as shown in Fig. 3.2(d). It is obvious that directed p-cycle protection earns protection capacity savings in terms of FSs so that it is more suitable and valuable to investigate directed p-cycles to protect asymmetric traffic in EONs.

The extra protection capacity allocated for asymmetric traffic in undirected p-cycles also causes more power consumption because the optical devices such as BVTs, BV-OXCs, and OAs consume power depending on the number of occupied FSs and modulation formats. However, power consumption can be reduced by allocating different FSs and modulation formats in directed p-cycles according to the traffic volume in each direction. Thus, we investigate directed p-cycle protection for asymmetric traffic with the objective of minimizing power consumption against single link failure in EONs. The main considerations in this study are summarized as follows:

1). Power Consumption

- e_m^{BVT} ***in BVT***: The power consumption of BVT for a single FS e_m^{BVT} in Eq. (3.2) depends on the Transmission Rate (TR) in terms of modulation formats, as shown in Tab. 3.2 [129].

$$e_m^{BVT} = 1.683 \cdot TR + 91.333 \tag{3.2}$$

Table 3.2: *Power consumption of a BVT with a single FS (12.5 GHz) at different modulation formats [129]*

Modulation Formats	TR (Gbps)	Power Consumption (W)
BPSK	12.5	112.374
QPSK	25	133.416
8QAM	37.5	154.457
16QAM	50	175.498

- e_v^{OXC} ***in BV-OXC***: The power consumption of a BV-OXC e_v^{OXC} in Eq. (3.3) depends on its nodal degree D_v, the add/drop degree α and the additional contributions (*e.g.*, power supply, control cards) [129]. Here, we treat add/drop degree α as 9 at each node, and it can be demonstrated that, assuming 1×9 WSSs.

$$e_v^{OXC} = 85 \cdot D_v + 100 \cdot \alpha + 150 \tag{3.3}$$

- e_a^{EDFA} ***in OA***: Erbium Doped Fiber Amplifier (EDFA) is set as OA with span distance 80 km between two neighboring EDFAs. The number of EDFAs varies on each link depending on the link length d_a. We assume that an EDFA consumes 100 W per direction [29, 129]. Then, power consumption of EDFAs e_a^{EDFA} along link a is calculated in Eq. (3.4).

$$e_a^{EDFA} = \lfloor \frac{d_a}{80} + 1 \rfloor \cdot 100 \tag{3.4}$$

2). FSs Allocation

- ***Spectrum continuity***: We assume that there is no spectrum conversion in the network. Thus, all the links in the same p-cycle should be assigned the same FSs.
- ***Spectrum contiguousness***: We assume that the FSs allocated to the p-cycles are adjacent on the optical spectrum except the required GB. Note that in order to efficiently utilize the spectrum resources, the p-cycles can share the same FSs if they do not have any common link.

3). Modulation Format Adaptation

- ***Protection capacity***: We consider the modulation format set M with BPSK, QPSK, 8-QAM and 16-QAM, then the protection capacity of one FS with each modulation format in M is 12.5, 25, 37.5 and 50 $Gbps$, respectively [129].
- ***Transmission reach***: The corresponding maximum transmission reaches of these modulation formats are assumed to be 9600, 4800, 2400 and 1200 km, respectively [146]. Note that in addition to the modulation formats, the maximum transmission reaches also depend on the exact spectral bandwidth that has to be reserved for the optical signal generated by the BVTs [104].

Table 3.3: *Parameters and variables in MILP model in* ***Chapter*** *3.*

Network Sets and Parameters	
I	The p-cycle set with maximum number $\|I\|$ allowed in EDPC, I_i indicates i-th p-cycle in I.
$G(V, A)$	Network topology with node set V and link set A.
N_v	The set of adjacent nodes of a node v.
M	The available modulation level set, we use $m = 0, 1, 2$ and 3 to indicate BPSK, QPSK, 8QAM and 16QAM, respectively.
d_{vu}	The length between node v and node u in $G(V, A)$.
L_{max}	The biggest link length in $G(V, A)$.
TR_m	The available bandwidth provided by one slot at modulation level m, which is 12.5, 25, 37.5 and 50 $Gbps$ for BPSK, QPSK, 8-QAM and 16-QAM, respectively.
e_m^{BVT}	The power consumption of the BVT at modulation m.
e_v^{OXC}	The power consumption of the BV-OXC at node v.
e_a^{EDFA}	The power consumption of all the EDFAs on link a.
h_m	Maximum transmission reach at modulation level m, which is 9600, 4800, 2400 and 1200 km for BPSK, QPSK, 8-QAM and 16-QAM, respectively [16]. h_{max}=9600 km, and h_{min}=1200 km.
N_G	The GB with one FS.
B	Set of FSs on each fiber link and $\|B\|$ is the total number of available FSs.
l_{vu}	Traffic load on unidirectional link $v \to u$ after routing.
β	A pre-defined fractional constant, $\frac{1}{\|V\|} \geq \beta > 0$.
Variables in EDPC	
$x_{vu}^i \in \{0, 1\}$	Equals 1 if link $v \to u$ is used by I_i, and 0 otherwise.
$y_v^i \in \{0, 1\}$	Equals 1 if node v is crossed by I_i, and 0 otherwise.
$f_v^i \in \{0, 1\}$	Virtual *voltage* value of node v in I_i.
$o_v^i \in \{0, 1\}$	Equals 1 if node v is the root node in I_i, and 0 otherwise.
$b_m^i \in \{0, 1\}$	Equals 1 if I_i operates at modulation level m, and 0 otherwise.
$q_{vu}^i \in \{0, 1\}$	Equals 1 if link $v \to u$ desires to be protected by I_i, and 0 otherwise.
$c_{ij} \in \{0, 1\}$	Equals 1 if I_i and I_j have at least one common link, and 0 otherwise.
$n_i \in [0, 32]$	The number of occupied FSs of I_i. The maximum FSs is 32 due to the capacity limitation in BVT.
$s_i \in [0, \|B\| - 1]$	The starting index of FSs in I_i. *e.g.*, one p-cycles uses FSs 1, 2 and 3, then the starting index of FSs s_i is 0, and the number of occupied FSs n_i is 3.
$o_{ij} \in \{0, 1\}$	Equals 1 if the starting index of FSs in I_i is smaller than that in I_j, and 0 otherwise.
$t_b \in [0, \|B\|]$	The maximum index of occupied FSs in all the p-cycles.
$\pi_{vu}^{im} \in [0, 32]$	The number of FSs provided by I_i to protect link $v \to u$ at modulation level m.
$n_{vu}^i \in [0, 32]$	The number of occupied FSs of I_i on link $v \to u$.

3.4 MILP formulation

In this section, we develop an MILP model called EDPC to design power-efficient directed p-cycles for EONs. Inspired by the advantage of cycle generation method without candidate cycle enumeration in [69], we explore directed p-cycle generation so that the proposed EDPC model is guaranteed to reach the optimal solution. An EON can be modeled as a digraph $G(V, A)$, which has the OXCs set V and the directed links set A. Between two adjacent optical OXCs, there are two directed links, *e.g.*, link $v \rightarrow u$ denotes the directed link from node v to node u, which also can be represented by $a \in A$. The notations are in Tab. 3.3. For the sake of readability, we use $\forall i$, $\forall v$, $\forall u$, $\forall m$, and $\forall a$ to denote $\forall i \in I$, $\forall v \in V$, $\forall u \in N_v$, $\forall m \in M$, and $\forall a \in A$, respectively.

3.4.1 MILP model

Objective:

$$\min \quad \theta_1 \cdot (E_{BVTs} + E_{OXCs} + E_{EDFAs}) + \theta_2 \cdot t_b \tag{3.5}$$

The objective is to minimize the total power consumption of directed p-cycles and the maximum index of FSs usage t_b. The optimization of t_b guarantees the *spectrum contiguousness* and potential spectrum sharing among p-cycles. θ_1 and θ_2 are adjustable parameters for weighting of these two metrics.

The total network power consumption is composed of:

1) E_{BVTs}: **The power consumption of BVTs**

$$E_{BVTs} = \sum_{i \in I} \sum_{m \in M} \sum_{a \in A} 2 \cdot e_m^{BVT} \cdot \pi_a^{im} \tag{3.6}$$

E_{BVTs} is introduced at the starting node and ending node of the protection path. It is the product of the number of occupied FSs and the power consumption of a single FS corresponding to the modulation format in Tab. 3.2.

2) E_{OXCs}: **The power consumption of OXCs**

$$E_{OXCs} = \sum_{i \in I} \sum_{v \in V} \sum_{u \in N_v} \frac{n_{vu}^i}{B} \cdot e_v^{OXC} \tag{3.7}$$

E_{OXCs} is calculated based on the proportion of resources that the protection path occupies in the links (number of occupied FSs with respect to the total FSs in a fiber).

3) E_{EDFAs}: **The power consumption of EDFAs**

$$E_{EDFAs} = \sum_{i \in I} \sum_{a \in A} \frac{n_a^i}{B} \cdot e_a^{EDFA} \tag{3.8}$$

E_{EDFAs} is calculated in the same way as E_{OXCs}.

Constraints:

The constraints in EDPC can be classified into **Directed cycle generation constraints** (3.9)-(3.13), **FSs allocation constraints** (3.18)-(3.22), **modulation adaptation constraints** (3.23)-(3.24) and **protection capacity constraints** (3.25)-(3.29).

1). Directed cycle generation constraints

Constraint (3.9) ensures that at most one unidirectional link between two nodes can be used in a directed p-cycle. Constraints (3.10) and (3.11) ensure that if node v is crossed by a p-cycle, then it must own one incoming link and one outgoing link. In order to guarantee that only a single cycle is generated, we further formulate constraints (3.12) and (3.13) to eliminate other cycles with *voltage* conflict and make sure the generated cycle is a connected graph, as shown in Fig. 3.3. These constraints enable to generate single directed p-cycle with either clockwise or counterclockwise. We prove it in Theorem 3.4.1.

$$x^i_{vu} + x^i_{uv} \leq 1, \qquad \forall i, \forall v, \forall u \tag{3.9}$$

$$\sum_{u \in N_v} x^i_{uv} - \sum_{u \in N_v} x^i_{vu} = 0, \qquad \forall i, \forall v \tag{3.10}$$

$$y^i_v = \sum_{u \in N_v} x^i_{vu}, \qquad \forall i, \forall v \tag{3.11}$$

$$f^i_u - f^i_v + o^i_u \geq (1+\beta) \cdot x^i_{vu} - 1, \qquad \forall i, \forall v, \forall u \tag{3.12}$$

$$\sum_{v \in V} o^i_v \leq 1, \qquad \forall i \tag{3.13}$$

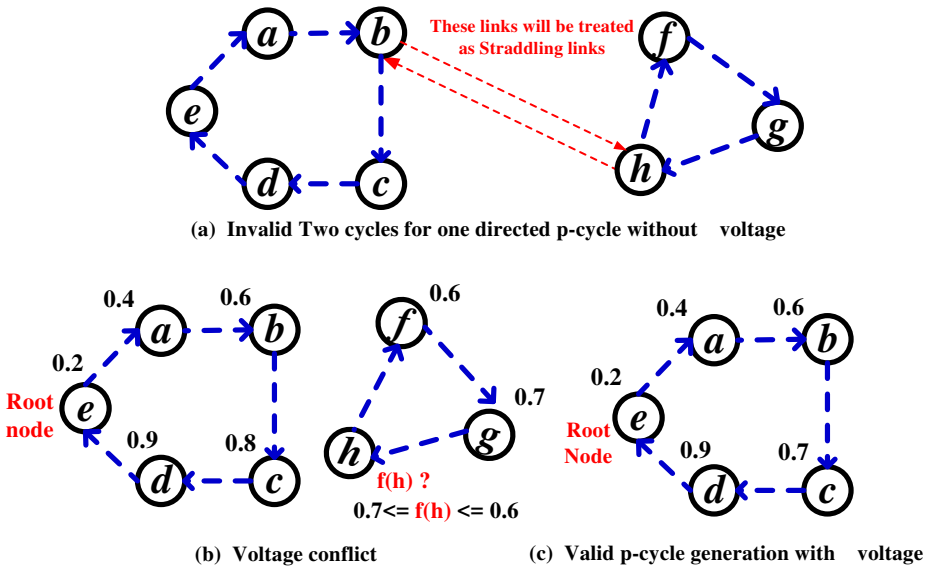

Figure 3.3: *Single directed cycle generation with voltage and root.*

Theorem 3.4.1. *Constraints (3.9)-(3.13) guarantee to generate a single directed p-cycle with either clockwise or counterclockwise for each $i \in I$.*

Proof. According to constraints (3.9)-(3.11), for each $i \in I$, each node in I_i either has both an incoming link and an outgoing link, or does not have any adjacent link. Thus, a single directed cycle or several ones are generated for I_i (clockwise or counterclockwise). In the latter case, several directed cycles can not be used as one directed p-cycle. As we can see from Fig. 3.3(a), if these two cycles are regarded as one p-cycle I_i, the links $b \rightarrow h$ and $h \rightarrow b$ would have the potential to be protected by I_i because nodes b and h are crossed by I_i. Obviously, this is not correct.

Next, we prove by contradiction that only a single cycle is permitted with the help of constraints (3.12) and (3.13). Without loss of generality, we suppose that two directed cycles are generated by constraints (3.9)-(3.11) in Fig. 3.3(b), and node r is the only *root node*, where the value beside each node indicates the corresponding voltage value. We can find that the cycle consisting of nodes e, g, h can not exist due a voltage conflict explained as follows. Since there is no root node, *i.e.*, $o_e^i = 0$, $o_h^i = 0$ and $o_g^i = 0$, we can get the following inequalities by using constraint (3.12),

$$f_e^i - f_h^i \geq \beta \tag{3.14}$$
$$f_g^i - f_e^i \geq \beta \tag{3.15}$$
$$f_h^i - f_g^i \geq \beta \tag{3.16}$$

Adding the three inequalities, a voltage conflict occurs: $0 \geq 3\beta$.

However, constraints (3.12) and (3.13) permit to generate a single cycle (*e.g.*, the cycle consisting of nodes a, b, c, d, r) with the root node in Fig. 3.3(c). From constraint (3.12), we can see that for each directed link, ending node has a bigger voltage than the starting node except the link $d \rightarrow r$ with ending root node e. However, by assigning $o_r^i = 1$ to the root node, the previous voltage conflict problem can be avoided. Thus, constraint (3.12) can be rewritten as

$$f_r^i - f_d^i + 1 \geq \beta \tag{3.17}$$

Here, root node r is able to have a smaller voltage than node d, then we will get $1 \geq \beta$ instead by adding all the inequalities. Thus, the proof follows. □

2). FSs allocation constraints

Constraints (3.18)-(3.20) allocate the order of FSs for each p-cycle. Constraint (3.18) indicates whether two p-cycles have any common link. Constraint (3.19) permits to compare the starting index of occupied FSs of each two p-cycles. Constraint (3.20) avoids spectrum conflict by adding one GB N_G and also ensures that two p-cycles can share the same FSs if they do not have any common link. Constraint (3.21) implies the maximum index of FSs, which is minimized in Eq. (3.5) to ensure *spectrum contiguousness*. Constraint (3.22) indicates the *spectrum continuity* along the links in

one p-cycle.

$$x_a^i + x_a^j - 1 \leq c_{ij}, \qquad \forall i,j,i \neq j, \forall a \tag{3.18}$$
$$o_{ij} + o_{ji} = 1, \qquad \forall i,j,i \neq j \tag{3.19}$$
$$s_i + n_i + N_G - s_j \leq B \cdot (2 - o_{ij} - c_{ij}), \qquad \forall i,j,i \neq j \tag{3.20}$$
$$s_i + n_i \leq t_b, \qquad \forall i \tag{3.21}$$
$$n_a^i = x_a^i \cdot n_i, \qquad \forall i, \forall a \tag{3.22}$$

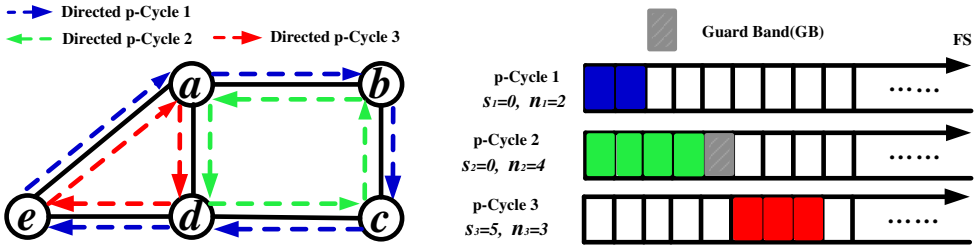

Figure 3.4: *FSs allocation for different directed p-cycles.*

An example of FSs allocation for three p-cycles is shown in Fig. 3.4. In each p-cycle, the same FSs are used on all the links. In addition, p-cycle 1 and p-cycle 2 can share some FSs with index 1 and 2 as they do not have any common link. However, for p-cycle 2 and p-cycle 3 with the common link $a \rightarrow d$, GB with index 5 should be reserved between the occupied FSs.

3). Modulation adaptation constraints

Constraint (3.23) guarantees modulation format selection with maximum transmission reach consideration. Constraint (3.24) ensures that only one modulation format can be assigned for one p-cycle.

$$\frac{\sum_{a \in A} d_a \cdot x_a^i - q_a^i \cdot d_a}{h_m} \leq \frac{h_{max}}{h_{min}} \cdot (1 - b_m^i) + \frac{L_{max}}{h_m} \cdot (1 - q_a^i) + b_m^i, \qquad \forall i, \forall m, \forall a \tag{3.23}$$
$$\sum_{m \in M} b_m^i \leq 1, \qquad \forall i \tag{3.24}$$

Note that the modulation format of a p-cycle is selected depending on the length of each protection path instead of the circumference of p-cycle so that more flexible modulation format can be assigned to ensure power-efficient p-cycle design. For instance, a p-cycle whose circumference exceeds 1200 km still can be assigned with 16-QAM if all of its protection paths are shorter than 1200 km. This is called path-length-limited p-cycle, which has the advantage over cycle-circumference-limited p-cycle as studied in [69, 78].

4). Protection capacity constraints

Constraints (3.25) and (3.26) indicate the desire of link $v \rightarrow u$ to be protected by I_i, providing that its two ending nodes v and u are crossed by I_i, and it is not an on-cycle link. Note that both the on-cycle links and straddling links are guaranteed to be protected only when they desire to be protected. Constraint (3.27) indicates the protection capacity of FSs that provided by I_i at modulation level m to protect link a. Constraint (3.28) ensures the maximum capacity of a BVT is 400 $Gbps$ [129]. Constraint (3.29) ensures 100% single link failure protection.

$$q_{vu}^{i} \leq \frac{1}{2}(y_v^i + y_u^i), \qquad \forall i, \forall v, \forall u \tag{3.25}$$

$$q_a^i \leq 1 - x_a^i, \qquad \forall i, \forall a \tag{3.26}$$

$$\pi_a^{im} \leq q_a^i \cdot b_m^i \cdot n_i, \qquad \forall i, \forall m, \forall a \tag{3.27}$$

$$\pi_a^{im} \cdot TR_m \leq 400, \qquad \forall i, \forall m, \forall a \tag{3.28}$$

$$\sum_{i \in I} \sum_{m \in M} \pi_a^{im} \cdot TR_m \geq l_a, \qquad \forall a \tag{3.29}$$

In order to ensure linearity, constraints (3.22) and (3.27) are rewritten as constraints (3.30) and (3.31), respectively.

$$\Longrightarrow \begin{cases} n_a^i \leq n_i, & \forall i, \forall a \\ n_a^i \leq x_a^i \cdot 32, & \forall i, \forall a \\ n_a^i \geq n_i - (1 - x_a^i) \cdot 32, & \forall i, \forall a \end{cases} \tag{3.30}$$

$$\Longrightarrow \begin{cases} \pi_a^{im} \leq n_i, & \forall i, \forall m, \forall a \\ \pi_a^{im} \leq q_a^i \cdot 32, & \forall i, \forall m, \forall a \\ \pi_a^{im} \leq b_m^i \cdot 32, & \forall i, \forall m, \forall a \end{cases} \tag{3.31}$$

Note that $|I|$ (the maximum number of p-cycle allowed in EDPC) is a predetermined parameter. It should be sufficiently large to ensure that the proposed EDPC manages to obtain the optimal solution. However, a larger $|I|$ will increase the execution time because for a given network the number of variables and constraints increases largely with $|I|$. For solving the EDPC, we set the number of p-cycles $|I|$ based on the protection capacity limitation in BVT. For each $a \in A$, we choose the possible number of p-cycles (with 400 $Gbps$) to protect it. Then, the total number of p-cycles $|I|$ can be estimated by Eq. (3.32) considering that a p-cycle can protect at least 3 links. In addition, a small positive integer δ is added in case that $|I|$ is not large enough.

$$|I| = \delta + \frac{1}{3} \sum_{a \in A} \lceil \frac{l_a}{400} \rceil \tag{3.32}$$

3.4.2 Discussion

In the proposed EDPC, directed p-cycles are designed with the objective of minimizing the total power consumption. As the power optimization has the priority over

the spectrum optimization, it may occur that more FSs are utilized in order to satisfy lower power consumption. Thus, there is a tradeoff between power and spectrum optimization when designing the p-cycle protection scheme for EONs. The model can be extended to represent the conventional p-cycle design without power consideration for asymmetric traffic protection by redefining the objective function of power consumption to total spectrum usage as follows:

$$\min \qquad \theta_1 \cdot S_{Total} + \theta_2 \cdot t_b \tag{3.33}$$

$$S_{Total} = \sum_{i \in I} \sum_{a \in A} n_a^i \tag{3.34}$$

Here, θ_1 and θ_2 are two adjustable parameters for the weights of total FSs allocated for protection capacity and the maximum index of the occupied FSs.

3.5 A two-step approach

Owing to the absence of candidate cycle enumeration, EDPC can reach the optimal solution, but its high computational complexity causes the scalability problem. This is why we decompose it into a two-step approach: improved cycle enumeration and a simplified ILP model called De-EDPC. As shown in the flow chart in Fig. 3.5, improved cycle enumeration is implemented by a Promising Power-efficient p-Cycles Selection (PPCS) algorithm to pre-compute the candidate cycle set for De-EDPC, while the latter is a simplified formulation decomposed from EDPC.

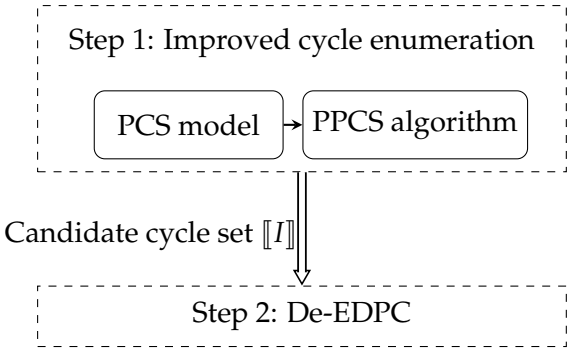

Figure 3.5: *Flow chart for the two-step approach.*

3.5.1 Improved cycle enumeration

The main idea of the improved cycle enumeration is that we select just enough p-cycles with different circumferences corresponding to maximum transmission reach limits so that the selected p-cycles for De-EDPC can be assigned diverse modulation formats power-efficiently. Thus, PPCS algorithm is developed to pre-compute the candidate cycle set and reduce the computation complexity for De-EDPC model, which will be

explained in detail in Subsec. 3.5.2. However, the method in [36] enumerates a large complete set $[\![\hat{I}]\!]$ of p-cycles, which results in high computation complexity. So we develop the following p-Cycle Selection (PCS) ILP model to select just enough p-cycles from $[\![\hat{I}]\!]$. The parameters and variables are shown in Tab. 3.4. The objective of PCS in (3.33) is to minimize the total number of links in all the selected p-cycles. Constraint (3.36) ensures that the selected p-cycles should be able to protect all the links that can be initially protected by p-cycles in the complete candidate cycle set $[\![\hat{I}]\!]$.

Table 3.4: *Additional notations in PCS*

Network Sets and Parameters in PCS	
$[\![\hat{I}]\!]$	Complete candidate cycle set obtained by the method in [36].
$x_a^i \in \{0,1\}$	Equals 1 if cycle $\hat{I}_i$ crosses link a, and 0 otherwise.
$z_a^i \in \{0,1\}$	Equals 1 if cycle $\hat{I}_i$ can protect link a, and 0 otherwise.
Variables in PCS	
$w_i \in \{0,1\}$	Equals 1 if cycle $\hat{I}_i$ is selected from $[\![\hat{I}]\!]$, and 0 otherwise.

$$min \quad \sum_{i \in [\![\hat{I}]\!]} \sum_{a \in A} w_i \cdot x_a^i \tag{3.35}$$

$$\sum_{i \in [\![\hat{I}]\!]} w_i \cdot z_a^i \geq z_a^i, \forall i, \forall a \tag{3.36}$$

Algorithm 3: PPCS Algorithm

Input : $G(V, A)$, h_m, $\forall m \in M$
Output: Selected candidate cycle set $[\![I]\!]$

```
1  for m ∈ M do
2      if m < 3 then
3          enumerate the complete cycle set [[Î]] whose circumference in the range
             (h_{m+1}, h_m] using the approach in [36];
4      end
5      else
6          enumerate the complete cycle set [[Î]] whose circumference in the range (0,
             h_3] using the approach in [36];
7      end
8      solve the PCS model with the complete cycle set [[Î]];
9      store the selected cycles obtained from PCS model in [[I]];
10 end
11 output [[I]]
```

Algorithm 3 shows the PPCS procedure. Considering the different maximum transmission reaches of modulation format set M, *Lines* 2-5 explain how to enumerate the complete cycle set with different circumferences. *Line* 6 performs PCS model to select just enough cycles from the enumerated cycles. We store the selected cycles in $[\![I]\!]$.

Thus, we obtain the candidate cycles with different circumferences for De-EDPC. For the PPCS algorithm, we only use it once to obtain the candidate cycle set in the network initialization.

3.5.2 Decomposed EDPC (De-EDPC)

Table 3.5: *Additional notations of De-EDPC*

New Network Sets and Parameters in De-EDPC	
$[\![I]\!]$	Selected candidate cycle set obtained by PPCS algorithm.
$x_a^i \in \{0,1\}$	Equals 1 if cycle I_i crosses link a, and 0 otherwise.
$z_a^i \in \{0,1\}$	Equals 1 if cycle I_i can protect link a, and 0 otherwise.
$c_{ij} \in \{0,1\}$	Equals 1 if cycle I_i and I_j have at least one common link, and 0 otherwise.

As De-EDPC is decomposed from EDPC in Sec. 3.5.2, the similar variables and constraints are used. We summarize the additional notations of De-EDPC in Tab. 3.5. Note that instead of using a specific cycle repeat variable, we use an equivalent method that scales the candidate cycle set $[\![I]\!]$ by repeating the cycles several times according to the total traffic volume. Thus, the parameters x_a^i, z_a^i and c_{ij} can be determined in advance. There are some changes in the objective functions Eqs. (3.7) and (3.8) as follows,

$$E_{OXC} = \sum_{i \in [\![I]\!]} \sum_{v \in V} \sum_{u \in N_v} \frac{x_{vu}^i \cdot n_i}{B} \cdot e_v^{OXC} \tag{3.37}$$

$$E_{EDFA} = \sum_{i \in [\![I]\!]} \sum_{a \in A} \frac{x_a^i \cdot n_i}{B} \cdot e_a^{EDFA} \tag{3.38}$$

The majority constraints in De-EDPC are the same as in EDPC, including ***FSs allocation*** (3.19)-(3.21), ***Modulation adaptation*** (3.23)-(3.24), ***Protection capacity*** (3.27)-(3.29). However, constraints (3.25) and (3.26) are replaced by constraint (3.39).

$$q_a^i \leq z_a^i, \qquad \forall i, \forall a \tag{3.39}$$

3.5.3 Computational complexity

The number of dominant variables and constraints in EDPC and De-EDPC are summarized in Tab. 3.6 (we assign $|M| = 4$ as we have four modulation formats). The number of dominant variables is the same in these two models while the number of dominant constraints in De-EDPC is largely reduced. The computational complexities in terms of dominant variables and constraints are still big for large-size networks, efficient heuristic algorithms will be developed as our future work. However, in this work, we mainly focus on studying the advantages of directed p-cycles for asymmetric traffic protection in EONs by developing ILP models.

Table 3.6: *Computational complexities of EDPC and De-EDPC.*

Models	Computational complexities	
	No. of dominant variables	No. of dominant constraints
EDPC	$max\{O(\|I\|\|A\|), O(\|I\|^2)\}$	$O(\|I\|^2\|A\|)$
De-EDPC	$max\{O(\|[\![I]\!]\|\|A\|), O(\|[\![I]\!]\|^2)\}$	$max\{O(\|[\![I]\!]\|\|A\|), O(\|[\![I]\!]\|^2)\}$

3.6 Simulation and performance evaluation

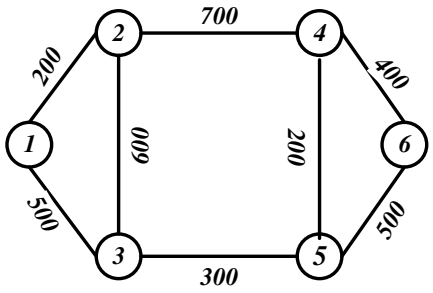

Figure 3.6: *Six-node network [16]*

We use CPLEX 12.06 to solve the proposed De-EDPC on an Intel Core PC equipped with a 3.5 GHz CPU and 8 GBytes RAM. The following test beds are used: six-node network (6 nodes, 16 directed links and average nodal degree 2.7) in Fig. 3.10(a), NSFNET (14 nodes, 44 directed links and average nodal degree 3.1) in Fig. 2.7(a) [46] and US Backbone networks (28 nodes, 90 directed links and average nodal degree 3.2) in Fig. 2.7(b) [46]. We regard θ_1 and θ_2 as 1 in the objective function Eq. (3.5) as it helps to improve the optimization speed for a high quality solution. Note that it has little impact on the first priority of total power consumption in our study. First, we evaluate the quality of solution in De-EDPC compared with the solution in EDPC. Then, extensive simulations are performed to show the power savings in De-EDPC in terms of TASY, AR and the number of DCs. AR is defined as the proportion of anycast traffic in the total traffic in the network. The following three metrics are used to evaluate the performance of p-cycles:

- ***Power consumption***: Our goal is to minimize the power consumption of p-cycles for asymmetric traffic protection.
- ***Power savings in De-EDPC***: This metric shows the advantage of power savings through power-efficient directed p-cycles in proposed De-EDPC.
- ***Total FS usage***: Total FS usage is an important feature that indicates the spare capacity usage of p-cycles.

Table 3.7: *Quality of solution and Execution Time in EDPC and De-EDPC.*

six-node network					
Traffic	EDPC ($\|I\| = 6$)		De-EDPC ($\|[\![I]\!]\| = 6$)		Gap
	Results	Execution Time	Results	Execution Time	
$1X$	4521.69	3146.89 s	4712.23	0.18 s	4.04%
$2X$	6357.91	2818.22 s	7018.97	0.52 s	9.42%
NSFNET network					
Traffic	EDPC ($\|I\| = 15$)		De-EDPC ($\|[\![I]\!]\| = 20$)		Gap
	Results	Execution Time	Results	Execution Time	
$1X$	10260.7	21270.66 s	10299.9	0.39 s	0.38%
$2X$	11084.6	26547.16 s	11997.4	0.57 s	7.61%

* The basic traffic 1X is 320 $Gbps$ and 100 $Gbps$ in six-node and NSFNET networks, respectively.

3.6.1 Quality of solution in De-EDPC

To verify the efficiency of the solutions in De-EDPC, we perform both EDPC and De-EDPC in six-node and NSFNET networks under traffic demands with low amount. A server with 500 GBytes memory is used due to the high computation complexity in EDPC while De-EDPC is solved in a PC with 8 GBytes memory. The traffic is generated with $TASY = 20\%$ and set up by Dijkstra's shorted-path routing. By using Eq. (3.32), we set the number of allowed cycles in EDPC as $|I| = 6$ and $|I| = 15$ in six-node and NSFNET networks, respectively. The number of candidate cycles in De-EDPC is obtained by PPCS algorithm with $[\![I]\!] = 6$ and $[\![I]\!] = 20$ in six-node and NSFNET networks, respectively.

Table 3.7 shows the results. Only a small traffic is shown because the EDPC exceeds the memory for a higher traffic. As we can see that De-EDPC achieves comparable solutions and dramatically reduces execution time compared with EDPC especially for a larger topology. For instance in NSFNET network, it requires more than 7 h to obtain the solution in EDPC while it takes less than 1 s in De-EDPC. The large reduction of execution time in De-EDPC is very attractive even though a small optimality gap is introduced. The optimality gap is because De-EDPC has relatively smaller feasible region compared with EDPC due to the fixed candidate cycles.

We can conclude that the proposed PPCS algorithm and De-EDPC offers a time-efficient way to solve the directed p-cycle design problem with high quality solutions.

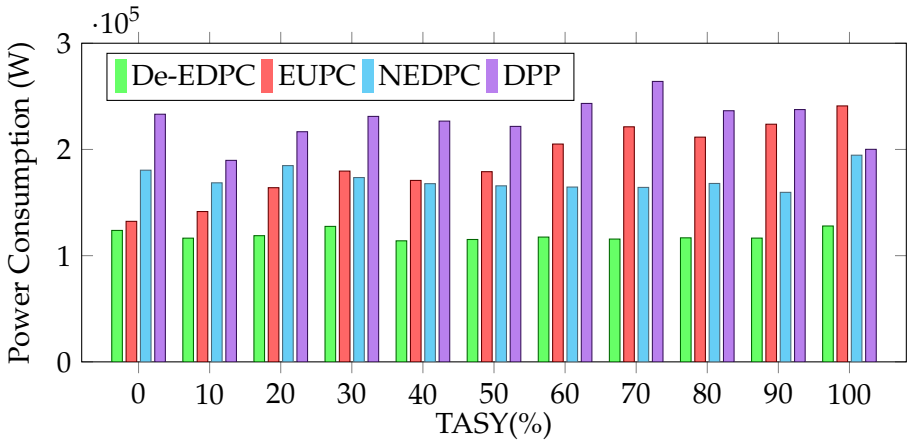

(a) Power Consumption in NSFNET network

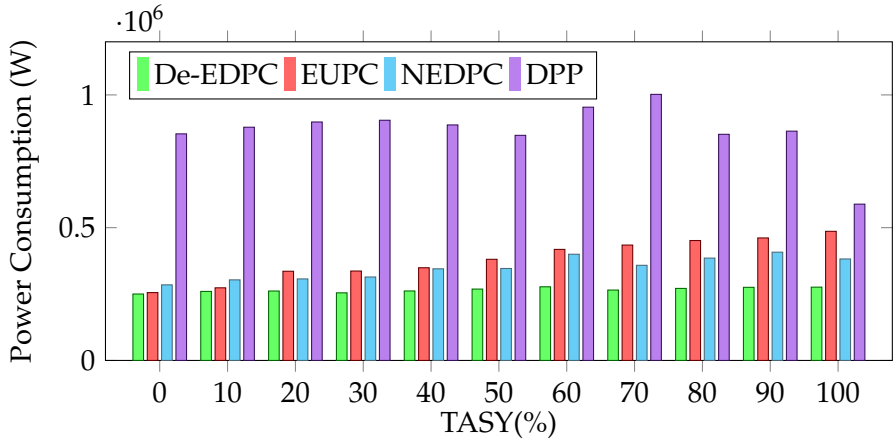

(b) Power Consumption in US Backbone network

Figure 3.7: *Power consumption as a function of TASY in NSFNET and US Backbone networks.*

3.6.2 Impact of $TASY$ on power savings in De-EDPC

We then study the power consumption of p-cycles for asymmetric traffic protection with De-EDPC in NSFNET and US Backbone networks. The traffic is generated with $TASY \in [0\%, 100\%]$. To evaluate the power savings of power-efficient directed p-cycles in De-EDPC, the following benchmarks are used:

- EUPC: It develops undirected p-cycles that minimize the total power consumption. We formulate the ILP model for EUPC based on De-EDPC. Note that EUPC enables the twice protection capacity for each straddling link.
- NEDPC: It is modified from the optimal p-cycle design in [137], which is formulated to minimize the sum of total FSs usage and maximum index of FSs. We add modulation formats and transmission reach limits in NEDPC to make a fair comparison.

- DPP: It is adapted from DP 1+1 protection in [129] by adding the same physical conditions as in De-EDPC. According to the working path calculated in advance, we compute K link-disjoint paths as candidate backup paths.

The total power consumption of all the potential single link failures in De-EDPC, EUPC, NEDPC and DPP are shown in Fig. 3.7 for NSFNET and US Backbone networks. As we can observe that DPP consumes more power than these p-cycle schemes, especially compared with the proposed De-EDPC. This is because that all the demands affected by the failed link in DPP need to be rerouted from the corresponding source nodes to the destination nodes while p-cycle protection schemes only reroute the traffic on the failed link between the two adjacent nodes. Thus, the more protection paths with longer length in DPP consume more power than the p-cycle protection. Among these three p-cycle schemes, De-EDPC consumes the lowest power for all of $TASY$, and the amount of power consumption in De-EDPC maintains the same level. As $TASY$ increases, the power consumption in EUPC goes up and it becomes the biggest. The power consumption in NEDPC also does not change too much with the increase of $TASY$.

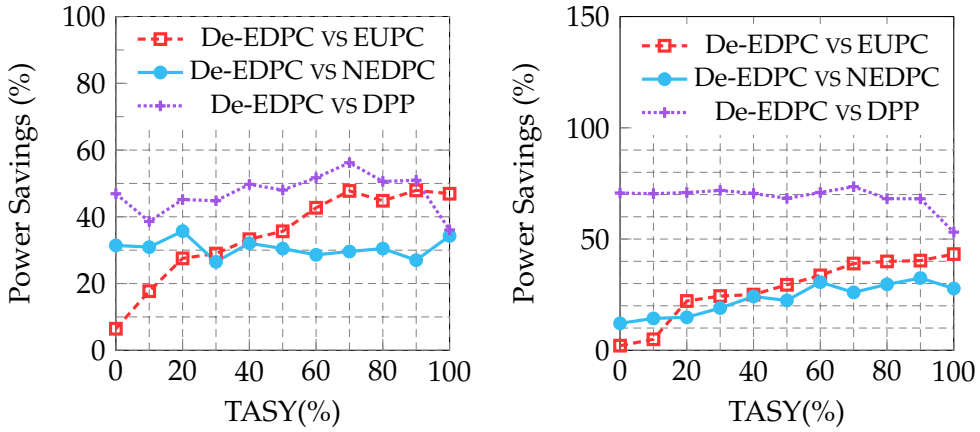

(a) Power Savings in NSFNET network (b) Power Savings in US Backbone network

Figure 3.8: *Power consumption as a function of TASY in NSFNET and US Backbone network.*

From Fig. 3.8(a) and Fig. 3.8(b), it is observed that the average power savings in De-EDPC compared with DPP are even 47.1% in NSFNET and 68.8% in US Backbone. For these p-cycle schemes, the power savings in De-EDPC compared with EUPC grow with the increase of $TASY$ from 0% to 100% (*i.e.*, from symmetric traffic to pure asymmetric traffic). For $TASY = 0\%$, the power saving is 6.46% in NSFNET network and 2.08% in US Backbone network. For $TASY = 100\%$, the power saving is even 46.91% in NSFNET network and 43.24% in US Backbone network. However, the power savings in De-EDPC compared with NEDPC do not show the same trend in NSFNET and US Backbone networks. It maintains among (26%, 36%) in NSFNET network, but it grows a little (from 12% to 33%) with the increase of $TASY$ in US Backbone network.

We also study the total number of used cycles and FSs usage in De-EDPC, EUPC,

Table 3.8: *Total number of p-cycles and FSs in NSFNET and US Backbone networks.*

TASY	NSFNET						US Backbone					
	De-EDPC		EUPC		NEDPC		De-EDPC		EUPC		NEDPC	
	Cycles	FSs	Cycles	FSs	Cycles	FSs	Cycles	FSs	Cycles	FSs	Cycles	FSs
0%	37	1385	36	1546	18	969	55	1635	50	1748	38	1349
20%	43	1247	38	2036	17	867	53	1834	54	2220	39	1563
40%	40	1194	46	2088	19	860	56	1903	56	2306	37	1603
60%	41	1334	42	2246	18	1018	58	2805	50	2788	39	2251
80%	40	1391	40	2546	20	1062	59	3057	56	3138	38	2483
100%	39	2007	40	3216	13	1482	58	3292	62	3278	40	2548

and NEDPC to make a fair comparison in Tab. 3.8. We can see that as $TASY$ increases, the total number of used p-cycles does not show many differences in De-EDPC, EUPC and NEDPC, respectively. However, the total number of FSs usage grows a lot with the increase of $TASY$ in these three p-cycle schemes. Among them, it is observed that NEDPC requires fewer p-cycles and FSs compared with De-EDPC and EUPC. This is because it is optimized to minimize spectrum usage, then high spectrum efficiency leads to fewer p-cycles. De-EDPC outperforms EUPC in terms of FSs usage because EUPC allocates twice the number of FSs for the undirected p-cycles without consciousness of the different traffic volume while De-EDPC effectively allocates the FSs according to the different traffic volume in each direction.

The simulation results demonstrate that directed p-cycles in De-EDPC provide a power-efficient way to protect asymmetric traffic in EONs. p-Cycle protection schemes consume less total power of all the potential link failures than the DPP scheme. De-EDPC earns significant power savings (up to 46.91%) against undirected p-cycles in EUPC, especially for asymmetric traffic with high $TASY$. De-EDPC also requires fewer FSs than EUPC. De-EDPC owns power consumption advantage over NEDPC, but it requires more FSs.

3.6.3 Impact of anycast ratio on power savings in De-EDPC

We then study the power savings in De-EDPC when both anycast and unicast services are considered. Specifically, the total traffic is composed of unicast traffic that generated between a pair of nodes, and anycast traffic that generated between the clients and DCs. We assume three DCs are located at nodes 1, 8 and 14 in NSFNET network, and six DCs are located at nodes 1, 7, 14, 19, 21 and 28 in US Backbone network. We use AR that corresponds to 0%, 20%, 40%, 60% and 80%. The total traffic is 4 $Tbps$ and 8 $Tbps$ in NSFNET and US Backbone networks, respectively.

Figure 3.9(a) and 3.9(b) illustrate the total power consumption of the three p-cycle schemes and power savings in De-EDPC in NSFNET and US Backbone networks, re-

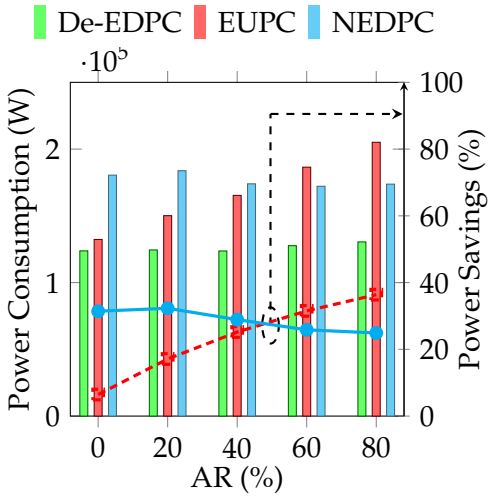

(a) Power consumption in NSFNET

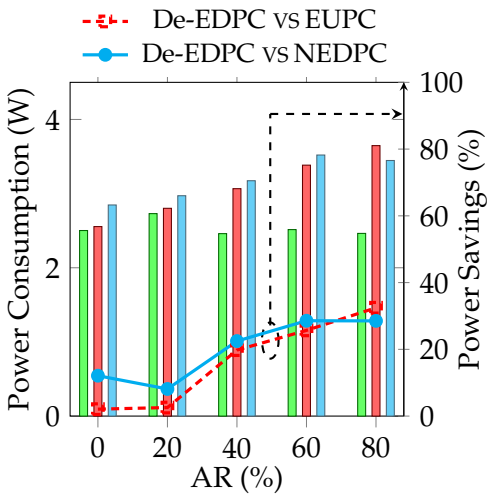

(b) Power consumption in US Backbone

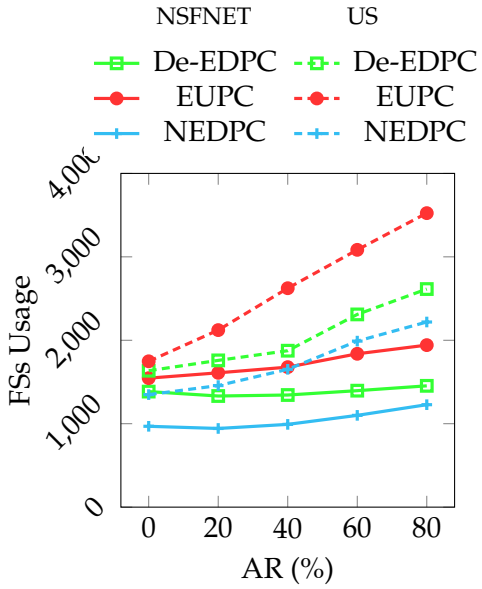

(c) FSs usage in NSFNET and US Backbone

Figure 3.9: *Power consumption and total FSs usage as a function of AR. (a) Power consumption and power savings in De-EDPC in NSFNET network. (b) Power consumption and power savings in De-EDPC in US Backbone network. (c) Total FSs usage in NSFNET and US Backbone networks.*

spectively. For the total power consumption, as the AR increases, De-EDPC consumes relatively stable power amount while EUPC requires more power in both NSFNET and US Backbone networks. We can see that the power savings in De-EDPC compared with EUPC increase from 6.46% (at $AR = 0\%$) to 36.38% (at $AR = 80\%$) in NSFNET, and it grows from 2.08% (at $AR = 0\%$) to 32.46% (at $AR = 80\%$) in US Backbone. However, the power savings in De-EDPC compared with NEDPC do not show the same trend in the two networks. This is because US Backbone network has bigger topology size and

nodal degree, then more efficient p-cycles can be generated as AR increases, while less topology size and nodal degree of NSFNET network make it less diversity of p-cycles. As a result, we can see that the power savings in De-EDPC compared with NEDPC maintains between 25% and 33% in NSFNET network while it increases a little from 8% to 28% in US Backbone network.

Figure 3.9(c) shows the total number of FSs usage. We can see the similar trend in NSFNET and US Backbone networks. Specifically, more FSs are required at a bigger AR for all the p-cycle schemes De-EDPC, EUPC and NEDPC. In addition, EUPC still consumes the most FSs because extra protection capacity is allocated for the asymmetric traffic while NEDPC requires the least owing to the optimization of FSs usage. The FSs usage in De-EDPC is much lower than in EUPC due to the consciousness of the different traffic volumes in the two directions.

3.6.4 Impact of DCs number on power savings in De-EDPC

Table 3.9: *DCs location in NSFNET and US Backbone networks.*

Networks	No. of DCs	Location of DCs
NSFNET	1	Node 8
	3	Nodes 1, 8, 14
	5	Nodes 1, 5, 8, 11, 14
	7	Nodes 1, 4, 5, 8, 9, 11, 14
US Backbone	4	Nodes 1, 12, 21, 28
	6	Nodes 1, 7, 14, 19, 21, 28
	8	Nodes 1, 7, 9, 12, 14, 19, 21, 28
	10	Nodes 1, 3, 7, 9, 12, 14, 19, 21, 24, 28

We further investigate the power savings in De-EDPC as a function of the number of DCs. The traffic is generated by setting $AR = 80\%$ and $TASY = 80\%$ so that the impact of number of DCs can be analyzed effectively. The number and location of DCs selected in the simulations are shown in Tab. 3.9, which is referred from [29].

Figure 3.10 shows the power consumption and FSs usage in De-EDPC, NEDPC and EUPC. From Fig. 3.10(a) and 3.10(b), we can see that the total power consumption does not show some trends in De-EDPC, NEDPC and EUPC with the increase of the number of DCs. However, compared with EUPC, the introduction of DCs brings the benefit of power savings in De-EDPC since it increases significantly from 6.5% to 46.1% in NSFNET network and from 2.1% to 38.5% in US Backbone network. This is because

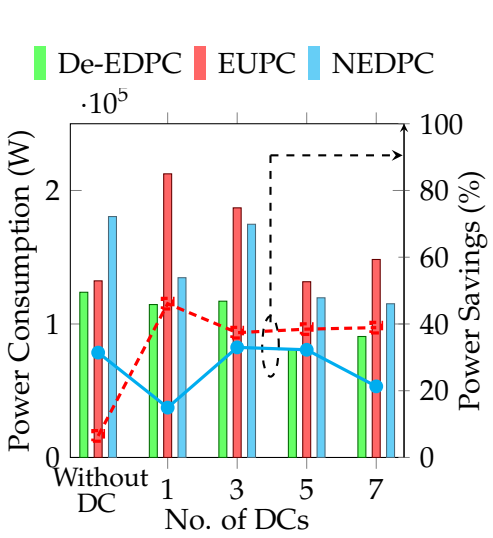

(a) Power consumption in NSFNET

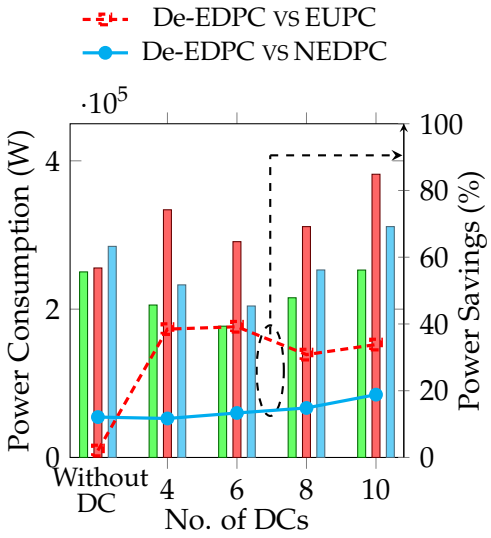

(b) Power consumption in US Backbone

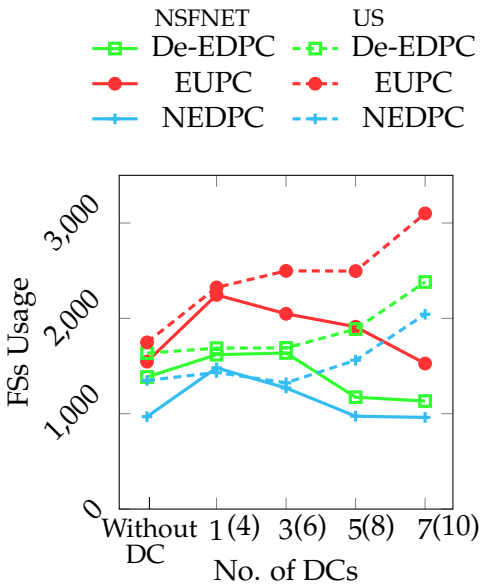

(c) FSs Usage in NSFNET and US Backbone

Figure 3.10: *Power consumption and total FSs usage as a function of the number of DCs. (a) Power consumption and power savings in De-EDPC in NSFNET network. (b) Power consumption and power savings in De-EDPC in US Backbone network. (c) Total FSs usage in NSFNET and US Backbone networks.*

anycast services in DCs bring asymmetric traffic in the network, then directed p-cycles in De-EDPC consume lower power. Nevertheless, as the number of DCs increases, the power savings in De-EDPC do not change too much even though the amount of power consumption varies in De-EDPC, NEDPC and EUPC, respectively. This is because the asymmetric traffic are set with fixed AR and *TASY*. Compared with NEDPC, power

savings in De-EDPC show different trends in NSFNET and US Backbone networks. It fluctuates with the increase of the number of DCs in NSFNET while it grows stably in US Backbone network.

The total FSs usage in Fig. 3.10(c) shows more differences in NSFNET and US Backbone networks. As we can see that in NSFNET network, the total FSs usage goes down with the increase of the number of DCs in De-EDPC, EUPC and NEDPC while it goes up in US Backbone network. However, it is still observed that EUPC requires the most FSs usage while NEDPC needs the least.

Comprehensive simulations of power consumption and FSs usage are performed in De-EDPC, EUPC and NEDPC for asymmetric traffic in terms of $TASY$, AR and the number of DCs. The results demonstrate that directed p-cycles in De-EDPC own significant power savings (up to 46.91%) compared with undirected p-cycles in EUPC, and the amount of power savings increase with the increase of $TASY$ or AR. In addition, De-EDPC also earns power savings compared with NEDPC, but the amount of power savings do not change too much as the $TASY$ or AR increases. It is also reserved that the introduction of DCs makes it more valuable to utilize directed p-cycles for protection in EONs in a power-efficient way.

3.7 Conclusion

In this chapter, we study power-efficient directed p-cycle protection for asymmetric traffic in EONs. Directed p-cycles enable to allocate different FSs and modulation formats for asymmetric traffic in each direction with the help of distinguishing traffic amount in two directions. Simulation results demonstrate that significant power savings are obtained by using directed p-cycles for asymmetric traffic protection in EONs, and the amount of power savings goes up as the traffic asymmetry or anycast ratio increases. In addition, it shows that the introduction of DCs makes it more valuable to utilize directed p-cycles in order to power-efficiently protect the anycast services while the amount of power savings with directed p-cycles does not depend on the number of DCs.

We find that spectrum usage large affects the power consumption of p-cycle protection as the dominant power consumption of BVTs depends on the number of FSs used. In addition to the optimization of directed p-cycle generation and modulation format adaption, spectrum usage savings can be achieved by designing shared protection schemes [83, 134, 148, 149]. Then, we further study the possibility of spectrum sharing of p-cycles and explore spectrum shared p-cycle protection scheme in the next chapter.

Chapter 4

Spectrum-efficient p-Cycle Design in EONs

Contents

4.1 Introduction

Efficient spectrum allocation has arisen as one key issue in EONs, which has been studied with new techniques, such as traffic grooming, defragmentation and survivability [12]. The spectrum allocation in EONs needs to address *spectrum contiguity* that restricts that the assigned FSs should be spectrally neighboring. In addition, EONs without spectrum conversion should ensure the *spectrum continuity* that the same FSs should be used on each link along the path. With the help of spectrum conversion in BV-OXCs, the *spectrum continuity* constraint can be relaxed to improve the overall spectrum efficiency [6]. Spectrum conversion is the capability of spectrum shifting in the frequency domain realized by all optical or O/E/O techniques [136], then the blocked requests can be converted accommodate into available contiguous spectrum slots [56, 74]. The study in [74] showed that incorporation of spectrum conversions significantly suppresses the request blocking probability and increases the traffic admissibility when the traffic load is low. In a congested network, when traffic load is larger, the performance is comparable with and without incorporation of spectrum conversion.

p-Cycle protection has been found very promising for network survivability due to its fast switching speed and efficient spare capacity for both on-cycle and straddling links [52]. The FSs assigned to the p-cycles are subject to the *spectrum contiguousness* constraint that the FSs should be spectrally neighboring except the required GB. Moreover, FSs allocation needs to consider spectrum conflict on the fiber links among p-cycles. In traditional p-cycle design, to avoid spectrum conflict, different FSs need to be assigned to p-cycles that have common link(s). However, S. Zhang et al.in [149] observed that p-cycles that have one common link still can share the same wavelength resource, which could greatly improves the spare capacity efficiency as much as 30% over the conventional no-shared p-cycle design. However, the potential of spare capacity sharing can be enhanced to p-cycles that have multiple common link(s), because the spectrum conflict only has influence on the links along protection paths not all the on-cycle links among p-cycles.

In this chapter, Spectrum Shared p-Cycle (SS-p-cycle) design for EONs is studied with/without spectrum conversion. SS-p-cycles allow to assign the same FSs for multiple p-cycles that have common link(s) as long as the protection paths provided by these p-cycles are guaranteed to do not have common link against single link failure. To this end, we first study the possibility of spectrum sharing among p-cycles that have common links. Then, two ILP models are formulated to address spectrum allocation of SS-p-cycle with/without spectrum conversion cases. An algorithm is developed for SS-p-cycle design without spectrum conversion. Extensive simulations are conducted of SS-p-cycles in comparison with conventional no-shared p-cycle design with/without spectrum conversion.

The significant aspects of this proposition are as follows:

- Propose the SS-p-cycle design for EONs to allow spectrum sharing among p-cycles even though they have multiple common links.

- Develop the ILP models to generate SS-p-cycles with optimal spectrum utilization with/without spectrum conversion as well as a scalable heuristic algorithm for SS-p-cycles in large instances.
- Spectrum allocation comparison between SS-p-cycles and conventional spectrum no-shared p-cycles.

4.2 Related work

In the literature, spectrum allocation in EONs has been extensively studied and several spectrum allocation methods for p-cycle design in EONs have been proposed [16, 63, 68, 137, 141]. The authors in [63] investigated dynamic p-cycle protection in EONs with spectrum planning related to PWCE p-cycle design and Hamiltonian cycle. They further studied FIPP p-cycles taking into account routing, modulation formats and spectrum allocation in [16]. In [141], an ILP model for p-cycle design in EONs was developed to minimize total spectrum usage with load balancing in the working paths. A comparison between ring cover technique and p-cycle protection was conducted in EONs in [137]. The effects of bandwidth squeezed restoration technique and the spectrum conversion capability were evaluated for p-cycle protection. The authors in [68] proposed the directed p-cycle design for asymmetric traffic in EONs and studied the power savings achieved in the optical equipments by directed p-cycle design.

However, in the literature, spectrum sharing has not been explored for p-cycle protection in EONs even though it has been well studied for path-based protection [83, 134]. The authors in [83] explored spectrum sharing in backup lightpaths enabled by the elasticity of the transponders. In [134], the distance adaptive dynamic RSA with SBPP was studied. In all the spectrum allocation for p-cycle protection above, different FSs are allocated for p-cycles that have common link(s). However, this spectrum conflict constraint will lead to spectrum wasting as these p-cycles still have the potential to share spare capacity as studied by S. Zhang et al. in WDM optical networks [148, 149]. They proposed shared p-cycles that can share the same wavelength resource if they only have one common link, and they observed that shared p-cycles can achieve better spare capacity efficiency as much as 30% over the conventional no-shared p-cycle design. Nevertheless, their shared p-cycles were only valid under wavelength conversion capabilities due to the absence of *wavelength continuity*. Moreover, the proposed shared p-cycles can not be applied into EONs since the challenging spectrum allocation is not considered.

Moreover, the spectrum sharing for p-cycles can be enhanced to p-cycles that have multiple common link(s). More specifically, p-cycles can share the same spectrum resources if their protection paths do not have common link under any single link failure. However, it is more challenging to explore the possible common link(s) on protection paths instead of only the on-cycle links among p-cycles, especially in EONs without spectrum conversion.

4.3 Problem statement

The topology of an EON is modeled as a graph $G(V, E)$, where V and E represent the sets of nodes and bidirectional links, respectively. We assume there are 300 FSs available in each fiber link. Note that we consider both cases of with/without spectrum conversion. SS-p-cycles are designed to allow spectrum sharing while maintaining sufficient spare capacity under the following considerations:

- *Sufficient spare capacity*: Enough spare capacity should be reserved on the p-cycles to ensure any single link failure.
- *Spectrum contiguity*: The FSs allocated to the paths should be neighboring on the optical spectrum, which is ensured by allocating a continued range of FS index.
- *Spectrum continuity (in the case of no spectrum conversion)*: All the links along the same working path or backup path should be assigned the same FSs.

In most of p-cycle designs, a candidate cycle set I is generated in advance based on network topology, then final p-cycles are chosen from set I by allocating spare capacity on on-cycle links. Efficient FSs allocation for p-cycles needs to take into account both spare capacity and maximum FSs usage. The main difference of p-cycle design with/without spectrum conversion is that the *spectrum continuity* constraint must be satisfied in EONs without spectrum conversion. More specifically, in each p-cycle, the same FSs should be assigned to each on-cycle link so that the protection path uses the same FSs along the traversing links. However, the *spectrum continuity* constraint can be neglected in p-cycle with spectrum conversion, which provides more flexible cycle selection and FSs allocation possibilities.

Conventional p-cycle design does not allow p-cycles to share the same FSs if they have common link(s). However, due to the property of p-cycle protection, only partial on-cycle links are combined as protection paths in one specific p-cycle. Thus, the ***spectrum conflict*** between p-cycles only occurs when their protection paths against one single link failure have common link(s). This inspires the potential to enhance spectrum sharing among p-cycles that have common link(s). The SS-p-cycle design is proposed in this study, which enables to allocate the same FSs to the p-cycles that have common link(s). Note that, they are different from the shared p-cycles proposed in [148, 149], in which the same wavelength resource can be shared by p-cycles that have at most one common link, however, the SS-p-cycles allow more potential spectrum sharing even if p-cycles have multiple common links.

The concept of SS-p-cycles and their spectrum sharing property are explained in Theorem 4.3.1. The SS-p-cycle problem is $\mathcal{NP}$-hard as the general p-cycle design without spectrum sharing has been shown to be $\mathcal{NP}$-hard [16, 52].

Theorem 4.3.1. *Two p-cycles can share the same spectrum iff all of their protection paths do not have common links against any single link failure. Thus, they are called* ***SS-p-cycles****.*

Proof. Considering two p-cycles I_1 and I_2, for any single link failure, *e.g.*, link e, $p^e_{I_1}$ and

$p^e_{I_2}$ are the protection paths in I_1 and I_2, respectively. We show first that the condition is sufficient. If $\forall e \in E$, $p^e_{I_1}$ and $p^e_{I_2}$ do not have any common link, then p-cycles I_1 and I_2 can share the same FSs, so they are **SS-p-cycles**. For the necessary condition, if two SS-p-cycles I_1 and I_2 can share the same FSs, it means that the protection paths $p^e_{I_1}$ and $p^e_{I_2}$ do not have any common link against any single link failure. Thus, the proof follows. □

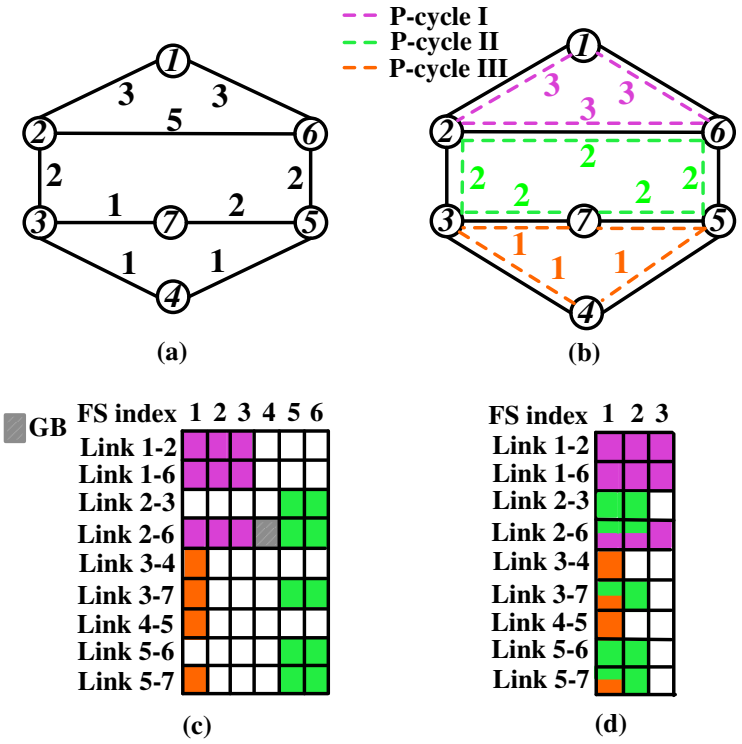

Figure 4.1: *(a) Working FSs on each link. (b) Protection capacity in terms of FSs for each link provided by p-cycles. (c) FSs allocation in conventional p-cycles without spectrum sharing. (d) FSs allocation in SS-p-cycles.*

Figure 4.1 shows an example of SS-p-cycle design with/without spectrum conversion compared with conventional no-shared p-cycle design. Figure 4.1 (a) shows the working FSs. Three p-cycles I, II and III are designed to provide the specific protection capacity, as shown in Fig. 4.1(b). Notice that p-cycle does not need to protect every on-cycle link or straddling link, for instance on link 3-7 with one working FS, only p-cycle III is required to protect it via path 3-4-5-7 with one FS protection capacity, even though p-cycle II also has the ability to protect it. The same case happens to link 7-5 which is only protected by p-cycle II with two FSs protection capacity. This property allows p-cycle II and III to share the same FSs since there is no common link on their protection paths under any single link failure. However, in conventional p-cycle design, p-cycles II and III can not share the same FSs as they have common links 3-7 and 7-5. Figure 4.1 (c) indicates the spectrum allocation in conventional p-cycle, the maximum index of occupied FSs is 6 and the spare capacity is 23. Nevertheless, in SS-p-cycles, the maxi-

mum index of occupied FSs is only 3 and the spare capacity is reduced to 19 in Fig. 4.1 (d) owing to the spectrum sharing. Moreover, more flexible spectrum allocation can be obtained if we consider the spectrum conversion in EONs. As shown in Fig. 4.1, the on-cycle links in one p-cycle can use different FSs, *ie.*, p-cycles II and III. It means that these p-cycles only need to reserve a sufficient number of contiguous FSs on on-cycle links, regardless the range of the assigned FSs. SS-p-cycles with spectrum conversion does not outperform p-cycles without spectrum conversion due to the size limit in this small topology, but the spectrum usage can be reduced among more SS-p-cycles in a bigger topology, which we will study later.

4.4 ILP formulation

Table 4.1: *Notations in the two ILP models in* ***Chapter*** *4.*

Network Sets and Parameters	
$G(V, E)$	Network topology with node set V and link set E.
I	The candidate p-cycle set, I_i indicates i-th p-cycle in I.
N_v	The set of adjacent nodes of a node v.
B	Set of FSs on each fiber link and $\|B\|$ is the total number of available FSs.
$x_e^i \in \{0,1\}$	Equals 1 if link e is on-cycle link in I_i, and 0 otherwise.
$z_e^i \in \{0,1,2\}$	Equals 1 if on-cycle link e can be protected by cycle I_i , 2 if straddling link e can be protected by cycle I_i, and 0 otherwise.
$y_v^i \in \{0,1\}$	Equals 1 if node v is crossed by I_i, and 0 otherwise.
l_e	Working traffic in terms of FSs on link e.
Variables in SS-PC-ILP	
$\delta_i \in \{0,1\}$	Equals 1 if cycle I_i is selected, and 0 otherwise.
$q_e^i \in \{0,1\}$	Equals 1 if cycle I_i is selected to protect link e, and 0 otherwise.
$s_i \in [0, \|B\| - 1]$	The starting index of occupied FSs in I_i.
$o_{ij} \in \{0,1\}$	Equals 1 if the starting index of occupied FSs of I_i is smaller than that of I_j, and 0 otherwise.
$c_{ij} \in \{0,1\}$	Equals 1 if I_i and I_j have spectrum conflict, and 0 otherwise.
$n_i \in [0, \|B\|]$	The number of occupied FSs of I_i.
$\pi_e^i \in [0, \|B\|]$	The number of FSs provided by I_i to protect link e.
$s_e^{min} \in [0, \|B\|]$	The minimum index of occupied FSs on link e.
$s_e^{max} \in [0, \|B\|]$	The maximum index of occupied FSs on link e.
Variables in SS-PC-SC-ILP	
$\pi_e^i \in [0, \|B\|]$	The number of FSs provided by I_i to protect link e.
$n_{ee'} \in [0, \|B\|]$	The number of FSs provided by link e to protect link e'.
$n_e \in [0, \|B\|]$	The total number of FSs provided by link e.

In this section, we first formulate an ILP model for SS-p-cycles in conventional opti-

cal networks without spectrum conversion case, named as SS-PC-ILP. In order to study the SS-p-cycles property with the help pf spectrum conversion, we also formulate an ILP model named SS-PC-SC-ILP. The notations are shown in Tab. 4.1. For the sake of readability, we use $\forall i$, $\forall v$, $\forall u$, and $\forall e$ to denote $\forall i \in I$, $\forall v \in V$, $\forall u \in N_v$, and $\forall e \in E$, respectively.

4.4.1 SS-PC-ILP Model (without spectrum conversion)

Objective:

The objective function (4.1) is to minimize the sum of occupied FSs margin on all the links and the maximum index of occupied FSs. θ_1 and θ_2 are used as adjustable weighting parameters. Note that by minimizing the first term in the objective function, spare capacity is indirectly minimized and spectrum defragmentation is also ensured by centralizing the FSs to the side of smaller FS index.

$$\min \quad \theta_1 \cdot \sum_{e \in E} (s_e^{max} - s_e^{min}) + \theta_2 \cdot t_b \tag{4.1}$$

Constraints:

$$q_e^i \leq z_e^i, \qquad \forall i, \forall e \tag{4.2}$$
$$\delta_i \geq q_e^i, \qquad \forall i, \forall e \tag{4.3}$$
$$\delta_i \leq \sum_{e \in E} q_e^i, \qquad \forall i \tag{4.4}$$
$$n_i \geq \delta_i, \qquad \forall i \tag{4.5}$$
$$\pi_e^i \leq n_i, \qquad \forall i, \forall e \tag{4.6}$$
$$\pi_e^i \leq q_e^i \cdot B, \qquad \forall i, \forall e \tag{4.7}$$
$$\sum_{i \in I} \pi_e^i \cdot z_e^i \geq l_e, \qquad \forall e \tag{4.8}$$
$$x_{e'}^i + x_{e'}^j + q_e^i + q_e^j - 3 \leq c_{ij}, \qquad \forall i, j, i \neq j, \forall e, e', e \neq e' \tag{4.9}$$
$$o_{ij} + o_{ji} = 1, \qquad \forall i, j, i \neq j \tag{4.10}$$
$$s_i + n_i + 1 - s_j \leq B \cdot (2 - o_{ij} - c_{ij}), \qquad \forall i, j, i \neq j \tag{4.11}$$
$$s_i + n_i \leq t_b, \qquad \forall i \tag{4.12}$$
$$s_i + n_i \leq \delta_i * B, \qquad \forall i \tag{4.13}$$
$$s_e^{max} \geq x_e^i \cdot (s_i + n_i), \qquad \forall i, \forall e \tag{4.14}$$
$$s_e^{min} \leq x_e^i \cdot s_i + (1 - \delta_i) * B, \qquad \forall i, \forall e \tag{4.15}$$

Constraints (4.2)-(4.4) determine whether p-cycle I_i is selected or not by checking if there exists at least one link that desires to be protected by I_i. Constraints (4.5)-(4.8)

guarantee the sufficient spare capacity against 100% single link failure. Constraints (4.9)-(4.11) enable spectrum sharing in SS-p-cycles. Specifically, the variable c_{ij} in constraint (4.9) determines whether p-cycles can share the same FSs by checking the possible common link(s) in their protection paths. Note that we use other link e' except the protected link e to indicate the possible links along protection paths. Constraint (4.11) ensures that one FS GB is reserved if two p-cycles have spectrum conflict, while for those p-cycles without spectrum conflict, the same FSs can be shared. It also guarantees the *spectrum contiguity* of FSs assigned to the p-cycles as the assigned FSs n_i is contiguous. Constraint (4.12) restricts the ending index of occupied FSs for each p-cycle. Constraint (4.13) is helpful to reduce the feasible solution region for fast optimization. Constraints (4.14)-(4.15) restrict the maximum index and minimum index of occupied FSs on each link, and they also guarantee *spectrum continuity* since the same FSs between $[s_i, s_i + n_i)$ is allocated for each on-cycle link, *e.g.*, $x_e^i = 1$ in p-cycle I_i.

4.4.2 SS-PC-SC-ILP model (with spectrum conversion)

Objective:

The objective is also to minimize the total occupied spare capacity and the maximum index of occupied FSs in the whole network as in SS-PC-SC-ILP model. θ_1 and θ_2 are adjustable parameters for weighting these two metrics.

$$\min \quad \theta_1 \cdot \sum_{e \in E} n_e + \theta_2 \cdot t_b \tag{4.16}$$

Constraints:

$$\pi_e^i \leq z_e^i \cdot B, \qquad \forall i, \forall e \tag{4.17}$$

$$\sum_{i \in I} \pi_e^i \cdot z_e^i \geq l_e, \qquad \forall e \tag{4.18}$$

$$n_{ee'} = \sum_{i \in I} \pi_{e'}^i \cdot x_e^i, \qquad \forall e, e', e \neq e' \tag{4.19}$$

$$n_e \geq n_{ee'}, \qquad \forall e, e', e \neq e' \tag{4.20}$$

$$n_e \leq t_b, \qquad \forall e \tag{4.21}$$

Constraint (4.17) indicates the ability of spare capacity in p-cycle to protect link e in terms of the number of FSs. Constraint (4.18) ensures that the spare capacity provided by all the p-cycles is sufficient to protect against 100% single link failure. Constraint (4.19) indicates the spare capacity in terms of FSs reserved on link e to protect link e'. Constraint (4.19) determiners the spare capacity needed to be reserved on link e under all the potential link failure. Constraint (4.21) restricts the maximum FSs reserved in the whole network, which is minimized in the objective function.

4.4.3 Discussion

Compared to p-cycles without spectrum sharing [137] and shared p-cycles [148, 149], FSs sharing in proposed SS-p-cycles are enhanced for p-cycles that even have multiple common links. To achieve the enhanced spectrum sharing, the proposed SS-PC-ILP and SS-PC-SC-ILP models need to check common link(s) on all the protection paths under any single link failure. This introduces the higher computational complexity and longer recovery time.

1). Computational complexity

Table 4.2: *Computational complexities of SS-PC-ILP and SS-PC-SC-ILP.*

Models	Computational complexities	
	No. of dominant variables	No. of dominant constraints
SS-PC-ILP (without spectrum conversion)	$max\{O(\|I\|\|E\|), O(\|I\|^2)\}$	$O(\|I\|^2\|E\|^2)$
SS-PC-SC-ILP (without spectrum conversion)	$max\{O(\|I\|\|E\|), O(\|E\|^2)\}$	$max\{O(\|I\|\|E\|), O(\|E\|^2)\}$

Thus, the reduction of FS utilization is obtained at the expense of higher complexity. We summaries the computational complexities of the ILP models for SS-PC-ILP and SS-PC-SC-ILP in terms of the number of dominant variables and constraints in Tab. 4.2. We can see that the number of dominant variables of these two models are comparable, however, SS-PC-ILP has higher computational complexity as the number of dominant constraints is $O(|I|^2|E|^2)$ while it is $max\{O(|I||E|), O(|E|^2)\}$ in SS-PC-SC-ILP. This is because that the constraints in SS-PC-ILP needs to ensure the spectrum continuity of SS-p-cycles.

2). Recovery time

The recovery time is defined as the time interval between the instant a failure happens and the instant the backup path is established [102]. The recovery process has several steps:

- The failure is detected by the adjacent node, which consumes $T_1 = 10\ \mu s$;
- The failure information is propagated to the nodes triggering protection switching operation, which requires a propagation delay $T_2 = 400\ \mu s/80km$ and message processing time at each node $T_3 = 10\ \mu s$;
- Configure, test and set up the cross-connects on the backup path, which requires $T_4 = 30\ ms$ at each node.
- Source node sends "set up" message to backup path and receives the "confirm" message, which corresponds to time T_2 and T_3.

The spectrum sharing property in SS-p-cycle protection contributes to the increased spectrum efficiency, however, it also brings in higher recovery time compared with the

conventional spectrum no-shared p-cycles. This higher recovery time results from the third step to configure, test and set up the optical cross-connects on the backup path because the optical OXCs are shared among different p-cycles.

4.5 Heuristic algorithm

Algorithm 4: SS-p-cycle Spectrum Allocation (SS-PC-SA)

Input : $G(V, E)$, traffic amount l_e, $\forall e \in E$, candidate cycle set I with hop limit n in $G(V, E)$

Output: Selected candidate cycle set $\mathbb{C}$, maximum index FS_{max} and total spare capacity FS_{total}

$\mathbb{C} \leftarrow \emptyset$, $\mathbb{C}_{FS} \leftarrow \emptyset$;
sort links in E in the descending order of traffic amount;
for $e \in E$ *with traffic amount* l_e **do**
  $Pro^e_{total} \leftarrow 0$, $R^e_{pro} \leftarrow (l_e - Pro^e_{total})$;
  if $\exists c \in \mathbb{C}, z^c_e > 0$ **then**
    $Pro^e_{total} \leftarrow \sum_{c \in \mathbb{C}} c_{FS} \cdot z^c_e$; $R^e_{pro} \leftarrow (l_e - Pro^e_{total})$;
    if $R^e_{pro} > 0$ **then**
      for $c \in \mathbb{C}, c_{FS} < B, z^c_e > 0$ **do**
        search the cycle c with smallest spare capacity requirement;
        while $R^e_{pro} > 0$ *and* $c_{FS} < B$ **do**
          c_{FS}++; $Pro^e_{total} \leftarrow (Pro^e_{total} + z^c_e)$; $R^e_{pro} \leftarrow (l_e - Pro^e_{total})$;
        end
      end
    end
  end
  else
    for $c \in I, c \notin \mathbb{C}, z^c_e > 0$ **do**
      if $R^e_{pro} > 0$ **then**
        search the cycle c with smallest spare capacity requirement, $\mathbb{C} \leftarrow c$;
        if $\lceil \frac{R^e_{pro}}{z^c_e} \rceil \leq B$ **then** $c_{FS} \leftarrow \lceil \frac{R^e_{pro}}{z^c_e} \rceil$;
        else $c_{FS} \leftarrow B$;
        $Pro^e_{total} \leftarrow (Pro^e_{total} + c_{FS} \cdot z^c_e)$;
        $R^e_{pro} \leftarrow (l_e - Pro^e_{total})$;
      end
    end
  end
end
get FSs conflict graph of p-cycles in $\mathbb{C}$ based on c_{ij} in Eq. (4.9);
allocate FSs for p-cycles in $\mathbb{C}$ with coloring method [140];

To overcome the lack of scalability of SS-p-cycle ILP model, *Algorithm* 4 a fast and efficient SS-p-cycle Spectrum Allocation (called SS-PC-SA) algorithm is proposed to perform cycle selection and FSs allocation without spectrum conversion. Note that, here the hop limit n is used to restrict the p-cycle generation, in a more realistic optical networks, distance-adaptive modulation formats can be allocated for different p-cycles with link distance consideration. *Line 1* is for the network initialization, where $\mathbb{C}$ is the selected p-cycles set and $\mathbb{C}_{FS}$ is the assigned FSs index set for the p-cycles in $\mathbb{C}$. *Line 2* sorts the links according to the descending amount of traffic demands. *Lines 3-37* explain how to select p-cycles with smallest spare capacity. More specifically, for each link e, the algorithm firstly tries to protect it with the selected candidate cycle set $\mathbb{C}$ by *Lines 4-15*, if enough protection capacity can not provided by $\mathbb{C}$, the algorithm will use new p-cycles $c \in I$ and put it(them) into $\mathbb{C}$ by *Lines 17-26*. *Line 28* constructs FSs conflict graph of SS-p-cycles based on Eq. (4.9). *Line 29* allocates FSs by using coloring method in [140]. Note that, *Algorithm* 4 can be easily modified to solve p-cycles without FSs sharing and with FSs sharing under one common link by recalculating the FSs conflict c_{ij} in *Line 28*. The time complexity of *Lines 3-27* is $O(|E| \cdot |I|^2)$, and it is $O(|\mathbb{C}|^3 \cdot \Delta)$ for coloring method in *Line 29* (Δ is the maximum degree in conflict graph). Thus, the time complexity of *Algorithm* 4 is $O(|E| \cdot |I|^2 + |\mathbb{C}|^3 \cdot \Delta)$.

4.6 Simulation and performance evaluation

We use CPLEX 12.06 to solve the proposed SS-PC-ILP and SS-PC-SC-ILP models with a 3.5 GHz CPU and 8 GBytes RAM. Traffic demands between each pair of nodes are randomly generated following a uniform distribution between 1 and X in units of FSs, and the traffic on each link is obtained by Dijkstra's shortest-path routing. COST239 (11 nodes and 26 links), and US Backbone (28 nodes and 45 links) networks are used as test beds. The following benchmarks are used:

- PC-ILP: conventional spectrum no-shared p-cycle design for EONs without spectrum conversion in [137].
- PC-SC-ILP: conventional spectrum no-shared p-cycle design for EONs with spectrum conversion in [137].

Note that we enable several p-cycles in PC-ILP and PC-SC-ILP to protect one working link for a fair comparison. The following two metrics are used to evaluate the performance:

- ***Maximum index of FSs***: It indicates the size of the occupied spectrum resource for the whole p-cycles.
- ***Spectrum Efficiency***: It is defined as the ratio of the total working capacity to the total spare capacity in the network.
- ***Spectrum Fragmentation Ratio (SFR)***: It is defined in [37] to evaluate the defragmentation efficiency.

We first identify the weighting value θ_1 and θ_2 regarding the sum of occupied FSs margin on all the links and the maximum index of occupied, respectively in the objective function (4.1) in the six-node topology [68]. Then, we conduct simulations to study how efficient the proposed SS-p-cycles is compared with the conventional spectrum no-shared p-cycles in PC-ILP in terms of FSs allocation and defragmentation efficiency. After that, we study the spectrum usage of proposed SS-p-cycles in the networks with and without spectrum conversion. In the end, we evaluate the performance of SS-PC-SA algorithm in larger instances.

Table 4.3: *FSs usage in terms of spare capacity and maximum index in six-node topology.*

Traffic with FSs in [1,X]	θ_1=1 θ_2=1					
	SS-PC-ILP		PC-ILP		% Reduction	
	Sum	Max	Sum	Max	Sum	Max
X=10	212	36	228	46	7.0%	21.7%
X=20	424	72	456	90	7.0%	20%
X=30	636	108	684	134	7.0%	19.4%
X=40	848	144	912	178	7.0%	19.1%
X=50	1060	180	1140	222	7.0%	18.9%
Traffic with FSs in [1,X]	θ_1=1 θ_2=0					
	SS-PC-ILP		PC-ILP		% Reduction	
	Sum	Max	Sum	Max	Sum	Max
X=10	212	36	228	53	7.0%	32.1%
X=20	424	72	456	105	7.0%	31.4 %
X=30	636	108	684	157	7.0%	31.2%
X=40	848	144	912	209	7.0%	31.1%
X=50	1060	180	1140	261	7.0%	31.0%
Traffic with FSs in [1,X]	θ_1=0 θ_2=1					
	SS-PC-ILP		PC-ILP		% Reduction	
	Sum	Max	Sum	Max	Sum	Max
X=10	248	36	228	46	-8.1%	21.7%
X=20	496	72	456	90	-8.1%	20%
X=30	744	108	684	134	-8.8%	18.7%
X=40	992	144	912	178	-8.8%	19.1%
X=50	1060	180	1140	222	7.0%	18.9%

SS-PC-ILP: Proposed SS-p-cycle design without spectrum conversion.
PC-ILP: Conventional spectrum no-shared p-cycle design without spectrum conversion in [137].
Sum: The total spare capacity of occupied FSs.
Max: The maximum index of occupied FSs.
% Reduction: SS-p-cycles over conventional spectrum no-shared p-cycles.

4.6.1 FSs allocation with different weighting θ_1 and θ_2

Table 4.3 shows the FSs allocation with different weighting θ_1 and θ_2 in three combination cases. When both spare capacity and maximum FSs index are minimized (θ_1=1 θ_2=1), the proposed SS-PC-ILP owns 7.0% and 19.8% FSs reduction compared with PC-ILP in average, respectively. When only spare capacity is minimized (θ_1=1 θ_2=0), the maximum index of FSs in SS-PC-ILP is much smaller than that in PC-ILP. It is because the spare capacity optimization of PC-ILP only needs to reserve a sufficient number of contiguous FSs for p-cycles, regardless of FSs range. While in SS-PC-ILP, the maximum index of FSs is also optimized since the FSs margin on each link is minimized. In the last case (θ_1=0 θ_2=1), the spare capacity in SS-PC-ILP is even bigger than that in PC-ILP, this is because without optimizing the FSs usage on each link, SS-PC-ILP satisfies minimum FSs index objective with more spectrum sharing at the expense of adding spare capacity. Thus, to make a fair comparison, we choose weighting θ_1=1, θ_2=1 in the following simulations.

4.6.2 FSs allocation advantage in SS-p-cycles

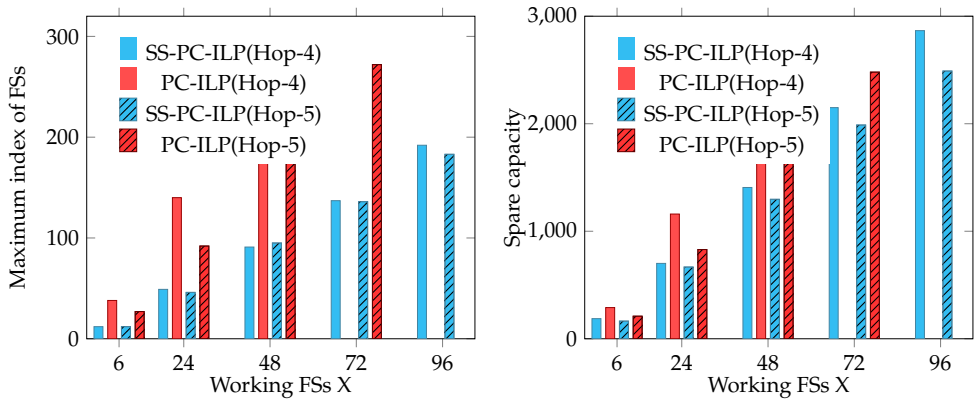

(a) Maximum index of FSs

(b) Spare capacity in terms of FSs

Figure 4.2: *FSs allocation in COST239 topology in SS-PC-ILP and PC-ILP in [137].*

We generate candidate p-cycles with different hop-count limits in COST239 and US Backbone typologies. A bigger hop-count limit results in more candidate p-cycles. The TiLim in CPLEX is set to be $\leq$ 3600 s. Figures 4.2 and 4.3 show the results on spare capacity and maximum index of FSs usage in SS-PC-ILP and PC-ILP, respectively. The SS-PC-ILP achieves 28.2% lower spare capacity and 57.5% lower maximum index of FSs in average than PC-ILP in COST239, and the amount is 14.8% and 30.8% in US Backbone, respectively. The bigger reduction in COST239 results from the more options for SS-p-cycles generation with efficient FSs allocation due to a bigger nodal degree. Moreover, for a relatively bigger working FSs, the PC-ILP method even could not obtain a solution (*e.g.*, X=72, 96 in Fig. 4.2), while it still can be solved by SS-PC-ILP. This is because the FSs allocation is much more efficient in SS-PC-ILP. If the hop-count limit

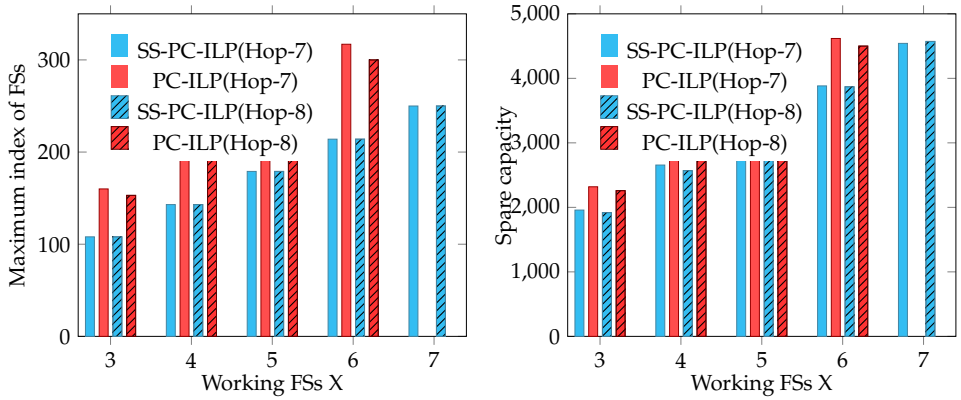

(a) Maximum index of FSs (b) Spare capacity in terms of FSs

Figure 4.3: *FSs allocation in US Backbone topology in SS-PC-ILP and PC-ILP in [137].*

increases, the FSs allocation in SS-PC-ILP does not change too much while it decreases a lot in PC-ILP (Note that it still could not obtain a solution with a bigger working FSs). It indicates that SS-PC-ILP has the priority to choose p-cycles with smaller hop-count limit, which also has advantage in utilizing the advanced modulation format with high spectral efficiency even though we do not consider it in this study.

4.6.3 Spectrum allocation in SS-p-cycles with/without spectrum conversion

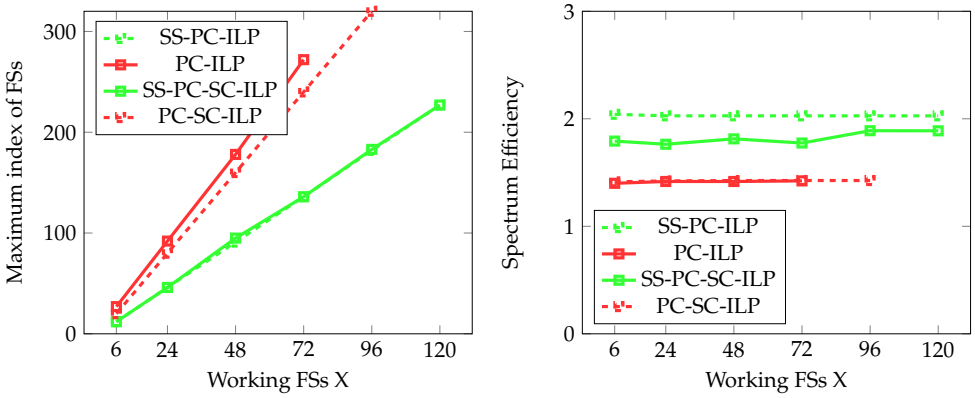

(a) Maximum index of FSs (b) Spectrum Efficiency

Figure 4.4: *FSs allocation in COST239 topology in SS-p-cycles and conventional no-shared p-cycles with/without spectrum conversion.*

Figure 4.4 shows spectrum allocation of p-cycles in COST239. We can see that the maximum index of FS' in the proposed SS-p-cycles is much smaller than the convectional no-shared p-cycles, and it is the same for SS-PC-ILP and SS-PC-SC-ILP. The reduction of maximum index of FS' in SS-p-cycles is about 50% and 44% with/without

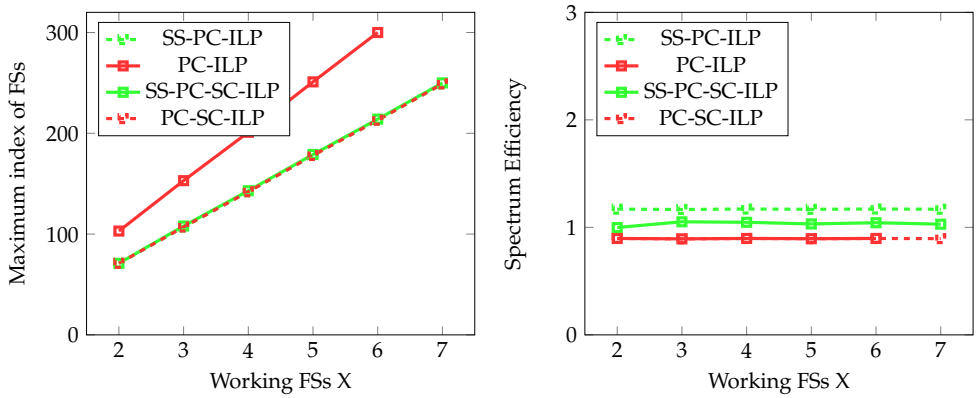

(a) Maximum index of FSs

(b) Spectrum Efficiency

Figure 4.5: *FSs allocation in US Backbone topology in SS-p-cycles and conventional no-shared p-cycles with/without spectrum conversion.*

spectrum conversion, respectively. For spectrum efficiency, SS-PC-SC-ILP earns the largest, PC-ILP and PC-SC-ILP obtain the smallest, and SS-PC-ILP lies in between. We also see that there are almost constant spectrum efficiency for all the four cases. More importantly, for a relatively higher working FS' (X=*96, 112*), the PC-ILP method could not obtain a solution even in the case with spectrum conversion. However, SS-p-cycles still can protect the higher working traffic. This is because the FS' allocation is much more efficient in SS-p-cycles with spectrum sharing.

Figure 4.5 shows spectrum allocation in US Backbone. We still can observe the SS-p-cycles require less amount of maximum index of FSs and earn higher spectrum efficiency than no-shared p-cycles. Specifically, the reduction of maximum index of FSs in SS-PC-ILP is about 29% than in PC-ILP. Again, the PC-ILP method could not obtain a solution for a relatively higher working FSs (X=*7*). However, it is a little different from the results in Fig. 4.4 as the PC-SC-ILP requires the same amount of maximum index of FSs as SS-PC-ILP and SS-PC-SC-ILP. This is because the bigger topology gives conventional spectrum no-shared p-cycle design more possibilities to earn better spectrum allocation. Nevertheless, the spectrum efficiency in conventional spectrum no-shared p-cycle design is still less than the proposed SS-p-cycles. We also see that spectrum conversion does not improve the spectrum efficiency in spectrum no-shared p-cycle.

We can see that SS-p-cycles requires the same maximum number of spectrum usage in the two cases while SS-p-cycle with spectrum conversion earns higher spectrum efficiency. Moreover, SS-p-cycles obtain better spectrum allocation than the conventional no-shared p-cycle. We also observe that the spectrum conversion does help p-cycle design to acquire better spectrum utilization, but it shows different impacts on maximum index of FSs and spectrum efficiency under different p-cycle design methods and different network nodal degrees. Moreover, even SS-p-cycles without spectrum conversion can obtain comparable or better spectrum allocation than conventional no-shared p-cycles with spectrum conversion.

Table 4.4: *SFR and Execution time.*

Traffic with FSs in [1,X]	SFR			Computation time		
	SS-PC-ILP	SS-PC-SA	PC-SA	SS-PC-ILP	SS-PC-SA	PC-SA
X=3	0.03854	0.00004	0.12871	3600 s	3.79s	3.75 s
X=4	0.03968	0	0.1614	3600 s	3.97s	3.96 s
X=5	0.12161	0.00297	-	3600 s	3.41s	-
X=6	0.07927	0.00447	-	3600 s	3.44s	-
X=7	0.11075	0.00074	-	3600 s	4.04s	-

4.6.4 Performance evaluation of SS-PC-SA algorithm

We then conduct simulations with SS-PC-SA algorithm in US backbone network (28 nodes and 45 links) under $|I| = 59$ and $n = 7$. To evaluate the comparative performance of SS-PC-SA algorithm, two references are used: the proposed SS-PC ILP, and a spectrum no-shared p-cycle algorithm PC-SA that is modified from SS-PC-SA.

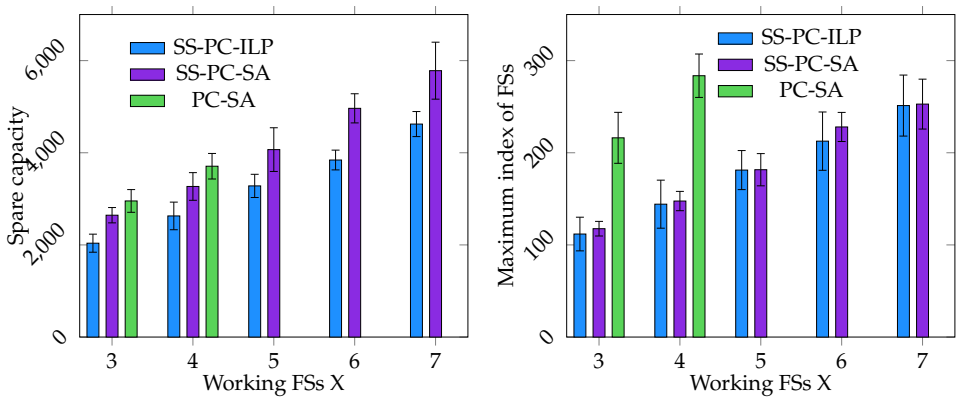

(a) Spare capacity (b) Maximum index of FSs

Figure 4.6: *FSs allocation in US backbone with SS-PC, SS-PC-SA and PC-SA.*

Figure 4.6 shows the FSs allocation results with confidence level 95% in SS-PC ILP, SS-PC-SA, and PC-SA. For all the traffic instances, SS-PC ILP needs the least FSs resource and SS-PC-SA requires a little more FSs, while PC-SA consumes the most FSs resource. Note that PC-SA can not even obtain a solution for a bigger working FSs (*e.g.*, $X = 5; 6; 7$) because the maximum FSs in PC-SA is beyond the limit $B = 320$. However, the spectrum sharing in SS-p-cycles results in efficient spectrum allocation so that fewer FSs are required. Overall, the reduction of spare capacity and maximum index of FSs in SS-PC-SA are about 12.6% and 46.8% compared with PC-SA, respectively, while a increase of these two metrics in SS-PC-SA are 20.9% and 3.0% when comparing with the results acquired in SS-PC ILP.

We also evaluate the spectrum defragmentation and computation time of SS-PC-

ILP, SS-PC-SA and PC-SA, which are shown in Tab. 4.4. It is observed that PC-SA has the biggest SFR due to its inefficient FSs allocation without spectrum sharing. It still can not obtain a solution for bigger working FSs (*e.g.*, $X = 5; 6; 7$). We notice that the SFR in SS-PC-SA is the smallest and even smaller than SS-PC ILP. This is because the coloring method used for FSs allocation in PC-SA forces to assign FSs from the smallest index side. The significant advantage on defragmentation efficiency in SS-p-cycles can also result in low blocking performance in dynamic case [37], which can be studied as future work. For the computation time, due to the high complexity of SS-PC ILP, we set parameter $TiLim$ (*i.e.*, computation time limit) in CPLEX to be 3600 s so that the solution can be obtained before exhausting all the memory, while SS-PC-SA and PC-SA take only about 4s to obtain the solution.

4.7 Conclusion

In this chapter, we have proposed SS-p-cycles to reduce FSs usage and SFR by leveraging special spectrum sharing and defragmentation for survivable EONs. To this end, both ILP formulation and efficient heuristic algorithm are developed. Simulation results have demonstrated that SS-p-cycles have significant advantages on both FSs allocation and defragmentation efficiency compared with conventional p-cycles without spectrum sharing. We also observe that the spectrum conversion does help SS-p-cycle design to acquire better spectrum utilization, but it shows different impacts on maximum index of FSs and spectrum efficiency under different p-cycle design method and different network nodal degrees.

In addition to the protection schemes against single link failure for MLR optical networks and EONs, another potential failure case, *i.e.*, large-area disaster, becomes an increasing threat on today's optical DCNs as all the links and nodes in the disaster area will be unavailable. Different from the previous single link failure, disaster failure in elastic DCNs needs to be addressed with DC location, content placement, spectrum allocation, *etc* [14, 80, 89, 142]. In the next chapter, we will study efficient protection schemes for elastic DCNs against disaster failure.

Part IV

Path Protection Schemes for Elastic Optical DCNs against Disaster

Chapter 5

Column Generation for Cloud Services in Disaster-Survivable Elastic Optical DCNs

Contents

5.1 Introduction

EONs and DCNs offer new opportunity with flexible spectrum usage and large-scale cloud services infrastructure with lower latency, higher availability and robustness [133][86]. However, the new failure scenario of large-scale disasters, such as earthquake, hurricane, or DC power disruptions, are being threatening the optical data DCNs [53]. Survivability against disaster for cloud service becomes a critical issue for elastic optical DCNs. Nowadays, the anycast technique benefits from that the required content/service can be served from one of many potential replica DCs [48]. It introduces an additional decision constraint to choose the serving DC compared with the conventional RSA problem in EONs. However, it permits to use the backup path from another DC with replicated content rather than from the original DC. Then, the service for a request can be guaranteed if the working path and backup path do not fall into the same DZ.

Among the recent disaster-survivable optical network studies [53, 55], provisioning DZ-disjoint working and backup paths is the most common approach. In disaster-survivable elastic optical DCNs, it is $\mathcal{NP}$-hard problem to address content placement, routing, protection of path and content as well as spectrum allocation. because DZ-disjoint routing problem has been shown a $\mathcal{NP}$-complete problem [59] and the RSA problem is $\mathcal{NP}$-hard [76]. Alternatively, heuristics were explored but they only gave locally optimal solutions rather than globally optimal one. In contrast, to guarantee the optimality, ILP formulation is possible to be tractable in larger instances by some decomposition approaches such as Lagrangian decomposition and Dantzig-Wolfe decomposition. For instance, CG approach has been used as a large-scale optimization tool for joint dimensioning of server and network infrastructure for resilient WDM networks [26]. It involves a Restricted Master Problem (RMP) that is restricted from the original problem with only a subset of variables, and a Pricing Problem (PP) that identifies new variables to enter the basis depending on the dual variables obtained from the master problem.

Nevertheless, not all the RSA ILP formulations for EONs can be decomposed by CG approach as studied in [126, 153]. The spectrum allocation techniques in Linear Programming (LP) can be categorized as slot-based and channel-based, which differs in FS assignment. Slot-based LP distinguishes each FS to be assigned. One of the slot-based LP is Slots Assignment (SA), which explicitly assigns all the FSs to be used for each request. The other one is Starting Slot Assignment (SSA), which only assigns the starting FS to each demand as the number of requested FSs is fixed and contiguous [126]. However, these slot-based LP formulations require a set of dedicated variables and constraints in order to guarantee the spectrum contiguity constraint. It can lead to infeasibility of a current dual solution of slot-based LP formulations with CG approach due to the dual variable of spectrum contiguity constraint [153]. Nevertheless, channel-based LP already ensures the spectrum contiguity once the channels are generated. The channels H is the pre-computed sets of spectrum contiguous FSs, for example, the channels set for a request with 2 FSs can be represented as, *i.e.*, $\{1,1,0,...,0,0,0\}$, $\{0,1,1,...0,0,0\}$, $\cdots\cdots$, $\{0,0,0,...,1,1,0\}$, $\{0,0,0,...0,1,1\}$. Thus, the channel-based

LP can be applied for CG approach to generate new columns of routing paths with determined channel.

In this chapter, we focus on CG approach for designing the disaster-survivable elastic optical DCNs with could services. We study both DEBPP and SEBPP that assigns dedicated or shared spectrum resources for backup paths with common link(s), respectively. The objective is to minimize the spectrum usage of both working and backup paths. First, DEBPP and SEBPP ILP models are designed based on slot-based SSA formulation, which can be optimally solved for small traffic instances. Then, a CG based decomposition method is proposed with channel-based formulation, which is shown to reach a near-optimal solution in a time-efficient way. To the best of our knowledge, it is the first time that the CG approach is studied for disaster-survivable elastic optical DCNs. Furthermore, extensive numerical simulations have been conducted to study the performance of DEBPP and SEBPP with different network design parameters.

5.2 Related work

Disaster-survivable optical DCNs have been attracting increasing interests over recent years with the deployment of DCNs and growing risk of the large-scale failures [45]. Note that some studies focused on DCNs protection referred to Shared Risk Group (SRG) which is a set of links or nodes that are vulnerable to a common failure (*e.g.*, a disaster) [26]. Most of the existing work focused on WDM network disaster or SRG protection by dimensioning anycast relocation [26, 45, 55, 109, 110]. The first disaster-resilient optical DCNs design was studied considering the content placement, routing, and protection of paths and content in [55]. A disaster-resilient backup reprovisioning with partial protection scheme was proposed by exploiting tolerated degraded service heterogeneity [110]. A disaster-aware service provisioning scheme was proposed by multipath routing with manycasting in cloud networks [109]. The joint dimensioning of server and network infrastructure was investigated under both Failure-Independent (FID) and Failure-Dependent (FD) cases against SRLG failure [26]. The survey in [45] classified different disaster survivable strategies for WDM optical networks into pre-disaster network design and post-disaster network recovery. A joint progressive DC recovery after disaster failure was studied to determine which DCs should be recovered to maximize the cumulative content reachability to users at each repair stage [39].

In addition to the disaster protection schemes in WDM optical networks, the disaster-survivable EONs have been studied recently with spectrum allocation [14, 80, 89, 142]. Based on k-node connectivity, k-node content connected provisioning scheme was proposed to design disaster-resilient elastic optical DCNs [80]. The provisioning scheme enabled to generate k independent end-to-content paths and allowed spectrum sharing by a matching-based principle. In [14], a shared path protection algorithm with spectrum-shared ability was proposed to minimize blocking probability and to improve spectrum efficiency. A bandwidth-adaptive protection scheme with content connectivity was proposed against disaster in elastic optical DCNs [89]. In [142], an ILP model for shared protection against disaster was proposed by utilizing the priori method to

first maximize the network throughput, and then to minimize used spectrum resources. However, all the proposed ILP models in [80, 89, 142] applied the SA-based spectrum allocation, which has been shown more computational complexity than SSA-based spectrum allocation [126]. There is no existing work about SSA-based spectrum allocation for disaster-survivable elastic DCNs.

Moreover, ILP approaches appear impractical for reasonably large scale studies with poor scalability while heuristics mostly produce locally optimal solutions not the globally optimal solutions. However, the exact optimal solution can be acquired in a scalable way using decomposition approaches, such as CG technique [60, 61]. There has not been related studies on CG-based protection for disaster-survivable elastic DCNs even though it has been explored with anycasting service protection in elastic DCNs [47]. A relocation protection scheme using CG approach was proposed in [60], which decomposed the original ILP into a RMP and a PP, which showed that the CG decomposition largely reduce computational complexity regarding scalability and running time. An efficient shared path protection for anycast routing was proposed with both ILP model and a CG optimization approach [114]. However, this CG-based anycasting service protection scheme for elastic DCNs only works for a single link or single DC node failure, but they are not able to maintain survivability for disaster because working path and backup path are not disaster-disjoint as well as the related spectrum allocation. Thus, it is important to explore efficient CG-based approach for disaster protection in elastic DCNs.

5.3 Problem statement

We use a digraph $G(V, A, D)$ to model elastic DCNs, in which V, A and D denote the set of nodes, symmetric directed links and DC nodes, respectively. A request $r(s_r, c_r, \phi_r)$ represents the source node s_r, content c_r and required number of FSs ϕ_r (we assume the traffic amount is requested by the number of FSs). Our objective is to minimize the spectrum usage with respect to the total FSs on all the links and the maximum index of the FSs in the network. We investigate the DC assignment and content placement, DZ-joint working path and backup path generation and spectrum allocation subproblems simultaneously, which is listed as follows:

1. **DC assignment and content placement**:
   Given the possible DC nodes location, the DC assignment and content placement subproblem determines each content is placed at which DC nodes depending on the maximum number replicas per content and DZ range. In order to ensure content survivability, the same content can not be placed at the DC nodes that can be affected by the same DZ.

2. **DZ-joint working path and backup path generation**:
   The working path and backup path should be DZ-joint so that the survivability of working path against single DZ failure can be guaranteed. The path generation in the network should follow the flow conservation constraint. Two types

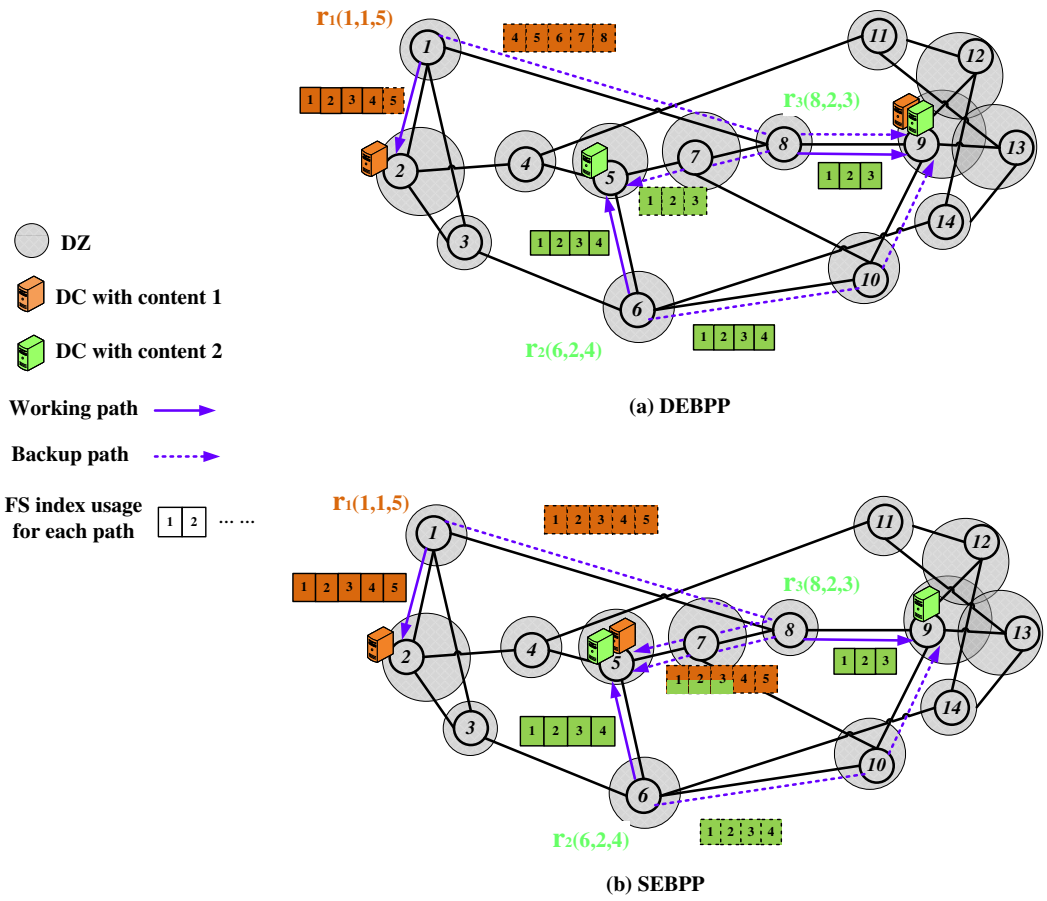

Figure 5.1: *Optimal solution acquired by DEBPP and SEBPP with three requests in NSFNET topology with 14 DZs.*

of backup path protection schemes are concerned in this chapter in terms of the spare capacity usage:

- DEBPP: The spare capacity on backup paths are dedicated for the corresponding working paths, and it can not be shared among different backup paths with common links.
- SEBPP: The spare capacity can be shared among different backup paths on their common links as long as their working paths are not be affected by the same DZ.

3. **Spectrum allocation**:
   A continuous range of FSs are allocated for each working path and backup path under the following principles.
   - *Spectrum continuity*: We assume that there is no spectrum conversion in the network. Thus, all the links along the working path or backup path should

Table 5.1: *Spectrum usage in DEBPP and SEBPP with three requests.*

Schemes	Total FSs usage	Link FSs usage	Maximal index FS
DEBPP	44	36	8
SEBPP	40	35	5

be assigned the same FSs.

- *Spectrum contiguity*: The FSs allocated to the paths should be neighboring on the optical spectrum, which is ensured by allocating a set of continues FS index.
- *Spectrum conflict*: The spectrum conflict may occur on the working-backup path pair that has common link among the same request or different requests. More spectrum conflict information is described depending on the type of DEBPP and SEBPP in Sec. 5.4. Note that in order to efficiently utilize the spectrum resources, the paths can share the same FSs as long as they do not have spectrum conflict.

The disaster-survivable problem involves the interdependencies in the optimization among the subproblems of DC location, content replica, and working path and backup path generation as well as the spectrum allocation. Apart from the difference in allocating FSs index in the spectrum allocation process, when multiple DCs are available for the content placement, there are a number of network parameters that can be controlled directly or indirectly to affect the spectrum allocation decision. This is because spectrum usage interrelates with the length and routes of working and backup paths, which is originally affected by the DC nodes location with content replica. Thus, the spectrum allocation, DC assignment and content placement, path generation and their interdependencies make service provisioning establishment in elastic DCNs very complicated. We aim at minimizing the spectrum usage while considering all the subproblems simultaneously in order to acquire the optimal solution of the disaster-survivable problem for elastic DCNs.

Here, a simple example in Fig. 5.1 shows how the total spectrum usage can be reduced by jointly optimizing the three subproblems. A NSFNET topology is given with 4 available DC nodes (at 2, 5, 9 and 11), 2 content and 14 possible DZs failure [55]. We assume that three requests, $r_1(1,1,5)$, $r_2(6,2,4)$ and $r_3(8,2,3)$, need to be provisioned with the maximum number of replica $K = 2$ per content. The optimal solution acquired by both DEBPP and SEBPP are illustrated in Fig. 5.1 with the working path, backup path and used FS index by jointly considering all the subproblems mentioned above. DEBPP and SEBPP have different content placement as well as the routes of working and backup paths. Specifically, we can see DEBPP places content 1 at DC nodes 2 and 9 while SEBPP places content 1 at DC nodes 2 and 5. This is because potential spectrum sharing in SEBPP can be achieved on the links 5-7 and 7-8 after generating the backup paths. The FS index besides each working and backup path shows the spectrum usage for provisioning the request under the spectrum conflict consideration. The spectrum

Table 5.2: *Notations*

Network Sets and Parameters	
$G(V, A, D)$	Network topology with node V, link set A and DC set D.
C	Set of content.
K	The maximum number of replicas per content.
Z	Set of DZs. As a subgraph of G, each z contains a set of edges and nodes.
S	Set of FSs on each fiber link and $\|S\|$ is the total number of available FSs.
R	Set of request $r(s_r, c_r, \phi_r)$, where s_r is the source node, c_r is the content, and ϕ_r is the required FSs.
Ψ_v^+	Set of outgoing links from node $v \in V$.
Ψ_v^-	Set of incoming links from node $v \in V$.
N_v	Set of adjacent nodes at node $v \in V$.
Variables in ILP formulations of DEBPP and SEBPP	
$p_{ra}^W \in \{0, 1\}$	Equals 1 if link a is used in the working path of request $r(s_r, c_r, \phi_r)$, and 0 otherwise.
$p_{ra}^B \in \{0, 1\}$	Equals 1 if link a is used in the backup path of request $r(s_r, c_r, \phi_r)$, and 0 otherwise.
$\Lambda_{rd}^W \in \{0, 1\}$	Equals 1 if DC d is used as the primary DC for request $r(s_r, c_r, \phi_r)$, and 0 otherwise.
$\Lambda_{rd}^B \in \{0, 1\}$	Equals 1 if DC d is used as the backup DC for request $r(s_r, c_r, \phi_r)$, and 0 otherwise.
$\alpha_{rz}^W \in \{0, 1\}$	Equals 1 if working path of $r(s_r, c_r, \phi_r)$ goes through DZ z, and 0 otherwise.
$\alpha_{rz}^B \in \{0, 1\}$	Equals 1 if backup path of $r(s_r, c_r, \phi_r)$ goes thorough DZ z, and 0 otherwise.
$R_d^c \in \{0, 1\}$	Equals 1 if content c is replicated at DC d, and 0 otherwise.
$g_r^W \in [0, \|S\| - 1]$	An integer variable denoting the assigned starting FS index of working path for request $r(s_r, c_r, \phi_r)$.
$g_r^B \in [0, \|S\| - 1]$	An integer variable denoting the assigned starting FS index of backup path for request $r(s_r, c_r, \phi_r)$.
$\beta_{rr'}^W \in \{0, 1\}$	Equals 1 if g_r^W of request $r(s_r, c_r, \phi_r)$ is smaller than $g_{r'}^W$ of request $r'(s_{r'}, c_{r'}, \phi_{r'})$, and 0 otherwise.
$\beta_{rr'}^B \in \{0, 1\}$	Equals 1 if g_r^B of request $r(s_r, c_r, \phi_r)$ is smaller than $g_{r'}^B$ of request $r'(s_{r'}, c_{r'}, \phi_{r'})$, and 0 otherwise.
$\beta_{rr'}^{WB} \in \{0, 1\}$	Equals 1 if g_r^W of request $r(s_r, c_r, \phi_r)$ is smaller than $g_{r'}^B$ of request $r'(s_{r'}, c_{r'}, \phi_{r'})$, and 0 otherwise.
$\gamma_{rr'}^W \in \{0, 1\}$	Equals 1 if the working path of request $r(s_r, c_r, \phi_r)$ and working path of request $r'(s_{r'}, c_{r'}, \phi_{r'})$ share at least one common link, and 0 otherwise.
$\gamma_{rr'}^B \in \{0, 1\}$	Equals 1 if the backup path of request $r(s_r, c_r, \phi_r)$ and backup path of request $r'(s_{r'}, c_{r'}, \phi_{r'})$ share at least one common link, and 0 otherwise.
$\gamma_{rr'}^{WB} \in \{0, 1\}$	Equals 1 if the working path for request $r(s_r, c_r, \phi_r)$ and backup path for request $r'(s_{r'}, c_{r'}, \phi_{r'})$ share at least one common link, and 0 otherwise.
$j_{raz}^B \in \{0, 1\}$	Equals 1 if backup path of request $r(s_r, c_r, \phi_r)$ is used upon disaster z, and 0 otherwise.
$T_a \in [0, \|S\|]$	The total number of spare capacity units (in FS) that should be served on link a.
$\Delta \in [0, \|S\|]$	The maximal index of used FSs.

usage of DEBPP and SEBPP is further summarized in Tab. 5.1. We can see that less spectrum (with link usage 35 FSs and maximal index 5 FSs) is required in the SEBPP owing to the spectrum sharing on the links 5-7 and 7-8. The spectrum sharing reduces not only the total FS used on all the links but also the maximum FS index. However, the dedicated FSs should be reserved for all the backup paths in DEBPP, which consumes link usage 36 FSs and maximal index 8 FSs.

5.4 Joint ILP formulations

In this section, we formulate two joint ILP models of dedicated end-to-content backup path protection and shared end-to-content backup path protection, respectively, namely DEBPP ILP and SEBPP ILP. We first present some notations in Tab. 5.2. For the sake of readability, we use $\forall v$, $\forall u$, $\forall a$, $\forall d$, $\forall c$, $\forall z$ and $\forall r$ to denote $\forall v \in V$, $\forall u \in N_v$, $\forall a \in A$, $\forall d \in D$, $\forall c \in C$, $\forall z \in Z$ and $\forall r \in R$, respectively.

Objective:

$$\min \quad \theta_1 \cdot (\sum_{a \in A} \sum_{r \in R} p_{ra}^{W} \cdot \phi_r + \sum_{a \in A} T_a) + \theta_2 \cdot \Delta \tag{5.1}$$

- Link-FSs: It is the first term that represents the sum of FSs usage on all the links of working paths and backup paths..
- Maximal-FSs: It is second term that represents the maximal index of occupied FSs.

DEBPP and SEBPP ILPs have the same objective function, which is shown in (5.1). The first term of the objective function is the total FSs usage on all the links of working paths and backup paths. The second term is the maximal index of occupied FSs. Their value affects the spectrum resource requirement and the overall spectrum utilization, respective. We minimize both of them using adjustable weighting parameters θ_1 and θ_2.

5.4.1 DEBPP ILP model

Constraints: *s.t.* (5.2)-(5.26)

The constraints in DEBPP ILP can be classified into **DC assignment and content placement constraints** (5.2)-(5.5), **flow-conservation constraints** (5.6)-(5.7), **disaster-zone-disjoint path constraints** (5.8)-(5.12) and **spectrum allocation constraints** (5.13)-(5.26).

1) **DC assignment and content placement constraints**:

Constraints (5.2)-(5.3) ensure only one primary DC and one backup DC are assigned for each request. Note that the backup DC should be different from the primary DC so

that the DZ-disjoint path constraints can be satisfied. Constraints (5.4)-(5.5) are established to conduct content placement in different DCs. For each content c, the number of replicas is limited to K. For each request r, the selection of primary DC and backup DC should make sure that the presence of the requested content c_r.

$$\sum_{d \in D} \Lambda_{rd}^{W} = 1, \qquad \forall r \tag{5.2}$$

$$\sum_{d \in D} \Lambda_{rd}^{B} = 1, \qquad \forall r \tag{5.3}$$

$$\sum_{d \in D} R_{d}^{c} \leq K, \qquad \forall c \tag{5.4}$$

$$\Lambda_{rd}^{W} + \Lambda_{rd}^{B} \leq R_{d}^{c_r}, \qquad \forall r, \forall d \tag{5.5}$$

2) **Flow-conservation constraints**:

Constraints (5.6)-(5.7) generate working path and backup paths through flow conservation. Specifically, the outgoing flow and incoming flow are equal unless it is a destination (DC) node, which has only incoming flow, or requesting node, which has only outgoing flow.

$$\sum_{a \in \Psi_v^+} p_{ra}^{W} - \sum_{a \in \Psi_v^-} p_{ra}^{W} = \begin{cases} 1, & v = s_r \\ -\Lambda_{rv}^{W}, & v \in D, \\ 0, & \text{otherwise} \end{cases} \qquad \forall r, \forall v. \tag{5.6}$$

$$\sum_{a \in \Psi_v^+} p_{ra}^{B} - \sum_{a \in \Psi_v^-} p_{ra}^{B} = \begin{cases} 1, & v = s_r \\ -\Lambda_{rv}^{B}, & v \in D, \\ 0, & \text{otherwise} \end{cases} \qquad \forall r, \forall v. \tag{5.7}$$

3) **Disaster-zone-disjoint path constraints**:

Constraints (5.8)-(5.9) and (5.10)-(5.11) are used to determine if the working path and backup path are affected by each disaster, respectively. More specifically, $\alpha_{rz}^{W}(\alpha_{rz}^{B})$ equals 1 if there exists link(s) in DZ z consisting the working(backup) path. Constraint (5.12) guarantees the DZ-disjoint property of working and backup paths.

$$\alpha_{rz}^{W} \leq \sum_{a \in z} p_{ra}^{W}, \qquad \forall r, \forall z \tag{5.8}$$

$$\alpha_{rz}^{W} \geq p_{ra}^{W}, \qquad \forall r, \forall z, \forall a \in z \tag{5.9}$$

$$\alpha_{rz}^{B} \leq \sum_{a \in z} p_{ra}^{B}, \qquad \forall r, \forall z \tag{5.10}$$

$$\alpha_{rz}^{B} \geq p_{ra}^{B}, \qquad \forall r, \forall z, \forall a \in z \tag{5.11}$$

$$\alpha_{rz}^{W} + \alpha_{rz}^{B} \leq 1, \qquad \forall r, \forall z \tag{5.12}$$

4) **Spectrum allocation constraints**:

Constraints (5.13) and (5.14) indicate whether the working paths of two requests have any common link, while constraints (5.15) and (5.16) determine whether the backup

paths of two requests have any common link. Constraint (5.17) indicates whether the working path of request r and the backup path of request r' have any common link. Constraints (5.18) and (5.19) make the comparison of starting index of FSs between the working paths of two requests and the backup paths of two requests, respectively. Constraints (5.20) and (5.21) imply the maximum index of occupied FSs.

$$p^W_{ra} + p^W_{r'a} - 1 \leq \gamma^W_{rr'}, \qquad \forall r, r', r > r', \forall a \tag{5.13}$$
$$\gamma^W_{rr'} = \gamma^W_{r'r}, \qquad \forall r, r', r > r' \tag{5.14}$$
$$p^B_{ra} + p^B_{r'a} - 1 \leq \gamma^B_{rr'}, \qquad \forall r, r', r > r', \forall a \tag{5.15}$$
$$\gamma^B_{rr'} = \gamma^B_{r'r}, \qquad \forall r, r', r > r' \tag{5.16}$$
$$p^W_{ra} + p^B_{r'a} - 1 \leq \gamma^{WB}_{rr'}, \qquad \forall r, r', r \neq r', \forall a \tag{5.17}$$
$$\beta^W_{rr'} + \beta^W_{r'r} = 1, \qquad \forall r, r', r > r' \tag{5.18}$$
$$\beta^B_{rr'} + \beta^B_{r'r} = 1, \qquad \forall r, r', r > r' \tag{5.19}$$
$$g^W_r + \phi_r \leq \Delta, \qquad \forall r \tag{5.20}$$
$$g^B_r + \phi_r \leq \Delta, \qquad \forall r \tag{5.21}$$

For two different requests r and r', the spectrum conflict principle in DEBPP is conducted as follows:

- Working-working path pair $p^W_r - p^W_{r'}, \forall r, r', r \neq r'$: the spectrum conflict occurs as long as the working-working path pair has at least one common link.
- Working-backup path pair $p^W_r - p^B_{r'}, \forall r, r', r \neq r'$: the spectrum conflict occurs as long as the working-backup path pair has at least one common link
- Backup-backup path pair $p^B_r - p^B_{r'}, \forall r, r', r \neq r'$: the spectrum conflict occurs as long as the backup-backup path pair has at least one common link.

Based on the SSA principle mentioned before, constraint (5.22) avoids spectrum conflict among working paths of all the requests and also allows that the working paths of two requests can share the same FSs if they do not have any common link. Note that the *spectrum contiguity* is ensured by setting a contiguous range of FSs ϕ_r for each request. Constraint (5.23) calculates the total FSs used for protection on each link in DEBPP. Constraints (5.24) and (5.25) avoid spectrum conflict among the working path of request r and backup path of request r' and also allows that the two paths can share the same FSs if they do not have spectrum conflict. As the DEBPP uses dedicated path for protection, then any two backup paths can not share FSs on common link, which is restricted by constraint (5.26).

$$g^W_r + \phi_r - g^W_{r'} \leq \Delta \cdot (2 - \gamma^W_{rr'} - \beta^W_{rr'}), \qquad \forall r, r', r \neq r' \tag{5.22}$$
$$T_a \geq \sum_{r \in R} p^B_{ra} \cdot \phi_r, \qquad \forall a \tag{5.23}$$
$$g^W_r + \phi_r - g^B_{r'} \leq \Delta \cdot (2 - \gamma^{WB}_{rr'} - \beta^{WB}_{rr'}), \qquad \forall r, r', r \neq r' \tag{5.24}$$
$$g^B_{r'} + \phi_{r'} - g^W_r \leq \Delta \cdot (1 - \gamma^{WB}_{rr'} + \beta^{WB}_{rr'}), \qquad \forall r, r', r \neq r' \tag{5.25}$$
$$g^B_r + \phi_r - g^B_{r'} \leq \Delta \cdot (2 - \gamma^B_{rr'} - \beta^B_{rr'}), \qquad \forall r, r', r \neq r' \tag{5.26}$$

5.4.2 SEBPP ILP model

Constraints: *s.t.* (5.2)-(5.22) and (5.28)-(5.31).

Different from DEBPP, the spectrum conflict principle in SEBPP is described as follows:

- Working-working path pair $p_r^W - p_{r'}^W, \forall r, r', r \neq r'$: The spectrum conflict occurs as long as the working-working path pair has at least one common link.
- Working-backup path pair $p_r^W - p_{r'}^B, \forall r, r', r \neq r'$: The spectrum conflict also depends on the corresponding working path ($p_{r'}^W$) of the backup path $p_{r'}^B$. The spectrum conflict occurs when the following two conditions happen: 1) p_r^W and $p_{r'}^B$ have at least one common link; 2) There exists at least one DZ z that does not affect $p_{r'}^W$ and p_r^W simultaneously. Otherwise, suppose DZ z_1 affects $p_{r'}^W$ but does not affect p_r^W, then when DZ z_1 failure occurs, both p_r^W and $p_{r'}^B$ need to use the spectrum resources on the common link.
- Backup-backup path pair $p_r^B - p_{r'}^B, \forall r, r', r \neq r'$: The spectrum conflict also depends on the corresponding working paths $p_{r'}^W$ and p_r^W. The spectrum conflict occurs when the following two conditions happen: 1) p_r^B and $p_{r'}^B$ have at least one common link; 2) $p_{r'}^W$ and p_r^W fall into at least one same DZ.

To perform spectrum sharing in SEBPP formulation, the constraints (5.23)-(5.26) are replaced by the following constraints (5.27)-(5.30).

$$T_a \geq \sum_{r \in R} p_{ra}^B \cdot \phi_r \cdot \alpha_{rz}^W, \qquad \forall a, \forall z \tag{5.27}$$

$$g_r^W + \phi_r - g_{r'}^B \leq \Delta \cdot (3 - \gamma_{rr'}^{WB} - \beta_{rr'}^{WB} - \alpha_{r'z}^W + \alpha_{rz}^W),, \qquad \forall r, r', r \neq r', \forall z \tag{5.28}$$

$$g_{r'}^B + \phi_{r'} - g_r^W \leq \Delta \cdot (2 - \gamma_{rr'}^{WB} + \beta_{rr'}^{WB} - \alpha_{r'z}^W + \alpha_{rz}^W), \qquad \forall r, r', r \neq r', \forall z \tag{5.29}$$

$$g_r^B + \phi_r - g_{r'}^B \leq \Delta \cdot (4 - \gamma_{rr'}^B - \beta_{rr'}^B - \alpha_{rz}^W - \alpha_{r'z}^W), \qquad \forall r, r', r \neq r', \forall z \tag{5.30}$$

Constraint (5.27) calculates the total FSs used for protection on each link in SEBPP. Note that SEBPP allows the backup paths of two requests to share the same FSs if their working paths are not affected by the same disaster. The formulation of spectrum allocation in SEBPP is based on the spectrum conflict principle. More specifically, working path of request r and backup path of request r' can also share the same FSs unless there exists a DZ z that affects the working path of r' rather than that of r. Constraints (5.28) and (5.29) allow to share FSs among the working path of request r and backup path of request r' even though they have common link(s). Constraint (5.30) permits to share FSs among the backup paths of requests even though they have common link(links).

In order to ensure linearity, constraint (5.27) is rewritten as constraints (5.31).

$$\Longrightarrow \begin{cases} T_a \geq \sum_{r \in R} j_{raz}^B \cdot \phi_r, & \forall a, \forall z \\ j_{raz}^B \geq p_{ra}^B + \alpha_{rz}^W - 1, & \forall r, \forall a, \forall z \\ j_{raz}^B \leq (p_{ra}^B + \alpha_{rz}^W)/2, & \forall r, \forall a, \forall z \end{cases} \tag{5.31}$$

5.4.3 Computational complexity

Table 5.3: *Computational complexities of DEBPP and SEBPP ILP models.*

No. of dominant variables	
DEBPP	$max\{O(\|R\|^2, \|R\|\|A\|, \|R\|\|Z\|, \|C\|\|D\|)\}$
SEBPP	$max\{O(\|R\|^2, \|R\|\|A\|, \|R\|\|Z\|, \|C\|\|D\|)\}$
No. of dominant constraints	
DEBPP	$max\{O(\|R\|^2\|A\|, \|R\|\|Z\|\|A\|)\}$
SEBPP	$max\{O(\|R\|^2\|A\|, \|R\|^2\|Z\|, \|R\|\|Z\|\|A\|)\}$

The number of dominant variables and constraints in DEBPP and SEBPP ILP models are summarized in Tab. 5.3. The number of dominant variables is the same in these two models while the number of dominant constraints in SEBPP ILP also depends on the $O(|R|^2|Z|)$ in addition to the $O(|R|^2|A|)$ and $O(|R||Z||A|)$ in DEBPP ILP.

5.5 Decomposition approach

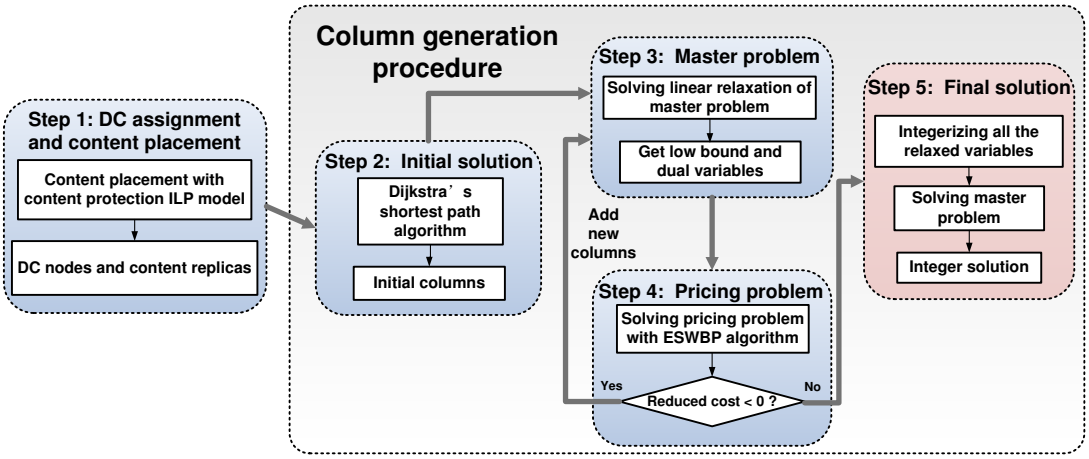

Figure 5.2: *Flow chart for the decomposition approach.*

In this section, decomposition is conducted to address the scalability issue of DEBPP and SEBPP ILP models. We first adapt the content placement ILP model with disaster-survivable content protection in [55] to obtain the DC assignment and content placement. Since there are an enormous number of lightpaths associated with spectrum allocation, the complexity of generating lightpaths and allocating spectrum is extremely large, and thus, it is computationally prohibitive to solve the full version of the DEBPP and SEBPP ILP models. Additionally, only those solutions that employ a limited number of lightpaths with spectrum allocation are clinically relevant. CG technique is applied to begin with an initial solution, then conducts as an iterative approach with the

following two problems:

1. Master problem: A restricted version of DEBPP and SEBPP ILP models with a confined set of lightpaths with spectrum allocation. This yields the optimal lightpaths with spectrum conflict consideration.

2. Pricing problem: Given the solution to the master problem, the pricing problem is solved to identify new promising lightpaths with spectrum allocation to be added to the lightpaths set to improve the objective function.

The procedure of the decomposition approach for DEBPP and SEBPP ILP models is explained in Fig. 5.2. Specifically, *Step 1* obtains the content replicas in the DC nodes through the ILP model proposed in [55]. *StepS 2-5* conduct the CG procedure. Specifically, an initial solution is achieved in *Step 2* using the ESWBP algorithm, which enables to generate the initial columns for working and backup paths of all the requests. Note that these initial columns are already configured with spectrum allocation. Then, *Step 3* solves the LPR of the master problem, from which we can get the value of the dual variable for each constraint in the master problem. After, the pricing problem in *Step 4* is executed to find new promising working and backup paths based on the value of dual variables. These new paths are confirmed to become the new columns in master problem as long as the reduced cost of the pricing problem is negative, which indicates that theses new paths would contribute to decreasing the objective function. The master-pricing loop is solved iteratively until no new column can be found, which occurs when the pricing problem returns a solution with non-negative reduced cost. *Step 5* integerizes the relaxed variables in master problem and solves it again to achieve a near-optimal integer solution by a solver like CPLEX. Note that the optimal integer solution can be acquired by re-solving the master problem using the branch-and-bound approach, which is neglected in this paper, but it can be left for future work due to its high complexity.

5.5.1 Step 1. DC assignment and content placement

We first calculate the DC node location and content replicas according to the traffic requests, DZ, and maximum number of replicas per content. The DC assignment and content placement problem can be solved by the ILP model in [55], whose objective is to place each content in K DC nodes such that the average distance from the requesting nodes to the destination DC nodes for all the requests is minimized. The efficient content placement is acquired by placing a content in those DCs closer to its popular region [1], which can reduce the spectrum resources used by working and backup paths. This ILP model ensure the existence of working path and backup path for each demand with requested content against any single DZ failure.

[1] It is defined as a region that includes most requesting nodes of this content.

5.5.2 Step 2. Initial solution

Step 2 is to give an initial solution that is essential for the master problem in the next step. Based on the DC location with content replicas acquired in the *Step 1*, we generate the initial working paths and backup paths as well as the associated spectrum usage. The initial solution is calculated in the following steps:

1). Computing initial working and backup paths

Dijkstra's shortest path algorithm is used to compute the initial working and backup paths. The working path with minimum hop count is acquired by comparing all the shortest paths from each possible primary DC. Based on the route of working path, the backup path is generated with disaster-disjoint consideration by removing all the nodes and links in the DZs that can affect the working path. Then, the backup path is also acquired by comparing all the shortest paths from each possible backup DC. Thus, the DZ-disjoint paths are guaranteed against single DZ failure.

2). Allocating spectrum usage

We construct a conflict graph to perform the spectrum allocation for the computed working and backup paths. In this conflict graph, each vertex represents a working/backup path, and an edge is added to link the two vertices if the path pair has spectrum conflict. Note that the path pair here indicates the arbitrary combination of working-working path pair, working-backup path pair and backup-backup path pair for the same request or different requests. The spectrum conflict of different path pair in DEBPP and SEBPP is conducted referred to Sec. 5.4. The adjacent vertices can not be assigned the same FS. Then, the spectrum allocation for those paths is transformed into a coloring problem in the constructed conflict graph. To this end, we apply a coloring heuristic to perform the spectrum allocation that minimizes the total number of spectrum usage on all the links [140]. Hence, the initial solution of the lightpaths is achieved with good quality in terms of disaster survivability and spectrum usage.

5.5.3 Step 3. Master problem

The master problem handles the selection of the most promising lightpaths under spectrum conflict consideration. Here, in order to get a CG formulation, we introduce the concept of a configuration $\omega \in \Omega$, where Ω denotes the overall set of configurations. A configuration $\omega \in \Omega_r$ is defined for a given request $r(s_r, c_r, \phi_r)$, and it describes a potential provisioning of the working and backup paths as well as the spectrum channels. The additional set, parameters and variables in master problem are summarized in Tab. 5.4.

We suppose that we know beforehand the overall set of configuration Ω containing the candidate promising lightpaths for each request. These promising lightpaths are first acquired in the initial solution, and then they are added and updated in each itera-

tion of the master-pricing loop until no promising lightpath can be found. The optimal solution is obtained in the master problem by optimizing the total spectrum usage, in which the objective is the same as that in the ILP models in Sec. 5.4. Thus, the master problem can be formulated as follows for DEBPP and SEBPP, respectively.

Table 5.4: *Additional set, parameters and variables in master problem*

Additional parameters in master problem	
H	Set of channels, *i.e.*, $H_r = \|S\| - \phi_r + 1$ for a specific $r(s_r, c_r, \phi_r)$.
h	Spectrum channel of working path.
h'	Spectrum channel of backup path.
B_h	Set of contiguous FSs occupied in channel $h \in H$.
Ω	The overall set of configurations. Ω_r indicates the set of configurations for a request $r \in R$.
$\omega \in \Omega_r$	The ω-th configuration for request r describes a pair of working and backup paths as well as the assigned channel.
$p^W_{\omega rah} \in \{0,1\}$	Equals 1 if link a is used by the working path of ω-th configuration for request r with channel h, and 0 otherwise.
$p^B_{\omega rah'} \in \{0,1\}$	Equals 1 if link a is used by the backup path of ω-th configuration for request r with channel h', and 0 otherwise.
$\alpha^W_{\omega rz} \in \{0,1\}$	Equals 1 if the working path of ω-th configuration for request r goes through DZ z, and 0 otherwise.
Variables in master problem	
$q^\omega_r \in \{0,1\}$	Equals 1 if ω-th configuration for request r is used including the working path, backup path and assigned channels, and 0 otherwise.
$e_{af} \in \{0,1\}$	Equals 1 if link a with FS f is used by the working or backup paths of all the requests, and 0 otherwise.
$o_f \in \{0,1\}$	Equals 1 if FS f is used, and 0 otherwise.

Objective:

$$\min \quad \theta_1 \cdot \sum_{a \in A} \sum_{f \in S} e_{af} + \theta_2 \cdot \sum_{f \in S} o_f \tag{5.32}$$

The objective of both DEBPP and SEBPP is to minimize the total spectrum usage, which is the sum of link spectrum usage and the maximal index. DEBPP and SEBPP have different constraints due to the different spectrum conflict principles.

Constraints:

1). DEBPP *s.t.* (5.33)-(5.36)

$$\sum_{\omega \in \Omega_r} q_r^{\omega} = 1, \qquad \forall r \tag{5.33}$$

$$\sum_{r \in R} \sum_{\omega \in \Omega_r} (p^W_{\omega rah} + p^B_{\omega rah'}) \cdot q_r^{\omega} \leq e_{af}, \qquad \forall a, \forall f \in B_h, B_{h'} \tag{5.34}$$

$$o_f \geq e_{af}, \qquad \forall a, \forall f \tag{5.35}$$

$$o_f \geq o_{f+1}, \qquad \forall f \tag{5.36}$$

Constraint (5.33) ensures that only one configuration can be selected for each request. Constraint (5.34) restricts the spectrum conflict for the working and backup paths of all the requests according to the principle of DEBPP in Sec. 5.4. Constraints (5.35) and (5.36) deal with the spectrum usage calculation for the link usage and the maximal index.

2). SEBPP *s.t.* (5.33), (5.35)-(5.38)

$$\sum_{r \in R} \sum_{\omega \in \Omega_r} p^W_{\omega rah} \cdot q_r^{\omega} \leq e_{af}, \qquad \forall a, \forall f \in B_h \tag{5.37}$$

$$\sum_{r \in R} \sum_{\omega \in \Omega_r} \{p^W_{\omega rah} \cdot (1 - \alpha^W_{\omega rz}) + p^B_{\omega rah'} \cdot \alpha^W_{\omega rz}\} \cdot q_r^{\omega} \leq e_{af}, \qquad \forall a, \forall f \in B_h, B_{h'}, \forall z \tag{5.38}$$

In addition to the same lightpath selection and spectrum usage calculation constraint (5.33), (5.35) and (5.36) in DEBPP, SEBPP deals with different spectrum conflict principle in constraint (5.37) and (5.38), which ensure that the same FS can not be shared by the paths pair with spectrum conflict. However, it also prohibits two paths to share the same FS even if they have at least a common link in two cases: i), working-backup paths pair: the working path and the corresponding working path of the backup path always fall into the same DZ. 2) backup-backup paths pair: the two working paths of the backup-backup paths pair never fall into the same DZ.

5.5.4 Step 4. Pricing problem

The goal of the pricing problem is to generate the configuration of promising working and backup lightpaths (promising columns) with negative reduced cost, and then add them to the overall set of configuration Ω in the master problem. We first define four dual variables of the constraints (5.33), (5.34), (5.38) and (5.37) in master problem, which will serve as the input parameters in the pricing problem.

Dual variables:

- μ_r : dual variable for DEBPP and SEBPP of constraint (5.33)
- $\zeta_{af} \geq 0$: dual variable for DEBPP of constraint (5.34)
- $\rho_{af} \geq 0$: dual variable for SEBPP of constraint (5.37)

- $\eta_{afz} \geq 0$: dual variable for SEBPP of constraint (5.38)

Reduced cost:

1). DEBPP

For each request r, once a configuration ω_r is generated with the working path on spectrum channel h and backup path on spectrum channel h', the reduced cost $\bar{c}^{DEBPP}_{\omega_r}$ of the configuration ω_r is given by

$$\begin{aligned}\bar{c}^{DEBPP}_{\omega_r} &= 0 - \{\mu_r - \sum_{a\in A}\sum_{f\in B_h\cup B_{h'}}(p^W_{\omega rah} + p^B_{\omega rah'})\cdot\zeta_{af}\} \\ &= -\mu_r + \sum_{a\in A} p^W_{\omega rah}\cdot Cost^W_{\omega rah} + \sum_{a\in A} p^B_{\omega rah'}\cdot Cost^B_{\omega rah'} \end{aligned} \tag{5.39}$$

Where $Cost^W_{\omega rah}$ and $Cost^B_{\omega rah'}$ in DEBPP is defined as

$$Cost^W_{\omega rah} = \sum_{f\in B_h}\zeta_{af} \tag{5.40}$$

$$Cost^B_{\omega rah'} = \sum_{f\in B_{h'}}\zeta_{af} \tag{5.41}$$

2). SEBPP

For each request r, once a configuration ω_r is generated with the working path on spectrum channel h and backup path on spectrum channel h', the reduced cost $\bar{c}^{SEBPP}_{\omega_r}$ of the configuration ω_r is given by

$$\begin{aligned}\bar{c}^{SEBPP}_{\omega_r} &= 0 - \left(\mu_r - \sum_{a\in A}\sum_{f\in B_h} p^W_{\omega rah}\cdot\rho_{af} - \sum_{a\in A}\sum_{f\in B_h\cup B_{h'}}\sum_{z\in Z}\left\{p^W_{\omega rah}\cdot(1-\alpha^W_{\omega rz}) - p^B_{\omega rah'}\cdot\alpha^W_{\omega rz}\right\}\cdot\eta_{afz}\right) \\ &= -\mu_r + \sum_{a\in A} p^W_{\omega rah}\cdot Cost^W_{\omega rah} + \sum_{a\in A} p^B_{\omega rah'}\cdot Cost^B_{\omega rah'} \end{aligned} \tag{5.42}$$

Where $Cost^W_{\omega rah}$ and $Cost^B_{\omega rah'}$ in SEBPP is defined as

$$Cost^W_{\omega rah} = \sum_{f\in B_h}\rho_{af} + \sum_{f\in B_h\cup B_{h'}}\sum_{z\in Z}(1-\alpha^W_{\omega rz})\cdot\eta_{afz} \tag{5.43}$$

$$Cost^B_{\omega rah'} = \sum_{f\in B_h\cup B_{h'}}\sum_{z\in Z}\alpha^W_{\omega rz}\cdot\eta_{afz} \tag{5.44}$$

For each $r \in R$, a promising configuration ω_r of working and backup paths is obtained by minimizing the reduced cost $\bar{c}^{DEBPP}_{\omega_r}$ and $\bar{c}^{SEBPP}_{\omega_r}$, respectively. From Eq. (5.39) and (5.42), we observe that the $Cost^W_{\omega rah}$ and $Cost^B_{\omega rah'}$ can be the link weight with associated request and spectrum channel. Then, $p^W_{\omega rah}$ and $p^B_{\omega rah'}$ become the decision variables in the pricing problem to determine the routes of working and backup path, respectively. *A simple way to resolve our pricing problem is*: applying the K shortest path algorithm in [34] to compute the working and backup paths pair $\forall r \in R$ under all the combination of

primary DCs, backup DCs, working spectrum channels and backup spectrum channels, and find the most promising one with the minimum negative reduced cost, which will be added to the overall configuration set Ω in the master problem for the next iteration. The authors in [100] proved that it is $\mathcal{NP}$-hard to solve the pricing problem of p-cycle design that generates the promising cycles. In our case, the path generation is even more complicated as not only the working and backup paths are required but also the primary and backup DC nodes as well as the working and backup spectrum channels. Thus, we develop an ESWBP algorithm to solve the pricing problem in a reasonable time. Considering that the number of available spectrum channels $H_r = S - \phi_r + 1$ for each request $r(s_r, c_r, \phi_r)$ largely increases the complexity of the pricing problem, ESWBP algorithm only considers a subset of spectrum channel range H_r for each $r \in R$ in each iteration. For instance, Fig. 5.3 shows the example of H_r in the first iteration, 10 candidate channels in the channel range H_r (indicating the available starting FS of each channel) are available per request and the interval of H_r for the two neighbor requests is 5 FSs. In our simulations, we set the maximum FSs of the each request as 10 and the maximum spectrum overlapping between different requests as 5. Note that the value 10 and 5 can be modified accordingly, and all the channels in H have the chance to be included in H_r because the pricing problem is solved iteratively until no column with negative reduced cost can be found.

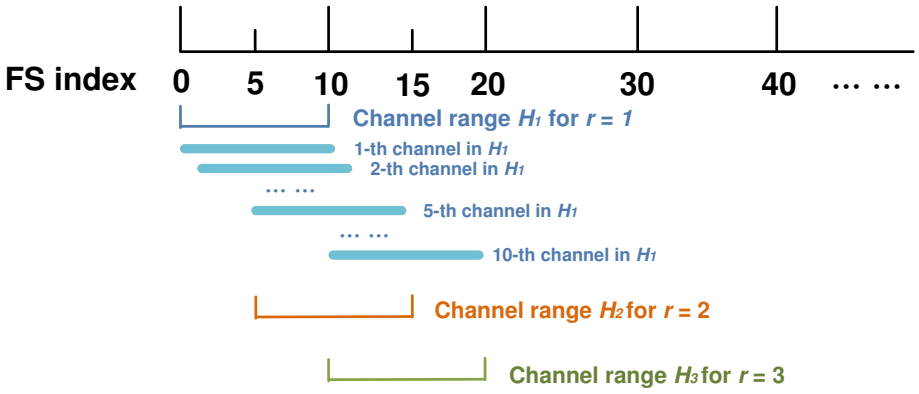

Figure 5.3: *A set of candidate channel range H_r in the first iteration for requests* 1, 2, *and* 3.

Algorithm 5 shows the detailed procedure of ESWBP algorithm. *Line 1* selects one request r and *Line 2* determines the available channel range H_r for r. *Lines 3-5* select the primary DC for r and *Lines 6-8* select the backup DC for r. *Lines 9-10* choose the working channel h and backup channel h' for r. *Line 11* calculates the link weight for working path. *Line 12* generates K shortest working path from the primary DC to s_r based on working link weight by K shortest path algorithm in [34], which is adapted to find the path with minimum negative reduced cost. Note that for working path generation in SEBPP, the term (1-$\alpha^W_{\omega rz}$) is neglected as the parameter $\alpha^W_{\omega rz}$ is unknown before the working path generation. For each $k \in K$, *Line 14* removes all the links and nodes in the DZs that affect the working path in order to ensure the disaster-disjoint

Algorithm 5: ESWBP Algorithm

Input : $G(V, A, D)$, $r(s_r, c_r, \phi_r)$, μ_r, ρ_{af}, ζ_{af}, η_{afz}, $\forall r \in R$, $\forall a \in A$, $\forall f \in S$, $\forall z \in Z$

Output: $P^W_{\omega rah}$, $\alpha^W_{\omega rz}$, $P^B_{\omega rah'}$, B_h, $B_{h'}$, $\forall r \in R$, $\forall \omega \in \Omega_r$, $\forall a \in A$, $\forall z \in Z$

1 **for** $r \in R$ **do**
2 Determine the available channel range H_r for r;
3 **for** $d \in D$ **do**
4 **if** $R^{c_r}_d = 1$ **then**
5 $\Lambda^W_{rd} \leftarrow 1$;
6 **for** $d' \in D, d' \neq d$ **do**
7 **if** $R^{c_r}_{d'} = 1$ **then**
8 $\Lambda^B_{rd'} \leftarrow 1$;
9 **for** $h \in H_r$ **do**
10 **for** $h' \in H_r$ **do**
11 Calculate working link weight $Cost^W_{\omega rah}$;
12 Generate K shortest working path $P^W_{\omega rah}$ from d to s_r with negative reduced cost based on $Cost^W_{\omega rah}$;
13 **for** $k \in K$ **do**
14 Update $\alpha^W_{\omega rz}$ and remove all a if a is in $z \in Z$ that affects $P^W_{\omega rah}$;
15 Calculate backup link weight $Cost^B_{\omega rah'}$;
16 Generate shortest backup path $P^B_{\omega rah'}$ from d' to s_r with negative reduced cost based on $Cost^B_{\omega rah'}$
17 **if** *Get a lower total reduced cost* **then**
18 Update $P^W_{\omega rah}, P^B_{\omega rah'}$;
19 **end**
20 **end**
21 **end**
22 **end**
23 **end**
24 **end**
25 **end**
26 **end**
27 **end**

working-backup path generation. *Lines 15-16* generate the shortest backup path based on backup link weight by Dijkstra's shortest path algorithm. *Line 17-18* updates the generated working-backup path pair in the configuration set ω_r if a lower total reduced cost is acquired, which ensures that the generated working-backup path pair has the minimum negative reduced cost.

This master-pricing path generation procedure is repeated until no qualified solution for a request (with negative reduced cost) can be found in the pricing problem. When the master-pricing iteration terminates, we conclude that the best solution for the LPR of the master problem is reached. A valid lower bound will be obtained for

the optimal integer solution. In order to get the optimal integer solution, we choose to use CPLEX optimizer to get an approximated optimal integer solution which is based branch-and-bound approach.

5.5.5 Discussion

The decomposition approach offers an efficient solution to solve the survivable network design problem for elastic optical DCNs. The introduction of ILP model [55] allows to pre-determine the DC node location and content replica, thus, the CG procedure can generate new lightpaths accordingly in the pricing problem. Otherwise, for each new iteration of working and backup paths pair generation, the DC position and content replica have to be determined, which may make the already determined lightpaths useless. However, the pre-determine DC node location and content replica would make the decomposition approach sub-optimal as it does not give the optimal DC nodes and content replicas with respect to final working paths, backup paths and spectrum usage. The gap introduced by the decomposition approach compared with the original ILP will be evaluated in Sec. 5.4.

5.6 Simulation and Performance Evaluation

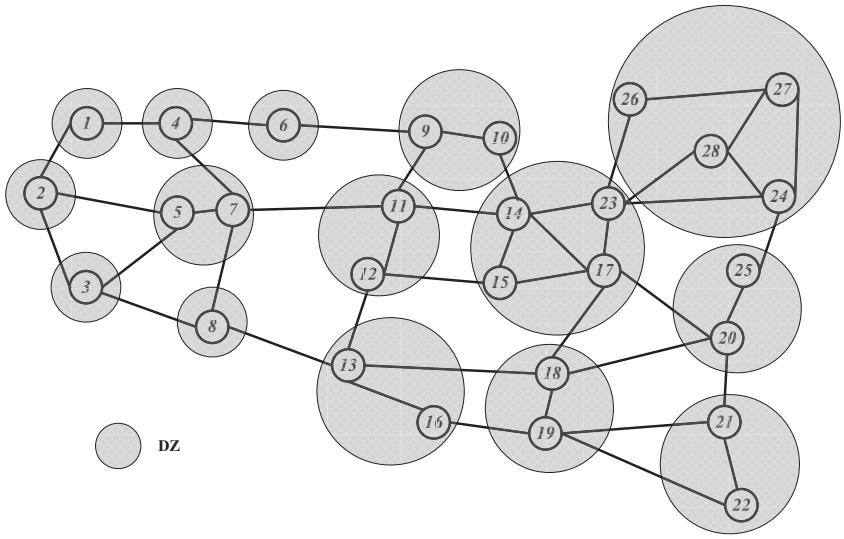

Figure 5.4: *US network topology with 15 DZs.*

We have performed extensive simulations to evaluate the spectrum usage in the proposed ILP model and CG approach for both DEBPP and SEBPP. We first studied the gap introduced by CG approach compared with the ILP model, and then evaluated the

Table 5.5: *Quality of Solution and Execution Time in CG approach and joint ILP models.*

No. Requests		Joint ILP models				CG approach								Gap	
		z_{1h}^{ILP}	FS_{total}	FS_{link}	t^{ILP}	$z^{initial}$	z^{LP}	z_{1h}^{CG}	FS_{link}	FS_{max}	t^{CG}	t_{LPR}^{CG}	t_{ILP}^{CG}	$Gap^{initial}$	Gap^{ILP}
NSFNET Network (3 DCs at nodes 2, 5 and 9, 14 DZs and 2 replicas for each content)															
10	DEBPP	**290**	260	30	8s	313	312	**312**	270	42	1s	1s	0s	-0.32%	**7.59%**
	SEBPP	**253**	233	20	448s	276	275	**275**	243	32	5s	5s	0s	-0.36%	**8.70%**
20	DEBPP	**448**	412	36	3600s	498	488	**493**	431	62	6s	6s	0s	-1%	**10.04%**
	SEBPP	**379**	345	34	3600s	437	424.733	**432**	388	44	7s	7s	0s	-1.14%	**13.98%**
30	DEBPP	**663**	613	50	3600s	700	691.998	**700**	630	70	7s	7s	0s	-0%	**5.58%**
	SEBPP	**614**	570	44	3600s	638	608	**630**	572	58	23s	23s	0s	-1.25%	**2.61%**
40	DEBPP	**867**	792	75	3600s	918	898.389	**912**	826	86	54s	8s	46s	-0.65%	**5.19%**
	SEBPP	**832**	765	67	3600s	808	761.612	**792**	719	73	49s	44s	5s	-2.0%	-
US Backbone Network (4 DCs at nodes 1, 12, 21 and 28, 15 DZs and 2 replicas for each content)															
10	DEBPP	**263**	232	31	317s	284	267	**268**	232	36	3s	2s	1s	-5.63%	**1.90%**
	SEBPP	**240**	216	24	3600s	278	253	**269**	230	39	11s	11s	0s	-3.23%	**12.08%**
20	DEBPP	**538**	503	35	3600s	571	537	**537**	503	36	58s	43s	15s	-5.95%	/
	SEBPP	**751**	714	37	3600s	471	428.625	**442**	405	37	78s	78s	0s	-6.16%	/
30	DEBPP	**949**	861	88	3600s	1115	993.75	**1027**	932	95	47s	24s	23s	-7.90%	**8.22%**
	SEBPP	-	-	-	-	896	824.639	**863**	786	77	135s	134s	1s	-3.68%	-
40	DEBPP	-	-	-	3600s	1462	1389.23	**1399**	1309	90	85s	85s	0s	-4.31%	-
	SEBPP	-	-	-	-	1215	1078.01	**1136**	1065	71	784s	776s	8s	-6.50%	-

- No feasible solution is obtained after one hour or exhausting all the memory.

/ The result obtained by ILP is even worse due to the existing optimality gap in CPLEX solver after exhausting the memory.

spectrum usage of DEBPP and SEBPP with respect to different number of requests, DC nodes, number of replicas per content in different network topologies.

5.6.1 Simulation setup

We implemented the proposed joint ILP models and CG approach in C++ with CPLEX 12.06. The simulations were conducted on an Intel Core PC with a 3.5 GHz CPU and 8G Bytes RAM. The following test beds are used: NSFNET network (14 nodes, 44 directed links and average nodal degree 3.1) [68] and US Backbone network (28 nodes, 90 directed links and average nodal degree 3.2) in [68]. We assume 14 DZs existing in NSFNET network in Fig. 5.1 and 15 DZs existing in US Backbone network in Fig. 5.4. We also assume that there are 300 available FSs in each fiber and 10 contents for the cloud services. The content and source node of each request are generated randomly, and the number of required FSs is randomly chosen among [1,10]. The weights θ_1 and θ_2 used in the objective function should be determined by the network operator, which represent the importance of total link spectrum usage and maximal spectrum usage. For simplicity, we set the same weight for them, *i.e.*, $\theta_1 = \theta_2 = 1$.

5.6.2 The efficiency of CG approach compared with ILP

To verify the efficiency of the solution acquired by the CG approach, we conducted simulations under small traffic demands (the number of requests varies from 10 to 40) with both ILP formulation and CG approach in NSFNET and US Backbone networks.

We assume that in NSFNET network there are 3 DCs (at nodes 2, 5 and 9) and 2 replicas per content, in US Backbone network there are 4 DCs (at nodes 1, 12, 21 and 28) and 2 replicas per content. The running time is limited to 3600 s in both joint ILP models and CG approach. Table 5.5 shows the solution of total spectrum usage and the execution time of DEBPP and SEBPP obtained by the ILP formulation and CG approach. z_{1h}^{ILP} and z_{1h}^{CG} show the value of final solution, t^{ILP} and t^{CG} show the total execution time for the acquired final solution. For the CG approach, t^{CG} consists of the execution time of solving LPR of the master problem t_{LPR}^{CG} and the execution time of solving the final ILP problem t_{ILP}^{CG}. Note that in some cases t_{ILP}^{CG} is $0s$ because we remove the columns whose q_r^{ω} equals 0 in the *Step 5* before integerizing all the relaxed variables.

In NSFNET network, we can see that the joint ILP models requires 3600 s with both DEBPP and SEBPP for the number of requests more than 20 while CG approach largely reduces execution time with the comparable solutions. In US Backbone network, SEBPP ILP model requires 3600 s for even 10 requests and it can not obtain a solution for more than 30 requests after exhausting all the memory or running for 3600 s. We also notice that the CG approach takes less time but introduces solution gap. The introduced gap is due to two reasons: 1) the DC assignment and content placement are pre-determined and solved separately before the using the CG approach; 2) the ESWBP algorithm ignores some spectrum channels that may contribute to a better solution. We also find the CG approach has relatively bigger gap for SEBPP than DEBPP because the working

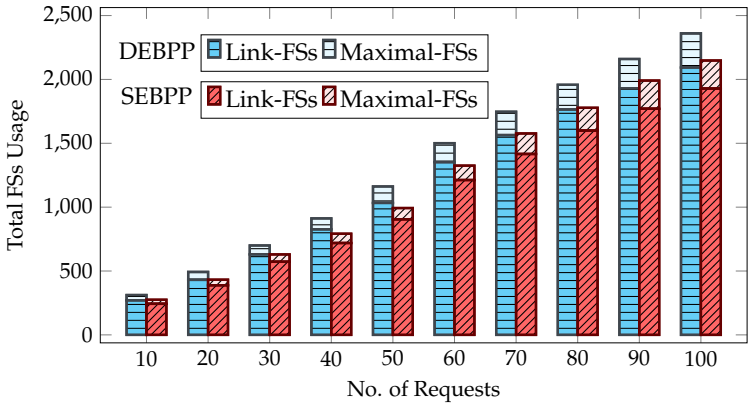

(a) Total FSs Usage in NSFNET

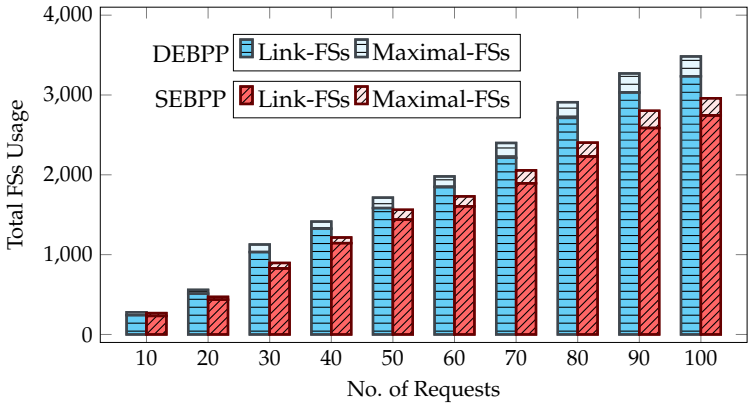

(b) Total FSs Usage in US Backbone

Figure 5.5: *Total FSs usage of DEBPP and SEBPP in terms of link-FSs and maximal-FSs in NSFNET and US Backbone networks.*

path generation in the pricing problem of SEBPP neglects the term $(1 - \alpha^{W}_{\omega rz})$ for link weight in Eq. (5.43).

We can conclude that joint ILP models are really time-consuming and they even can not obtain a solution after exhausting all the memory. The proposed CG approach can acquire a comparable solution in a reasonable time. Thus, the CG approach offers a time-efficient way to solve the disaster-survivable cloud services provisioning problem in elastic DCNs.

5.6.3 Spectrum usage VS no. requests

We then studied the spectrum usage of CG approach in terms of total link FSs usage and maximal FS index as a function of the number of requests. We still assume that in NSFNET network there are 3 DCs and 2 replicas per content, in US Backbone network there are 4 DCs and 2 replicas per content. We set the number of traffic requests from

10 to 100 and the running time no more than 3600 s. The traffic requests used in the simulations are generated randomly with the required FSs among [1,10]. The FSs usage of DEBPP and SEBPP is shown in Fig. 5.5.

In NSFNET network, we see that the overall FSs usage of both DEBPP and SEBPP increases as the number of requests goes up while SEBPP requires less FSs usage than DEBPP. The amount of the total FSs savings in SEBPP is achieved between 7.82% and 14.54% with an average value of 10.94%, the small FSs savings in NSFNET network is due to less spectrum sharing in the SEBPP case. This is because the fixed DC locations in DCNs are more likely to provision the traffic from the same DC as the number of traffic increases, then the working paths of these traffic demands are more likely to traverse the same DZ, which will results in the less possibility to share FSs on their backup paths. We also notice that the FSs savings in maximal index (18.23% on average) is higher than that in the total link FSs usage (9.99% on average).

In US Backbone network, the tendency of overall FSs usage in DEBPP and SEBPP are quite similar to those in NSFNET network when increasing the number of traffic requests. However, we observe that a more FSs savings and more steady tendency is acquired as the number of traffic demands increases compared with the results in NSFNET network. The average amounts of overall FSs usage savings, total link FSs usage and maximal FS index in SEBPP are 15.1%, 15.80% and 7.48%, respectively. The more savings in SEBPP acquired in US Backbone network comes from the fact that large topology allows more geographically distributed paths routing provisioned from the fixed DC nodes. Then, to achieve the FSs sharing, the working paths have more possibility to not traverse the same DZs. So, it is likely to permit the spectrum sharing among the lightpaths using SEBPP in a larger network.

The simulation results demonstrate that SEBPP achieved spectrum usage savings compared with the DEBPP for disaster-survivable cloud service provisioning. The amount of the spectrum savings in SEBPP over DEBPP varies in different topologies, it is bigger in a larger network. This is because a large network gives more possibility to the geographical distribution of working and backup paths routing.

5.6.4 Spectrum usage VS number of DCs location and content replicas

We further investigated the total spectrum usage of DEBPP and SEBPP when varying the number of DC nods and content replica in NSFNET and US Backbone networks. The number and location of DCs selected in the simulations are shown in Tab. 5.6, which is referred from [55, 68]. We first evaluated the spectrum usage with different DCs while maintaining the replicas per content $K = 2$. Then, we studied the total spectrum usage with different replicas per content under the fixed DCs.

Figure 5.6 shows the total spectrum usage of DEBPP and SEBPP in NSFNET network as the number of DCs and content replicas vary. We can see from Fig. 5.6 (a) that for a small number of requests, the spectrum usage in DEBPP does not show many differences when increasing the number of DCs, and the same tendency is observed for SEBPP. After the number of requests becomes bigger than 60, spectrum savings can

Table 5.6: *DCs location in NSFNET and US Backbone networks.*

Networks	No. of DCs	Location of DCs
NSFNET	2	Node 5, 9
	3	Nodes 2, 5, 9
	4	Nodes 2, 5, 9, 11
	5	Nodes 2, 5, 6, 9, 11
US Backbone	4	Nodes 1, 12, 21, 28
	6	Nodes 1, 7, 14, 19, 21, 28
	8	Nodes 1, 7, 9, 12, 14, 19, 21, 28

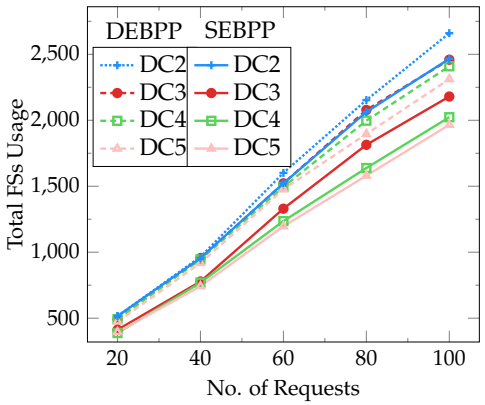

(a) Total FSs usage vs. No. of DCs

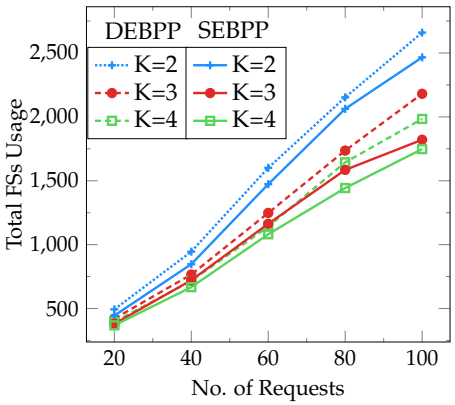

(b) Total FSs usage vs. No. of replicas K (No. of DCs = 4)

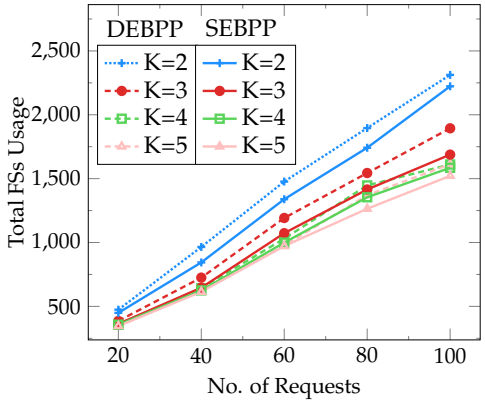

(c) Total FSs usage vs. No. of replicas K (No. of DCs = 5)

Figure 5.6: *Total FSs usage of DEBPP and SEBPP for different No. of DCs and No. of replicas in NSFNET network.*

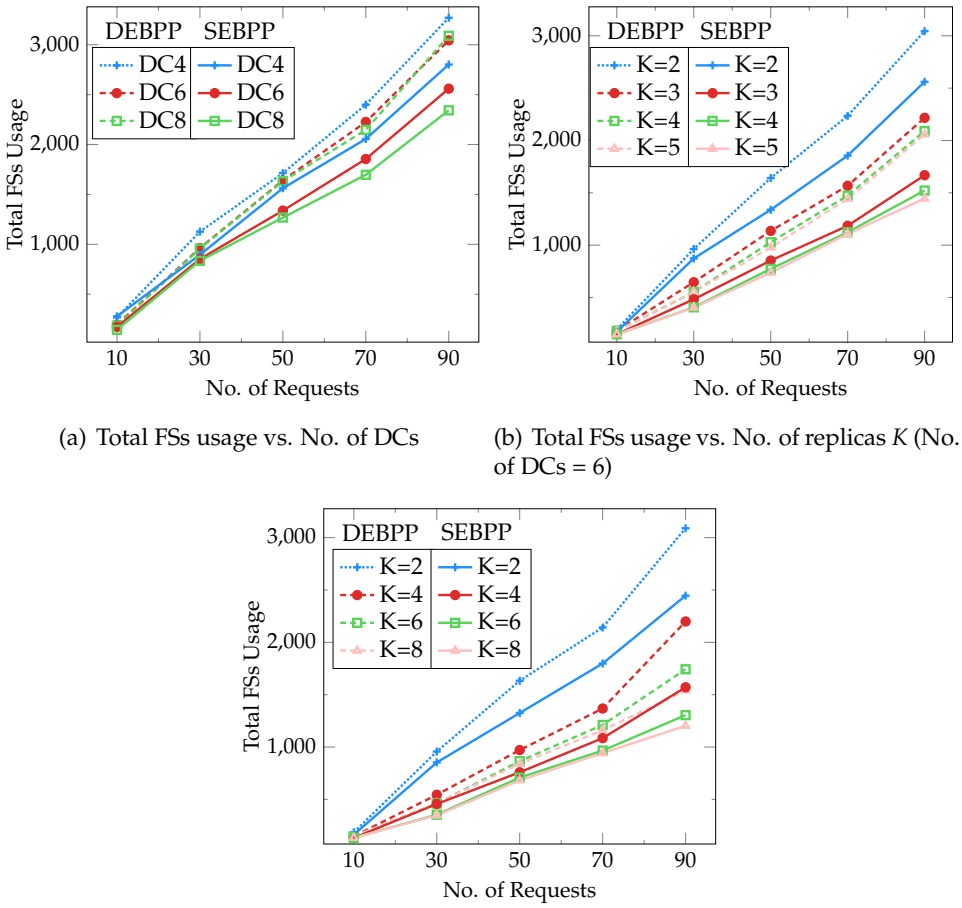

(a) Total FSs usage vs. No. of DCs

(b) Total FSs usage vs. No. of replicas K (No. of DCs = 6)

(c) Total FSs usage vs. No. of replicas K (No. of DCs = 8)

Figure 5.7: *Total FSs usage of DEBPP and SEBPP for different No. of DCs and No. of replicas in US Backbone network.*

be acquired in both DEBPP and SEBPP by using more DCs, and significant savings is observed in SEBPP. But it also can be seen that after a certain value (4 DCs), increasing the number of DCs does not help much to reduce spectrum usage. For four DCs, Fig. 5.6 (b) shows the spectrum usage with different content replicas K. The spectrum usage is reduced largely for both DEBPP and SEBPP when K changes from 2 to 3. We also observe that the spectrum savings of SEBPP over DEBPP goes up as the number of content replicas increases. For the 5 DCs in Fig. 5.6 (c), the similar tendency is observed that significant spectrum savings in DEBPP and SEBPP is acquired from $K = 2$ and 3, and it does not reduce too much for K after 3. We still see that the most spectrum savings in SEBPP over DEBPP is acquired at $K = 3$.

Figure 5.7 shows the spectrum usage of DEBPP and SEBPP in US Backbone network as the number of DCs and content replicas vary. In Fig. 5.7 (a), we see the spectrum usage is reduced with the increase in the number of DCs and the significant spectrum

savings in SEBPP still can be observed for 8 DCs. In Fig. 5.7 (b) and (c), we observe the similar results to Fig. 5.6 (b) and (c) in NSFNET network. Significant spectrum savings occurs for both DEBPP and SEBPP when the number of content replicas changes from $K = 2$ to 3 for 6 DCs and $K = 2$ to 4 for 8 DCs. The most spectrum savings acquired in SEBPP over DEBPP is at $K = 3$ for 6 DCs and $K = 4$ for 8 DCs, and it dose not reduce too much after adding more content replicas.

We can conclude that as the number of DCs and number of replicas per content increase, the total spectrum usage reduces significantly and the spectrum savings in SEBPP over DEBPP goes up. However, the spectrum savings do not decrease too much after the number of DCs and replica achieve a certain value, thus just using a reasonable number of DCs with efficient content replicas in network design can achieve significant spectrum usage savings for disaster-survivable cloud service provisioning.

5.7 Conclusion

We have investigated disaster-survivable cloud service provisioning problem in elastic DCNs. Concerning the content placement, routing, protection of path and content, and spectrum allocation, we first develop the joint ILP models for dedicated path protection and shared path protection to minimize the total spectrum usage. To overcome scalability drawback of the joint ILP models, a CG-based decomposition approach is proposed to solve original problem in several steps with respect to content placement, initial solution, master problem and pricing problem. Simulation results have shown that the CG-based decomposition approach produces comparable results in shorter time than the joint ILP models. The results acquired by the CG-based decomposition have shown that just using a small number of DCs with efficient content replicas in network design enables to achieve significant spectrum usage savings for disaster-survivable cloud service provisioning.

Part V

Conclusions and Perspectives

Chapter 6

Conclusions and Perspectives

6.1 Summary

In this thesis, the protection schemes for next generation optical networks are studied with the objective to reduce the resources usage with respect to spectrum, cost and energy. Specifically, we focus on single link failure protection and large area disaster failure protection. *p*-Cycle protection is proposed to address the single link failure of the on-cycle links and the straddling links in MLR WDM and EONs. Disaster failure protection is studied by both DEBPP and SEBPP in elastic DCNs with content placement consideration. The proposed protection schemes are tackled from the aspects of transmission rate, optical equipment cost, energy consideration as well as wavelength/spectrum allocation. Against each aspect, either the optimal solutions (*i.e.*, the MILP / ILP models) are developed for searching exact results for small instances, or the heuristic solutions are proposed for large-scale cases. Aiming at acquiring the optimal *p*-cycle design, a *p*-cycle design without candidate cycle enumeration is proposed rather than its conventional cycle enumeration in advance. In order to solve the disaster protection in larger instances, a column generation based decomposition is developed to reduce the complexity while achieving a near-optimal result.

At the beginning of the thesis, a brief background is given to the evolution of optical networks from fixed-grid to flexible-grid as well as the key technologies of EONs. Then, the critical importance of survivability in optical networks is addressed involving the classical protection schemes and the challenges of next generation optical network protection. In the end, the literature regarding the cost-effective, power-efficient and disaster-survivable protection schemes are reviewed.

In Chapter 2, the low-cost *p*-cycle design without candidate cycle enumeration is proposed for MLR optical networks. The *p*-cycle protection scheme considers the cycle generation, line rate selection as well as the transmission reach and transponder cost at different line rates. Distance-adaptive *p*-cycles are generated based on path-length-limited *p*-cycles with 10/40/100 Gbps line rate. An MILP model is formulated to address those consideration simultaneously, which allows to obtain the optimal solution

in small instances. Moreover, GPA algorithm and EI algorithm are developed to make the proposed MILP model scalable. GPA algorithm permits to partition the network topology into small sub-graphs in average while EI algorithm estimates the number of p-cycles required in the MILP model. The simulations show that the proposed p-cycle design achieves significant cost savings for MLR optical networks, especially the transponder cost savings, in comparison with p-cycle design with SLR and that with candidate cycle enumeration.

In Chapter 3, the power-efficient directed p-cycle protection for EONs under asymmetric traffic is studied. We first present the advantage of directed p-cycle over undirected p-cycle for asymmetric traffic protection. Then, we formulate the MILP model of directed p-cycles to minimize the total power consumption of optical equipments concerning adaptive modulation formats, spectrum allocation and protection capacity. Finally, we decompose the MILP model by using a two-step approach consisting of the improved cycle enumeration and a simplified ILP model. We conduct extensive simulations of the proposed directed p-cycles compared with the conventional undirected p-cycles in terms of power consumption and spectrum usage. The results show that directed p-cycles own significant power savings (up to 46.91%) compared with the conventional undirected p-cycles, and the amount of power savings increases with the increase of traffic asymmetry and anycasting ratio. Moreover, we also compare the proposed power-efficient directed p-cycles with spectrum-efficient directed p-cycles. The results show that power-efficient directed p-cycles earn power savings, but the amount of power savings does not change too much whatever the traffic asymmetry or anycasting ratio it is. It is also observed that the introduction of DCs makes it more valuable to utilize directed p-cycles for protection in EONs in a power-efficient way.

In Chapter 4, we further study the efficient spectrum allocation for p-cycle protection scheme in EONs. The SS-p-cycle design is proposed to allow spectrum sharing among multiple p-cycles that have common link(s). We first propose a theorem to state the spectrum sharing principle and prove it. Then, two ILP models are formulated to design the SS-p-cycles with and without spectrum conversion. To increase the scalability, an algorithm is also developed for SS-p-cycle design without spectrum conversion. The results show that SS-p-cycles are promising to reduce spectrum utilization compared with conventional p-cycles without spectrum sharing. Moreover, the proposed algorithm obtains comparable solution as the proposed ILP model within a short time in large topologies. Moreover, the results also show that the spectrum conversion does help p-cycle protection to acquire better spectrum utilization, but it shows different impacts on maximum index of FSs and spectrum efficiency under different p-cycle design methods and network with different nodal degrees.

In Chapter 5, we study the disaster-survivable path protection for cloud services in elastic DCNs, which involves the content placement, routing, protection of path and content, and spectrum allocation. First, both DEBPP and SEBPP schemes are formulated by the ILP models to minimize the spectrum usage based on slot-based starting slot assignment formulation, which can be optimally solved in small traffic instances. To improve the scalability, the ILP models are decomposed into a master problem and a pricing problem based on the CG approach with channel-based formulation. Simu-

lation results show that the CG-based decomposition approach produces comparable results as the ILP formulation in a short time. As the number of DCs and number of replicas per content increase, the total spectrum usage reduces significantly and the spectrum savings in SEBPP over DEBPP goes up. We can conclude that a reasonable number of DCs with efficient content replicas in network design enables to achieve significant spectrum usage savings for disaster-survivable cloud service provisioning.

6.2 Future work

Lots of important issues on p-cycle protection with the spectrum, cost and energy issues are covered in this thesis as well as the path protection schemes for disaster-survivable DCNs. But many issues are still open for better supporting protection in optical networks with the advanced technologies. Several potential perspectives are suggested below for the future work:

1. **Cost and energy issues in p-cycle protection scheme with multiflow optical transponders**

As proven in this thesis, the directed p-cycle protection scheme is power-efficient for EONs with asymmetric traffic provisioning. Significant power savings can be acquired in the BVTs, BV-OXCs and OAs, especially in BVTs. Nowadays, the multiflow optical transponders have attracted lots of interests owing to its efficient multiple optical paths accommodation even though most of the current work only makes use of the BVTs for lightpath provisioning. It has been shown that cost-effective and power-efficient network design can be achieved by employing multiflow optical transponders [67, 121]. A multiflow optical transponder allows client data flows that come from a single client interface to be mapped to multiple optical flows, which is promising to achieve potential reduction in the number of router interfaces and considerable potential for cost and energy savings. In conventional EONs with BVTs, each optical path is supported by the BVT with the minimum spectral width necessary. It occurs that a 400 Gb/s capacity BVT may accommodate only 40 Gb/s optical path demand. However, with the capability of multiflow optical transponder, the transponder utilization efficiency can be improved by generating a wide variety and multiple optical flows in a single transponder. As a result, the cost-effective and power-efficient p-cycle protection should be further addressed with the heterogeneous traffic demands, which is far beyond the current protection scheme with BVTs.

2. **Traffic grooming and regenerators placement in p-cycle protection scheme**

The p-cycle protection schemes studied in this thesis concern the transparent optical network protection without electronic signal processing at intermediate OXCs. However, the quality of an optical signal degrades as it travels though several optical components from its source to destination. To address this issue, we consider the maximum transmission reach of each protection path in the thesis so that distance-adaptive modulation format can be assigned for each p-cycle. However, such quality degradation

can be addressed by placing regenerators at intermediate OXCs to regenerate the optical signal [42]. Moreover, traffic grooming can be used to aggregate low rate traffic into high rate lightpaths to improve utilization of network resources, which also has the additional benefit of providing optical signal regeneration at intermediate OXCs [42, 106]. The employment of traffic grooming and regenerators will improve the resource utilization for survivable network design at the expense of cost and energy. In addition to the spectrum resources, cost and energy optimization problem of p-cycle protection, this also involves the decision of either placing the regenerators or grooming equipments on the p-cycles. Thus, the cost-effective and power-efficient p-cycle protection should be further studied concerning the traffic grooming and regenerators.

3. **Dynamic content management in disaster-survivable DCNs with failure risk consideration**

As proven in the thesis, the column generation based decomposition is very useful for the disaster protection for elastic DCNs. We have considered the static path protection against disaster failure, in which the DC and content placement are decided once and they do not change later. However, the study conducted in [38] has demonstrated that the dynamic content-management solution can highly benefit service providers in designing disaster-resilient cloud networks. Under dynamic case, the probability of disasters and content properties (demands and importance) can be time-varying, and a change in disaster probabilities can make a currently safe DC location become risky at a later time. Moreover, most of the time the DZs are difficult to pre-calculate, it is very expensive for network operators to prevent connections from disasters, and recover them after disasters. Given the set of possible DZs, the study in [28] developed a probabilistic risk model to analyze the loss/penalty, and provided a mathematical model to reduce the risk and decrease the disaster loss by a proactive traffic engineering solution. Consequently, the places for a content to be replicated can be dynamically changed over a fixed set of DCs so that risk is reduced in terms of expected content loss. In addition to the initial content placement, the dynamic content-management solution is enhanced to the initial placement to make the network adaptable to changing conditions and disaster alerts [38, 71]. Thus, the column generation based disaster-aware protection schemes can be further investigated for dynamic content-management with the consideration of failure risk.

List of Figures

List of Tables

Bibliography

[1] G.694.1 : Spectral grids for wdm applications: Dwdm frequency grid. [Online]. Available: https://www.itu.int/rec/T-REC-G.694.1/en, 2012.

[2] Pankaj K. Agarwal, Alon Efrat, Shashidhara K. Ganjugunte, David Hay, Swaminathan Sankararaman, and Gil Zussman. The resilience of WDM networks to probabilistic geographical failures. *IEEE/ACM Trans. Netw.*, 21(5):1525–1538, Oct. 2013.

[3] Jude Akpuh and John Doucette. Sizing eligible route sets for restorable network design and optimization. In *Proc. IEEE Int. Conf. Commun.*, pages 5292–5299, May 2008.

[4] Jude Akpuh and John Doucette. Enhanced failure-specific p-cycle network dual-failure restorability design and optimization. *J. Opt. Netw.*, 8(1):1–13, Jan. 2009.

[5] Rodolfo Alvizu, Guido Maier, Navin Kukreja, Achille Pattavina, Roberto Morro, Alessandro Capello, and Carlo Cavazzoni. Comprehensive survey on T-SDN: Software-defined networking for transport networks. *IEEE Commun. Surv. Tut.*, 19(4):2232–2283, Jun. 2017.

[6] Norberto Amaya, Georgios Zervas, and Dimitra Simeonidou. Introducing node architecture flexibility for elastic optical networks. *J. Opt. Commun. Netw.*, 5(6):593–608, Jun. 2013.

[7] N. Georges Anoh, JoËl Christian Adépo, Michel Babri, and BOKO Aka. Hybrid protection scheme for elastic optical networks with regenerator and efficient energy consideration. *J. Comput. Sci. Telecommun.*, 6(10), Nov. 2015.

[8] Rachna Asthana and Yatindra Nath Singh. Distributed protocol for removal of loop backs and optimum allocation of p-cycles to minimize the restored path lengths. *J. Lightw. Technol.*, 26(5):616–627, Mar. 2008.

[9] Joseph Berthold, Adel A. M. Saleh, Loudon Blair, and Jane M. Simmons. Optical networking: Past, present, and future. *J. Lightw. Technol.*, 26(9):1104–1118, May 2008.

[10] Jin-Xing Cai, Carl R. Davidson, Alan Lucero, Hongbin Zhang, Dmitri G. Foursa, Oleg V. Sinkin, William W. Patterson, Alexei N. Pilipetskii, Georg Mohs, and

Neal S. Bergano. 20 Tbit/s transmission over 6860 km with sub-nyquist channel spacing. *J. Lightw. Technol.*, 30(4):651–657, Feb. 2012.

[11] Cicek Cavdar. Energy-efficient connection provisioning in WDM optical networks. In *Proc. Opt. Fiber Commun. Conf.*, pages 1–3, Mar. 2011.

[12] Bijoy Chand Chatterjee, Nityananda Sarma, and Eiji Oki. Routing and spectrum allocation in elastic optical networks: A tutorial. *IEEE Commun. Surv. Tut.*, 17, May. 2015.

[13] Bowen Chen, Jie Zhang, Weisheng Xie, Jason P. Jue, Yongli Zhao, and Gangxiang Shen. Cost-effective survivable virtual optical network mapping in flexible bandwidth optical networks. *J. Lightwave Technol.*, 34(10):2398–2412, May 2016.

[14] Bowen Chen, Yongli Zhao, and Jie Zhang. Survivable spectrum-shared ability in flexible bandwidth optical networks with distributed data centers. *Photon. Netw. Commun.*, 33(2):102–111, Apr. 2017.

[15] Xiaoliang Chen, Fan Ji, and Zuqing Zhu. Service availability oriented p-cycle protection design in elastic optical networks. *J. Opt. Commun. Netw.*, 6(10):901–910, Oct. 2014.

[16] Xiaoliang Chen, Shilin Zhu, Liu Jiang, and Zuqing Zhu. On spectrum efficient failure-independent path protection p-cycle design in elastic optical networks. *J. Lightw. Technol.*, 33(17):3719–3729, Sept. 2015.

[17] Piotr Chołda and Andrzej Jajszczyk. Reliability assessment of p-cycles. In *Proc. IEEE Global Commun. Conf.*, volume 1, page 5, Nov. 2005.

[18] Pulak Chowdhury, Massimo Tornatore, Avishek Nag, Ezra Ip, Ting Wang, and Biswanath Mukherjee. On the design of energy-efficient mixed-line-rate MLR optical networks. *J. Lightw. Technol.*, 30(1):130–139, Jan. 2012.

[19] Konstantinos Christodoulopoulos, Konstantinos Manousakis, , and Emmanouel (Manos) Varvarigos. Reach adapting algorithms for mixed line rate WDM transport networks. *J. Lightw. Technol.*, 29(21):3350–3363, Nov. 2011.

[20] Kostas Christodoulopoulos, Konstantinos Manousakis, and Emmanouel Varvarigos. Comparison of routing and wavelength assignment algorithms in WDM networks. In *Proc. IEEE Global Commun. Conf.*, pages 1–6, Nov. 2008.

[21] Kostas Christodoulopoulos, Ioannis Tomkos, and Emmanuel A. Varvarigos. Elastic bandwidth allocation in flexible OFDM-based optical networks. *J. Lightw. Technol.*, 29(9):1354–1366, May 2011.

[22] Cisco. Cisco global ip traffic forecast. [Online]. Available: https://www.cisco.com/c/en/us/solutions/collateral/service-provider/visual-networking-index-vni/vni-hyperconnectivity-wp.html, 2016.

[23] Infinear corporation. White paper: The evolution of next-gen optical networks. Technical Report WP-NGON-10-2014, Infinera Corporation.

[24] Raja Datta and Indranil Sengupta. Static and dynamic connection establishment in wdm optical networks: A review. *IETE J. Research*, 51(3):209–222, 2005.

[25] Jose Roberto de Almeida Amazonas, German Santos-Boada, Sergio Ricciardi, and Josep Sole-Pareta. Technical challenges and deployment perspectives of sdn based elastic optical networks. In *Proc. Int. Con. Transparent. Opt. Netw.*, pages 1–5, Jul. 2016.

[26] Chris Develder, Jens Buysse, Bart Dhoedt, and Brigitte Jaumard. Joint dimensioning of server and network infrastructure for resilient optical grids/clouds. *IEEE/ACM Trans. Netw.*, 22(5):1591–1606, Oct. 2014.

[27] M. Nishan Dharmaweera, Rajendran Parthiban, and Y. Ahmet Sekercioglu. Toward a power-efficient backbone network: The state of research. *IEEE Commun. Surv. Tut.*, 17(1):198–227, Jul. 2015.

[28] Ferhat Dikbiyik, Massimo Tornatore, and Biswanath Mukherjee. Minimizing the risk from disaster failures in optical backbone networks. *J. Lightw. Technol.*, 32(18):3175–3183, Sept. 2014.

[29] Xiaowen Dong, T.E.H. El-Gorashi, and J.M.H. Elmirghani. On the energy efficiency of physical topology design for IP over WDM networks. *J. Lightw. Technol.*, 30(12):1931–1942, Jun. 2012.

[30] John Doucette, Peter A. Giese, and Wayne D. Grover. Combined node and span protection strategies with node-encircling p-cycles. In *Proc. Design Reliable Commun. Netw. Workshops*, pages 213–221, Oct. 2005.

[31] John Doucette, Donna He, and Oliver Yang Wayne D. Grover and. Algorithmic approaches for efficient enumeration of candidate p-cycles and capacitated p-cycle network design. In *Proc. Design Reliable Commun. Netw. Workshops*, pages 212–220, Oct. 2003.

[32] Hamza Drid, Nicolas Brochier, Esther Le Rouzic, and Nasir Ghani. P-cycle design for mixed-line rate optical networks. In *Proc. Opt. Netw. Des. Model. Conf.*, pages 1–4, Apr. 2012.

[33] Hamza Drid, Bernard Cousin, Miklos Molnar, and Samer Lahoud. A survey of survivability in multi-domain optical networks. *Comput. Commun.*, 33(8):1005–1012, May. 2010.

[34] D. Anthony Dunn, Wayne D. Grover, and Mike H. MacGregor. Comparison of k-shortest paths and maximum flow routing for network facility restoration. *IEEE J. Sel. Areas Commun.*, 12(1):88–99, Jan. 1994.

[35] Georgios Ellinas, Dimitri Papadimitriou, Jacek Rak, Dimitri Staessens, James P.G. Sterbenz, and Krzysztof. Practical issues for the implementation of survivability and recovery techniques in optical networks. *Opt. Switching Netw.*, 14:179–193, 2014.

[36] Abdelhamid E. Eshoul and Hussein T. Mouftah. Survivability approaches using p-cycles in WDM mesh networks under static traffic. *IEEE/ACM Trans. Netw.*, 17(2):671–683, Apr. 2009.

[37] Wenjian Fang, Minhua Lu, Xiahe Liu, Long Gong, and Zuqing Zhu. Joint defragmentation of optical spectrum and IT resources in elastic optical datacenter interconnections. *IEEE J. Opt. Commun. Netw.*, 7(4):314–324, Apr. 2015.

[38] Sifat Ferdousi, Ferhat Dikbiyik, M. Farhan Habib, Massimo Tornatore, and Biswanath Mukherjee. Disaster-aware datacenter placement and dynamic content management in cloud networks. *J. Opt. Commun. Netw.*, 7(7):681–694, Jul. 2015.

[39] Sifat Ferdousi, Ferhat Dikbiyik, Massimo Tornatore, and Biswanath Mukherjee. Joint progressive recovery of optical network and datacenters after large-scale disasters. In *Proc. Opt. Fiber Commun. Conf.*, page Tu3E.5. OSA, 2017.

[40] Michele Flammini, Alberto Marchetti-Spaccamela, Gianpiero Monaco, Luca Moscardelli, and Shmuel Zaks. On the complexity of the regenerator placement problem in optical networks. *IEEE/ACM Trans. Netw.*, 19(2):498–511, Apr. 2011.

[41] Paola Frascella, Naoise Mac Suibhne, Fatima C. Garcia Gunning, Selwan K. Ibrahim, Paul Gunning, and Andrew D. Ellis. Unrepeatered field transmission of 2 tbit/s multi-banded coherent WDM over 124 km of installed SMF. *Opt. Express*, 18(24):24745–24752, Nov. 2010.

[42] Chengyi Gao, Hakki C. Cankaya, Ankitkumar N. Patel, Jason P. Jue, Xi Wang, Qiong Zhang, Paparao Palacharla, and Motoyoshi Sekiya. Survivable impairment-aware traffic grooming and regenerator placement with connection-level protection. *J. Opt. Commun. Netw.*, 4(3):259–270, Mar. 2012.

[43] David J. Geisler, Nicolas K. Fontaine, Ryan P. Scott, Tingting He, Loukas Paraschis, Ori Gerstel, Jonathan P. Heritage, and S. J. B. Yoo. Bandwidth scalable, coherent transmitter based on the parallel synthesis of multiple spectral slices using optical arbitrary waveform generation. *Opt. Express*, 19(9):8242–8253, Apr. 2011.

[44] Ori Gerstel, Masahiko Jinno, Andrew Lord, and S.J. Ben Yoo. Elastic optical networking: A new dawn for the optical layer? *IEEE Commun. Mag.*, 50(2):s12–s20, Feb. 2012.

[45] Teresa Gomes, János Tapolcai, Christian Esposito, David Hutchison, F. Kuipers, J. Rak, A. de Sousa, A. Iossifides, R. Travanca, J. André, L. Jorge, L. Martins, P. O. Ugalde, A. Pašić, D. Pezaros, S. Jouet, S. Secci, and M. Tornatore. A survey

of strategies for communication networks to protect against large-scale natural disasters. In *Proc. Resil. Netw. Design Model. Workshops*, pages 11–22, Sept. 2016.

[46] Long Gong, Xiang Zhou, Xiahe Liu, Wenwen Zhao, Wei Lu, and Zuqing Zhu. Efficient resource allocation for all-optical multicasting over spectrum-sliced elastic optical networks. *J. Opt. Commun. Netw.*, 5(8):836–847, Aug. 2013.

[47] Róza Goścień. On the efficient column generation-based optimization of anycast traffic in survivable elastic optical networks. In *Proc. Int. Con. Transparent. Opt. Netw.*, pages 1–4, Jul. 2017.

[48] Róża Goścień, Krzysztof Walkowiak, and Mirosław Klinkowski. Gains of anycast demand relocation in survivable elastic optical networks. In *Proc. Reliable Netw. Des. Model. Workshops*, pages 109–115, Nov. 2014.

[49] Róza Goścień, Krzysztof Walkowiak, and Mirosław Klinkowski. Joint anycast and unicast routing and spectrum allocation with dedicated path protection in elastic optical networks. In *Proc. Design Reliable Commun. Netw.*, pages 1–8, Apr. 2014.

[50] Róza Goścień, Krzysztof Walkowiak, and Mirosław Klinkowski. Tabu search algorithm for routing, modulation and spectrum allocation in elastic optical network with anycast and unicast traffic. *Comput. Netw.*, 79:148–165, Jan. 2015.

[51] Wayne D. Grover and John Doucette. Advances in optical network design with p-cycles: Joint optimization and pre-selection of candidate p-cycles. In *Proc. Lasers Electro-Optics Society*, pages 49–50, Nov. 2002.

[52] Wayne D. Grover and Demetrios Stamatelakis. Cycle-oriented distributed preconfiguration: ring-like speed with mesh-like capacity for self-planning network restoration. In *Proc. IEEE Int. Conf. Commun.*, pages 537–543, Jun. 1998.

[53] M. Farhan Habib, Massimo Tornatore, Ferhat Dikbiyik, and Biswanath Mukherjee. Disaster survivability in optical communication networks. *Comput. Commun.*, 36(6):630–644, 2013.

[54] M. Farhan Habib, Massimo Tornatore, Marc De Leenheer, Ferhat Dikbiyik, and Biswanath Mukherjee. A disaster-resilient multi-content optical datacenter network architecture. In *Proc. Int. Con. Transparent. Opt. Netw.*, pages 1–4, Jun. 2011.

[55] M. Farhan Habib, Massimo Tornatore, Marc De Leenheer, Ferhat Dikbiyik, and Biswanath Mukherjee. Design of disaster-resilient optical datacenter networks. *J. Lightw. Technol.*, 30(16):2563–2573, Aug. 2012.

[56] Mohammad Hadi and Mohammad Reza Pakravan. Spectrum-convertible BVWXC placement in OFDM-based elastic optical networks. *IEEE Photon. J.*, 9(1):1–12, Feb. 2017.

[57] Wensheng He. Survivable design in WDM mesh networks. In *Retrospective Theses and Dissertations*, 2006.

[58] Riu Hirai, Nobuhiko Kikuchi, and Takayoshi Fukui. High-spectral efficiency dwdm transmission of 100-gbit/s/lambda IM/DD single sideband-baseband-nyquist-pam8 signals. In *Proc. Opt. Fiber Commun. Conf.*, pages 1–3, Mar. 2017.

[59] Jian Qiang Hu. Diverse routing in optical mesh networks. *IEEE Trans. Commun.*, 51(3):489–494, Mar. 2003.

[60] Brigitte Jaumard, Jens Buysse, Ali Shaikh, Marc De Leenheer, and Chris Develder. Column generation for dimensioning resilient optical grid networks with relocation. In *Proc. IEEE Global Commun. Conf.*, pages 1–6, Dec. 2010.

[61] Brigitte Jaumard, Christophe Meyer, and Babacar Thiongane. On column generation formulations for the RWA problem. *Discrete Appl. Math.*, 157(6):1291–1308, Mar. 2009.

[62] Caroline Rochaand Brigitte Jaumard and Pierre-Etienne Bougué. Directed vs. undirected p-cycles and FIPP p-cycles. In *Proc. Int. Netw. Optim. Conf.*, Apr. 2009.

[63] Fan Ji, Xiaoliang Chen, Wei Lu, Joel J. P. C Rodrigues, and Zuqing Zhu. Dynamic p-cycle protection in spectrum-sliced elastic optical networks. *J. Lightw. Technol.*, 32(6):1190–1199, Mar. 2014.

[64] Masahiko Jinno. Elastic optical networking: Roles and benefits in beyond 100-gb/s era. *J. Lightw. Technol.*, 35(5):1116–1124, May. 2017.

[65] Masahiko Jinno, Takuya Ohara, Yoshiaki Sone, Akira Hirano, Osamu Ishida, , and Masahito Tomizawa. Elastic and adaptive optical networks: possible adoption scenarios and future standardization aspects. *IEEE Commun. Mag.*, 49(10):164–172, Oct. 2011.

[66] Masahiko Jinno, Hidehiko Takara, Bartlomiej Kozicki, Yukio Tsukishima, Yoshiaki Sone, and Shinji Matsuoka. Spectrum-efficient and scalable elastic optical path network: architecture, benefits, and enabling technologies. *IEEE Commun. Mag.*, 47(11):66–73, Nov. 2009.

[67] Masahiko Jinno, Hidehiko Takara, Yoshiaki Sone, Kazushige Yonenaga, and Akira Hirano. Multiflow optical transponder for efficient multilayer optical networking. *IEEE Commun. Mag.*, 50(5):56–65, May 2012.

[68] Min Ju, Fen Zhou, Shilin Xiao, and Zuqing Zhu. Power-efficient protection with directed p-cycles for asymmetric traffic in elastic optical networks. *J. Lightw. Technol.*, 34(17):4053–4065, Sept. 2016.

[69] Min Ju, Fen Zhou, Zuqing Zhu, and Shilin Xiao. Distance-adaptive, low CAPEX cost p-cycle design without candidate cycle enumeration in mixed-line-rate optical networks. *J. Lightw. Technol.*, 34(11):2663–2676, 2016.

[70] Ahmed Zaky Kasem, RRoberto Gallardo, and John Doucette. An enhanced ILP design model for node-encircling p-cycle networks. In *Proc. Design Reliable Commun. Netw. Workshops*, pages 1–7, Apr. 2014.

[71] Mohammad Ali Khoshkholghi, Azizol Abdullah, Rohaya Latip, Shamala Subramaniam, and Mohamed Othman. Disaster recovery in cloud computing: A survey. *Comput. Inform. Sci.*, 7(4):39, 2014.

[72] Mohammad S. Kiaei, Chadi Assi, and Brigitte Jaumard. A survey on the p-cycle protection method. *IEEE Commun. Surv. Tut.*, 11(3):53–70, Jan. 2009.

[73] Kazuro Kikuchi. Coherent optical communication technology. In *Proc. Opto-Electron. Commun. Conf.*, pages 1–1, Oct. 2016.

[74] Nattapong Kitsuwan, Praphan Pavarangkoon, Bijoy Chand Chatterjee, and Eiji. Oki. Performance of elastic optical network with allowable spectrum conversion at intermediate switches. In *Proc. Int. Conf. Commun.*, pages 1–4, Jul. 2017.

[75] Axel Klekamp and Ulrich Gebhard. Performance of elastic and mixed-line-rate scenarios for a real IP over DWDM network with more than 1000 nodes [invited]. *J. Opt. Commun. Netw.*, 5(10):A28–A36, Oct. 2013.

[76] Mirosław Klinkowski and Krzysztof Wakowiak. Routing and spectrum assignment in spectrum sliced elastic optical path network. *IEEE Commun. Lett.*, 15(8):884–886, Aug. 2011.

[77] Mirosław Klinkowski and Krzysztof Walkowiak Walkowiak. On the advantages of elastic optical networks for provisioning of cloud computing traffic. *IEEE Netw.*, 27(6):44–51, Nov. 2013.

[78] Adil Kodian, Anthony Sack, and Wayne D. Grover. The threshold hop-limit effect in p-cycles: Comparing hop- and circumference-limited design. *Opt. Switching Netw.*, 2(2):72–85, Sept. 2005.

[79] Cedric F. Lam. Optical network technologies for datacenter networks. In *Proc. Opt. Fiber Commun. Conf.*, pages 1–3, Mar. 20160.

[80] Xin Li, Shanguo Huang, Shan Yin, Bingli Guo, Yongli Zhao, Jie Zhang, and Wanyi Gu. Shared end-to-content backup path protection in k-node (edge) content connected elastic optical datacenter networks. *Opt. Express*, 24(9):9446–9464, May 2016.

[81] Menglin Liu, Massimo Tornatore, and Biswanath Mukherjee. New strategies for connection protection in mixed-line-rate optical WDM networks. *J. Opt. Commun. Netw.*, 3(9):641–650, Sept. 2011.

[82] Menglin Liu, Massimo Tornatore, and Biswanath Mukherjee. Efficient shared subconnection protection in mixed-line-rate optical WDM networks. *J. Opt. Commun. Netw.*, 5(11):1227–1235, Nov. 2013.

[83] Menglin Liu, Massimo Tornatore, and Biswanath Mukherjee. Survivable traffic grooming in elastic optical networks-shared protection. *J. Lightw. Technol.*, 31(6):903–909, Mar. 2013.

[84] Jorge López, Paola Soto, Yabin Ye, and Peter M. Krummrich. Differentiated quality of protection: An energy- and spectral-efficient resilience scheme for survivable static and dynamic optical transport networks with fixed- and flexible-grid. *Opt. Switching Netw.*, 19(Part 2):78–96, 2016.

[85] Jorge López, Yabin Ye, Víctor López, Felipe Jiménez, Raúl Duque, Peter M. Krummrich, Francesco Musumeci, Massimo Tornatore, and Achille Pattavina. Traffic and power-aware protection scheme in elastic optical networks. In *Proc. Telecommun. Netw. Strategy Plann. Symposium*, pages 1–6, Oct. 2012.

[86] Ping Lu, Liang Zhang, Xiahe Liu, Jingjing Yao, and Zuqing Zhu. Highly efficient data migration and backup for big data applications in elastic optical inter-datacenter networks. *IEEE Network*, 29(5):36–42, Sept. 2015.

[87] Yunlei Lui, Gangxiang Shen, Weidong Shao, and Sanjay Kumar Bose. Green ip over WDM optical network design for mixed line rates and limited transmission reaches. In *Proc. COIN*, pages 1–6, 2013.

[88] Ulrike Von Luxburg. A tutorial on spectral clustering. *Stat. Comput.*, 17(4):395–416, Dec. 2007.

[89] Chen Ma, Jie Zhang, Yongli Zhao, Zilian Jin, Yachao Shi, Yang Wang, and Meng Yin. Bandwidth-adaptability protection with content connectivity against disaster in elastic optical datacenter networks. *Photon. Netw. Commun.*, 30(2):309–320, Jun. 2015.

[90] Konstantinos Manousakis, Archontoula Angeletou, and Emmanouel (Manos) Varvarigos. Energy efficient RWA strategies for WDM optical networks. *J. Opt. Commun. Netw.*, 5(4):338–348, Apr. 2013.

[91] Darli A. A. Mello, Andre´ N. Barreto, Tiago C. de Lima, Thiago F. Portela, Lotfollah Beygi, and Joseph M. Kahn. Optical networking with variable-code-rate transceivers. *J. Lightw. Technol.*, 32(2):257–266, Jan. 2014.

[92] Toshio Morioka, Masahiko Jinno, Hidehiko Takara, and Hirokazu Kubota. Innovative future optical transport network technologies. *NTT Rev.*, 9(8):1–8, 2011.

[93] Hussein T. Mouftah and Pin-Han Ho. *Optical networks: architecture and survivability*. Springer Science & Business Media, 2012.

[94] Biswanath Mukherjee. WDM optical communication networks: progress and challenges. *IEEE J. Sel. Areas Commun.*, 18(10):1810–1824, Oct. 2000.

[95] Biswanath Mukherjee. *Optical WDM networks*. Springer Science & Business Media, 2006.

[96] Avishek Nag, Massimo Tornatore, and Biswanath Mukherjee. Optical network design with mixed line rates and multiple modulation formats. *J. Lightw. Technol.*, 28(4):466–475, Feb. 2010.

[97] Tania Panayiotou, Georgios Ellinas, and Neo Antoniades. p-cycle-based protection of multicast connections in metropolitan area optical networks with physical layer impairments constraints. *Opt. Switching Netw.*, 19(P2):66–77, Jan. 2016.

[98] Helder A. Pereira, Daniel A. R. Chaves, Carmelo J. A. Bastos-Filho, and Joaquim F. Martins-Filho. OSNR model to consider physical layer impairments in transparent optical networks. *Photon. Netw. Commun.*, 18(2):137–149, 2008.

[99] Jordi Perelló, Annalisa Morea, Salvatore Spadaro, Albert Pagés, Sergio Ricciardi, Matthias Gunkel, and Gabriel Junyent. Power consumption reduction through elastic data rate adaptation in survivable multi-layer optical networks. *Photon. Netw. Commun.*, 28(3):276–286, May. 2014.

[100] Deepak Rajan and Alper Atamturk. Survivable network design: routing of flows and slacks. In *Proc. Tele. Netw. Des. Maneg.*, pages 65–81, 2003.

[101] Byrav Ramamurthy and Biswanath Mukherjee. Wavelength conversion in WDM networking. *IEEE J. Sel. Areas Commun.*, 16(7):1061–1073, Sept. 1998.

[102] Sumathi Ramamurthy, Laxman Sahasrabuddhe, and Biswanath Mukherjee. Survivable WDM mesh networks. *J. Lightw. Technol.*, 21(4):870–883, Apr. 2003.

[103] Rajiv Ramaswami, Kumar Sivarajan, and Galen Sasaki. *Optical networks: A practical perspective*. Morgan Kaufmann, 2009.

[104] Cristina Rottondi, Massimo Tornatore, and Giancarlo Gavioli. Optical ring metro networks with flexible grid and distance-adaptive optical coherent transceivers. *Bell Labs Tech. J.*, 18(3):95–110, Dec. 2013.

[105] Lu Ruan, Fangcheng Tang, and Chang Liu. Dynamic establishment of restorable connections using p-cycle protection in WDM networks. *Photon. Netw. Commun.*, 11(3):301–311, May. 2006.

[106] Alvaro Rubio-Largo, Miguel A. Vega-Rodriguez, Juan A. Gomez-Pulido, and Juan M. Sanchez-Perez. Multiobjective metaheuristics for traffic grooming in optical networks. *IEEE Trans. Evol. Computat.*, 17(4):457–473, Aug. 2013.

[107] Adel A. M. Saleh and Jane M. Simmons. Evolution toward the next-generation core optical network. *J. Lightw. Technol.*, 24(9):3303–3321, Sept. 2006.

[108] Nicola Sambo, Piero Castoldi, Antonio D'Errico, Emilio Riccardi, Annachiara Pagano, Michela Svaluto Moreolo, Josep M. Fábrega, Danish Rafique, Antonio Napoli, Silvano Frigerio, Emilio Hugues Salas, Georgios Zervas, Markus Nölle, Johannes K. Fischer, Andrew Lord, and Juan P.F.-P Gimenez. Next generation sliceable bandwidth variable transponders. *IEEE Commun. Mag.*, 53(2):163–171, Feb. 2015.

[109] S. Sedef Savas, Ferhat Dikbiyik, M. Farhan Habib, Massimo Tornatore, and Biswanath Mukherjee. Disaster-aware service provisioning with manycasting in cloud networks. *Photon. Netw. Commun.*, 28(2):123–134, Sept. 2014.

[110] S. Sedef Savas, Chen Ma, Massimo Tornatore, and Biswanath Mukherjee. Backup reprovisioning with partial protection for disaster-survivable software-defined optical networks. *Photon. Netw. Commun.*, pages 186–195, 2016.

[111] Dominic A. Schupke. An ILP for optimal p-cycle selection without cycle enumeration. In *Proc. Opt. Netw. Des. Model. Conf.*, Feb. 2004.

[112] Dominic A Schupke, Claus G Gruber, and Achim Autenrieth. Optimal configuration of p-cycles in WDM networks. In *Proc. Int. Conf. Commun.*, pages 2761–2765, Apr. 2002.

[113] Samir Sebbah and Brigitte Jaumard. An efficient column generation design method of p-cycle-based protected working capacity envelope. *Photon. Netw. Commun.*, 24(3):167–176, Dec. 2012.

[114] Ali Shaikh, Jens Buysse, Brigitte Jaumard, and Chirs Develder. Anycast routing for survivable optical grids: Scalable solution methods and the impact of relocation. *J. Opt. Commun. Netw.*, 3(9):767–779, Sept. 2011.

[115] Gangxiang Shen and Wayne D. Grover. Survey and performance comparison of dynamic provisioning methods for optical shared backup path protection. In *Proc. Broad. Netws.*, pages 1310–1319 Vol. 2, Oct. 2005.

[116] Gangxiang Shen, Hong Guo, and SanjayK. Bose. Survivable elastic optical networks: survey and perspective. *Photon. Netw. Commun.*, 31(1):71–87, Feb. 2016.

[117] Zhi-shu Shen, Hiroshi Hasegawa, Ken ichi Sato, Takafumi Tanaka, and Akira Hirano. A novel elastic optical path network that utilizes bitrate-specific anchored frequency slot arrangement. *Opt. Express*, 22(3):3169–3179, Feb. 2014.

[118] William Shieh, Hongchun Bao, and Yan Tang. Coherent optical OFDM: theory and design. *Opt. Express*, 16(2):841–859, Jan. 2008.

[119] Adam Smutnicki and Krzysztof Walkowiak. Optimization of p-cycles for survivable anycasting streaming. In *Proc. Design Reliable Commun. Netw.*, pages 227–234, Oct. 2009.

[120] Thomas A. Strasser and J. L. Wagener. Wavelength-selective switches for ROADM applications. *IEEE J. Sel. Top. Quantum Electron.*, 16(5):1150–1157, Sept. 2010.

[121] Takafumi Tanaka, Akira Hirano, and Masahiko Jinno. Advantages of IP over elastic optical networks using multi-flow transponders from cost and equipment count aspects. *Opt. Express*, 22(1):62–70, Jan. 2014.

[122] Ioannis Tomkos, Siamak Azodolmolky, Josep Solé-Pareta, Davide Careglio, and Eleni Palkopoulou. A tutorial on the flexible optical networking paradigm: State of the art, trends, and research challenges. *Proc. IEEE*, 102(9):1317–1337, Sept. 2014.

[123] Bogdan Uščumlić, Yvan Pointurier, Annalisa Morea, and Sébastien Bigo. On the cost of protection in optical slot switching rings with elastic transponders. In *Proc. Opt. Fiber Commun. Conf.*, page Th2A.46. Optical Society of America, 2015.

[124] Chaitanya S. K. Vadrevu, Rui Wang, Massimo Tornatore, Charles U. Martel, and Biswanath Mukherjee. Degraded service provisioning in mixed-line-rate WDM backbone networks using multipath routing. *IEEE/ACM Trans. Netw.*, 22(3):840–849, Jun. 2014.

[125] Emmanuel A. Varvarigos and Kostas Christodoulopoulos. Algorithmic challenges in flexible optical networks. In *Proc. Int. Comput. Netw. Commun.*, pages 236–241, Feb. 2014.

[126] Luis Velasco, Mirosław Klinkowski, Miroslaw Ruiz, and J. Comellas. Modeling the routing and spectrum allocation problem for flexgrid optical networks. *Photon. Netw. Commun.*, 24(3):177–186, Dec. 2012.

[127] Luis Velasco, Alba P. Vela, Fernando Morales, and Marc Ruiz. Designing, operating, and reoptimizing elastic optical networks. *J. Lightwave Technol.*, 35(3):513–526, Feb. 2017.

[128] Jorge Lopez Vizcaino, Yabin Ye, Víctor López, Felipe Jiménez, Raúl Duque, and Peter Krummrich. On the energy efficiency of survivable optical transport networks with flexible-grid. In *Proc. European Conf. Opt. Commun.*, page P5.05. OSA, 2012.

[129] Jorge López Vizcaíno, Yabin Ye, Víctor López, Felipe Jiménez, Francesco Musumeci, Massimo Tornatore, Achille Pattavina, and Peter M. Krummrich. Protection in optical transport networks with fixed and flexible grid: Cost and energy efficiency evaluation. *Opt. Switching Netw.*, 11:55–71, 2014.

[130] Krzysztof Walkowiak. Anycasting in connection-oriented computer networks: Models, algorithms and results. *Int. J. Appl. Math. Comput. Sci.*, 20(1):207–220, 2010.

[131] Krzysztof Walkowiak, Róza Goścień, and Mirosław Klinkowski. Evaluation of impact of traffic asymmetry on performance of elastic optical networks. In *Proc. Opt. Fiber Commun. Conf.*, page Th1I.2, Mar. 2015.

[132] Krzysztof Walkowiak, Mirosław Klinkowski, Róza Goścień, and Andrzej Kasprzak. Multiflow transponders for provisioning of asymmetric traffic in elastic optical networks with dedicated path protection. In *Proc. European Conf. Opt. Commun.*, pages 1–3. OSA, Sept. 2014.

[133] Bin Wang, Zhengwei Qi, Ruhui Ma, Haibing Guan, and Athanasios V. Vasilakos. A survey on data center networking for cloud computing. *Comput. Netw.*, 91:528–547, 2015.

[134] Chao Wang, Gangxiang Shen, and Sanjay Kumar Bose. Distance adaptive dynamic routing and spectrum allocation in elastic optical networks with shared backup path protection. *J. Lightw. Technol.*, 33(14):2955–2964, Jul. 2015.

[135] T. L. Weems. How far is far enough. *Disaster Recovery J.*, 16(2), 2003.

[136] Yue Wei, Gangxiang Shen, and Sanjay Kumar Bose. Span-restorable elastic optical networks under different spectrum conversion capabilities. *IEEE Trans. Rel.*, 63(2):401–411, Jun. 2014.

[137] Yue Wei, Kai Xu, Yuling Jiang, Heming Zhao, and Gangxiang Shen. Optimal design for p-cycle-protected elastic optical networks. *Photon. Netw. Commun.*, 29(3):257–268, 2015.

[138] Sheryl L. Woodward, Weiyi Zhang, Balagangadhar G. Bathula, Gagan Choudhury, Rakesh K. Sinha, Mark D. Feuer, John Strand, and Angela L. Chiu. Asymmetric optical connections for improved network efficiency. *J. Opt. Commun. Netw.*, 5(11):1195–1201, Nov. 2013.

[139] Bin Wu, Kwan L. Yeung, and Pin-Han Ho. ILP formulations for p-cycle design without candidate cycle enumeration. *IEEE/ACM Trans. Netw.*, 18(1):284–295, Feb. 2010.

[140] Haitao Wu, Fen Zhou, Zuqing Zhu, and Yaojun Chen. On the distance spectrum assignment in elastic optical networks. *IEEE/ACM Trans. Netw.*, 25(4):2391–2404, Aug. 2017.

[141] Jingjing Wu, Yejun Liu, Cunqian Yu, and Ying Wu. Survivable routing and spectrum allocation algorithm based on p-cycle protection in elastic optical networks. *J. Light Electron Opt.*, 125(16):4446–4451, 2014.

[142] Rui Xu, Bin Chen, Mingjun Dai, Xiaohui Lin, and Hui Wang. Disaster survivability in elastic optical datacenter networks. In *Proc. IEEE Optoel. Global Conf.*, pages 1–3, Sept. 2016.

[143] Raghav Yadav, Rama Shankar Yadav, and Hari Mohan Singh. P-cycle based network design to control the optical path lengths in restored state of transparent network. In *Proc. Int. Conf. Comput. Commun. Technol.*, pages 355–359, Sept. 2010.

[144] Yabin Ye, Felipe Jiménez Arribas, Jaafar Elmirghani, Filip Idzikowski, Jorge López Vizcaino, Paolo Monti, Francesco Musumeci, Achille Pattavina, and Ward Van Heddeghem. Energy-efficient resilient optical networks: Challenges and trade-offs. *IEEE Commun. Mag.*, 53(2):144–150, Feb. 2015.

[145] Feng Zhang and Wen-De Zhong. Applying p-cycles in dynamic provisioning of survivable multicast sessions in optical WDM networks. In *Proc. Opt. Fiber Commun. Conf.*, page JWA74. Optical Society of America, Mar. 2007.

[146] Liang Zhang, Wei Lu, Xiang Zhou, and Zuqing Zhu. Dynamic RMSA in spectrum-sliced elastic optical networks for high-throughput service provisioning. In *Proc. Int. Conf. Comput. Netw. Commun.*, pages 380–384, Jan. 2013.

[147] Liang Zhang and Zuqing Zhu. Spectrum-efficient anycast in elastic optical inter-datacenter networks. *Opt. Switching Netw.*, 14:250–259, Aug 2014.

[148] Zhenrong Zhang, Lixin Zhu, Zhengbin Li, and Anshi Xu. Shared-p-cycles method for design of survivable WDM networks. *Front. Electr. Electron. Eng. China*, 4(4):362–370, Dec. 2009.

[149] Wen-De Zhong and Zhen-Rong Zhang. Design of survivable WDM networks with shared-p-cycles. In *Proc. Opt. Fiber Commun. Conf.*, volume 1, pages 554–556, Feb. 2004.

[150] Dongyun Zhou and Suresh Subramaniam. Survivability in optical networks. *Netw.*, 14(6):16–23, Nov. 2000.

[151] Fen Zhou. Multicast provision in transparent optical networks with Mixed Line Rates. In *Proc. Opt. Netw. Des. Model. Conf.*, pages 125–130, Apr. 2013.

[152] Zuqing Zhu, Masaki Funabashi, Zhong Pan, Bo Xiang, Loukas Paraschis, and S. J. B. Yoo. Jitter and amplitude noise accumulations in cascaded all-optical regenerators. *J. Lightw. Technol.*, 26:1640–1652, Jun. 2008.

[153] Mateusz Źotkiewicz, Michal Pióro, Miroslaw Ruiz, Mirosław Klinkowski, and Luis Velasco. Optimization models for flexgrid elastic optical networks. In *Proc. Int. Con. Transparent. Opt. Netw.*, pages 1–4, Jun. 2013.

Acronyms

SLR	Single-Line-Rate
WDM	Wavelength-Division Multiplexing
MLR	Mixed-Line-Rate
EON	Elastic optical network
DSP	Digital Signal Processing
***p*-Cycle**	pre-configured Cycles
DEBPP	Dedicated End-to-content Back-up Path Protection
SEBPP	Shared End-to-content Back-up Path Protection
BVTs	Bandwidth-Variable Transponders
FS	Frequency Slot
BV-OXCs	Bandwidth-Variable Optical cross-Connects
DPPC	Disaster Protecting *p*-Cycle
CG	Column Generation
CAPEX	Capital Expenditures
MILP	Mixed Integer Linear Programming
GPA	Graph Partitioning in Average
ILP	Integer Linear Programming
SS-*p*-cycle	Spectrum Shared *p*-cycle
SFR	Spectrum Fragmentation Ratio
SS-SA	SS-*p*-cycle Spectrum Allocation
DCs	Data Centers
DCNs	Data Center Networks
OAs	Optical Amplifiers

TDM Time Division Multiplexing

EDFA Erbium-Doped Fiber Amplifier

CAGR Compound Annual Growth Rate

SLICE spectrum-SLICEd "elastic optical path" network

DWDM Dense Wavelength-Division Multiplexing

DFB Distributed Feedback

WSS Wavelength-Selective Switches

ROADM Reconfigurable Optical Add/Drop Multiplexer

DP-QPSK Dual-Polarization Quadrature Phase Shift Keying

RWA Routing and Wavelength Assignment

RWRA Routing, Wavelength, and Rate Assignment

OOK On/Off Key

DPSK Differential Phase Shift Keying

BER Bit-Error Rate

OFDM Orthogonal Frequency-Division Multiplexing

RSA Routing and Spectrum Assignment

SDN Software-Defined Network

BPSK Binary Phase-Shift Keying

16-QAM 16-Quadrature Amplitude Modulation

CoWDM Coherent Wavelength-Division Multiplexing

CO-OFDM Coherent Optical Orthogonal Frequency-Division Multiplexing

OAWG Optical Arbitrary Waveform Generation

S-BVT Sliceable Bandwidth-Variable Transponder

FEC Forward Error Correction

BV-WSS Bandwidth-Variable Wavelength Selective Switches

MEMS Micro Electro Mechanical Systems

LICOS Liquid Crystals On Silicon

PLCs Planar Lightwave Circuits

SBPP Shared Backup Path Protection

DZ Disaster Zone

CDNs	Content Delivery Networks
VM	Virtual Machine
MLR-p	MLR-at-p-lightpath protection
MLR-l	MLR-at-lightpath protection
MLR-g	MLR-with-backup-flow-grooming protection
SSP	Shared Subconnection Protection
DP	Dedicated Protection
SP	Shared Protection
MPLS	Multi-Protocol Label Switching
Diff QoP	Differentiated Quality of Protection
EI	Estimation of cycle numbers $\|I\|$
RRA	Routing/Rate Assignment
WA	Wavelength Assignment
O/E/O	Optical-Electrical-Optical
PLI	Physical-Layer Impairment
VPN	Virtual Private Networks
TASY	Traffic Asymmetry
AR	Anycast Ratio
DPP	Dedicated Path Protection
TS	Tabu Search
PWCE	Protected Working Capacity Envelope
FIPP	Failure-Independent Path Protection
FSs	Frequency Slices
TR	Transmission Rate
GB	Guard Band
PPCS	Promising Power-efficient p-Cycles Selection
PCS	p-Cycle Selection
SFR	Spectrum Fragmentation Ratio
SA	Slots Assignment
SSA	Starting Slot Assignment

SRG	Shared Risk Group
FID	Failure-Independent
FD	Failure-Dependent
RMP	Restricted Master Problem
PP	Pricing Problem
ESWBP	Enhanced Shortest Working and Backup Paths
LPR	Linear Programing Relaxation

List of Publications

International Journals:

[J1]: **Min Ju**, Fen Zhou, Shilin Xiao and Haitao Wu."Leveraging Spectrum Sharing and Defragmentation to *p*-Cycle Design in Elastic Optical Networks." *IEEE Commun. Letters.*, vol. 21, no. 3, pp. 508-511, Mar. 2017.

[J2]: **Min Ju**, Fen Zhou, Shilin Xiao and Zuqing Zhu."Power-Efficient Protection With Directed *p*-Cycles for Asymmetric Traffic in Elastic Optical Networks." *J. Lightwave Technol.*, vol. 34, no. 17, pp. 4053-4065, Sep. 2016.

[J3]: **Min Ju**, Fen Zhou, Zuqing Zhu and Shilin Xiao."Distance-adaptive, Low CAPEX Cost *p*-Cycle Design Without Candidate Cycle Enumeration in Mixed-Line-Rate Optical Networks." *J. Lightwave Technol.*, vol. 34, no. 11, pp. 2663-2676, Jun. 2016.

[J4]: **Min Ju**, Fen Zhou, and Shilin Xiao."Column Generation for Cloud Services in Disaster-Survivable Elastic Optical Datacenter Networks." *IEEE Trans. Commun.*, 2017 (To be submitted).

[J5]: Fen Zhou, **Min Ju**, and Amine Ait-Ouahmed."Joint Optimization for Multicast Provisioning in Mixed-Line-Rate Optical Networks with Column Generation Approach." *J. Lightwave Technol.*, vol. PP, no. pp, pp. 1-14, 2017.

International Conferences:

[C1]: Cao Chen, **Min Ju**, Shilin Xiao, Fen Zhou, and Xuelin Yang."Minimizing Total Blocking By Setting Optimal Guard Band In Nonlinear Elastic Optical Networks." *Proceedings of 19th International Conference on Transparent Optical Networks (ICTON).*, Giroda, Spain, Jul. 2017, pp. 1-4.

[C2]: **Min Ju**, Fen Zhou, Shilin Xiao and Torres-Moreno, Juan-Manuel."Spectrum Shared p-Cycle Design in Elastic Optical Networks with/without Spectrum Conversion Capabilities." *Proceedings of International Conference on Network Games, Control, and Optimization (NETGCOOP).*, Avignon, France, Feb. 2017, pp. 147-157.

[C3]: **Min Ju**, Fen Zhou, Shilin Xiao and Zuqing Zhu. "Energy-efficient Protection with Directed *p*-Cycles for Asymmetric Traffic in Elastic Optical Networks." *Proceedings of European Conference on Networks and Optical Communications (NOC)*, Lisbon, Portugal, Jun. 2016. pp. 94-99.

[C4]: Fen Zhou, Haitao Wu, **Min Ju**, Jérémy Omer, Imane Sefrioui, Luis Flores, Bruno Rosa, Samuel Deleplanque and Marcos de Melo da Silva. "Routing and Scheduling Problem of N-Side." *Proceedings of European Study Group with Industry*, Avignon, France, May 2016.

[C5]: **Min Ju**, Fen Zhou, Zuqing Zhu and Shilin Xiao. "p-Cycle design without candidate cycle enumeration in mixed-line-rate optical networks." *Proceedings of 16th International Conference on High Performance Switching and Routing (HPSR)*, Budapest, Hungary, Jul. 2015. pp. 1-6.

[C6]: Zexi Yu, Shilin Xiao, Yinan Hou, **Min Ju** and Weisheng Hu. "Simulation of adaptive OFDM white-LED visible light communication system using high-order QAM based on FPGA." *Proceedings of Asia Communications and Photonics Conference (ACPC)*, Nov. 2014, Shanghai, China. pp. ATh3A.181.

[C7]: Juan Du, Shilin Xiao, Hao He, Zhao Zhou and **Min Ju**."Novel Time-Domain Compensation Scheme for Transmitter IQ mismatch in CO-OFDM System." *Proceedings of Asia Communications and Photonics Conference (ACPC)*, Nov. 2014, Shanghai, China. pp. ATh3A.131.

[C8]: **Min Ju** and Shilin Xiao."Design principles and applications of a novel electromagnetic spectrum table." *Proceedings of the International Symposium on Antennas and Propagation (ISAP)*, Oct. 2013, Nanjing, China. pp. 184-187.

[C9]: **Min Ju**, Shilin Xiao, Weiqiang Sun, Meihua Bi, Zhao Zhou and Tao Qi."Effects of Optical Filters on 10-Gb/s RSOA-Based Upstream Transmission in WDM-PON System." *Proceedings of Asia Communications and Photonics Conference (ACPC)*, Nov. 2013, Beijing, China. pp. AF2F.60.